PyrSat – Prevention and response to wild fires with an intelligent Earth observation CubeSat

Mónica Estébanez Camarena

Department of Electrical Engineering

University of Cape Town

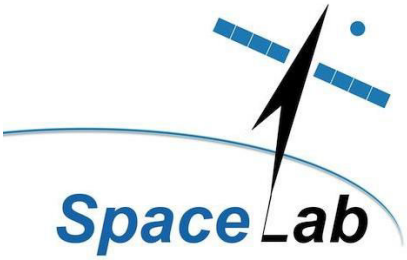

February 2018

SL18 – 02M

Authorship declaration

"I know the meaning of plagiarism and declare that all the work in this document, save for that which has been properly acknowledged, is my own. This dissertation has been submitted to the Turnitin module and I confirm that my supervisor has seen my report and any concerns revealed by such have been resolved with my supervisor."

Mónica Estébanez Camarena

Signed by candidate

Date: 17th February 2018

APPLICATION FORM

Please Note:
Any person planning to undertake research in the Faculty of Engineering and the Built Environment (EBE) at the University of Cape Town is required to complete this form **before** collecting or analysing data. The objective of submitting this application *prior* to embarking on research is to ensure that the highest ethical standards in research, conducted under the auspices of the EBE Faculty, are met. Please ensure that you have read, and understood the **EBE Ethics in Research Handbook** (available from the UCT EBE, Research Ethics website) prior to completing this application form: http://www.ebe.uct.ac.za/ebe/research/ethics1

APPLICANT'S DETAILS		
Name of principal researcher, student or external applicant		Monica Estebanez Camarena
Department		Electrical Engineering
Preferred email address of applicant:		ESTMON001@myuct.ac.za
If Student	Your Degree: e.g., MSc, PhD, etc.	MPhil
	Credit Value of Research: e.g., 60/120/180/360 etc.	120
	Name of Supervisor (If supervised):	Prof Peter Martinez
If this is a researchcontract, indicate the source of funding/sponsorship		
Project Title		PyrSat – Prevention and response to wild fires with an intelligent Earth Observation CubeSat

I hereby undertake to carry out my research in such a way that:

- there is no apparent legal objection to the nature or the method of research; and
- the research will not compromise staff or students or the other responsibilities of the University;
- the stated objective will be achieved, and the findings will have a high degree of validity;
- limitations and alternative interpretations will be considered;
- the findings could be subject to peer review and publicly available; and
- I will comply with the conventions of copyright and avoid any practice that would constitute plagiarism.

SIGNED BY	Full name	Signature	Date
Principal Researcher/ Student/External applicant	Monica Estebanez Camarena	Signed by candidate	**19 Dec 2017**

APPLICATION APPROVED BY	Full name	Signature	Date
Supervisor (where applicable)	Peter Martinez	Signed by candidate	19/12/17
HOD (or delegated nominee) Final authority for all applicants who have answered NO to all questions In Section1; and for all Undergraduateresearch (Including Honours).	Olabisi Falowo	Signed by candidate	13/2/18
Chair : Faculty EIR Committee For applicants other than undergraduate students who have answered YES to any of the above questions.			

Abstract

Forest fires are a pervasive and serious problem. Besides loss of life and extensive environmental damage, fires also result in substantial economic losses, not to mention property damage, injuries, displacements and hardships experienced by the affected citizens.

This project proposes a low-cost intelligent hyperspectral 3U CubeSat for the production of fire risk and burnt area maps. It applies Machine Learning algorithms to autonomously process images and obtain final data products on-board the satellite for direct transmission to users on the ground.

Used in combination with other services such as EFFIS or AFIS, the system could considerably reduce the extent and consequences of forest fires.

Acknowledgements

I would like to thank my supervisor, Peter Martinez, for his tireless motivation, help and support. Since I had the idea to develop this dissertation, he always supported me and made me believe in it. It is because of him that this thesis became, besides the academic requirement to fulfil my MPhil degree, a personal project that I have developed as if it were going to be reality. Today, I strongly believe in the concept presented in this work as a means to open the access to space to a wider community of users and to address social and environmental issues.

Peter did not only help me in the development of my dissertation but also during the two-year period of my Masters programme. He is doing an excellent job in preparing postgraduate students with the ambition to change the space arena. He also supported me in my applications to international competitions and national conferences. In particular, the PyrSat space mission concept won the award of Best Proposal Prepared by an Individual in the ESA's Sentinel Small Sat (S^3) competition and was finalist in the ESA's Space for Sustainability Awards.

I also want to thank George Sithole, from the Geomatics Department, who was willing to help me and provide me with all possible resources for the design of the on-board classification software. Every time that I needed help he found the time to give me advise on my dissertation and he made me always feel welcome.

Lastly, I want to thank the extraordinary SpaceLab team, that during this time have become close friends of mine and a great support for the development of my MPhil and extra-curricular matters. They all are outstanding people and students, with brilliant ideas and the potential and motivation to realise them.

The completion of this dissertation would not have been possible with the contribution of all of them.

Table of Contents

Chapter III. System design

Chapter IV. Autonomous on-board image analysis and classification

Chapter V. Schedule, cost and funding

Chapter VI. Regulatory and space policy issues

Chapter VII. Conclusions and future work

List of acronyms

ADCS	Attitude Determination and Control System
ADR	Active Debris Removal
AFIS	Advanced Fires Information System
COPUOS	Committee on the Peaceful Uses of Outer Space
COTS	Commercial off-the-shelf
EPS	Electrical Power System
EC	European Commission
EFFIS	European Forest Fires Information System
EO	Earth Observation
ESA	European Space Agency
EU	European Union
FOV	Field of View
GIS	Geographic Information System
GSD	Ground Sample Distance
IARU	International Amateur Radio Union
IFOV	Instantaneous Field of View
ISIS	Innovative Solutions in Space
ITU	International Telecommunications Union
LEO	Low Earth Orbit
LTAN	Local Time of the Ascending Node
LTDN	Local Time of the Descending Node
MODIS	Moderate Resolution Imaging Spectroradiometer
NASA	National Aeronautics and Space Administration
NDVI	Normalized Difference Vegetation Index
NIR	Near Infrared
NN	Neural Networks

OBDH	On-board Data Handling
OBC	On-Board Computer
OST	Outer Space Treaty
OTB	Orfeo ToolBox
PCA	Principal Component Analysis
PCB	Printed Circuit Board
PSR	PyrSat Requirement
RF	Radio Frequency
SVM	Support Vector Machine
SWIR	Short-Wave Infrared
TIR	Thermal Infrared
TOA	Top of the Atmosphere
UCT	University of Cape Town
UHF	Ultra High Frequency
UN	United Nations
UNOOSA	United Nations Office for Outer Space Affairs
US	United States

Chapter I. Introduction

Wild fires are a global phenomenon that can have serious consequences for the environment, population and property. Earth observation satellites can play an important role in the entire fire management cycle, from risk assessment, to mitigation and response. Furthermore, the space industry and technology in general is evolving at a fast pace and applying these advances to fire applications could potentially reduce the extent of consequences of forest fires around the world.

The goal of this Chapter is to set the context for an intelligent CubeSat mission for Earth observation that will focus on wild fires. Firstly, the problem and current approach to wild fires will be introduced. Secondly, the methodology and history of Earth observation applications for forest fire management will be presented. This will lead to an introduction to the existing fire services and the EO satellites dedicated to fire management. Then, the chapter will move on to an explanation of some technological and conceptual advances in the space sector, namely, hyperspectral Earth observation, Earth observation data product formats and the CubeSat standard. Finally, a last section will be dedicated to the combination of the three technologies that are the base of the PyrSat project: CubeSats, hyperspectral sensors and on-board processing.

1.1. Introduction to the problem of wild fires and the importance of fire management

1.1.1. Fire: a global challenge

Vegetation fires are an important issue affecting a variety of environment, ecosystem and climate functions and structures. They are one of the most relevant factors affecting vegetation succession, vegetation composition and carbon budgets worldwide.

Of special relevance at a global scale is the high volume of smoke emitted, which changes atmospheric composition, deteriorates air quality and contributes to global warming and climate change (Fuchs et al., 2015). Forests fires emit mainly Carbon Dioxide (around a 90%), the main greenhouse gas (Carrielo and Anderson, 2007). Africa alone accounts for 40% of global annual carbon emissions, with the highest incidence of vegetation fires in the world (Tsela et al., 2014). The atmospheric chemistry change is a highly complex factor to include in the emission models. Estimations are primarily based on the amount of biomass consumed, derived from burned area mapping, pre-fire biomass information and knowledge of the degree of fires combustion completeness (Bastarrika, Chuvieco and Martín, 2011).

Uncontrolled fires have many socio-economic implications. In developed regions such as Australia, Greece, Portugal, Russia or the State of California in the United States these implications are especially acute as a result of the large numbers of severe fires that have taken place in recent years due to the growing urbanization of forested areas (Bastarrika, Chuvieco and Martín, 2011).

On the one hand controlled or prescribed burning (also known as hazard reduction burning), fuel management activities and forest thinning can reduce fire occurrence and intensity, and increase the survival of some forest classes. Additionally, the spatial patterns of fuel management can in principle affect the growth and spread rate of large fires. The division into blocks of large areas with high fire

risk and danger potential is also crucial for fire prevention and suppression (Saglam et al., 2008).On the other hand, human actions can also alter natural fire occurrences and with them the responses of organisms to fire, distribution of land cover types and nutrient cycling (Antunes et al., 2014).

All in all, fire is an essential factor in many forest ecosystems and should therefore be taken into account in the management of a forest. However, due to the inherent complexity of the topic, management strategies and procedures are generally difficult to define (Saglam et al., 2008).

1.1.2. Fire behaviour and detection in different biomes

Although wildfire is a global phenomenon, its consequences are different in each location. Not surprisingly, different biomes exhibit different responses to fire, and this has been well documented in the literature. A compilation of this information for different ecosystems obtained from a literature review is presented below:

- *Tropical rainforests:* Although they cover less than six percent of the total surface of the Earth, tropical rainforests contain more than 50 percent of the world's biodiversity (Anderson and Imandaand, 1999). Despite the conditions of these forests, normally too humid to present frequent occurrences of natural fire, some land use practices can increase this frequency. For example, in Southeast Asia and Latin America, land use practices resulted in wild fires burning more than 20 million hectares in the period 1997-1998 (Cochrane, 2003). In Africa, however, these forests do not normally burn. An exception of this was the outbreak of fires in the Congo Basin caused by the severe drought brought about by the 2015-2016 El Niño year (Verhegghen et al., 2016).
- *Pine forests:* In general, dense forest formations are less easily penetrated by fire. The most recurrent fire occurrences in this biome take place at an understory level.
  A high tree canopy compromises the detection accuracy of burn scars and understory fires (Tsela et al., 2014).
- *Grassland biome:* Fires here are generally widely spaced with large burns of 120-1000 ha and above. There is also a significant presence of smaller burns (<100 ha) that are often undetected by the commonly used coarse spatial resolution sensors (Tsela et al., 2014).
- *Savannah:* Observations in the Kruger National Park of South Africa revealed that, depending on the degree of brightness, even in the case of small fires, they could easily be detected at lower resolution. However, small fires with complex shapes were more often undetected (Tsela et al., 2014). This biome generally accounts for the most frequent fire occurrences. In the dry season, it is most commonly due to the flammability of the vegetation. Lightning is a potential cause in the wet season (Antunes et al., 2014).
- For the specific case of South Africa, it is also important to consider the *fynbos biome*, characteristic of the Western Cape. Here, the majority of burned areas are in the range of 0.36-1000ha and exhibit a simple morphology. Spectral pre- and post- fire difference are not large (Tsela et al., 2014). Because of the similarity of the pre- and post- fire spectral responses, a considerable number of the fires were not detected (Tsela et al., 2014).

In general, fire is more prone to start in open vegetation formations and close to savannah formations or roads. Recent and abandoned logging roads are also a potential facilitator for forest fires (Verhegghen et al., 2016).

Uncontrolled coal burning is also a global-scale phenomenon, more importantly in countries such as the US, former USSR, South Africa, Venezuela, India and China, with significant levels of coal mining activity. In most of the cases, a fire ignited in an active mine can be suppressed by the operating company. The problem appears however in abandoned coal sites, especially where small-scale mining with inadequate technologies has taken place and where the mining activities have not been properly closed down. In these cases, fire often results in severe environmental consequences as well as significant economic losses (Lorenz et al., 2015).

1.1.3. The relevance of fire management

Fire management encompasses activities carried out at local and national levels in different institutional, economic, social environmental and geographical contexts with the goal of controlling the frequency, area, intensity and impact of fires (Flasse et al., 2004).

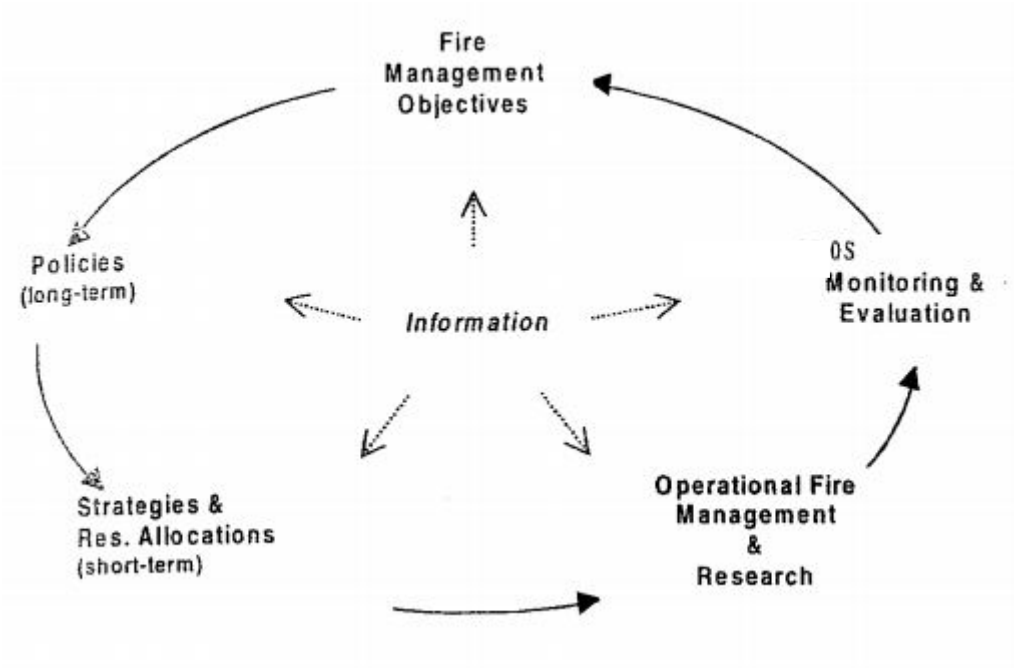

Figure 1.1: Typical fire management cycle (Flasse et al., 2004).

The typical fire management cycle has different phases, all of which have a requirement for reliable information. These are: Definition of the fire management objectives, determination of policies and strategies for effective fire management, research, monitoring and evaluation of the implementation. The output of this last phase will be the input for repeating the cycle (Flasse et al., 2004).

Each phase of the fire management cycle requires different kinds of information. For example, some ecosystems with frequent fire occurrence present a cyclic behaviour with vegetation recovery and biomass accumulation following fire events. Fire management should thus consider this and other aspects of the biological cycle and avoid fuel accumulation and the increased risk of more severe fires that threaten the local flora and fauna. Attention and assignment of resources should be focused on zones with identified high occurrence of fires (Antunes et al., 2014).

Traditional field measurements are still useful and indeed often needed for validation and local applications of space-derived fine data products. However, they are highly labour extensive, costly and difficult to extrapolate over large areas (Saglam et al., 2008). Thus, due to the often vast extent of fires and the very dynamic nature of the process, they cannot provide sufficiently accurate and updated information to consistently serve as a basis for fire management. This is especially true for locations with limited resources and staff, or with poor accessibility (Flasse et al., 2004, Pereira, 2007).

1.2. Remote sensing of fires from space

Spaceborne remote sensing can obtain products for fire management in the different phases of a fire event: Before (fuel load, vegetation status and rainfall), during (active fires) and after the fire (burned areas). However, analysis and interpretation of the reflectance data captured by the sensors is necessary to obtain these useful final products (Flasse et al., 2014).

1.2.1. Advantages and limitations of remote sensing for fire monitoring

Remote sensing offers a timely, easy and cost-effective tool for fire research and monitoring (Saglam et al., 2008). Its accuracy, repeatability, speed of data acquisition, longer historical data and ease of combination with other thematic data such as roads, fire units, plantations, villages or protected forests make remote sensing especially suited for fire management tasks (Antunes et al., 2014, Flasse et al., 2004).

Some of these characteristics derive from the orbits of the satellites that give regular, frequently updated, reliable, systematic observations. Because of their high vantage point, satellites are also capable to observe in a more economical and timely way vast and remote areas, where there is no easy access by other means. Lastly, satellites capture data in a wider range of the electromagnetic spectrum, which allows them to gather data of more diverse nature about the observed objects (Flasse et al., 2004).

However, remote sensing of fires from space also has the following limitations:

- *Obscuration of burned areas by smoke and clouds:* Thick smoke is opaque to visible wavelengths and can complicate the discrimination of burned areas in the long-wave thermal infrared (through temperature contamination) and in the near infrared. However, it is almost transparent to middle-infrared wavelengths, which makes this region useful in areas such as most of Africa, where thick smoke is frequent during the dry season. Thick clouds obscure the surface in the whole spectral region from NIR to TIR and can be mistaken for burned areas. Dense tree canopy can also cover underlying fires by absorbing and reflecting their emitted radiant energy (Flasse et al., 2004) and (Fuchs et al., 2015).
- *Masking of burned areas:* Post-fire regrowth and green-up of the surface can remove the signal of burned areas. This is especially critical where these processes happen shortly after the fires (Flasse et al., 2004).
- *Misclassification of burn scars:* On soils with high moisture content, “patchy fires” (a mosaic of small and non-continuous fires) are frequent. In these circumstances, the whole soil extent can be misclassified as burned areas (Flasse et al., 2004).

- *Variable spectral signatures:* Spectral and spatial variability due to viewing, atmosphere and surface conditions at different places and times often make it impossible to generalize the fire detection methods. That is, a specific method that obtain robust results for a certain geographic region and under certain circumstances may not be accurate when extrapolated to other sites and times (Flasse et al., 2004, Fuchs et al., 2015).

The variable accuracy of maps obtained with remote sensing data should also be taken into account and assessed, normally through obtaining complementary ground truth data (Flasse et al., 2004).

1.2.2. Fire-related products obtained with remote sensing

Fire produces four kinds of specific signal observable from space: Direct radiation from the flame front (heat and light), aerosols (smoke), solid residue (char and ash) and altered vegetation structure (scar) (Pereira, 2007).

Two products are traditionally derived from satellite observations: active fire and burned area maps. Because of the temporal constraints that make an active fire only observable if a satellite passes over it when it is burning, burned area is a more suitable measurement of the impact of fires. Over the years a variety of fire products have become publicly available, although due to the fact that these fire products are usually derived for a specific site, they are normally only valid regionally (Tsela et al., 2014).

Fire risk and danger potential maps (FRDP)

Fire danger and risk estimates in a spatio-temporal scale are crucial for fire management planning and the simulation of fire growth and development in a landscape (Saglam et al., 2008).

Saglam et al. (2008) define fire risk as the '*probability of ignition depending on the presence and activities of causative agents (i.e. man, lightning, etc)´*and fire danger, as the '*sum of constant and variable factors affecting the ignition, spread and resistance to control, and subsequent fire damage*'.

Fire risk and danger potential (FRDP) maps are digital cartography of fire ignition risk and severity and are based on stand characteristics, topographic features and land uses in a specific location. They are the result of incorporating satellite and field observations in an index representing fire ignition probability and fire danger (Saglam et al., 2008).

In the same work, analytical expressions for both fire risk potential and fire danger potential indices (FRI and FDI) are presented.

$$FRI = 10\,SC_i + 2\,AL_j + 2\,SA_k + 3S_l + 2IS_m$$

$$FDI = SC_i^2\,(CC_n + SD_p + S_l + IS_m)$$

These indices are based on seven factors, namely: the species composition (SC); the proximity of agricultural lands to forests (AL); the proximity to settlement areas (SA);the slope (S); the insolation (IS);the stand crown closure (CC); the stages of stand development (SD). Each variable factor is divided into several classes, and each class is assigned a fire risk and a fire danger rating (extreme, high, moderate, low). Table 1.1 shows this rating for the case of fire risk.

Table 1.1: Weights and ratings assigned to variables and classes for fire risk (Saglam et al., 2008).

Variables	Classes		Value Assigned	Fire Risk
Species composition	(1) Calabrian pine		5	Extreme
(weight = 10)	(2) Calabrian pine + black pine		5	Extreme
	(3) Shrub		4	High
	(4) Degraded areas		2	Moderate
	(5) Oak + Coppice		1	Low
Slope	(6) 0 – 5 %		1	Low
(weight = 3)	(7) 5 – 15 %		2	Moderate
	(8) 15 – 35 %		3	High
	(9) > 35 %		5	Extreme
Insolation	(10) 0- 23	N	1	Low
(weight =2)	(11) 23- 68	NE	2	Moderate
	(12) 68 -113	E	2	Moderate
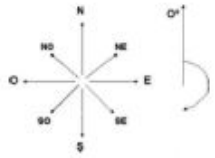	(13) 113 – 158	SE	3	High
	(14) 158 – 203	S	5	Extreme
	(15) 203 – 248	SW	5	Extreme
	(16) 248 – 293	W	2	Moderate
	(17) 293 – 338	NW	2	Moderate
	(18) 338 – 360	N	1	Low
Proximity of Agricultural Lands	(19) 0-100		5	Extreme
to Forest (m)	(20) 100-200		3	High
(weight = 2)	(21) 200-300		2	Moderate
	(22) 400 <		1	Low
Proximity to Settlement Areas (m)	(23) 0-100		5	Extreme
(weight = 2)	(24) 100-200		3	High
	(25) 200-300		2	Moderate
	(26)400 <		1	Low

*non-vegetated sites were assigned a "0" fire risk rating

Slope does not necessarily have an impact on fire ignition but it definitely affects the fire evolution once a fire starts. Steeper scenarios cause a faster fire propagation, and thus have higher fire danger. As for **insolation**, southern and south-western exposures have a greater fire danger potential in the northern hemisphere; in the southern hemisphere, this is true for northern and north-eastern exposures. The **stage of development** is an indicator of the structure of the forest and its diverse processes. The older and more developed a stand is, the more crown accumulation and surface fuels, less vertical continuity and less fire danger potential. The **species composition** indicates the site conditions, vegetation flammability and speed of fire propagation. Deciduous forest stands present a low fire danger, whereas it is high for coniferous and Mediterranean shrubs. **Crown closure** indicates the ease of fire to spread. The higher it is, the more intensely fire burns. The **proximity of agricultural lands to the forest** and the **distance from settlements areas** provide an indicator of how much human activities affects the fire risk (Saglam et al., 2008).

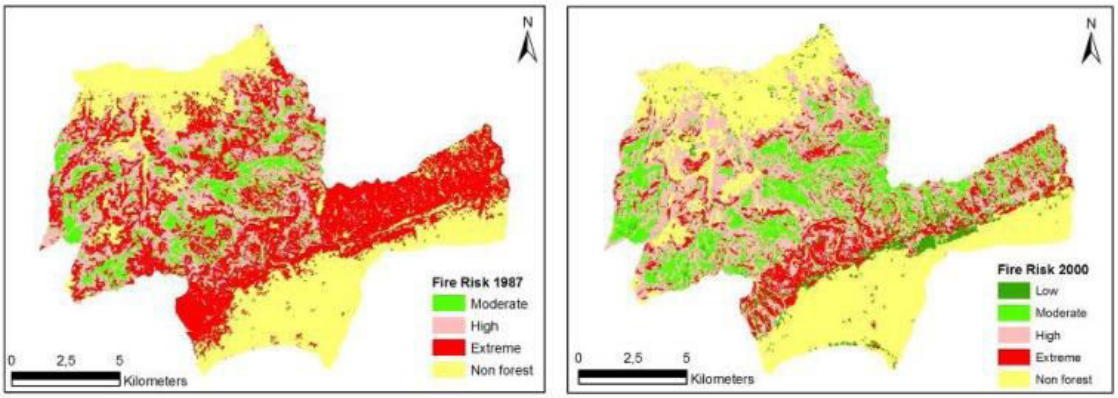

Figure 1.2: Spatial fire risk maps for the Korudag Forest District, north-western Turkey, derived from 1987 and 2000 Landsat (Saglam et al., 2008).

Anderson and Imandaand (1999) identified three means to study the vegetation fire risk:

1. A mapped history of previous fire occurrence. This can allow the identification of patterns, such as the relation between the number and severity of fires and the vegetation type, rainfall and land uses, and fire-prone areas.

2. A drought or soil dryness index (SDI). Although rainfall is the primary inhibitor and suppressant of vegetation fires and is therefore usually used as the main fire danger indicator, the soil dryness index provides more practical and realistic predictions. This method follows a water balance approach, using daily weather data (daily rainfall and estimated evapotranspiration derived from the land temperature) to estimate the SDI.

3. Indices of current relative vegetation dryness (susceptibility to fire): The Normalized Difference Vegetation Index (NDVI) represents the greenness or photosynthetic activity of vegetation. It is one of the most widely used vegetation indices and correlates the red and infrared bands. It can be linked to the susceptibility of vegetation to fire as the dryer vegetation is, the more it reflects in the red and the less it reflects in the infrared, thus resulting in a smaller NDVI index (USDA-ARS Jornada Experimental Range et al., 2013)

   Although seasonal change can be detected from the NDVI images, this method has certain limitations that may invalidate its predictions. Firstly, different land uses and vegetation types result in local variations of the NDVI. Furthermore, scenes such as burn scars, flooded areas or areas cleared for agriculture are also problematic as their low reflectance can lead to mistaking them for dry vegetation. Thus, knowledge of field conditions is required in order to use this index as a fire risk indicator.

   Combining the SDI and NDVI indices might be the best method to predict vegetation fire danger. However, is it important to note that these methods reflect the susceptibility of vegetation to burn. The occurrence of fire is irrevocably related to anthropogenic causes (Anderson and Imandaand, 1999).

Additionally, climate change may also increase the fire occurrence (Antunes et al., 2014).

Active fire detection

Active fire detection is most efficiently carried out with thermal sensors. Although the spectral signature of a fire is quite specific, there may still be some confusion with other sources such as oil refineries and volcanic eruptions. One of the main challenges with active fire detection is that the signals are very short lived (Pereira, 2007).

For operational applications, timeliness of information provision is essential. To be really useful the data have to be updated as often as possible and distributed in near-real time (Flasse et al, 2004).

Remote sensing of burned areas

Detection of burned areas is based on the detection of char and scar signals. Because these signals are longer lasting than active fire signals, burned area analysis is commonly used to study the ecological and economic effects of the fire (Pereira, 2007).

Most burned area analysis is based on multi-temporal change detection. Changes in the albedo, temperature, photosynthetic signals and soil/ vegetation moisture can be diagnostic of burned areas (Pereira, 2007).

Burned areas have three observable characteristics that allow them to be observed from space:

- Vegetation is cleared. Methods based on this effect include vegetation spectral indices such as NDVI, GEMI and atmospherically resistant ARVIs. They are of relevant application in areas such as pine and evergreen forests where primarily photosynthesising vegetation burns. However, for grassland, shrubs and deciduous woodland vegetation, deterioration can occur previously to a fire, reducing the detection rate. Some human activities reducing the vegetation density can have the same effect.
- Char combustion residues, much darker than unburned vegetation, are deposited over the burned area. This darkening is especially observable in NIR wavelengths. However, the main drawback of relying on this method is that the signal produced by deposition of residues is very short-lived and can be removed by wind or rain. Additionally, other dark objects such as water bodies can be misinterpreted as burned areas. In these cases, the use of other regions of the spectrum can help resolve this confusion. Another potential source of error with this method arises where more efficient combustion leaves bright ash residues that merge with the surrounding vegetation.

- The temperature of these areas is higher than that of their surroundings, especially during the day. Detecting burn scars as temperature anomalies is generally done with bands in the thermal infrared. Although this technique is often efficient, some situations, such as temperatures that saturate a sensor making therefore impossible to differentiate signals over a certain intensity threshold, low night temperature difference and cool features in smoke plumes over the fire can result in omission errors (Flasse et al., 2004).

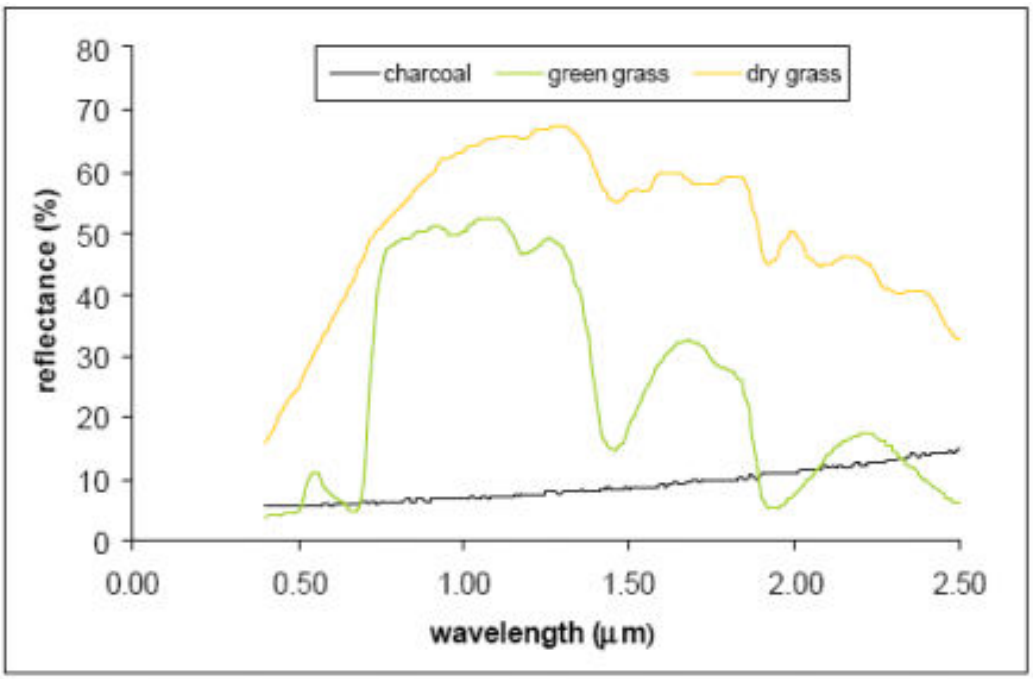

Figure 1.3: Spectral signature of charcoal, green grass and dry grass (Pereira, 2007).

Burn scar data products produced from these three types of signals are useful at all stages of the fire management cycle: They can provide useful baseline data such as fire frequency maps combining maps from different years, seasonal fire maps or fire intensity and severity assessment by means of the date and pattern of the mapped burned areas or from the spectral reflectance of the burned residues. More homogeneous scars normally indicate high fire intensity and occur late in the dry season. The contrary is true for patchy scars.

Frequency maps can also indicate areas where more active fire prevention measures should be implemented and burned area maps can assist the fire suppression teams in planning their activities (e.g. a fire advancing towards a recently burned area may not need instant suppression). These products can also be used for monitoring and evaluation of management activities and ultimately, to refine regional and national fire policy.

As with any application of remote sensing to detect physical features or phenomena, the detection of fire scars is subject to confusion with other sources, such as other land cover types or shadows. The main drawbacks of these methods are:

- Target variability / Spectral separability: The spectral signal of surface darkening due to charcoal deposition immediately following a fire is very specific. However, the later vegetation scar signal is less specific and can be obliterated by agricultural practices or vegetation defoliation by pathogenic agents.

  In the visible spectral region, charcoal can be confused with dense, dark vegetation, water, dark soils, wetlands, cloud and terrain shadows. Some of these confusions may also appear in the SWIR, although in this region the burning of dense, dark vegetation produces an increase in the reflectance. The NIR is doubtlessly the best spectral region to characterize burned areas. The most characteristic fire-induced signal is produced in the NIR-SWIR bi-

plane (with a negative reflectance change in the NIR and a positive change in the SWIR). The best colour composite to visualize burned areas is therefore R-SWIR, G-NIR and B-VIS (Pereira, 2007).

- Signal persistence: Burn scar features are generally short-lived (weeks or sometimes months) due to removal of burned particles by wind or rain. This is especially true for areas where the fuel burned is very thin, such as tropical savannah. In other areas, such as forests, where burning produces larger particles and more biomass burned, the signals persist longer.

- Clouds: One of the limitations of spaceborne optical remote sensing is that clouds and smoke can hide or reduce the visibility of the observed scene. The mean probability of observing clouds in any given remote sensing image is 62% in the Northern Hemisphere and 53% in the Southern Hemisphere. However, fires normally occur in the dry season, when these probabilities are generally lower. A multi-temporal composite can overcome this problem, especially when a thermal channel is available (Pereira, 2007).

- Smoke: Smoke aerosols in the atmosphere are an effective solar scattering and absorbing mechanism that affects surface observations and reduces the spectral differences between different land covers and conditions. A very smoky atmosphere renders the visible range of the EM spectrum unusable for observing burn scars, whereas the SWIR can produce much better observations. In temperate and boreal forests, where the signature of a fire lasts longer, one can wait until the end of the dry-season to avoid this problem. However, in tropical savannahs and temperate grassland, because the short duration of fire signatures, waiting is not an option (Pereira, 2007). Thus, fires remain more frequently undetected with optical sensors.

- Vegetation canopy / understory fires: Surface fires without canopy burning are more common in tropical forests and savannahs. In such cases, canopy radiation interception and shadowing can interfere with the detection of understory fires (Pereira, 2007).

- Target spatial pattern / fragmentation: There is a large global variability in the extent of burning, spatial patterns of fires and fire size distributions. This diversity can often not be captured by the traditionally used low spatial resolution sensors. The most problematic areas are mosaic-burning fires (i.e. fires that cause a patchy burned area pattern), such as in some tropical savannahs, where the probabilities of getting a wrong estimation of total area burned are high (Pereira, 2007).

Few countries have programs to systematically map burned areas. Portugal is an exception, keeping an annual registry of burned area maps derived visually from Landsat (Bastarrika, Chuvieco and Martín, 2011).

Because of the spatial and spectral variety of burned areas, automated classification is difficult. Spectral response can change with different observation conditions, fire severity, time since the fire was extinguished, type of vegetation and soil exposure (Antunes et al., 2014). Most algorithms try to

balance the omission and commission errors and obtain reasonable results at a local scale, but when extrapolated to other sites the omission and commission errors highly differ (Bastarrika, Chuvieco and Martín, 2011).

Expert visual interpretation, often supported by ground truthing, obtains reliable results and is normally used for the validation of other classification algorithms. In many occasions, these results are indeed better than those obtained with any automated method. On the other hand, the former are generally more expensive and time consuming than the latter (Antunes et al., 2014). Other considerations in favour of automated algorithms are practicality, objectivity and repeatability (Bastarrika, Chuvieco and Martín, 2011).

Spectrally, the near and thermal infrared wavelengths can help discern between burned and unburned areas better than the visual wavelengths (Flasse et al., 2004).Bastarrika, Chuvieco and Martín (2011) studied the ability of different combinations of Landsat spectral bands and spectral indices to discern burned areas. The best results were obtained with one visual, one NIR and two SWIR bands, as this combination was more spectrally complete. The most distinctive spectral indices were multitemporal comparisons of BAI and BAIM. NDVI also helped to reduce the confusion with urban areas and other land covers. Other post-fire spectral indices, namely NDVI, GEMI, NBRL, BAI, MIRBI and NBRS, contributed to reduce misclassification errors. A dependency of the results on the acquisition time after the fire and on the ecosystem succession pace was observed.

1.2.3. Integration with other sources of data

One of the more relevant advantages of remote sensing data for fire management is their easy integration with other geolocated data to obtain other more informative thematic products.

In this context, Geographic Information Systems (GIS) software provides a useful platform. Through the simultaneous analysis of different spatially registered layers information such as maps of infrastructure, administrative boundaries, fire history, planned ignition points and maps made on the ground, spatial models can be constructed (Flasse et al., 2004).

1.2.4. Methods

Whatever the study may be, the first step in analysing remote sensing data is pre-processing it. This includes spatial and radiometric corrections and potentially other tasks such as image segmentation, data dimensionality and co-registration of different images in the case of sensor data fusion or temporal analysis.

Only once these necessary pre-processing operations are completed can classification be performed. The target classes can be different kinds of vegetation or other relevant factors for fire risk and damage assessment, active fires or burn scars. Supervised classification is more commonly used than unsupervised. The features normally selected for the classification are the reflectance valuesin the sensed spectral bands andvarious spectral indices. The latter give a clearer physical meaning to the reflectance values. Some classifiers that have been used for cover types classification in fire applications are decision trees (Verhegghen et al., 2016) and supervised maximum likelihood (Saglam et al., 2008). For detection of burned areas, some classifiers that have been applied are supervised Mahalanobis distance with a visual expert post-classification (Antunes et al., 2014),

supervised non-parametric random forest (Roy, 2016), parallelepiped supervised classification (Hudak and Brockett, 2004), non-supervised Isogeg algorithm (Carrielo and Anderson, 2007) and the Jeffries-Matusita distance method (J-M) (Bastarrika, Chuvieco and Martín, 2011).

The classification is normally validated with data obtained from other independent sources. For instance, high spatial resolution *data from other remote sensors* are widely used. Verhegghen et al. (2016) used data from the GeoEye-1 satellite, with a resolution of 0.4 m. In (Antunes et al., 2014), a vegetation map produced by visual interpretation of SPOT images (5 m) is used. SPOT Multispectral data (20 m) is also used as a reference in (Hudak and Brockett, 2004). Other sources of validation data are *field inspection* and *validated data and maps produced by recognised agencies*. For example, forest cover types and burned areas maps, produced by governmental agencies and derived from satellite imagery, field inspection and other methods are used in (Saglam et al., 2008), (Hudak and Brockett, 2004) and (Bastarrika, Chuvieco and Martín, 2011). Finally, *widely validated products* such as the MODIS active fire and burned area products, VIIRS data and other ESA-funded burned area products are also used for validation of automated classification results (Roy, 2016). Commonly the validation is carried out by visual comparison between the sensed data in question and the validation data.

The obtained products are often further processed and analysed in combination with other data to produce more informative and application-oriented products that can potentially assist in a more practical way fire management and related administrative decisions. For example, Antunes et al. (2014) used historical burned area data to calculate the annual burned area and integrated burned area maps with natural vegetation maps in order to assess the impact of fire on the landscape structure in the Brazilian Savannah.

In general, algorithms developed for certain areas obtain reasonable results but cannot be globally generalised. Thus, local algorithms result in much higher fidelity outputs than global ones. To overcome this limitation, Tsela et al. (2014) highlight the apparent importance of designing generalized algorithms that can be adapted locally by local experts through the setting of parameters to better account for local vegetation properties and the spatial and spectral properties of local burned areas.

1.2.5. Earth observation for fire applications

Although there are some free sources of satellite fire data, such as those acquired by the AVHRR sensor, more often than not these data are highly costly, especially if one needs data with better spatial resolution. Lately, the trend is that more organizations are distributing their data online. Such are the cases of the MODIS open data and the commercially available SPOT VEGETATION data. Higher resolution data are still only available for certain users (Flasse et al., 2004).

For **fire risk and damage potential studies**, Landsat, MODIS, SPOT and AVHRR can provide information on fuel moisture and characterization, fire risk and danger and fire frequency. On the local-scale, LiDAR and airborne HS sensors are more suitable and have been widely used to analyse vertical forest structure and estimate crucial parameters for fire behaviour (Saglam et al., 2008).

Many authors have used different sensors and techniques for **burned area mapping**, for which an important part of the existing research has been done using Landsat. Other sensors with lower

spatial but higher temporal resolution have been also employed, such as MODIS, SPOT-VEGETATION, AVHRR, ATSR-2 and GOES, although they fail to discern small and patchy burned areas. For these situations finer resolution sensors obtain better results.

(Bastarrika, Chuvieco and Martín, 2011) proposes a 2-step algorithm of global applicability to reduce at the same time omission and commission errors in burned area mapping using Landsat images.

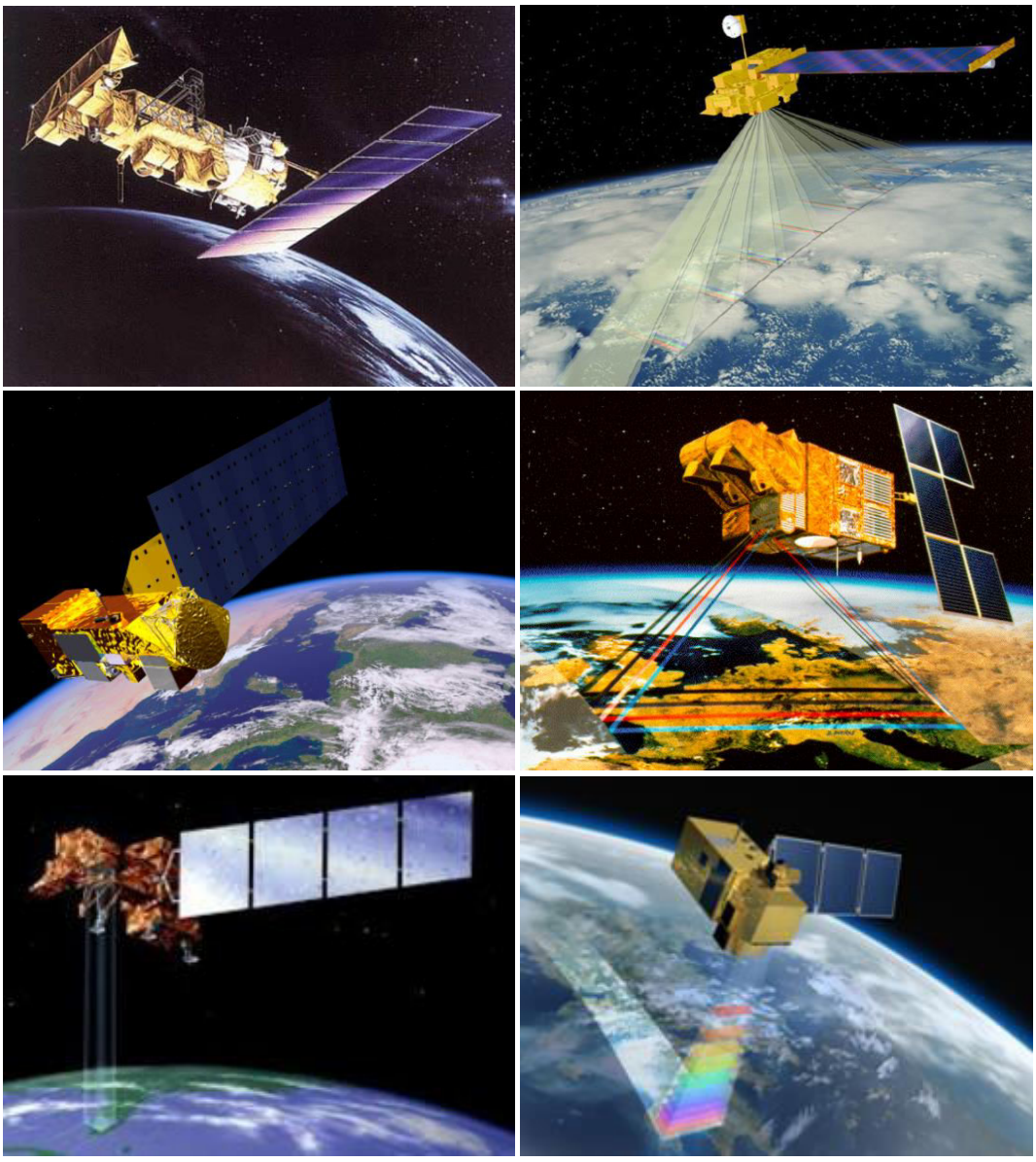

Figure 1.4: Instruments traditionally used for fire managament. From the top left corner they are, from the top to the bottom and for left to right: AVHRR on-board NOAA (NASA, n.d.a); Terra (Vassili Group, n.d.) and Aqua (Stöckli, n.d.), both carrying MODIS; SPOT-4 with the VEGETATION sensor (VITO NV, 2010), Lansat-7 (Irons, Taylor and Rocchio, 2017) and Sentinel-2A (Helen, 2017).

MODIS produces two different 500-m burned area products: MCD45A1 from the 500-m MODIS cloud-free surface reflectance time series data using a predictive bidirectional reflectance modelling approach. Both products are widely validated and in some instances used as validation data to assess the accuracy of the algorithms developed for other satellites' sensors. MCD64A1 makes use of the active-fire based burned area mapping algorithm and applies it to the 500-m MODIS cloud-free surface reflectance images. Because this later product uses active fire training data, it may not fully

represent small or fragmented burned areas, giving rise to omission errors. MCD45A1 does not use training data and relies only on the surface change of reflectance and a statistical wavelength threshold for burned area mapping (Tsela et al., 2014).

Tsela et al. (2014) have evaluated the performance of these two products and that of a combined burned area product derived particularly for that study for six different ecosystems in South Africa. The validation is done with reference to 30-m Landsat 5 Thematic Mapper (TM) data and to national vegetation and land cover maps. The sites covered are the most fire prone biomes that normally burn every year: savannah (Southern Kruger National Park and Thabazimbi), grassland (Middelburg and Free State), fynbos (Western Cape) and pine forest (Sabie). The results were different for the different sites but the general trend was that the merged product produced better results and fires smaller than a pixel can produce commission errors in the MCD64A1 product.

Because of its spectral, spatial and temporal characteristics, Landsat is appropriate to map burn scars: Landsat 1, 2 and 3 carried the Multispectral Scanner (MSS) sensor, with 4 bands and 57 to 80 m spatial resolution. The Thematic Sensor (TM) on board the Landsat 4 and 5 and Enhanced TM plus (ETM+) on board Landsat 7 have 6 bands with 25 to 30 m resolution (Hudak and Brockett, 2004). Landsat 8, launched in 2013, added two sensors to the Landsat collection, OLI and THIRST. The Operational Land Imager (OLI) has nine bands, comprising the six bands in ETM+ and also a New Deep Blue band and another SWIR band, both with a 30 m resolution the and a 15 m resolution PAN band. The sensor THIRST observes in the thermal infrared. Since the launch of Landsat 1 in 1973, the Landsat series has produced more than 40 years of Earth observation historical data (Fuchs et al., 2015).

Landsat ETM+ data is used in (Carrielo and Anderson, 2007) to assess the BAI index suitability for the study the forest fires dates in the Mato Grosso state, in the Brazilian Amazon. Only the red and infrared bands were used. The index was proven to improve the detection rate of recent scars when compared to data acquired in an independent spectral band while also avoiding false positives such as in the case of rivers (Carrielo and Anderson, 2007).

Hudak and Brocket (2004) provide another example of the use of Landsat imagery to map fire scars. In this work, the region under observation was the Madikwe Game Reserve in South Africa and its bordering areas in Botswana and South Africa.

Landsat TM and ETM+ images were also used to classify and map the main factors affecting the fire risk and damage potential in North Western Turkey (Saglam et al., 2008).

In (Antunes et al., 2014), Landsat TM data are used to obtain fire distribution information for wildfire management in the Cerrado, which is the second largest Brazilian biome and the savannah with the highest biodiversity in the world.

As for **active fires** the use of SPOT and Landsat data for operational applications is limited because of their cost, low temporal resolution and centralized receiving stations. On the other hand, Meteosat and NOAA high temporal resolution (30 minutes and 12 hours, respectively) together with their free-of-charge data broadcast policy allows local acquisition, analysis in-situ and fast distribution of fire information (Flasse et al., 2004).

In 1999 a NOAA-based fire early system was developed for field-level prevention, detection and control of vegetation fires in Sumatra (Anderson and Imandaad, 1999).

The sensor on-board the NOAA satellites is the Advanced Very High Resolution Radiometer (AVHRR), an across-track scanning system with five spectral bands, a spatial resolution of 1.1 km and that scans the Earth twice a day (Department of Commerce of the United States of America, n.d).

This sensor has in fact been commonly used for fire management. One of the most recurrent applications, with many operational algorithms developed by diverse authors, is the detection of active fires. An example of that is the DLR project Timeline, aiming at processing thirty years of AVHRR historical data over Europe into L1b, L2 and L3 products and offering them online through a free and open data policy. For validation, this projects uses the internationally recognised and widely validated MODIS active fire product (Fuchs et al., 2015).

The main drawback of the AVHRR sensor for the application of active fire detection is the low saturation threshold of the middle-infrared channel 3, which can be caused not only by the high temperature of a fire but also by highly reflective bare soils and sunglint. Its low spatial resolution and the high distortion at the image borders (2.5 km x 7 km) due to a wide scan angle (+/- 55º) also limit the applicability of the sensor (Fuchs et al., 2015).

Pereira (2007) presents a general review of spaceborne fire remote sensing based on the data obtained with NOAA / AVHRR, SPOT-Vegetation, ERS-2/ASTR, ENVISAT/AATSR and Meteosat, with spatial resolution of 1 to 5 km.

More recently, ESA's Sentinel satellites, in the frame of the Copernicus Earth observation program, have introduced new promising capabilities for fire monitoring. The series will comprise six missions, out of which four have already been launched. Sentinel-1 (S1), composed of two satellites, is a radar mission for land and ocean applications. Sentinel-2 (S2), also comprising two satellites in orbit, is a multispectral high resolution mission for land applications and that can also serve for emergency response. Sentinel-3, with currently only the satellite Sentinel-3A operative, is a multi-instrument mission that has, among others, the SLSTR instrument with bands optimized for fire monitoring. Finally, the Sentinel-5 Precursor, or Sentinel-5P, was launched in October 2017 and is the forerunner of Sentinel-5, that will study air quality and climate change (ESA, n.d.a and n.d.b).

The low spatial (300 m - 1 km) but high temporal (daily revisit cycle) MODIS, AVHRR, VEGETATION and MERIS sensors are broadly used to monitor wildfires at a global scale. However, their limited spatial resolution results in underestimations in the case of small burned areas. It also makes difficult the precise identification of the vegetation in the burned areas. Therefore, fusion of these data with those obtained from finer spatial but lower temporal resolution satellites, such as Landsat, ASTER or RapidEye, as well as with radar data able to overcome any weather condition and the frequent cloud coverage in tropical evergreen forests can give better and more complete results (Verhegghen et al., 2016).

Roy (2016) proposes a prototype of a global burned area product combining NASA-USGS' Landsat-8 and ESA's S2 data. The main motivations for this combination is an improved quantization and signal/noise characteristics of Landsat-8, the longer historical coverage of Landsat and the higher temporal resolution of S2.

Verhegghen et al. (2016) assessesthe ability of a combination between the Sentinel 1 and 2 for mapping of burned areas in the Congo Basin forests after the outbreak of fires produced by the 2015-2016 el Niño Year, and other tropical forests.

A first detection of active fires is done by MODIS and later S1 and S2 images are used to map the location, extent and spreading speed of the fire. Maps of burned areas at 20-25 m spatial and 10 day temporal resolution were produced, with only a 63% spatial coherence between the maps obtained with the two satellites. While S2 does not observe some areas because of clouds, S1 only senses a smaller extent of the burned areas, due to a conservative threshold defined to avoid confusion with vegetation water content. S2 detects changes in the surface reflectance while S1 detects changes in vegetation structure and moisture, thus probably only detecting the most severe fires that produce more dramatic changes in the vegetation. All in all, the simultaneous use of both sensors achieved a higher detection rate for burned areas (Verhegghen et al., 2016).

1.3. Existing services

1.3.1. The European Forest Fires Information System (EFFIS)

The European Forest Fires Information System (EFFIS) originated in 1998. It is supported by the Expert Group on Forest Fires, registered under the Secretariat General of the European Commission and formed by experts from 40 countries in Europe, Middle East and North Africa. Since 2015, EFFIS has been part of the Emergency Management Services of the EU Copernicus programme.

EFFIS provides services such as fire danger forecasting, active fire detection and fire damage assessment. The fire danger forecast is derived from meteorological information from different sources, with a spatial resolution up to 10 km. Information about active fires and burnt areas for rapid damage assessment is obtained from MODIS (250 m spatial resolution, updated daily). Higher spatial resolution satellites, including Landsat and Sentinel, are used for a finer fire damage assessment after the fire season.

Although EFFIS focuses on Europe and the Mediterranean Basin, it also contributes to the Global Wildfire Information System (GWIS), a service expanded to the whole world (European Commission, n.d.a). GWIS is a cooperative initiative of the GEO and Copernicus Programs. Its main goal is to serve as a platform to put together different existing fire information sources, both at regional and national level, in order to provide a comprehensive and complete view and evaluation tool for global fire monitoring. It is framed in the activities of EFFIS, the Global Terrestrial Observing System (GTOS) Global Observation of Forest Cover- Global Observation of Land Dynamics (GOFC-GOLD) Fire Implementation Team (GOFC Fire IT), and their associated Regional Networks. The development of GWIS is supported by diverse partner organizations and space agencies, including NASA through its ROSES program (European Commission, n.d.b).

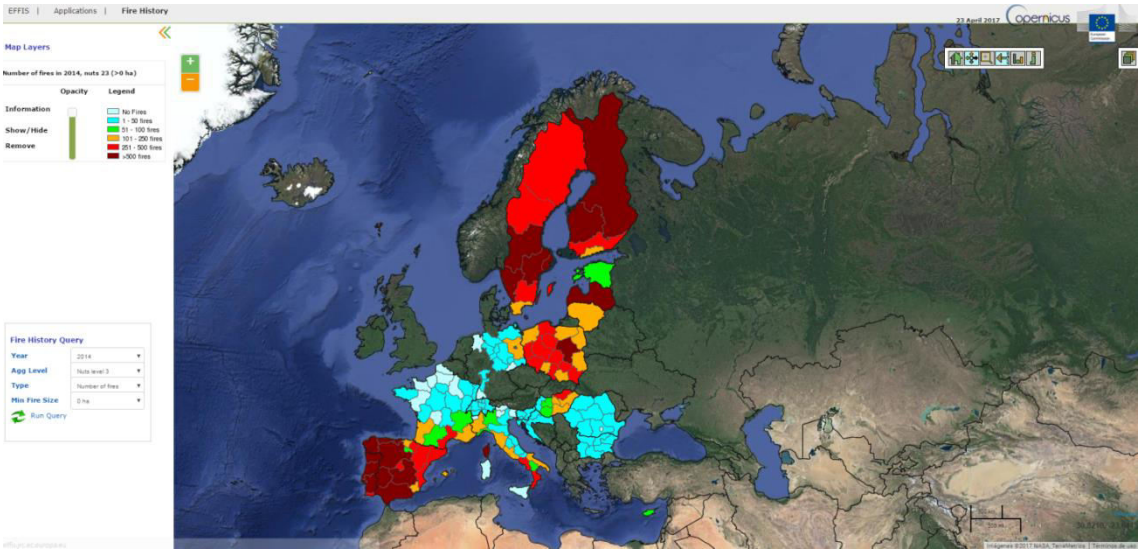

Figure 1.5: Number of fires in the 2014 fire season recorded in the European Fire Database from EFFIS web interface (European Commission, n.d.a) .

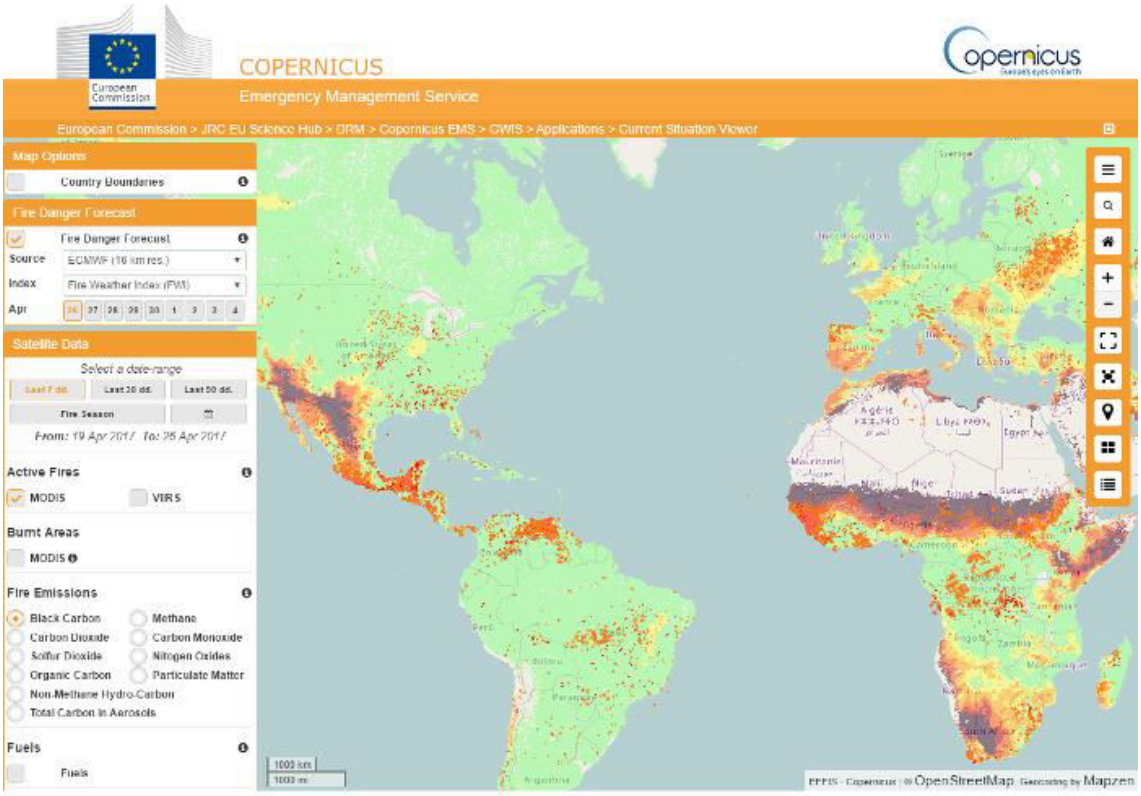

Figures1.6: Diplay of the GWIS viewer (European Commission, n.d.b).

1.3.2. The Advanced Fire Information System (AFIS)

The Advanced Fire Information System (AFIS) is a satellite-based global fire information tool developed by the South African Council for Scientific and Industrial Research (CSIR). It provides fire managers near-real time information worldwide. It provides a unique tool to distribute information about fire risk close to some critical sites such as critical infrastructure, property, electrical power transmission grids or forest plantations. Based on Earth observation satellites, weather forecast

models and Information and Communication Technologies, it offers fire prediction, detection, monitoring, alerting, planning and reporting services and products.

The products provided by AFIS are: Active fire detection based on GEO (MSG/GOES) and LEO (VIIRS/MODIS) satellites data, fire danger rating, four-day fire danger predictions based on the Canadian Fire Weather Forecast Index or any other user-defined model. The weather forecast data is obtained from the European Centre for Medium-range Weather Forecasting (ECMWF). Additionally, it also offers burned area products by fusion of the MODIS MCD45 and MCD64 products and Landsat fire products (AFIS, n.d.).

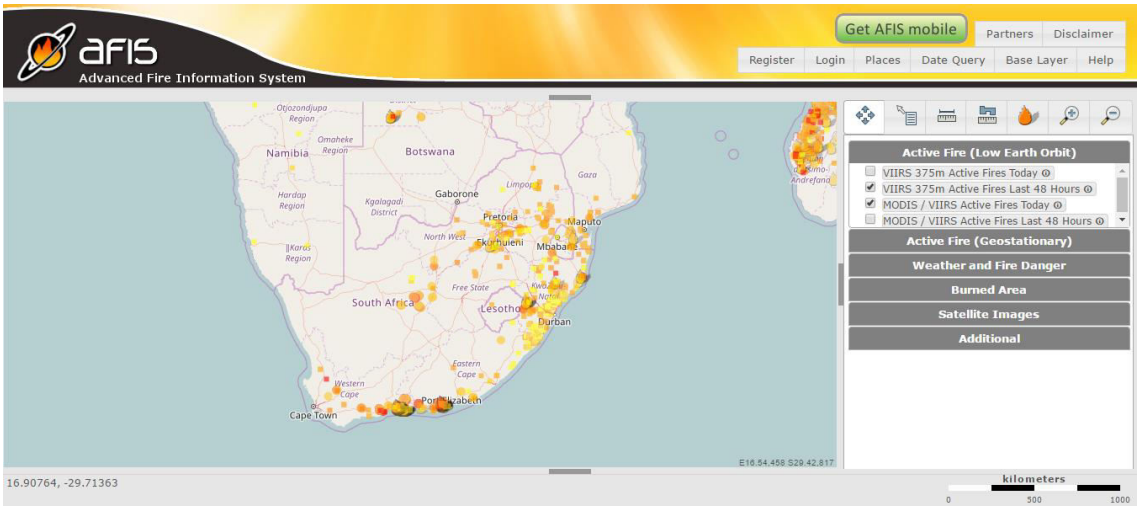

Figure 1.7: AFIS viewer in Southern Africa as for the 8th of June 2017 (AFIS, 2017).

1.3.3. Project Pharos

There are other fire information platforms around the globe. One of them is the Project Pharos by the German DLR, still under development. It is a software mediation platform to support decision making. It will integrate data from EO satellites and in-situ sensors, process it and provide the results to a series of key services for disaster management in its different phases, such as risk and threat simulation tools, decision support services and public alert systems. The implementation core elements are: Decision Support Services (DSS), Simulation and Modelling Services (SMS), Alert Gateway, Processors and services (Fuchs et al., 2015).

Fire hotspot detection will be done with MODIS and the meteorological Meteosat Second Generation (MSG) satellite data. For the recovery, mitigation and preparation phase: high-resolution images will be used (<30 m or <2.5 m) to produce thematic products (burn scars) and maps. The service will be provided with a temporal resolution better than one day.

The products will be created manually on demand with expert knowledge. The data will be provided by the Copernicus Space Component (CSC) - Data Access and through DLR science service data access (TerraSAR- X and FireBIRD missions). The dataset for the application area will be provided by Landsat 7 and 8, FireBIRD, Spot 5, 6 and 7, WorldView 2 and 3, TerraSAR-X and potentially Sentinel 1 and 2. Thus, Pharos will include a wide range of images with different spectral, spatial and temporal resolutions that will facilitate capturing data in all the possible circumstances.

Remote sensing data will be combined with other layers of data to produce thematic maps. E.g. the affected population will be derived from the combination of population layers and burn scar maps. The produced thematic maps will be: Geographic Reference Map, Fire Extent Map, Damage Assessment Map, and Fire Monitoring Map. For the fire hotspots, drawing data from EFFIS is being considered. The thematic layers and maps will potentially be produced by DLR ZKI Service as well as Copernicus EMS Services (Fuchs et al., 2015).

1.4. Dedicated Earth Observation satellites for fire management applications: FireBIRD

It is worth noting that most of the remote sensing products for fire management are derived from imagery taken by "multi-purpose" satellites, i.e. Earth Observation satellites from whose data different types of information, including fire-related information, can be extracted.

However, there are also some sensors for which fire applications served as a design driver. This is the case, for example, of Sentinel 3 SLSTR that incorporates bands optimized for fire detection.

A satellite especially conceived for fire applications is DLR's FireBIRD, an infrared remote sensing mission. It comprises two satellites, namely TET-1 and BIROS, based on the DLR's Bispectral and Infrared Remote Sensing Detection (BIRD) satellite and its IR sensor. FireBIRD is a scientific mission with the objective of detecting fires as hot temperature anomalies with the IR sensors, as well as identifying thermal patterns for other ecological processes. Because of its research nature, the ultimate goal of the mission is to provide data for scientific research and semi-operational use to a wide group of users (Lorenz et al., 2015).

Figure 1.8: Satellites in the FireBIRD mission: TET-1 and BIROS (Halle and Terzibaschian, n.d.).

FireBIRD has a spatial resolution of 165 m and a revisit period of less than 5 days, which means a higher spatial but lower temporal resolution than MODIS and Sentinel 3 SLSTR and a lower spatial

but higher temporal resolution than the TIRS sensor on-board the Landsat Continuity Mission. Thus, FireBIRD can cover a unique window of observation opportunities (Klein at al., 2013).

Active fire detection and information is performed on board by implementing the Bi-Spectral Method. In this way, the data to be downloaded is reduced to a list of detected high-temperature events containing the parameters analysed. This reduces considerably the on-board memory and downlink requirements.

On-board the two satellites there are two infrared cameras and a multispectral pushbroom sensor with four channels: green, red, NIR and TIR. The spatial resolution is 39 m for the visual and NIR channels and 165 m for the TIR; the swath is 202 km and 167 km, respectively. With the two satellites in orbit, a revisit period of 3.5 days should be achieved. Furthermore, an off-nadir tilt of up to 30° enables imaging the same area on consecutive days. The on-board storage and downlink rate limit the amount of images that can be captured per day. To free the on-board memory and be able to take more images, additional downlink-only ground stations are considered.

In addition to level 1b and 1c products (refer to Table 1.4), other products containing fire-related information are available to download as text files and kml files. They comprise the fire location, fire radiative power (FRP) and for fires with a FRP greater than 20 MW fire line length, also optionally the fire temperature and burned area of fire.

MODIS active fire products commonly used for fire monitoring have 1 km resolution. FireBIRD aims to provide a high spatial resolution compliment to these fire products and others of coarse resolution such as Suomi NPP VIIRS and Joint Polar Orbiting Satellite System (JPSS). TET-1 and BIROS are intended to be the precursors for a Fire Monitoring Constellation (FMC).

All the data will be archived centrally and, once processed, distributed to the users via FTP. Any data will be also accessible later on the EOWEB catalogue of DFD. The data received in the network of additional downlink-only ground stations will be sent to the central archive. Observations may be requested through a proposal process. The acquisition planning will be only carried out by the FireBIRD project principle investigator and the science coordinator.

Due to the scientific nature of the mission, the data will be open and free. Although in principle FireBIRD has also a commercial potential, the small coverage and low downlink rate will not allow a large-scale monitoring, for which a constellation would be necessary. However, the open and free data policy will promote the use of FireBIRD and prove its usability for other applications (Lorenz et al., 2015).

1.5. Hyperspectral satellite missions

Hyperspectral sensors can sense light in hundreds of narrow contiguous wavebands spanning a wide range of wavelengths from ultraviolet to longwave infrared (though usually not the entire range in a single sensor). Thus, they capture much more information about the sensed objects and are a useful tool to differentiate them.

The image data are often represented as a hyperspectral image cube, in which the horizontal layers depict the obtained image (spatial data) in the different wavelengths of the spectrum (spectral data). Thus, each pixel generates a different spectrum, as shown in Figure 1.9 (Varshneyand Arora, 2004).

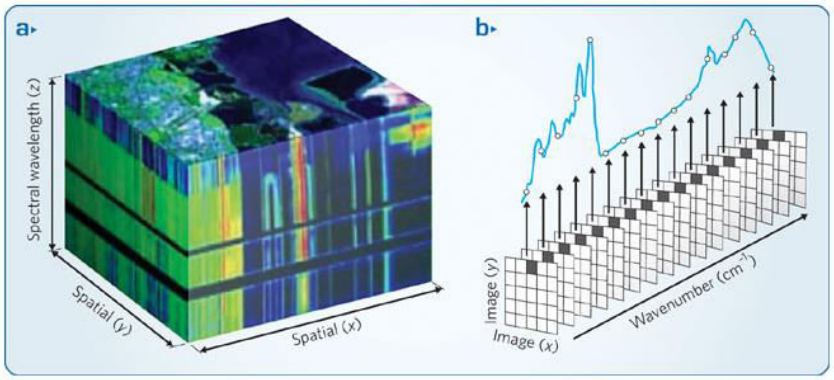

Figure 1.9: Hyperspectral imaging (Bannon, 2009).

Hyperspectral remote sensing offers numerous advantages for a wide variety of applications, including precision agriculture, biotechnology, environmental monitoring, food security and monitoring and security and defence. However, the large amount of data requires high on-board storage capacity and powerful communication links to transmit it to the ground.

Figure 1.10 shows in a graphic way the difference between visual, multispectral and hyperspectral sensors.

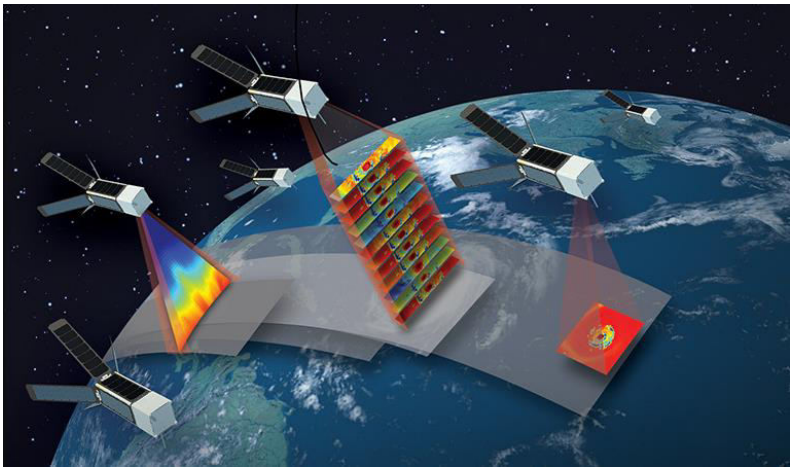

Figure 1.10: Visual, multispectral and hyperspectral sensors (NASA, n.d.b)

However, despite the numerous advantages that hyperspectral sensors have, only a small number of them have been put in orbit in Earth observation missions. The first one, in the year 2000, was Hyperion on-board the satellite EO-1. Since then, these missions have always been reserved for larger satellites, with cameras normally weighting 100 kg or more (ESA, 2018). Table 1.2 shows the hyperspectral sensors that have been launched into space since EO-1 and the missions that are planned to be launched in the near future. As far as the author of this work is aware, the table covers all the existing satellites with hyperspectral sensors previously launched and/or still in orbit at the time of this writing.

Table 1.2: Spaceborne hyperspectral sensors for Earth observation. The data compiled in this table was extracted from the eoPortal website, with the following exceptions: [1] (Zhang et al., 2014), [2] (Enmap, n.d.), [3] (Matsunaga et al., 2011) and [4] (NASA, 2017) and (Hochberg et al., 2015).

Mission name	Operator	HS Instrument	Launch	Mission status as of February 2018	Orbit	Spacecraft		Instrument			
						Dimensions	Mass	No. bands	Spectral range [µm]	Spectral resolution [nm]	Spatial resolution[m]
EO – 1	NASA	Hyperion	2000	End-of-life: 2017 Expected re-entry: 2056	Sun-synch. circular polar orbit, H = 705 km, i = 98.7º, T = 99 min, LTDN = 10:15	Hexagonal 1.25 m diameter 0.73 m high	Launch mass: 588 kg Dry mass: 410 kg	220	0.4 – 2.5 0.4 - 1 (VNIR); 0.9 – 2.5 (SWIR)	0.1	30
MightySat II	Air Force Research Laboratory	FTHSI	2000	Reentered 2002	Sun-synch. circular orbit, H = 556 km, i = 97.3º, T = 95.5 min LTDN = 11:15	68.6 cm x 89 cm x 89 cm	Launch mass: 123.7 kg Payload mass: 37 kg	256	0.4 – 2.5	1.7 nm @ 450 nm	28 x 30
PROBA – 1	ESA	CHRIS	2001	Operational	Sun-synch. elliptical polar orbit, perigee= 542 km, apogee=657 km (mean altitude of 615 km), i = 97.9º, T = 96.97 min, LTDN = 10:30	60 cm x 60cm x 60 cm	Launch mass: 94 kg	18 (17m GSD) 61 (34m GSD)	0.41 - 1.05	1.3-11.3 nm	17m at 560km
Huan Jing-1 (HJ-1: Environmental Protection & Disaster Monitoring Constellation)	China Centre for Resources Satellite Data and Application (CRESDA)	HSI (on-board HJ-1A)	HJ-1A and HJ-1B in 2008	Operational	Sun-synch. circular orbit, H = 650 km, i = 97.95º, T = 97.4 min LTDN = 10:45	1.2 m x 1.1 m x 1.03 m	Launch mass: 470 kg	110-128	0.45 - 0.95	n.d.	100

IMS-1 (Indian Microsatellite-1)	ISRO	HySI	2008	Planned mission life of 2 years	Sun-synch. near-circular orbit, H = 635 km, i = 97.94º, T = 97.4 min, LTDN = 9:30	0.6 m x 0.98 m x 1.13 m	Launch mass: 83 kg	64	0.4 - 0.95	< 15 nm	550 m
TacSat 3 (Military)	Air Force Research Laboratory	ARTEMIS	2009	Re-entry: 2012	Near-circular LEO, H = 420 km × 449 km, i =40.4º, T = 93.6 min	n.d.	Launch mass: < 400 kg	400 +	0.4 - 2.5	5 nm	n.d.
Tiangong-1 Space Lab (manned)	China	HSI	2011	Unexpected end-of-life: 2016 Expected re-entry: March 2018	Near circular orbit, H = 380-400 km, T ~ 92 min i = 42.77º	10.4 m in length and 3.35 m in diameter	Orbital mass: 8506 kg	64 64	0.4 – 1 1 – 2.5	10 nm 23 nm	10
YouthSat / IMS-1A	ISRO and Roskosmos	LiVHySI	2011	Planned mission life of 2 years	Sun-synch. near-circular orbit, H = 822 km, i = 98.78º, T = 101.35 min, LTDN: 10:30	0.6 m x 0.98 m x 1.13 m	Launch mass: 92.8 kg	n.d.	0.450 – 0.950	8 nm	4 km (To study the atmosphere)
STSat - 3	KARI (Korea Aerospace Research Institute)	COMIS	2013	End-of-life in 2015	Sun-synch. near-circular orbit, H = 600 km, T = 96.4 min i = 97.8º, LTDN = 10:30	1.02 m x 1.03 m x0.88 m	~ 175 kg	64	0.4 - 1.05	2~15 nm	30 / 60 (selectable by command)
GomX-4B	ESA	HyperScout	2018	Operational	Sun synch. circular orbit, H = 500 km, i = 97.32º, T = 94.6 min, LTDN: 14:00	20 cm x 30 cm x 10 cm	~ 8 kg	45	0.4 - 1	12 nm	40 m

China Commercial Remote-sensing Satellite System - A (CCRSS - A) [1]	China	CCRSS – A HRS	n.d. Scheduled for 2016 – No more information available online	n.d.	n.d.	1.02 m x 0.98 m x 0.55 m	147 kg	328	0.4-2.5	n.d.	30
PRISMA	Italian Space Agency ASI	PRISMA	Scheduled for 2018	Planned	Sun-synch. circular, H = 615 km, i = 97.85°, T = 96.6 min, LTDN = 10:30	1.7 m x 1.5 m x 3.4 m	Launch mass: < 550 kg	~ 250 bands	0.4 -2.5	12 nm	30
EnMAP [2]	DLR	HSI	Scheduled for 2019	Planned	Sun - synch. circular, H = 652 km, i = 97.98°, T = 97.57 min LTDN ~ 11:00	3.1 m × 2 m x 1.7 m	Launch: 936 kg (55 kg hydrazine)	244	0.42–2.45	6.5 nm (VNIR), 10 nm (SWIR)	30
ALOS – 3 [3]	JAXA	HISUI HS	≥2019	Planned	Sun - synch. Circular, H = 618 km, i = 97.9°, T = 97 min LTDN = 10:30	n.d.	n.d.	185 (VNIR:57 SWIR:128)	0.4 - 2.5	10 nm (VNIR), 12.5 nm (SWIR)	30
HyspIRI [4]	NASA	VSWIR	n.d.	Planned	n.d.	n.d.	n.d.	212	0.38–2.5	10 nm	30
Sentinel – 10	ESA	n.d.	2028	Planned	n.d.	n.d.	n.d.	n.d.	n.d.	n.d.	n.d.

From Table 1.2 we are able to make the following observations:

- To date, only nine hyperspectral missions have been launched into space and only two are still operational, namely, PROBA-1 and Huan Jing-1. The most remarkable and widely known sensors are NASA's Hyperion and ESA's CHRIS. All of these missions are quite heavy; PROBA-1 the lightest one, weighs in at 96 kg.
- Among the launched missions, two are from the Air Force Research Laboratory. This is consistent with the faster technology development in the military.
- China, Korea and India have all launched research satellites with hyperspectral imagers.
- NASA, ESA and JAXA, three of the biggest space players worldwide, have plans for hyperspectral satellite missions.
- The spatial resolution of the spaceborne hyperspectral sensors is surprisingly good, with an apparent ground resolution of 30 m for many of them.
- As expected, and in accordance with the general trend of Earth observation missions, most of the missions listed in Table 1.2 are in, or intended for, a Sun-synchronous circular polar orbit.
- However, it can be observed that the number of hyperspectral missions compared with the overall number of Earth observation missions developed since 2000 is quite low. Generally, missions selecting certain wavelengths or focused in a specific region of the spectrum for a given application have been preferred. Nevertheless, for classification with Machine Learning algorithms, probably increasing the number of wavelengths and thus the number of features produces better results, as a continuum spectrum is more representative of an object.

1.6. Earth observation data products formats

1.6.1. New paradigms: Analysis-Ready Data and the CEOS Data Cube

The increase in the data volumes produced by Earth Observation missions has raised interest among the different CEOS member agencies and other players in developing new approaches to handle these data with a view to offering information more closely directed to meet end-user requirements. These efforts have led to the Analysis Ready Data (ARD) strategy of USGS (which will drive its entire Landsat ground segment design in future) and Future Data Architectures, such as the CEOS Data Cube concept.

The Data Cube concept was first successfully developed by Geoscience Australia and the Australian Space Agency (CSIRO). It basically consists of a multi-dimensional (space, time, data layers) data composition in which the data are organised temporally and spatially. This can be used in a diverse number of applications, making the analysis and interpretation easier to the final-users of the data (Killough, 2015).

Analysis-Ready Data (ARD) are data already processed and organized by Space Agencies or other parties in order to give the users data ready to use without the need of traditional time-consuming image preparation. It incorporates corrections for instrument calibration (gains, offsets), geolocation (spatial alignment) and radiometry (solar illumination, incidence angle, topography, atmospheric

interference). Additionally, these data have a defined structure with auxiliary metadata, quality flags and products. The CEOS organization is promoting the use of ARD in its Data Cube infrastructure.

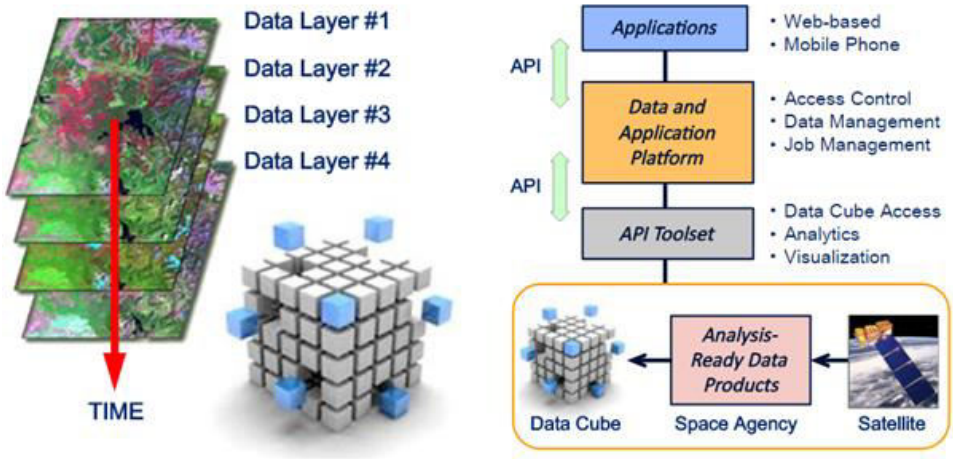

Figure 1.11: Data Cube concept and general architecture (Killough, 2015).

Examples of this kind of data are the Landsat Surface Reflectance (SR) and the ALOS Annual Mosaic product. The former consists of geolocated and calibrated surface reflectance together with quality indicators, land classification and cloud masks. The latter includes geolocation and backscatter corrections (topography and incidence angle), and associated metadada (Australian Geoscience, 2015).

1.6.2. Standard data processing levels

The Committee on Earth Observation Satellites (CEOS) defines the data processing levels for Earth observation data shown in Table 1.3. Sublevel definition is however less standardized and varies according to the specific mission. For example, the products available for the users in the FireBIRD mission are described in Table 1.4.

Table 1.3: Data level definition by CEOS (Hagolle, 2014).

Data Level	CEOS Definition
Level 0	Reconstructed unprocessed instrument data at full space &time resolution with all available supplemental information to be used in subsequent processing (e.g., ephemeris, health and safety) appended.
Level 1	Unpacked, reformatted level 0 data, with all supplemental information to be used in subsequent processing appended. Optional radiometric and geometric correction applied to produce parameters in physical units. Data generally presented as full time/space resolution. A wide variety of sub level products are possible.
Level 2	Retrieved environmental variables (e.g., ocean wave height, soil moisture, ice concentration) at the same resolution and location as the level 1 source data.
Level 3	Data or retrieved environmental variables which have been spatially and/or temporally re-sampled (i.e., derived from level 1 or 2 products). Such re-sampling may include averaging and compositing.
Level 4	Model output or results from analyses of lower level data (i.e., variables that are not directly measured by the instruments, but are derived from these measurements).

Table 1.4: FireBIRD data products, according to ESA (Klein et al., 2013).

Data level	Description
Level-0 (Archive Data)	Raw data after restoration of the chronological data sequence for the instruments operating in observation mode, at full space/time resolution with all supplementary information to be used in subsequent processing appended. Data are time-tagged. - One image file per band - Two auxiliary files (black body baffle calibration measurements) - Data of GPS, star tracker sensors, control moment gyros, Sun vector - Quick look and archive metadata - On-Board Fire parameters
Level-1B	Level 0 data not re-sampled, quality-controlled (saturation mask) and radiometrically calibrated, spectrally characterized, geometrically characterized - bands are coregistered - annotated with satellite position and pointing and preliminary pixel classification (cloud mask). The Level 1 product consists of Top of Atmosphere (TOA) radiance ($W/m^2 \cdot sr \cdot \mu m$). - File format is HDF5.
Level-1C	Level 1 data ortho rectified, re-sampled to a specified grid. Image re-sampling is performed using a selectable re-sampling method including bi-cubic, bi-linear and nearest neighbour. - File format is HDF5.
Level-2B	Contains the Fire products: location (Latidute /Longitude), Fire Radiative Power (FRP) and optional for fires with a FRP greater than 20 MW fire line length, fire temperature and burned area. - File format is a text-file and KML

1.7. CubeSats

1.7.1. The CubeSat standard

In 1999, the California Polytechnic State University at San Luis Obispo and the Stanford University's Space Systems Development Lab created the CubeSat standard. Although in principle their objective was to offer students access to space, the standard was quickly adopted by hundreds of organizations all around the world. This includes not only universities and other educational institutions, but also private companies and government organizations.

The main reason for the global adoption to this standard is that it facilitates frequent and affordable access to space, made possible by a wide spectrum of launch opportunities (California Polytechnic Institute of Technology, n.d.).

1.7.2. Launch opportunities for CubeSats

The launch cost is usually the most expensive element in a CubeSat project. Many of the current CubeSat launches are done on converted Russian rockets by companies such as Eurokot or Kosmotras. Currently, the launch cost on Kosmotras is about US$50 000 per single cube (1U). CubeSats can also be launched as a secondary payload on larger rockets, with a cost in the range of

(US$2.7K - US$12K)/Kg. NASA's CubeSat Launch Initiative offers universities and schools a free launch opportunity on board rockets that are going to be launched (Madry, 2016).

Additionally, there are some launch opportunities developed specifically for CubeSats:

- The Japanese ISS module has an airlock that can be used to launch CubeSats. The cost of this service is not published.
- Nanoracks also launches from the ISS, with a price of US$85000 per cube.
- Sherpa Containerized, by Spaceflight Industries, offer launch to LEO for 3U - 12U CubeSats at a cost of US$295 – US$995 (Madry, 2016).

Other organizations, such as Cal Poly, Innovative Solutions in Space (ISIS), Spaceflight Industries, Inc., TriSept Corporation and Tyvak offer a spectrum of launch procurement and support services (California Polytechnic Institute of Technology, n.d.).

1.7.3. Component providers

Since the creation of the CubeSat concept, many entities have joined the CubeSat "revolution". This has had a profound impact on the space industry and the conception of many missions worldwide. Since the appearance of the concept, the number of space entities has increased significantly. In view of this new market niche, many companies have been established or have re-adapted their product offerings to develop CubeSat components for all these new nanosatellite missions.

The website www.cubesatshop.com acts as intermediate distributor and gathers CubeSat products from different companies. Namely, AMR Propulsion Innovations, CrystalSpace, CubeSpace, DHV Technology, Ecuadorian Space Agency, EyasSat, HEAD HCT, IQ Wireless, ISIS, Kubos, Lens R&D, Maryland Aerospace Inc., Microspace, NewSpace, Pumpkin, RUAG, SCS Space, SolarMEMS, Soleniz, Theia Space, Thoth and TY-Space.

It is important to note how this new way of developing a satellite mission constitutes a total disruption in the space industry.

1.8. Where CubeSats, hyperspectral sensors and on-board processing meet: NASA and ESA projects

The usual size of hyperspectral sensors and the vast amount of information to be downloaded normally restrict this capability to large satellites and high-performance ground stations. Highly skilled image processing experts are also needed to process the images in order to extract useful information products for end users. All these requirements limit the reach of the technology to a reduced number of users.

Hyperspectral CubeSat missions can change this paradigm. However, the low on-board storage, power and downlink capabilities of CubeSats are important limiting factors. On-board data processing holds out the hope of overcoming these limitations. In this section, two missions by ESA and NASA that incorporate on-board processing capability are presented.

In November 2000, **NASA's Earth Observing 1 (EO-1)** satellite was launched as part of the NASA New Millennium Program, a project dedicated to validating new revolutionary technologies that would be used in the future space missions. Its main payload was the Advanced Land Imager (ALI), which

aimed to produce the same multispectral data than Landsat 7 with a higher signal-to-noise ratio, better spatial performance and at a lower cost. One of the ten new millennium technologies aboard the satellite that comprise the ALI is the hyperspectral camera Hyperion (Perry, 2001).

Since 2003, the Autonomous Sciencecraft Experiment (ASE) has operated on-board EO-1. ASE is autonomous decision-making software able to process and analyse EO images through machine learning and pattern recognition techniques. This allows for intelligent downlink of only selected data and autonomous retargeting to increase the science return (NASA, 2005).

Figure 1.12 shows the procedure for automated on-board image analysis by EO-1. It has three steps:

1. Pre-processing: The image is reduced to a subset of 11-bands to adapt it to the computational power on-board EO-1.
2. Superpixel segmentation: Spectrally-homogeneous contiguous areas in the image are grouped for a new representation. This improves noise while reducing the data set size by a factor of ~100.
3. Endmember detection: Identification of endmembers through numerical methods and automatic feature detection. A summary product of 50KB can then be delivered within 6 hours of acquisition. Alternatively, the entire hyperspectral image is transmitted in about 5 days (Thompson et al, 2012).

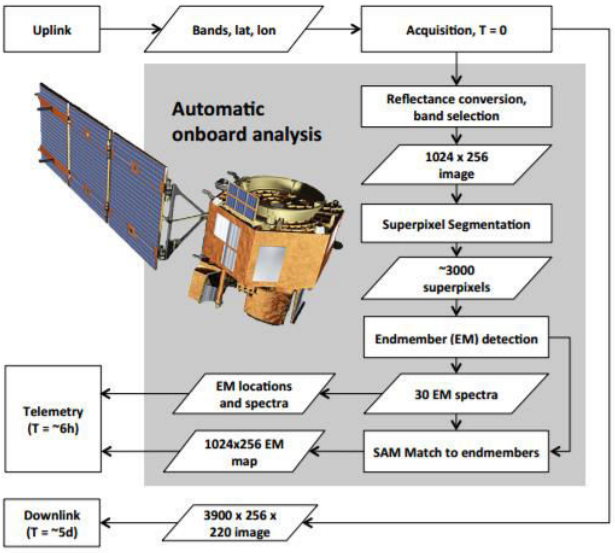

Figure 1.12: Procedure for on-board processing and summary downlink by EO-1 (Thompson et al, 2012).

The spacecraft bus has dimensions and mass of a large satellite: i.e. a diameter of 1.25 m and a height of 0.73 m, and an overall mass up to 480 kg, with the payload weighing up to 110 kg (eoPortal Directory, n.d.).

In 2016, part of the team working in the EO-1 mission proposed a **hyperspectral CubeSat constellation** that would image the surface of the Earth on a daily basis, with the kind of on-board image analysis incorporated in EO-1. The CubeSats would have a 6U form factor and their development would cost less than US$1 million each (Mandl et al., 2016).

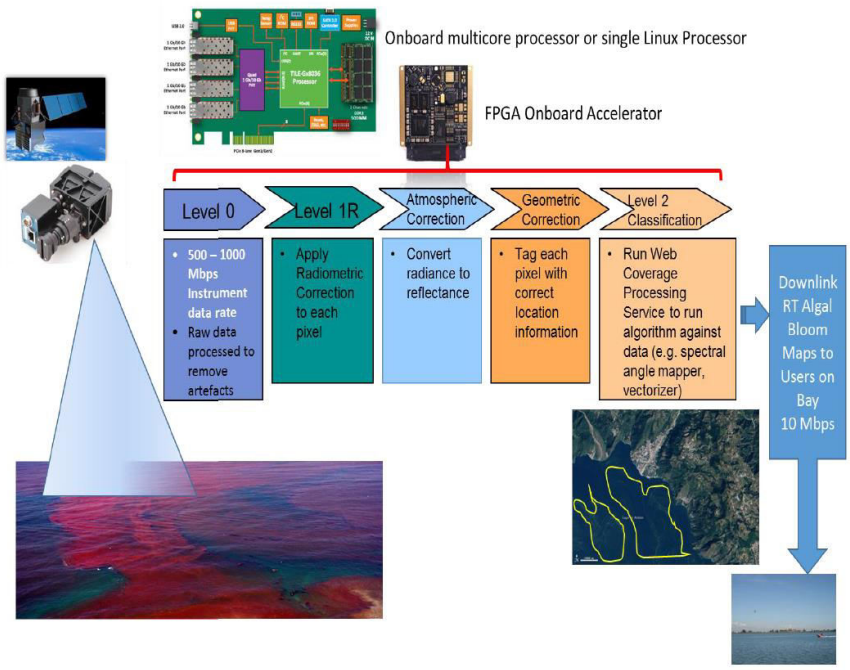

Figure 1.13: Basic data processing steps for a space-based imaging spectrometer that typically was done on the ground, but can now be done on-board a satellite, in realtime at low power consumption with new on-board processing technology (Mandl et al., 2016).

On the 2nd of February 2018, ESA successfully launched the 6U CubeSat **GomX-4B**. The satellite is part of a two-satellite constellation, the GomX-4, a research and development mission by GomSpace in partnership with DALO (Danish Defence Acquisition and Logistics Organization), TUD (Technical University of Denmark) of Lyngby, Denmark, and ESA (European Space Agency). The satellite GomX-4B carries an intelligent hyperspectral sensor called HyperScout (eoPortal directory, 2018). **HyperScout** was designed by the Dutch company Cosine and is envisioned as a commercially exploitable intelligent hyperspectral sensor for future satellite missions, from nano to larger satellites (Cosine, 2016).The HyperScout Onboard Data Processing Software (ODPS) converts the raw hyperspectral data (L0) into application-level data (L2B). The image processing levels within this mission are:

- Level 0 to Level 1A: Geometric processing. Geolocation of the image. This is done using the satellite attitude data as well as a model of the Earth previously stored on-board the satellite.
- Level 1A to Level 1B: Radiometric processing. Converts each pixel digital number into top of atmosphere (TOA) radiance value.
- Level 1B to 1C: Data reshaping. Converts a sequence of frame images to a set of band images.
- Level 1C to Level 2A: Projection. Using the geolocated data, the image is regridded and spatially corrected so as to form a hyperspectral cube.
- Level 2A to Level 2B: Application-level processing. A subset of the data is selected and classified or subjected to other transformations, such as calculating physical indices. Classification is done following a detection change approach. Other possible operations include the calculation of vegetation or moisture spectral indices.

Possible applications of HyperScout include *biomass monitoring, Leaf Area Index (LAI), tree cover, deforestation, large forest fires, drought conditions, crop water requirements, delineation of flooded areas, land cover and land use changes* (Soukup et al., 2016).

Chapter II. Requirements definition

2.1. Mission statement

To design, manufacture and deploy in orbit an intelligent hyperspectral CubeSat for fire management in Africa.

2.2. Mission objectives

2.2.1. Primary objectives

1. To demonstrate the possible and powerful combination of CubeSat, hyperspectral and on-board processing technologies in space.
2. To build a low-cost satellite able to produce on-board vegetation fire risk and burned area maps based on hyperspectral data.

2.2.2. Secondary objectives

1. To raise the profile of South Africa and other African nations in the space arena internationally.
2. To build expertise and capacity in space technology and its application in Africa.
3. To give South Africa and other African nations independence in the production and utilization of space resources; in particular, spaceborne hyperspectral imagery.
4. To demonstrate the possibility of producing a system of these characteristics for a low cost.
5. To incorporate this mission as a complement to other international fire management services such as EFFIS and AFIS.

2.3. Schematic of the PyrSat project

The mission proposed in this study is an intelligent hyperspectral Earth observation CubeSat for fire monitoring. Traditionally, hyperspectral remote sensing has been restricted to larger and more costly satellites due to a number of factors. On the space segment side, these factors include the usual size of the hyperspectral sensors and the strong downlink requirements posed by the vast amount of data produced which must be subsequently downloaded. On the ground segment side, high-performance antennae are usually needed to receive the vast amount of data produced on-board. Additionally, expertise on the ground to process and extract meaningful information from the images and to distribute the products to the end users or customers is also required. All these constraints usually reduce the reach of this powerful tool to a limited number of users. Although data from the existing hyperspectral sensors in space can be obtained and processed according to specific interests, not many data are free and open. Furthermore, when it is, it may not contain the ideal characteristics and observations needed for a specific application.

This project is an initiative to overcome these issues and give independent means to obtain low-cost application-specific data for fire management. The core idea is to equip a CubeSat with a miniaturized hyperspectral sensor and give it the ability to perform on-board the image processing

and analysis tasks traditionally carried out on the ground. The final data product to be downloaded will be a GIS layer ready to be used and integrated with other thematic layers, which can be critical infrastructure, specific key locations such as hospitals, schools or airports, or important corridors, such as railways, major roads or power lines. This will reduce the requirements posed on both the downlink capacity and the ground infrastructure and expertise while supporting an efficient fire prevention, damage assessment and forest rehabilitation.

An initial concept of the mission architecture is presented below. The system will be further developed and characterized in the subsequent chapters of this dissertation.

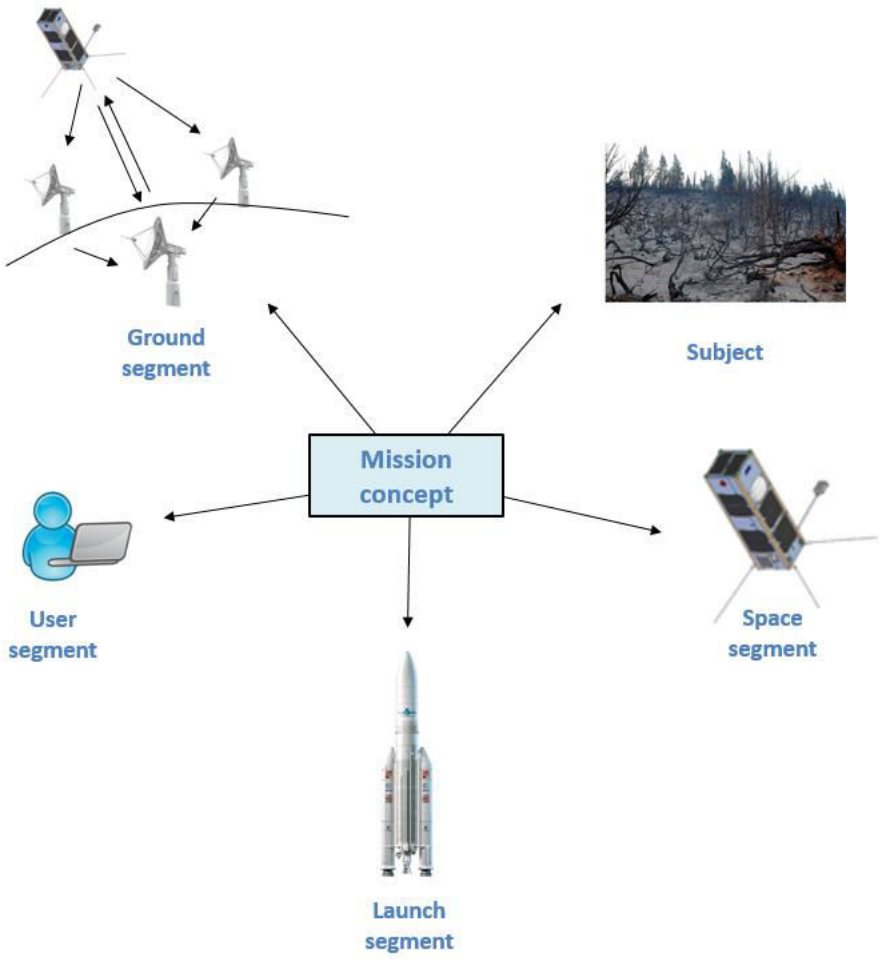

Figure 2.1: Space mission architecture.

The *subject* of the mission will be fire scars and vegetation susceptibility to burn in different ecosystems and scenes, in principle in Africa, although ideally it will be extended to other regions of the world. The *space segment* will consist of a CubeSat with the necessary subsystems to provide orbit and attitude maintenance, power, command, telemetry and data handling, structure and thermal control (spacecraft bus) and a hyperspectral sensor, together with a dedicated computer for image processing (payload). The *orbit*, also part of the space segment, is selected for its suitability to address the subject. The satellite will be placed in a polar Sun-synchronous orbit because of the multiple advantages of this orbit for Earth observation.

The *launch segment* will depend on the final application orbit, and will presumably be provided by one of the traditional launch operators for CubeSats. As for the *ground segment*, there will be a master ground station tracking, commanding and receiving telemetry and data from the satellite. Additional options such as a network of receiving ground stations or direct download to the users is uncertain at this stage and will be further evaluated. Different ground segment schemes will entail different command, control and communication architectures.

Finally, the *end users* will mainly be fire response units and administrative decision makers.

2.4. Mission requirements analysis

2.4.1. Customer/ User needs

- Vegetation fire risk maps:
    - To obtain geolocated and ready-to-use information about especially susceptible areas in order to increase the level of alert and minimize the response time in the case of a fire.
        - Spatial resolution better than 250 m, which is the currently provided by EFFIS with the MODIS sensor.
        - Monthly information updates in the wet season and weekly in the dry season.
        - Location accuracy of 50 m or better in order to ensure an efficient and appropriate management and protect especially vulnerable areas.
- Burned area products:
    - To receive accurate information about the location of fire scars for fire response, rehabilitation and other studies such as annual and historical registers.
        - Spatial resolution greater than 250 m.
        - Daily coverage for the case of the burn scars left by active fires, punctual image captures after a fire and weekly or monthly updates afterwards.
        - Location accuracy of 50 m.

2.4.2. Constraints

Derived from the top-level objectives and directly affecting the requirements definition, the following system constraints must be taken into consideration:

1. The satellite will conform to the CubeSat standard.
2. The image processing will be done on-board.
3. The sensor will be a hyperspectral sensor. This decision is derived directly from the objective of demonstrating this technology in a CubeSat. It nevertheless has an identified motivation; with automated on-board image processing, in principle the more wavebands captured by the sensor, the more reliable the results will be.

4. The main goal of this project is to provide the power of hyperspectral spaceborne remote sensing for a low cost, in order to serve a wider community of end users than is the case with current hyperspectral data products.

Clearly, such a mission will require a significant financial investment by South Africa and other African countries. It will also have to be affordable by these countries. The mission cost has to be weighed against the cost of fires. It is therefore instructive to weigh up the costs of space activities against financial losses caused by fires.

Figure 2.15 presents international space budgets as of 2016. Only spacefaring nations with an expenditure of at least US$10 million are represented:

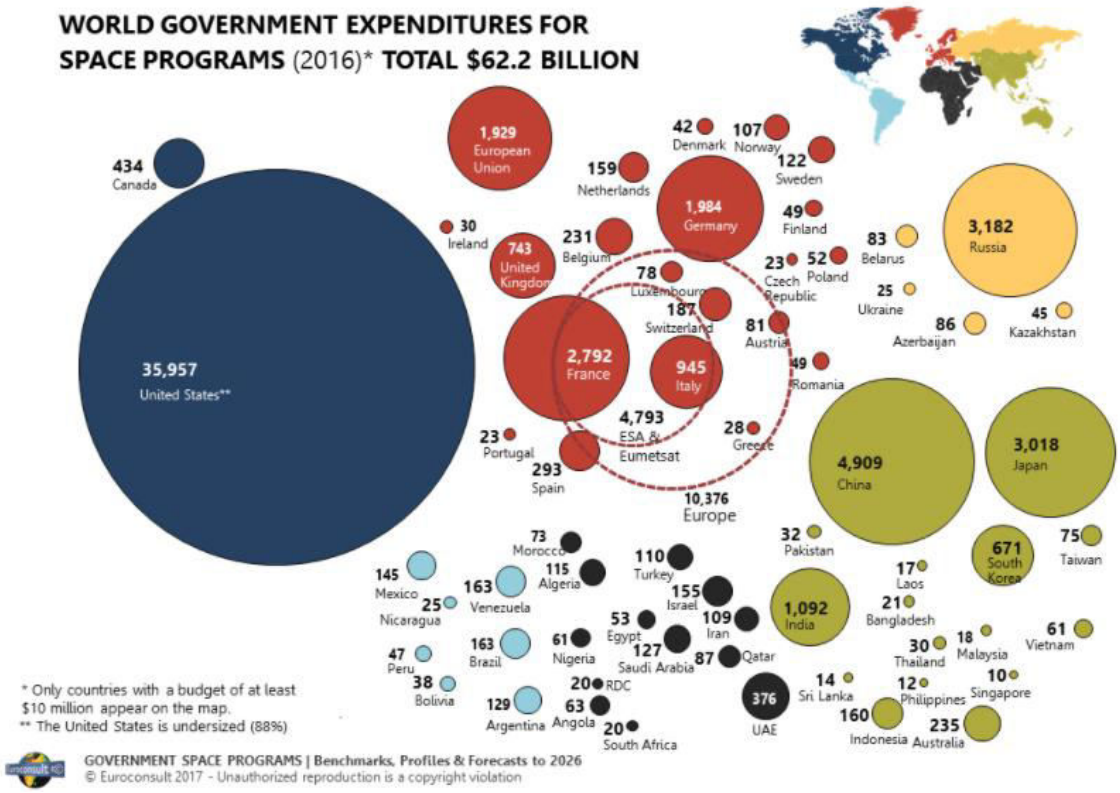

Figure 2.2: International space budget as of 2016 (Euroconsult, 2017).

Information about budgets allocated to fire services is not easily accessible on the internet. In South Africa, the mid-term estimate for fire-related services budgets is 3.1, 3.3 and 3.5 million Rands in the periods 2015/2016, 2016/2017 and 2017/2018, respectively (National Treasury Republic of South Africa, 2016). In Euros, these amounts are €214 480, €228 250 and €242 100, respectively. On the other hand, the corresponding expenses in the Mediterranean basin are significantly higher. In a report published by the World Wildlife Fund (WWF) in the frame of the project FIREFIGHT in the Mediterranean Region in 2001, it is estimated that the general cost of fire services in this region was on the order of 1 billion Euros annually at the time of the report. In the same epoch, the annual budget dedicated to forest protection against fires in Spain was 360 million Euros at the time of the report (Dimitrou, Mantakas and Kouvelis, 2001).

In light of these figures, a cost target of €500 000 for the whole project, from satellite development to launch is deemed to be low-cost for a mission of these characteristics.

2.5. Requirements definition

Having determined our user needs and constraints, we now turn to a definition of our functional and operational requirements for such a mission. The nomenclature given to designate the requirements, PSR, stands for “PyrSat Requirement”.

2.5.1. Functional requirements

These are requirements that define how well the system must perform to meet its objectives.

PERFORMANCE

PSR 1: The system must achieve a spatial resolution of 250 m.

PSR 2: The system must locate burned areas and areas of high fire risk with a location accuracy of 50 m.

COVERAGE

PSR 3: The mission must provide monthly information updates to monitor the evolution of burn scars and the vegetation fire risk in the wet season.

PSR 4: The system must also provide weekly coverage of burn scars to monitor their evolution and the progress of rehabilitation efforts and to keep an updated track of the vegetation fire risk.

PSR 5: Daily coverage must be guaranteed for the burned area product for active fires. Punctual coverage must also be available after a fire.

PSR 6: The system must cover the African continent, with special emphasis on southern Africa, and must have the capability of extending coverage to other regions.

RESPONSIVENESS

PSR 7: Both burned area and vegetation fire risk products must be sent to the users within one hour after the desired observation has taken place.

PSR 8: For an active fire, the system must perform a requested observation within the same day it is requested.

PSR 9: For monitoring burned areas and fire risk evolution, the system must obtain the required observations either weekly or monthly in specific scheduled days according to the application requirements and system availability.

2.5.2. Operational requirements

The operational requirements describe how the system will operate and how users will interact with it to achieve the mission objectives.

DURATION

PSR 10: The mission shall be operational for a minimum of two years.

AVAILABILITY

PSR 11: With the exception of the necessary time to charge batteries and imaging disruptions due to weather conditions such as clouds, the system should be available 90 % of the time. The idle time when the satellite is not tasked with imaging or data downloads must be used for system testing and updates when appropriate.

SURVIVABILITY

PSR 12: The spacecraft and all the components in it must be able to endure the space environment (especially radiation and temperature conditions) without degradation in the performance for at least two years.

DATA DISTRIBUTION

PSR 13: There must be one only master ground station to command and track the satellite as well as to receive its telemetry.

PSR 14: An additional network of receiving ground stations must be established in order to disseminate data to end users rapidly as to accomplish the previous requirements.

DATA CONTENT, FORM AND FORMAT

PSR 15: The image processing and analysis must be performed on-board.

PSR 16: The final data product shall be a GIS layer representing the burn scars and the different levels of vegetation fire risk classes, and it must be easily integrated with other geolocated information.

PSR 17: The data products downloaded must be manageable with open source software.

PSR 18: The burned area maps must have only two classes: Burned and not burned.

PSR 19: The vegetation fire risk maps must have four different risk levels.

PSR 20: The system must also offer the option to download the raw data for analysis on the ground in order to give mission planners and analysts the means to evaluate the system performance, improve calibrations, and fix errors.

PSR 21: The downloaded product must be accompanied by ancillary data such as the date and time of the capture and the level of confidence.

2.5.3. Constraints

Lastly, the constraints limit cost, schedule and implementation techniques available for the system design.

COST

PSR 22: The satellite development and launch must be achievable for under €500 000.

SCHEDULE

PSR 23: The development time must be of under two years.

PSR 24: The initial operational capability must be achieved within the first semester in orbit.

PSR 25: The final operational capability must be achieved within, at least, the fourth semester in orbit.

REGULATIONS

PSR 26: The mission shall comply with the applicable South African and international legal frameworks.

PSR 27: The mission must comply with applicable intellectual property and technology transfer frameworks.

POLITICAL

PSR 28: The program must promote international cooperation in terms of the covered areas and the data policy, download and distribution. It must involve at least one partner country in Africa and a partner in Europe.

PSR 29: The mission shall complement but not duplicate other fire services such as AFIS and EFFIS.

ENVIRONMENT

PSR 30: The satellite must be able to naturally de-orbit in a period of no more of 25 years after the end of its operational life.

PSR 31: The orbit altitude must be high enough to minimize the atmospheric drag and guarantee an operational life of at least two years but low enough to avoid the inner Van Allen radiation belt.

INTERFACES

PSR 32: The ground operators must retransmit to the user the final data product produced on-board the satellite.

PSR 33: The data received in the download-only ground stations must be immediately retransmitted to the master ground station.

PSR 34: The receiving ground stations must also be capable of transmitting the data directly to the users.

PSR 35: The users must send their requests to the master ground station that will schedule and command the observations.

DEVELOPMENT CONSTRAINTS

PSR 36: The satellite shall adopt the CubeSat standard.

PSR 37: The hardware must be built up using commercial off-the-shelf (COTS) components.

PSR 38: The on-board software must be open-source.

PSR 39: The entire development process must be well reported in complete and traceable documents.

Chapter III. System design

In this Chapter we will discuss a conceptual system design for a proof-of-concept CubeSat Earth observation mission with on-board data processing capabilities for fire applications. We will first consider the space segment for such a mission (the orbit design and the spacecraft payload and bus), followed by ground segment, the user segment and the launch segment, respectively.

3.1. Space segment

3.1.1. Orbit design

The choice of a LEO orbit is essential for this mission in order to achieve the required spatial resolution. The CubeSat form factor does not allow for large telescopes with a high spatial resolution. Hence the hyperspectral sensors available for satellites of this form factor generally provide a limited resolution. Thus, a higher orbital altitude would result in unacceptably low spatial resolutions.

Another important consideration to bear in mind in the orbit selection is that, as a proof-of-concept mission, this mission will achieve its objectives in a short time. After this time, it should de-orbit within 25 years (PSR 30) to minimize its impact on the debris situation in LEO. No propulsive capabilities for orbit maintenance are envisioned.

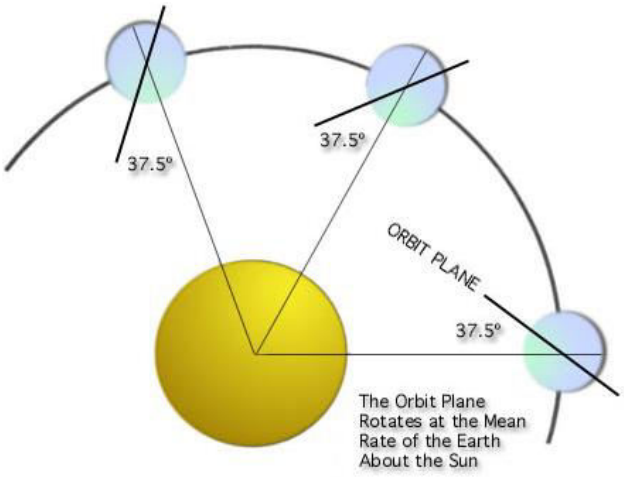

Figure 3.1: Sun-synchronous orbit for the case of Landsat 7 (NASA, 2016).

A Sun-synchronous orbit, this orbit provides multiple advantages for Earth observation missions (Boain, 2004). The nearly fixed position of the line of nodes with respect to the sun's direction has several useful characteristics:

- Almost constant lighting conditions of the observations throughout the mission;
- The thermal environment of the satellite remains almost the same, facilitating the engineering and survivability of the systems;

- The orbit always has the same "dark-side", which can help to avoid some thermal control problems and also has advantages such as enabling a fixed position of the solar panels always pointing to the sun, thus being more efficient and avoiding frequent "search for the sun" attitude control manoeuvres to charge batteries.

Another advantage of these orbits is that the altitude can be selected within a wide range (200 - 1680 km) allowing for different viewing geometries and conditions to best serve different applications. Due to the circular nature of the orbit, the captured images are nearly homogeneous. Furthermore, discrete altitudes can be chosen to provide a repeated ground-track over a certain number of days. Thus, complete and repeatable global coverage can be ensured.

Being nearly polar, this orbit also provides roughly global coverage for. However, for the specific application of fires, coverage of the Arctic Circle is not necessary.

Some of these characteristics, such as the homogeneous lighting conditions and image geometry, are especially relevant for this mission due to the already high spectral and spatial variability of the sensed subject.

Because the satellite does not have its own propulsion system, the launcher will inject it directly into the operational orbit. Without a propulsion system, the satellite will also be unable to perform orbital corrections and thus, the zonal harmonic coefficients of the Earth's gravitational field J2 and J3 will trigger orbital perturbations. To avoid this effect, a **frozen orbit** could be selected. In order to achieve this orbit, the **argument of perigee** (ω) must be 90 or 270 degrees, thus positioning the orbit perigee over the North or South Pole, and the **eccentricity** 0.001. For most NASA Sun-synchronous missions ω is 90 degrees. That is, the argument of perigee is over the North Pole (Boain, 2004).

For the selection of the orbital **altitude** within the LEO region, a lower limit of 500 km should be considered due to the strong atmospheric drag that could cause a too rapid de-orbiting below this altitude (Boain, 2004). In order to maximize the time in orbit while achieving a good spatial resolution, an altitude of 550 km will be selected.

The choice of the **local time at the ascending node** (LTAN) is generally a compromise between different constraints. Namely, to obtain the best solar lighting conditions for the regions observed; to reduce the risks of antisolar or specular reflection; to take meteorological factors into account, e.g., a certain region may be under cloud cover every day in the middle of the morning; to take into account the crossing time of other Sun-synchronous satellites carrying out the same type of mission; to limit periods of solar eclipse and to limit thermal variations during each revolution (Capderou, 2005).

Energy-wise, the best suited orbit is one with LTAN 6:00 or 18:00, known as dusk-dawn orbit, as it minimizes the time the satellite is in eclipse. Radar satellites and other satellites studying the dynamics of the atmosphere normally use this orbit, because of the high power demand posed by their payloads. This orbit is also useful to keep the temperature variations low (Capderou, 2005).

However, the observation requirements may be better accomplished with a different LTAN. To avoid specular reflections, a midday crossing time at the node should not be chosen. Mission designers normally consider that the best time slot for viewing lasts for 3 hours and takes place from 10:30 to 13:30. Thus, for Earth observation satellites is it common to have the LTAN at 10:30 or 13:30, depending on meteorological factors such as cloud coverage at certain times of the day in some

regions. Examples of this are the seven Landsat and the five SPOT satellites, with descending nodes at the end of the morning (Capderou, 2005).

In the case of this project, a dusk-dawn orbit is an interesting choice due to the power limitations of CubeSats as well as the softer thermal variations achieved with this orbit. However, in order for the observations to be more useful probably a LTDN at 13:30 would be most suitable.

Because of the low altitude of the orbit and the limited aperture angles of the on-board sensor (11.77 degrees semi-vertical angle and 14.13 degrees semi-horizontal angle), presented in detail further in this Chapter, the potential observations considering fixed orientation of the sensor to nadir are very limited. Thus, we must evaluate other alternatives for the orbit trying to produce only daytime observations over the areas of interest in this mission.

For the purpose of this study, we selected the regions of interest to be the Western Cape, in Southern Africa, and Spain. In particular, the cities of Cape Town and Barcelona were selected.

In order to assess the applicability of different orbits to this mission, different LTAN were simulated in STK. Namely, 6:00, 10:00, 10:05, 10:10, and 10:30 LTAN and 13:30 LTDN. The propagation time interval is from the 1st of December 2017 until the 1st of December 2018.

The results of the simulation showed that the dusk-dawn orbit, with LTAN at 6:00 in the morning, was not useful for this mission. The observations over Cape Town achievable with this orbit are all between 3:00 and 3:15 in the morning and between 14:20 and 14:30 in the afternoon. In other locations more to the east of the country, such as East London and Pretoria, the time of the observations advances to earlier in the morning and afternoon. Therefore, only the descending segment of this orbit offers useful observations. In total, there are 85 observations over Cape Town in the time interval of the propagation, meaning that the space between useful observations is too wide to consider this orbit for this application in South Africa. Furthermore, the total of 93 observations over Barcelona given by this orbit take place in the morning between 3:20 and 3:30 and in the evening between 16:10 and 16:25, meaning also only one segment of the orbit produces useful observations and they are too widely spaced.

The same is true for the orbit with LTDN at 13:30. This orbit only produces observations over Cape Town between 9 am and 10 am and between 10 pm and 11 pm. In total, there are 86 observations in the simulation time window. There is also one segment of the orbit that always produces observations in the middle of the night over Barcelona. Thus, the number of daytime observations is again unacceptably low and the orbit is not a viable option.

Among the other options, the orbit with LTAN at 10:10 seems to be a better choice. It produces observations in the approximate interval times of 7:10 - 7:20 and 18:30- 18:40 over Cape Town and 7:30 - 7:40 and 18:20 - 18:30 over Barcelona.

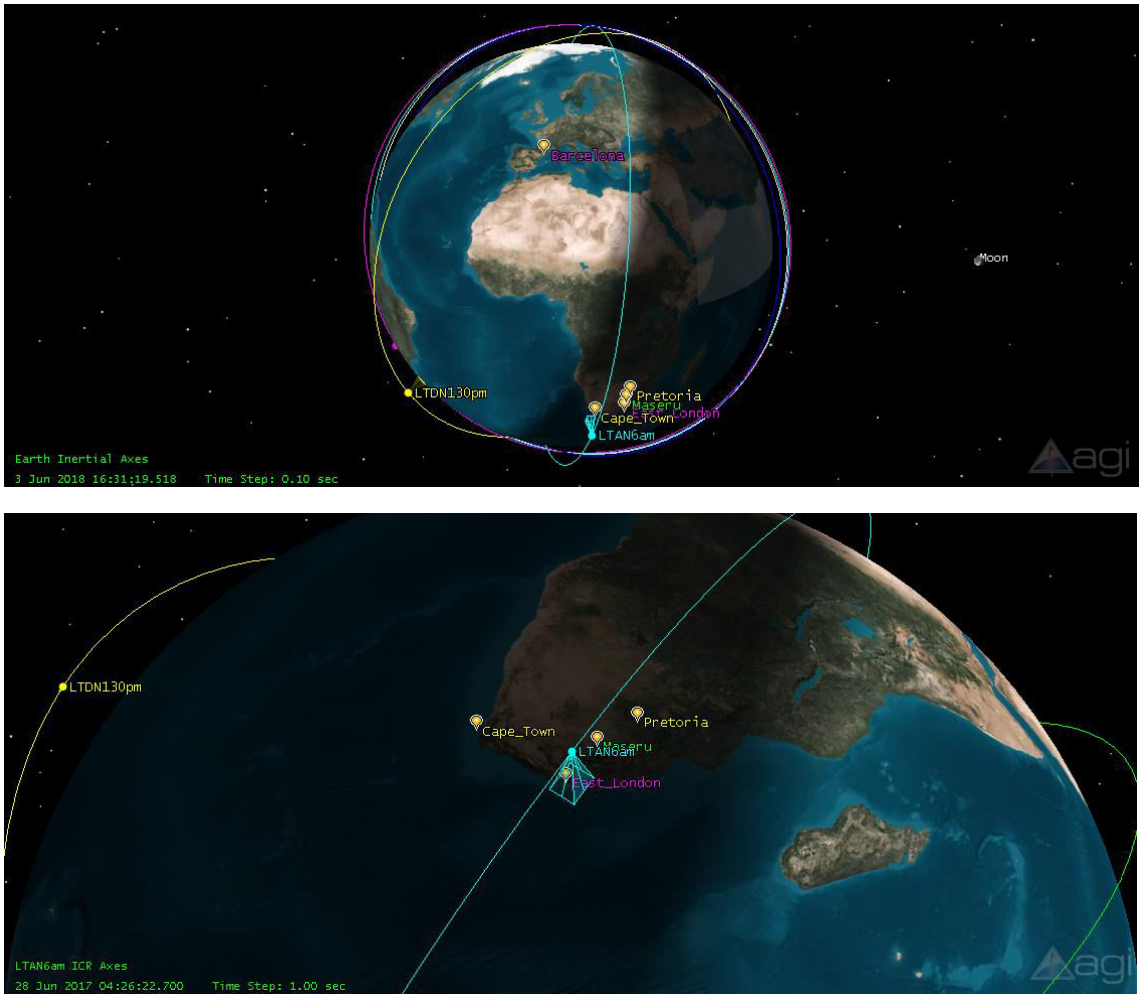

Figure 3.2: Orbital simulation in STK. The image at the top shows the simulated orbits. The image at the bottom shows the visibility of the sensor on-board the satellite in an orbit with 6 am LTAN in its pass over East London in the Eastern Cape, South Africa. In this image a small part of other orbits is also visible.

According to the insurance industry, in the Western Cape the fire season is from December to April. Taking into consideration the sunrise and sunset times in Cape Town during these months in 2017 and the passing times of the orbit previously stated, it can be concluded that all the passes at the beginning of the fire season will occur in daylight. This is the case until the 2nd of April, when one of the evening passes will already take place during the night. On the 9th of April all the evening passes will be at night. On the 18th of April the first morning pass will be lost but there will be still some daytime coverage until the end of the month. Thus, the area will be covered during the whole fire season, although the frequency of the observations will gradually reduce.

On the other hand, the fire season in the Mediterranean Basin is from May to September (Ager et al., 2013), so coverage should be maximized in these months. As in the case of Cape Town, all the passes over Barcelona occur after sunrise at the beginning of the fire season. On the 26th of August, the first evening pass will be already after sunset. All the evening passes occur after sunset from the 2nd of September. On the 12th of September the first morning pass will occur before sunrise and thus will not produce useful observations, but some morning coverage will be maintained until the 22nd of September, almost at the end of the fire season.

Although this orbit will have only night passes over both cities for a considerable part of the year, during most of the fire season there will only be daytime passes, minimizing the time between useful observations.

During the time when the satellite cannot serve the main interest areas of South Africa and the Mediterranean Sea, it will be available for other regions in the world. Furthermore, as the processing occurs on-board and there are multiple passes in which the satellite has access to the ground stations, both in Cape Town and Barcelona, there will be plenty of free mission time and on-board memory space and that could also be used to image other areas.

The daytime passes over Cape Town are presented in Table 3.1. The access refers to all the accesses of the sensor included in the propagated time interval. The complete list of accesses of the sensor to Cape Town and Barcelona are included in Annex A and B, respectively.

Table 3.6: Day accesses of the on-board sensor to Cape Town.

Access	Start time (SA)	Duration (sec)
1	3Dec2017 07:18:36	14.9
2	4Dec2017 07:15:13	14.9
3	20Dec2017 18:37:00	14.9
4	21Dec2017 18:33:22	14.9
5	31Dec2017 07:18:47	14.9
6	1Jan2018 07:15:25	15.0
7	17Jan2018 18:37:12	15.0
8	18Jan2018 18:33:49	15.0
9	28Jan2018 07:18:59	15.0
10	29Jan2018 07:15:36	15.0
11	14Feb2018 18:37:23	15.0
12	15Feb2018 18:34:00	14.9
13	25Feb2018 07:19:11	14.9
14	26Feb2018 07:15:48	14.9
15	14Mar2018 18:37:35	15.0
16	15Mar2018 18:34:12	14.9

Access	Start time (SA)	Duration (sec)
17	25Mar2018 07:19:23	14.9
18	26Mar2018 07:16:00	14.9
21	22Apr2018 07:19:34	14.9
22	23Apr2018 09:16:12	14.9
39	10Sep2018 07:17:10	14.9
40	11Sep2018 07:13:48	15.0
41	26Sep2018 18:38:57	0.1
42	27Sep2018 18:35:34	14.9
43	8Oct2018 07:17:22	14.9
44	9Oct2018 07:13:59	15.0
45	25Oct2018 18:35:46	14.9
46	5Nov2018 07:17:36	14.9
47	6Nov2018 07:14:11	15.0
48	22Nov2018 18:35:58	14.9
49	23Nov2018 18:32:48	1.6

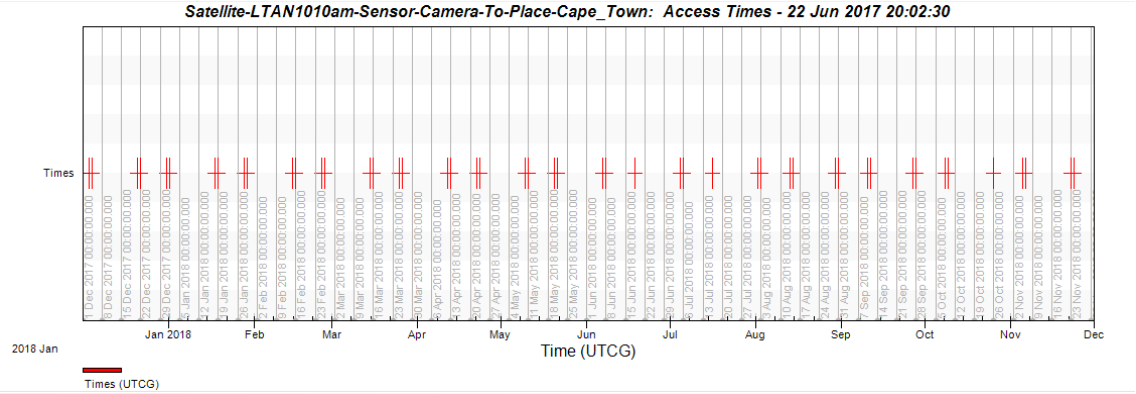

Figure 3.3: Total accesses of the on-board sensor to Cape Town.

Thus, in total there are 31 daytime accesses of the sensor to Cape Town, and therefore, the same number of potential observations. Out of these, 20 occur in the fire season 2017-2018. Then there are roughly four and a half months until the next daytime observation on the 10th of September. During this whole period, the satellite produces two observations roughly every two weeks. Later on, from this date until the next fire season the resources should be exploited to assess the recovery of the previous fire season and to monitor the vegetation fire risk in order to prevent fires in the next fire season.

The preceding analysis assumes a nadir-viewing satellite with a 10.8 x 1.3 FOV. Off-nadir viewing would increase the number of useable passes considerably.

The total accessibility of the satellite to a theoretical ground station in Cape Town, this time without taking the sensor into account, is summarized below. There are a total of 1767 accesses, with multiple accesses a day. Although a significant number of them happen at an elevation too low with respect to the ground station for the satellite to acquire images, this high number highlights the possibility of increasing the frequency of observations by tilting the satellite to acquire off-nadir observations.

Indeed, tilting the satellite should be done given the reduced number of nadir-pointing observations. However, even in the case of failure of this mode, the satellite would still have some functionality as it can produce fire risk maps more frequently updated than those currently available and burned scar maps also approximately every two weeks.

Global Statistics

Min Duration	1202	6 Aug 2018 11:14:18.495	6 Aug 2018 11:14:24.204	5.709
Max Duration	228	17 Jan 2018 20:31:16.660	17 Jan 2018 20:43:27.478	730.818
Mean Duration				575.363
Total Duration				1016666.135

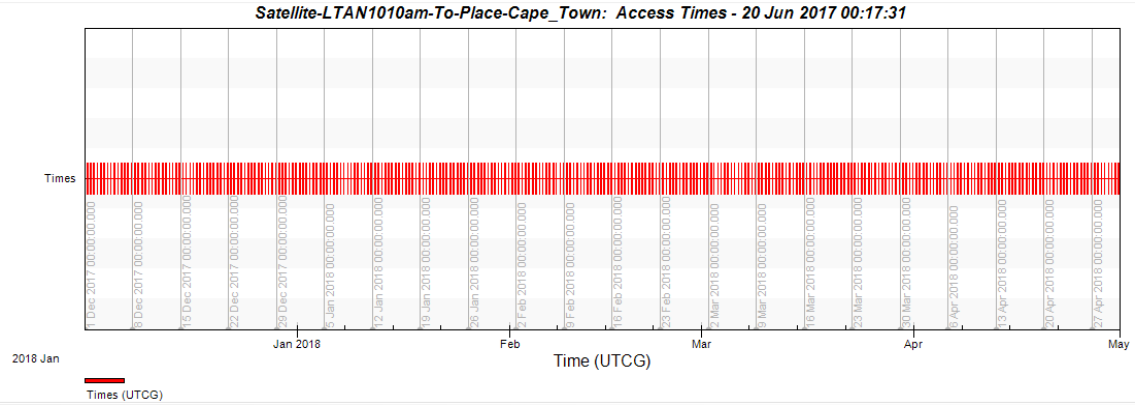

Figure 3.4: Accesses of the satellite to Cape Town during the fire season.

At this point it is necessary to note that with this orbit and its revisit period it will not be possible to guarantee daily coverage as specified in the requirement PSR 5 with one single satellite, although significant improvements could be achieved with an attitude control system able to tilt the satellite. The options here then would be to increase the number of satellites to add to the constellation, to increase the orbital altitude or to dispense with this capability for this satellite and rely on the information offered by other satellites and fire services. Increasing the orbital altitude would lead to unacceptably low spatial resolutions with the available technology. As one of the main objectives of this satellite is to serve as technology demonstration, creating a constellation is not deemed prudent

until the technology has been proved functional. For the moment the mission will limit its capabilities to a weekly and monthly coverage and rely on other services for a more frequently updated product.

Table 3.2 summarizes the characteristics of the designed operational orbit:

Table 3.2: Orbital parameters of the designed operational orbit.

Type of orbit	Sun-synchronous
Altitude	550 km
Orbital period	95.21 min
Inclination	~ 97 deg (polar orbit)
Eccentricity	0.001 (near-circular)
Argument of perigee	90 deg
LTAN	10:10

The orbital period (shown in Table 3.2) and the orbital velocity of the satellite, for the case of a circular orbit, can be computed using the following equations:

$$P = 2\pi\sqrt{\frac{r^3}{\mu}};\ v = \sqrt{\frac{\mu}{r}}$$

where *r* is the orbital radius[km], which corresponds to the orbital altitude added to the radius of the Earth (6357 km at the poles), and μ is the gravitational parameter [km^3/s^2], 3.986 × 10^5 km^3/s^2 for Earth. The resultant orbital velocity is 7.6 km/s.

Finally, since the orbit is Sun-synchronous with a determined altitude, the inclination is also determined. Figure 3.5 shows the orbital radius versus the inclination for a Sun-synchronous orbit.

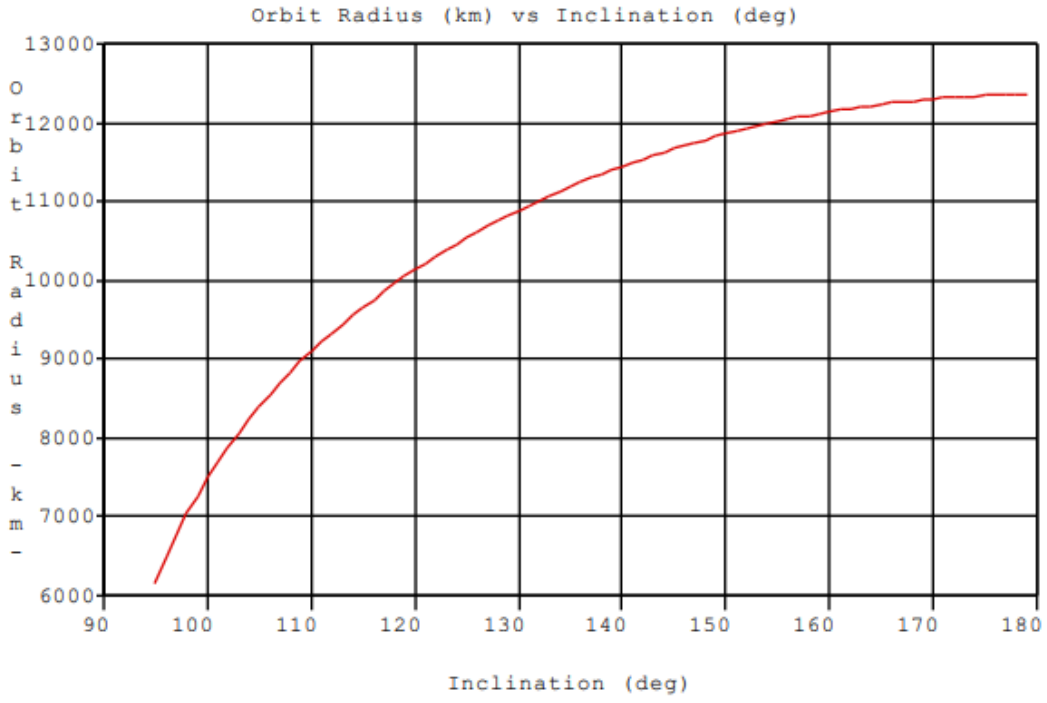

Figure 3.5: Orbital radius versus orbital inclination for circular Sun-synchronous Earth Orbits (NASA, n.d.c).

Thus, for an orbital radius of 6907 km (6357 km + 550 km), the inclination is approximately 97 degrees.

3.1.2. Space payload design and sizing

As stated in the objectives, this mission aims to demonstrate technologically the possibility of processing hyperspectral data on-board a CubeSat. Thus, the payload is composed of a hyperspectral sensor and a dedicated computer. After an image has been captured, the computer will process the raw data, apply a radiometric correction, geolocate each image pixel and finally, perform the classification and create either the burned area or vegetation fire risk products, both in a GIS layer format (shape file). In this way, the final data product is created on board the satellite and is ready to be used on the ground.

It must be remembered here that, for both the payload and satellite subsystems, the requirement PSR 37 states that all the components must be COTS.

On-board sensor

In the choice of the hyperspectral camera, the main design driver was the cost. Generally, this technology is extremely costly, and the standard market price would have increased the total cost of the mission unacceptably. For example, Mandl et al. (2016) propose the camera Nano-Hyperspec by Headwall for their Hyperspectral Cubesat Constellation for Rapid Natural Hazard Response. They estimate a total cost of $200 000, including an upgrade to make the camera space capable. Using hyperspectral cameras designed for drones was also considered, but in general their dimensions were larger than the CubeSat form factor.

However, the company XIMEA produces miniaturized multispectral and hyperspectral sensors for a price well below the market average. Thus, this was the chosen provider. Their hyperspectral cameras weigh 32 g and measure 26 x 26 x 31 mm, and are thus compatible with the CubeSat form factor. Both snapshot and pushbroom options are available. Additionally, it is claimed in the products description that because of their robustness and resistance they could have space applications, such as remote sensing, space exploration or astronomy (XIMEA, 2016a).

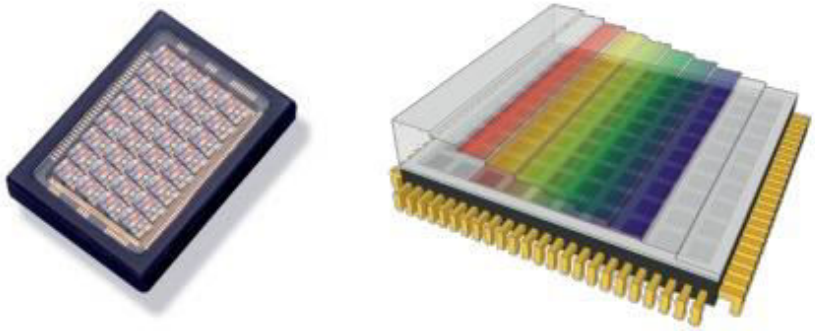

Figure 3.6: Snapsot Mosaic and Linescan mechanisms (XIMEA, 2016a).

The least costly cameras, at a price of US$17 700 are the LS100 (spectral range 630-970 [nm], 100+ spectral bands in steps of 4 nm, each with a size of 2048 x 8 pixels line scan sensor), MS4X4 (470-630 [nm], 16 bands, snapshot sensor) and MS5X5 (600-950/975 [nm], 25 bands, snapshot sensor)

(XIMEA, 2016a). Among these, the MS4X4 seems to be the less useful one due to the spectral range and the number of bands.

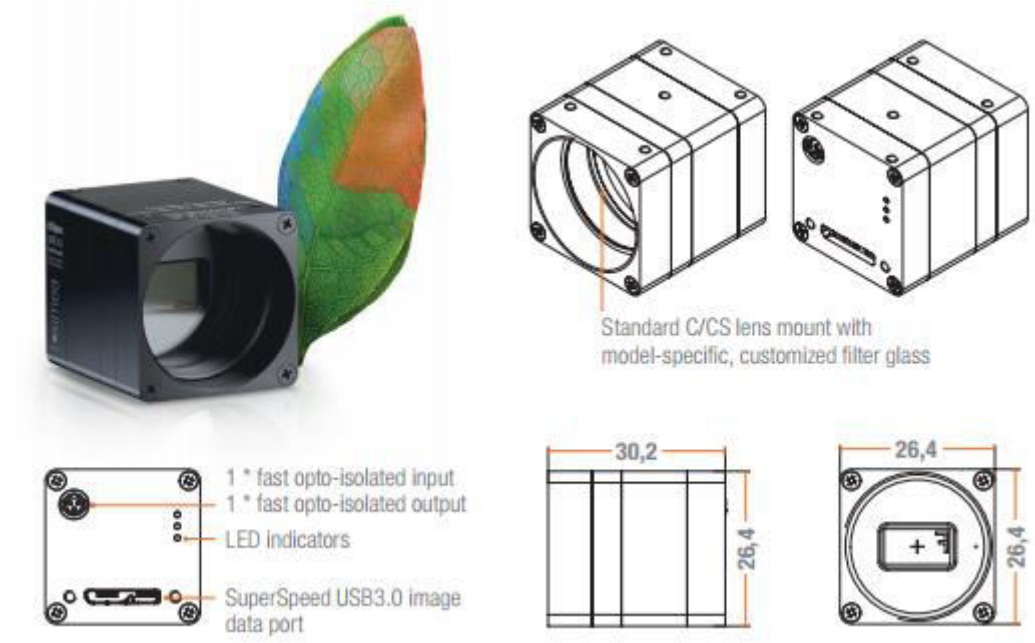

Figure 3.7: xiSpec cameras by XIMEA (XIMEA, 2016a).

Indeed, only the LS100 camera can be considered hyperspectral, because of the number of bands it features, and will therefore be the one selected for the mission. Although snapshot sensors present the advantages of avoiding scanning mechanisms with rotary or mobile parts, which gives them increased robustness or compactness, as well as the ability of gathering all the information in the image at the exact same instant, which allows for a better observation of dynamic scenes (Hagen et al, 2012), it can be assumed that for the applications of this project the scenes are going to be of a relatively static nature. Furthermore, the increased number of bands should improve the performance of Machine Learning image classification.

Thus, the on-board hyperspectral sensor for this mission will be the LS100 camera by XIMEA, which consumes 1.6 W and can be connected to a USB3 Vision Compliant port (XIMEA, 2016a).

The geometric specifications of the sensor are described in Table 3.3:

Table 3.3: LS100 camera geometric specifications.

Focal length (f) [mm]	16, 25, or 35 mm. The latter will be employed to obtain better spatial accuracies
Detector dimensions (d_{det}) [pix]	2048 pix (H) x 1088 pix (V)
Pixel dimensions (d_{pix}) [µm]	4.3 µm (H) x 6.07 µm (V)
iFOV	0.122857 mRad(H) x 0.173429 mRad(V)
FOV	10.78 deg (H) x 14.34 deg (V)

The focal length and dimensions of the detector and pixel size were extracted from the XIMEA website (2016). The iFOV and FOV angles were calculated through simple trigonometric relations from the f, d_{det} and d_{pix}.

Considering the sensor characteristics, the approximate spatial resolution on the ground (GSD) and swath width (sw) - without taking into account the curvature of the Earth - from an orbit of 550 km can be calculated applying the Thales theorem to Figure 3.8.

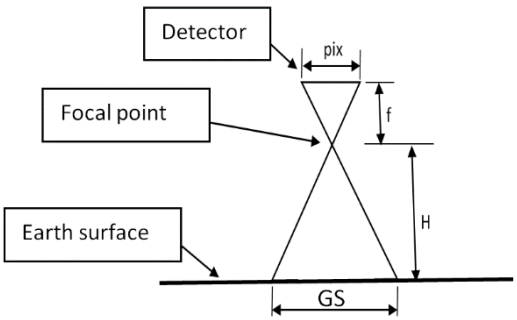

Figure 3.8: Sensor spatial resolution.

$$\frac{\mathrm{GSD}}{\mathrm{H}} = \frac{\mathrm{d_{pix}}}{\mathrm{f}} \rightarrow GSD_{550km} = 67.57\ m\ (across-track)\ \mathrm{x}\ 95.39\ m\ (along-track)$$

$$\frac{\mathrm{sw}}{\mathrm{H}} = \frac{\mathrm{d}}{\mathrm{f}} \rightarrow sw_{550km} = 138.29\ km\ (accross-track)\mathrm{x}\ 103.71\ km\ (along-track)$$

Although this resolution is generally considered as medium resolution, it is already higher than that of MODIS products (250 m), accomplishing requirement PSR 1. The fire danger forecast offered by the EFFIS service is derived from meteorological information from different sources and has a spatial resolution of 10 km. This service also obtains the information about active fires and a burned area rapid damage assessment from MODIS (250 m), which is updated daily. For a finer fire damage assessment after the fire season, higher spatial resolution satellites such as Landsat and Sentinel are used (European Commission, n.d.c).

Thus, because of the spatial and temporal resolution of the proposed system, it could obtain higher resolution burned area products than those of MODIS and more frequently updated than those of higher resolution satellites. It could also play an important role in fire danger forecasting with the finer resolution vegetation fire risk products that could be combined with weather information to obtain a more significant product. This would also enable more accurate fire prevention that could be of special interest to specific key locations such as hospitals, schools or airports, or important corridors, such as railways, major roads or power lines.

A limitation of the LS100 camera however is that the sensed spectral range does not include the MIR and TIR wavelengths traditionally used for fire management activities. However, it is expected that the multiple continuous bands are sufficient accomplish the classification tasks required for this mission. In any case, if the technology was successfully proved in orbit and a constellation was to be

formed, developing IR satellites to combine their information with that of the hyperspectral ones would be a powerful initiative.

Dedicated computer

Different options were considered for the dedicated computer. Namely, the Raspberry Pi 3 model B, because of its outstanding price-quality relation, and NVIDIA Jetson TK1 and TX1, because of their high computational power and remarkable graphics unit.

Requirements for the dedicated computer:

The criteria applied to the evaluation process were derived from the requirements for the selected computer. The nomenclature given to designate the requirements, PSR DC, stands for "PyrSat Requirement Dedicated Computer".

- PSR DC 1: In line with the main objective of the mission, low cost is one of the most important design drivers for the selection of the computer.

- PSR DC 2: The computer must perform its data reduction and classification tasks in a time sufficiently short to allow the transmission of the final data products to the ground station in the pass immediately following that in which the image was captured.

- PSR DC 3: The power consumption must be minimised and limited to the available power in CubeSats.

  Typically, the 1U, 2U, and 3U CubeSats' maximum power budgets range from 1 to 2.5 watts, 2 to 5 watts, and 7 to 20 watts, respectively (Sterling Arnold, Nuzzaci and Gordon-Ross, 2012).

- PSR DC 4: In order to reduce launch cost, which is the most expensive element in a CubeSat mission, the computer mass must be minimised.

- PSR DC 5: The dimensions of the computer must be compatible with the CubeSat form factor and as small as possible. Smaller computers will result in more free space available for the rest of subsystems and lighter satellites, with the subsequent lower overall cost.

  The dimensions of a single CubeSat unit are (l x w x h): 98.4 x 98.4 x 98.4 mm for the inner envelope and 100 x 100 x 113.5 mm for the outer envelope (ISIS and CubeSatShop.com, n.d.).

- PSR DC 6: The computer must be able to survive and operate in the space environment (temperature, radiation) as well as survive the vibrations and mechanical loads experienced during launch.

  In space, the temperature can undergo extreme variations. Depending on its aspect and its time in direct sun light, a metal plate in LEO will cycle from –170°C to 123°C. (Antunes, 2012).

On the ground and during the launch, the satellite is subjected to high mechanical loads, such as its integration with the launch vehicle, the transportation of the latter to the launch pad, the vibrations during the ignition of the engines and the huge accelerations during the lift off and injection in orbit.

Out of the protective atmosphere, radiation coming from the Sun and galactic cosmic rays can endanger satellites' surfaces and electronic and other components, such as the lenses of the optical instruments.

Although the thermal subsystem, the structure and protective layers withstand part of these conditions, the satellite subsystems, including the dedicated computer, must also be resistant to both electromagnetic and particle radiation.

- PSR DC 7: The availability of resources such as pre-compiled libraries and detailed documentation must be considered in the selection of software development tools.

  Currently, large developers' communities produce a significant amount of resources for known common tasks, such as image processing and classification.

  Using these already existing resources can allow for a more efficient effort and time assignments in the development of a project, i.e. instead of creating new redundant software, emphasis can be put into the resolution of certain tasks specific of the project.

  Also, the more information available about a certain system and the bigger the users' platforms, the easier it is to use it and resolve any given problem.

  These aspects must thus be considered for the choice of the dedicated computer.

- PSR DC 8: The dedicated computer must have some sort of cooling system. Overheating of the computer can not only lead to its malfunctions but also induce problems in other satellite subsystems. One of the consequences of overheating could be degraded or blurry images.

- PSR DC 9: The computing power and memory of the computer must be enough to accomplish the demanding tasks of this mission.

  On the one hand, on-board image processing and classification has the advantage of lowering the communications subsystems requirements, as less data has to be sent to the ground, which is one way to cope with the communications limitations of CubeSats. Furthermore, it reduces the necessary on-ground equipment and the number of qualified professionals necessary to process the satellite images. On the other hand, it makes the command and data handling subsystem critical for supporting the compute-intensive mission functionality. For instance, a multispectral camera generally produces image data cubes ranging in size from hundreds of Megabytes to Gigabytes (Sterling Arnold, Nuzzaci and Gordon-Ross, 2012).

  In this project, the dedicated computer will be responsible for tasking the camera to take images, receiving the images after they have been captured, and processing and classifying them to produce the final data products.

As specified by XIMEA, an image captured by the chosen LS100 camera has a detector size of 2048 × 1088 pixels, with 8, 10 bits per pixel (RAW pixel data) and 100 bands, meaning an image size of up to 278.53 MB.

The dedicated computer must be able to perform the following tasks:

1. Image pre-processing
   1.1. Geometric and radiometric corrections
   1.2. Geolocation
2. Image analysis: Classification
3. Creation of the final product: Burned area and vegetation fire risk maps in the format of GIS layers (shape files).

Comparison of alternative computers:

Three different processors were considered for this project:

- Raspberry Pi: Because of its unprecedented price-performance ratio. Due to its higher computational power, only the **Raspberry Pi 3 model B** was considered for this mission.

- NVIDIA Jetson Tegra: Although more expensive than the Raspberry Pi, NVIDIA produces well-known graphic processing units (GPUs) and that are able to carry out more computationally demanding tasks. As stated on their website, the NVIDIA Jetson is "*the world's leading AI computing platform for GPU-accelerated parallel processing in the mobile embedded systems market*". Both the **NVIDIA Jetson TK1 and TX1** incorporate CUDA processors, which turns the GPU into a general-purpose graphics processor unit (GPGPU).

NVIDIA provides carriers for both TK1 and TX1, under the name of "developer kits". However, in order to be able to utilize the credit card sized TX1, which would fit in a 1U form factor and is thus one of its major advantages, an alternative carrier was also considered: Orbitty by Connect Tech. This carrier is developed specifically for the NVIDIA Jetson TX1, is of its same size and has an extended temperature range of -40°C to +85°C, which makes it better suited for space applications in accordance with the requirement PSR DC 6.

Table 3.4: Comparison of considered dedicated computers and carriers considered for this mission.

	Power consumption	Mass	Dimensions	Availability of resources	Cooling system	Processing power	Memory	CSI	Price
Raspberry Pi 3 model B	3.57 – 5.1 W *[1]	45 g *[2]	85.60x56x 21 mm*[2]	Large user community Not very supported for image classification	No	1.2 GHz 64-bit quad-core ARMv8 CPU + VideoCore IV 3D graphics core *[3]	1 GB RAM + microSD slot*[1]	CSI-2 2 Gbps bandwidth 5 MP resolution*[4]	US$39.98 *[5]
NVIDIA Jetson TK1 Developer Kit	5 W under typical load 10 W with the module fully utilized*[6]	120 g *[7]	127x127 mm*[6] (board)	Large developer community CUDA should support Caffe and others, but not Maxwell™ Architecture	Yes	NVIDIA 4-Plus-1™ Quad-Core ARM® Cortex™-A15 CPU + NVIDIA Kepler GPU (192 CUDA Cores) *[8]	2 GB x16 Memory with 64-bit Width + 16 GB 4.51 eMMC Memory *[8]	Two fast CSI-2 MIPI camera ports (one 4-lane and one 1-lane) *[9] + USB3.0 A*[8]	US$192*[5&]*[8] (US$129 with an academic discount, for US and Canada)
NVIDIA Jetson TX1 (module)	1 W idle 8 – 10 W under typical CUDA load Up to 15 W with the module fully utilized*[10]	144 g (with heatsink); 75 g (w/o heatsink) *[11]	50x87 mm*[12]	Large developer community Libraries for deep learning (cuDNN) *[8]	Heatsink*[8]	64-bit ARM® A57 CPUs + 1 TFLOP/s 256-core with NVIDIA Maxwell™ Architecture (256 CUDA cores) *[8]	4 GB LPDDR4 | 25.6 GB/s + 16 GB eMMC, SDIO, SATA*[8]	-	US$ 344 *[8]
+ Developer Kit	-	386 g*[13]	170x170 mm*[13]	-	Extra fan *[8]	-	-	Up to six cameras | 1400 Mpix/s + USB3.0 A*[8]	US$ 499 (US$299 with an academic discount, for US and Canada)*[8]
Orbitty Carrier *[11]	-	41 g	87x50 mm	-	No	-	-	USB 3.0	US$174 *[14] (Total: US$ 518)

*[1] https://www.raspberrypi.org/documentation/hardware/raspberrypi/power/README.md

*2 https://www.raspberrypi.org/
*3 http://www.petervis.com/Raspberry_PI/Raspberry_Pi_CSI/Raspberry_Pi_CSI_Camera_Module.html
*4 https://www.raspberrypi.org/help/faqs/#generalDimensions
*5 https://www.amazon.com/
*6 http://elinux.org/Jetson_TK1
*7 http://www.itpro.co.uk/desktop-hardware/22731/nvidia-jetson-tk1-review
*8 http://www.nvidia.com/object/embedded-systems.html
*9 http://elinux.org/Jetson/Cameras
*10 https://devblogs.nvidia.com/parallelforall/nvidia-jetson-tx1-supercomputer-on-module-drives-next-wave-of-autonomous-machines/
*11 http://www.connecttech.com/pdf/ASG003.pdf
*12 http://elinux.org/Jetson_TX1
*13 http://images.nvidia.com/content/tegra/embedded-systems/pdf/JTX1-DevKit-Product-sheet.pdf
*14 http://www.connecttech.com/sub/products/ASG003.asp

Evaluation of options:

From the Table 3.4 in the previous section, we can conclude that although the NVIDIA Jetsons are more expensive than the Raspberry Pis, the price difference is negligible compared to the overall mission cost. Furthermore, their processing power, camera interfaces and availability of resources make the Jetsons especially attractive for this project.

On the one hand, the NVIDIA Jetson TX1 is clearly more computationally powerful than the TK1, has NVIDIA Maxwell™ Architecture incorporated in the GPU (specifically designed for image classification) and fits in one CubeSat unit (if the Orbitty Carrier is considered). On the other hand, the TK1 model seems to have enough computational power for this task and is considerably cheaper than the TX1. It also has CUDA processors, which would potentially suffice for the required tasks. However, its main drawback is that because of its dimensions, it would only fit in a CubeSat of 4U or larger. Since 6U CubeSats are much more widely used than 4U, the availability of components and resources for them is higher and thus, this design would be considered. Manufacturing and launching a 6U CubeSat would require a significant increase in the overall project budget.

For example, the company ISIS (www.isispace.nl) offers 3U CubeSat structures for a price ranging between US$3 936.67 and US$4 206.31, while 6U CubeSat structures are priced between US$7 927.27 and US$8 466.54.

The price difference for the launch, the most expensive element in a CubeSat mission, would be around US$150 000 for three extra units if launching with Kosmotras, the most widely used operator.

Considering that requirement PSR 22 targets a mission cost (development and launch) of €500 000, this price difference seems excessive.

Thus, the NVIDIA Jetson TX1 with the Orbitty Carrier was considered the most appropriate choice of on-board computer for this project.

Figure 3.9: Orbitty carrier shown with NvidiaJetson TX1 module (Connect Tech, 2017).

Note: During the development of this dissertation, the Nvidia Jetson TX2 became commercially available. Although the TX2 is more powerful than the TX1, it has not been included in this study

because it would unnecessarily increase the computing power at the expense of an increase in the power demand, with a peak of 19.6 V (Arrow Electronics, 2018), unaffordable for this satellite.

3.1.3. Spacecraft subsystems

The main drivers in the selection of the spacecraft subsystems are:

- Once again, the cost must be treated as a powerful design driver (PSR 22).
- All the subsystems must be compatible with the CubeSat form factor (PSR 36).
- All the components must be COTS and thus commercially available (PSR 37).
- The system must be designed to survive in the space environment for a minimum of two years (PSR 10). In this sense, thermal and radiation protection must be taken into consideration. Utilizing COTS components with flight heritage or that have already successfully passed the pertinent mechanical tests is thus beneficial.

Attitude determination and control subsystem

Attitude determination and control is essential for spaceborne remote sensing, both to achieve good quality images and to correctly geolocate them. This is especially relevant in the case of this project, due to the autonomy of the satellite and the absence of expert interpretation of the images. Thus, a solid ADCS subsystem is one of the most important elements for the success of the mission.

A satellite's attitude or orientation can be described by three rotations: yaw, pitch and roll, as represented in Figure 3.10.

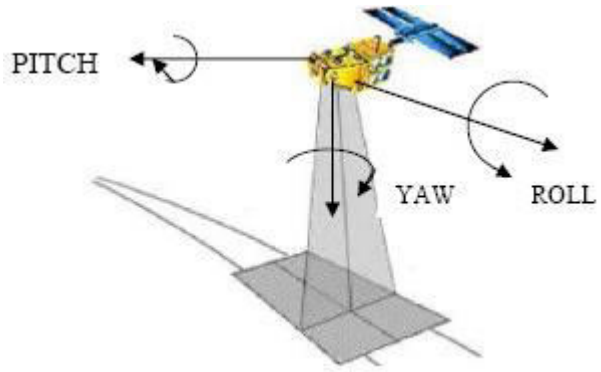

Figure 3.10: Roll, pitch and yaw rotations defining the satellite attitude (Bense, 2007).

PyrSat will be 3-axis stabilized and nadir-looking in all operation modes, although of course this is more relevant for the observation mode. The antenna used to communicate with the ground will be nearly omni-directional and thus no pointing is needed. For the first phase of the in-orbit technology demonstration the observations will be only to nadir, but tilting the satellite should be considered further in the mission. Being in a Sun-synchronous orbit, the orientation of the satellite with respect to the sun will be maintained constant. The attitude control system must be able to counter-balance disturbance torques and control the satellite attitude during maneuvers and after transient events, such as the satellite separation and deployment after launch, and following recovery from any ADCS failures.

The satellite's attitude model, represented in the satellite's body-fixed reference system, will be as follows:

- The origin of the reference system is on the satellite's centre of mass.
- The Z_{SC}-*axis* is pointing to nadir. This axis is perpendicular to one of the four side faces (30 cm x 10 cm) of the spacecraft.
- The Y_{SC}-*axis* is aligned with the velocity vector. This axis is perpendicular to one of the two bases (10 cm x 10 cm) of the spacecraft. This means that the satellite will be "lying down" on a lateral face parallel to the Earth's surface just below it.
- TheX_{SC}-*axis* is chosen so that the body fixed reference system is a right-handed coordinate system.

Nearly all the systems selected for the designed ADCS subsystem described below are provided by CubeSpace (South Africa) and are especially designed to interface perfectly with each other. Furthermore, CubeSpace also conceives CubeControl to work together with the OBDH CubeComputer, also. In this way, the project is promoting the national space industry in South Africa. All of them, except the GPS receiver, are available on CubeSatShop.com.

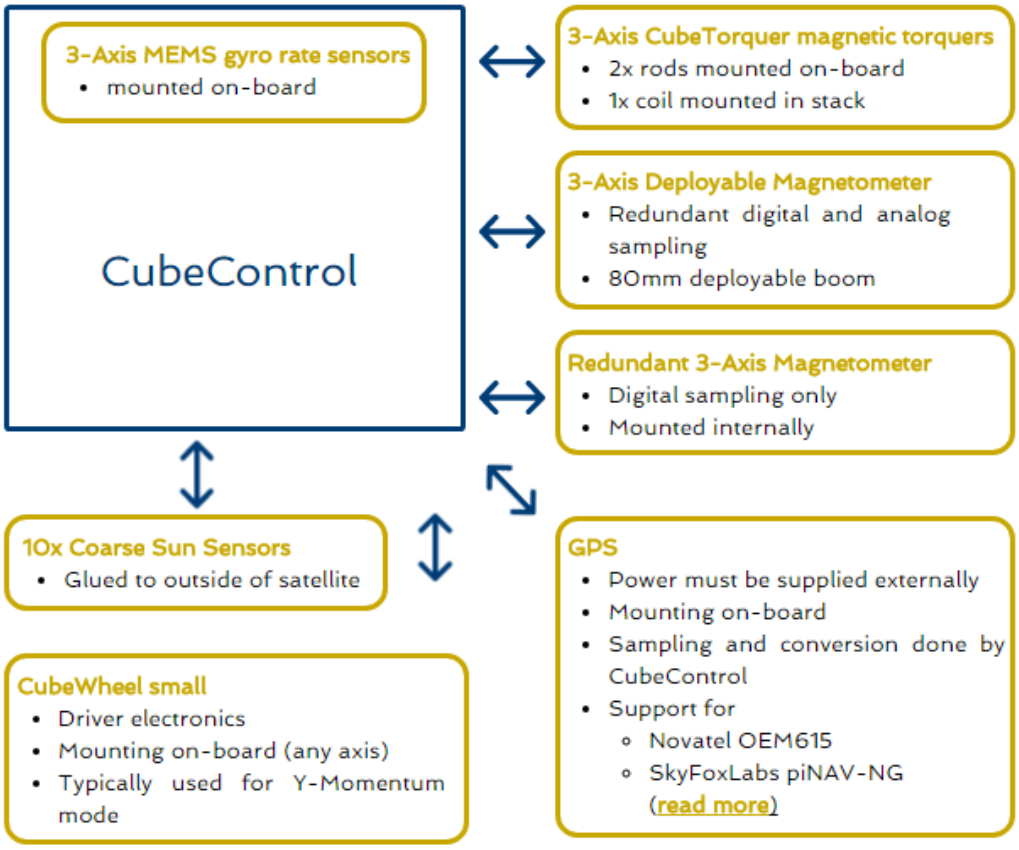

Figure 3.11: CubeSpace ADCS structure (CubeSpace, n.d). Out of these modules, the ones implemented in this mission will be the 3 - Axis Cube Torquer magnetic torquers, one CubeWheel small and a GPS unit.

CubeControl:

CubeControl is the actuator and sensor driver board that interfaces with all the ADCS elements. It was designed to integrate perfectly with other CubeSpace products (CubeSpace, n.d). As of June 2017, its price on CubeSatShop.com is 4 800 Euros.

This module has 3-axis micro-electro-mechanical MEMS rate sensors. It can be used together with others ADCS devices as shown in Figure 3.11.

CubeControl has a PC/104 form factor, compatible with CubeSat standard. The board and the rest of components, as well as the OBDH computer, have all flown on-board the QB50 precursor satellites. Its size and mass depend on the ADCS configuration and the installed systems. Without actuators, its power consumption is 250 mW and its operational voltage is in the range of 3.3 to 5 V. Its horizontal dimensions are 90 x 96 mm (CubeSpace, 2016a). As stated in CubeSatShop.com, the measurement updates of the on-board MEMS is 1 Hz.

From CubeSpace (2016a) and CubeSpace (2016b) it can be deduced that the mass of CubeControl is 56 g. Its price on CubeSatShop.com is €4 800.

CubeSense:

CubeSense is a fine Earth and sun sensor module compatible with many COTS CubeSat components. It is based on CMOS technology, featuring two different cameras that act like sensors and use on-board processing algorithms for image interpretation (processing of nadir and sun centroids). It has dual FPGA/SRAM system for redundancy and measurement updates at 1 Hz.

The nadir sensor has an accuracy of up to 0.2 degrees with the full planet in the field of view (FOV) of the sensor and the sun sensor also has an accuracy of 0.2 degrees over the whole FOV. The CMOS sensors have a resolution of 1024 x 1024 pixels, fisheye lenses of 180 degrees effective FOV and their locations can be configurable.

The operating voltage is from 3.3 V to 5 V, with a typical power consumption of 150 mW and a peak consumption of 360 mW. The dimensions of the PC104 board are 90 x 96 x 10 mm and those of the camera modules, 40 x 31 x 19 mm. Its operating temperature is in the range of -10 to 70 °C. Its mass is 80 g, including the cameras (CubeSpace, n.d.c). Its price is €4 800 (CubeSatShop.com).

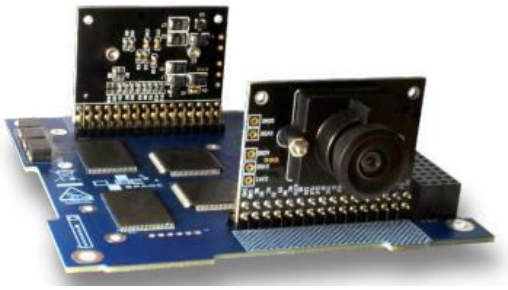

Figure 3.12: CubeSense (CubeSpace, 2016b).

3-Axis magnetic torquers: CubeTorquer&CubeCoil:

The CubeTorquer and CubeCoil are magnetic actuators designed by CubeSpace for CubeSat attitude control. Whereas the former has a ferromagnetic core, the latter has an air core.

The CubeTorquer is designed for near-perfect linearity. The low-profile design of the CubeCoil minimizes its weight. Both come with all the necessary interfaces to be mounted on CubeControl (CubeSpace, 2016b).

Two rods and one coil can be acquired through CubeSatShop.com for €1 600.

Their characteristics are summarized in Table 3.5:

Table 3.5: Properties of CubeTorquer and CubeCoil (CubeSpace, 2016b).

Properties	**CubeTorquer**	**CubeCoil**
Resistance	29 - 31 Ohm	80 - 83 Ohm
Inductance	150 Mh	60 mH
Nominal moment	± 0.24 Am^2	± 0.13 Am^2
Saturation moment	± 1.5 Am^2	-
Linearity	2.5 %	-
Residual moment	< 0.48 mAm^2	0 Am^2
Mass	28 g	46 g
Dimensions	Rod only: 60 (L) x 10 (Ø) mm With brackets and PCB: 18 x 14 x 62 mm	No PCB or fasteners: 90 x 96 x 6 mm

CubeWheel Small:

The miniaturized momentum wheel, CubeWheel small, is designed by CubeSpace to mount on CubeControl, via I2C, UART or CAN. It includes a brushless DC motor with vacuum-rated bearings, drive electronics and speed control algorithms.

It is mountable in the satellite's three body-fixed reference system axes. For the case of this project, it will control the Y_{SC}-axis. Controlling the rotation on the Y_{SC}-axis aims to reduce the geometric distortions due to varying satellite roll angle in the image.

Its performance is characterized by a speed range of up to 8000 rpm, a speed control accuracy better than 5 rpm, a maximum torque of 0.23 mNm and a momentum storage capacity of 1.7 mNms (at 8000 rpm).

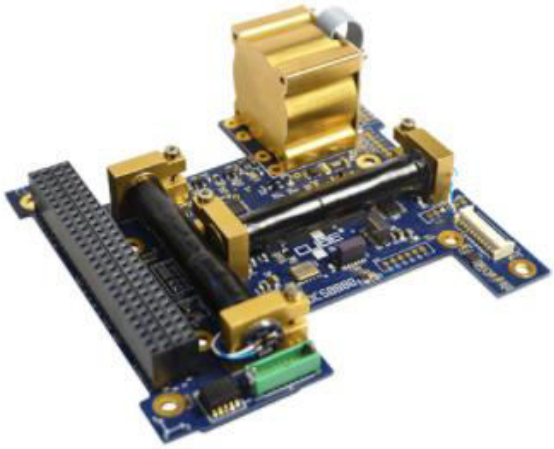

Figure 3.13: CubeControl with CubeWheel small and the two CubeTorquers (CubeSpace, 2016a).

The small version of CubeWheel measures 28 x 28 x 26.1 mm and weighs 60 g. The operating voltage is 3.3 V, while the battery can operate in a range of 6.5 V to 16 V. Although the typical power consumption is 120mW (at 2000 rpm), it can reach a peak of 720mW for the maximum torque. These power consumption values refer to a battery operating voltage of 8 V (CubeSpace, 2016d). The price of this unit on CubeSatShop.com is €4 300.

GPS Receiver and Antenna:

The selected GPS system comprises the piNAV-NG CubeSat GPS receiver and the piPATCH-L1 GPS antenna, produced by the company SkyFox Labs from Czech Republic. As derived from direct correspondence with the provider, both subsystems are space qualified and have already flown on-board the QB50 Pegasus satellite.

The GPS receiver is designed to receive GPS L1 signals and achieves the following performances:

- Position Accuracy +/- 10 m (95%, 2 sigma, on LEO)
- Velocity Accuracy +/- 10 cm/s (95%, 2 sigma, on LEO)
- Time Accuracy +/- 100 ns (95%, 2 sigma, on LEO)

It presents a very low power consumption (125 mW at 3.3 V) and is operational up to an altitude of 3600 km (SkyFox Labs, 2018).

The GPS antenna is a patch active antenna able to receive both GPS L1 signals and GLONASS signals. It allows satellite tracking even with nadir pointing. It is compatible with a power supply in the range of 2.7 to 5.5 V. At 3.3 V it presents a power consumption of 66 mW (SkyFox Labs, 2017).

The price of the whole system is €8 800 (€6 900 for the receiver and €1 900 for the antenna).

Communications subsystem

The uplink and downlink requirements will dictate what the telecommunications subsystem must be able to accomplish. The uplink will carry the telecommands sent by the ground station to the satellite; the downlink, the telemetry about the health and status of the satellite and its different subsystems, as well as the data product of the payload. By default, the latter will be a shape file. The operators will be able to choose another option in which the shape file will be downloaded together with information necessary to recreate the image on the ground in order to detect and correct errors.

Because of the similarity of the transmitted data, the two NASA projects mentioned earlier in this document can serve as a reference to choose an appropriate communications subsystem. EO-1's downlink capacity was 105 Mbps to be transmitted in S-band (variable to 2 Mbps), and X-band (105 Mbps). The uplink band was S-band (2 Kbps) (eoPortal Directory, n.d.b).

The RF communications system proposed for the hyperspectral CubeSat constellation is a SCR-102 S-Band radio, by Innoflight (Mandl et al., 2016). It can transmit (downlink) in the range of 2200-2300 MHz at up to 4.5 Mbps. The receiver (uplink) operates in the range of 2025-2110 MHz and up to 100 kbps, as specified in the Innoflight website innoflight.com.

Wertz and Larson (1999) establish as the typical requirements for uplink and downlink data rates:

- Command: 4000 bps typical (range of 2000 bps - 8000 bps).
- Health & status telemetry: 8000 bps is common (range of 40 - 10 000 bps).
- Mission/science: Low < 32 bps; Medium = 32 bps - 1 Mbps; High > 1 Mbps - 1 Gbps

They also highlight the advantage of selecting a large-beam-width antenna to be able to communicate with the ground station in a wide variety of viewing angles. Indeed, communications systems are often designed to receive signals over at least a hemisphere. In the case of this project a wide-beam antenna is suitable as opposed to a high-gain, directional one.

The mission/science telemetry downlink data rate is mission dependant. For this project, the mean access time of the satellite to a ground station in Cape Town is 575 sec or 9 min 35 sec. The size of a typical shapefile is in the order of several MB; in this project we will target 5 MB. Thus, if we want the mission data to be downloaded in one pass, the downlink rate must be on the order of 70 kbps.

In this line, an S band transmitter and antenna seem the most suitable option for this project. Early in the design and because of their competitive cost, the HISPICO transmitter with the antenna dedicated for it (by IQ wireless) were considered. Both are available online on www.cubesatshop.com. However, the simulation of the antenna in STK (with an aperture of up to 85 degrees) showed poor results. Because during the development of this work the UCT SpaceLab did not have a license for STK Communications, the antenna was simulated as a sensor with a cone half angle of 42.5 degrees. This should give good results for the analysis of the accesses of the antenna to Cape Town. There were 175 accesses in the total simulation time. Starting from the 1st of December 2017, there was a pass a day roughly during intervals of six days with intervals of twelve and six days in between. This would trigger the need for adding additional rely ground stations to the network. Furthermore, establishing an uplink

to command the satellite may be necessary in the intervals without connection. Thus, at least another fully operational (uplink/downlink) ground station should be installed in a different location. The global statistics of these accesses shown below:

Global Statistics

Min Duration	31	1 Feb 2018 09:05:35.454	1 Feb 2018 09:05:37.173	1.719
Max Duration	157	25 Oct 2018 20:35:17.172	25 Oct 2018 20:36:29.929	72.757
Mean Duration				56.570
Total Duration				9899.760

As the ideal ground station network for the mission is only one master ground station (for centralized control) and multiple downlink-only ground stations to accelerate the data distribution, this combination of antenna and transmitter was discarded at the expense of a price increase.

Other options available on CubeSatShop.com, such as the UHF/VHF ISIS full duplex transceivers, have a downlink data rate in the order of 1.2 to 9.6 kbps. Even in the case of the latter, the necessary time to download a packet of 10 Mbytes would be 1 h 9 min 27 sec, needing thus several passes to download it.

Thus, an option with a higher downlink rate is needed. The Bulgarian company EnduroSat offers CubeSat components at highly competitive prices. Although their flight heritage is not as established as for other companies, their products have successfully undergone mechanical and thermal tests (i.e. functional test, random vibration, sinusoidal vibration, pyroshock test, thermal cycling and some still must undergo the total ionization test) that qualify them for space. Selecting the components of the communication subsystem from them seems thus a reasonable option. Furthermore, a combination of an S-band/UHF transceiver (€7 000) and an S band patch antenna (€3 000) will result in a lower total cost than the previously considered system (€4 600 for the S-band patch antenna and €6 500 S-band HISPICO transmitter, without even considering an additional receiver that should be added to the system).

Antenna:

The EnduroSat S-band patch antenna features the following relevant characteristics (EnduroSat, 2016a):

- Impedance Matched Bandwidth (S11< -10dB): 2300-2500 MHz;
- RF output power: up to 4 W
- RF connector: Right angle MCX
- Insertion loss: less than 0.6 dB
- Gain up to 8.3 dBi
- Circularly polarized: Left Hand Circular Polarization (LHCP)
- Half Power Beam Width (HPBW) 71deg
- Compatible with lens up to 21 mm
- Weight: 64 g
- Dimensions: 98 mm x 98 mm x 12 mm

Simulating the antenna as a sensor with a cone half angle of 71 deg, the results obtained are satisfactory. The number of accesses of the satellite to a theoretical ground station in Cape Town, without considering obstacles that will depend on the location on the ground receiver antenna, is the

same as the previously computed accesses of the satellite to Cape Town (without the antenna): 1767, occurring five or six times a day during the simulated year. The total access duration is however somewhat reduced, but the difference is negligible (1016666.13 seconds versus the previous 1016666.14 seconds), with equal minimum, maximum and mean access duration.

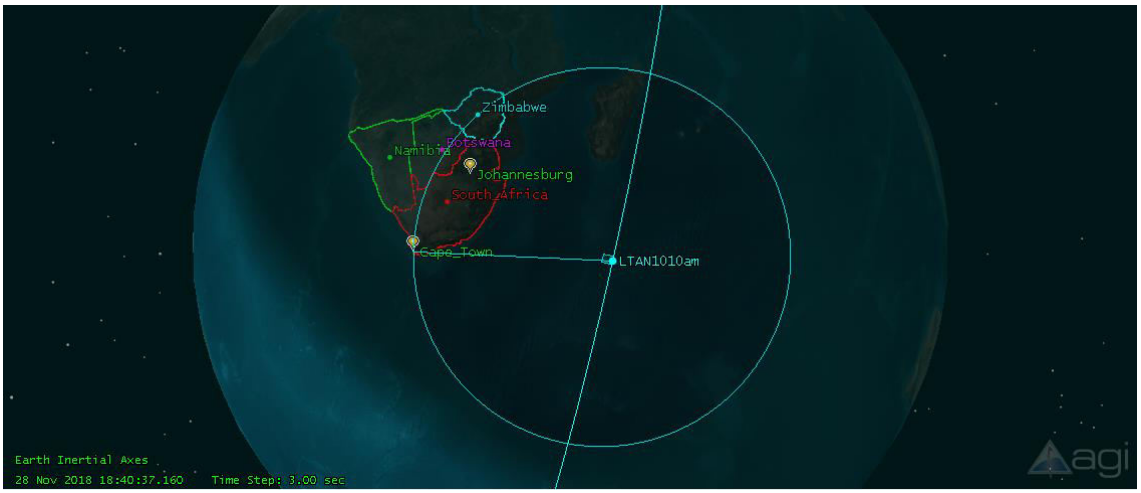

Figure 3.14: Coverage area of the antenna in one of the most unfavourable simulated passes, lasting only 181.82 sec, on the 28th of November 2018.

A UHF antenna must be installed on-board the satellite in order to be able to receive the telecommands sent by the ground station. The selected antenna, in order to ensure compatibility with the rest of the telecommunications subsystem, is a UHF antenna developed by EnduroSat.

The UHF antenna is circularly polarized and operates in the range 385 – 388 MHz. has a gain larger than 0 dBi and a maximum RF output power of 3.5W. Being the input voltage 5 V, the antenna presents a power consumption of 5 mV in sleep mode, and 1.25 W to 2.5 W for the antenna deployment (EnduroSat, 2017). The antenna will only be deployed once, as soon as the satellite reaches its operational orbit, and thus the power consumption during normal operations will only be 5 mV.

Transceiver:

The EnduroSat S/UHF transceiver module measures 90.2 mm x 95.9 mm x 25.2 mm and weighs 125 g. It offers dual-frequency communication via two independent transceivers on a single PCB. The UHF link is more suitable for telemetry and telecommand while the S-band link is dedicated to payload data. However, both can be used for uplink/downlink and provide redundancy to the system. The output power is also modifiable depending on the specific downlink requirements. The half-duplex UHF transceiver has two available data rates that can be programmed in-orbit. The S-band transceiver has four (250 kbps, 500 kbps, 1 Mbps and 2 Mbps).

UHF will be used for the uplink and S-band for the downlink. The 5MB data will be downloaded in 4 seconds at a downlink data rate of 2 Mbps. The UHF receiver has a power demand in the range of 0.109 to 0.231 W, with a typical value of 0.125 W. The S-band transmitter at a data rate of 1 Mbps has a power consumption of 4.9 W for data packages of 30 bytes and 5.38 W for packages of 120 bytes (EnduroSat, 2016a).

The main features of this transceiver are listed in Table 3.6 (Endurosat, 2016b):

Table 3.6: Properties of the communication module by EnduroSat.

Transceiver	S - Band	UHF
Frequency range	2400 - 2480 MHz	430 - 440 MHz
Typical transmit power	2 W (33 dBm)	1.5 W
Power amplifier efficiency	> 40 %	> 70 %
Power supply	5 V +/- 0.25 V	3.2 - 3.4 V
Typical current consumption	up to 1.35 A	0.82 A
Frequency stability	+/- 10 ppm	+/- 2.5 ppm
Data rate	250 kbps – 2 Mbps	200 - 1200 bps
Sensitivity	-94 to -86 dBm	-113 to -121 dBm
Interfaces	SPI (SLAVE)	UART @ 9600 bps / I2C (optional)

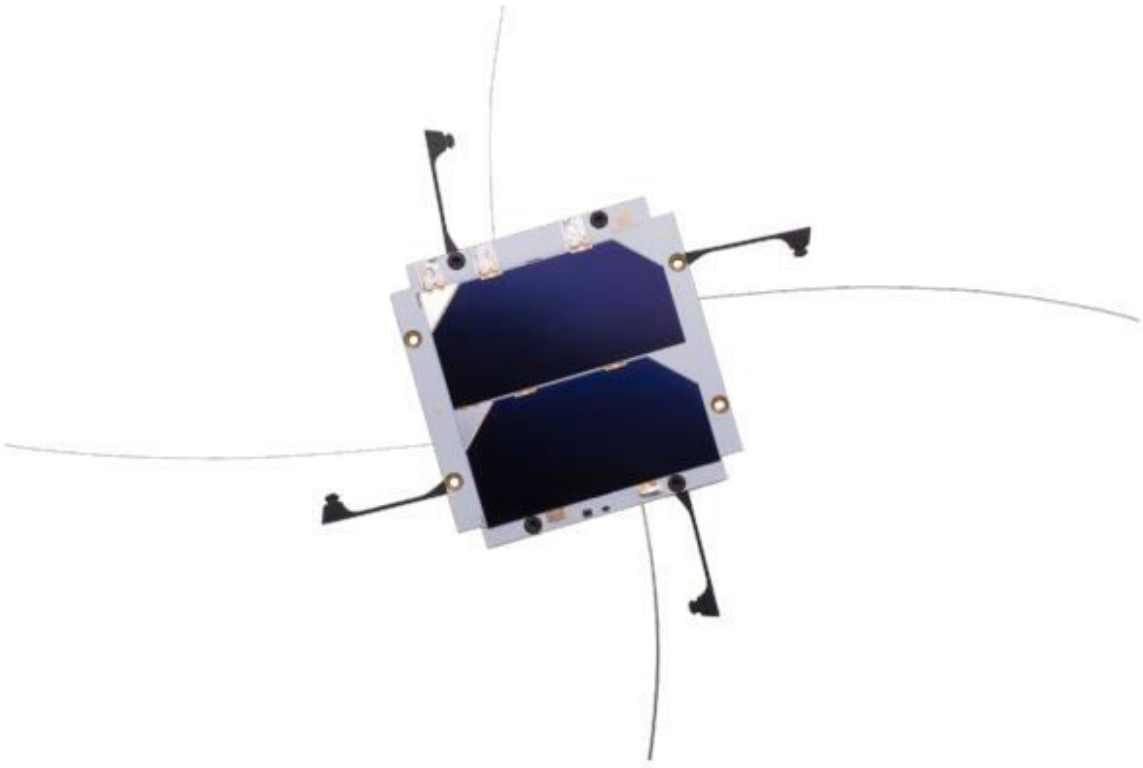

Figure 3.15: EnduroSat UHF antenna. The solar cell shown in the Figure is not included in the antenna pack but can be acquired separately from EnduroSat (Endurosat, 2017).

Figure 3.16: (From left to right) EnduroSat patch S-band antennaand UHF/S-band transceiver (Endurosat, 2016a and 2016b).

Command and data handling subsystem

As mentioned earlier, the selected on-board computer is CubeComputer, a general purpose OBC by CubeSpace. This computer has an ARM Cortex-M3 MCU, achieving high performance at a very low power. It is compatible with the CubeSat standard and many existing CubeSat components. It is suitable for command and data handing (CD&H), telemetry, tracking and command (TT&C), mass storage and ADCS.

The available memory is: 256 KB EEPROM, 4 MB flash for code storage and 2 external 1 MB SRAM for data storage. It also has a socket for a MicroSD of up to 2 GB.

CubeComputer is protected against radiation through complex error detection and correction techniques and the operating temperature is from -10 to 70 °C (CubeSpace, 2016e).

Its operating voltage is 3.3 V, with a typical power consumption of 200 mW. Its mass is up to 70 g and its dimensions are 90 mm x 96 mm x 10 mm (CubeSpace, 2016e). Its price is €4 500 (CubeSatShop.com).

Figure 3.17: CubeComputer (CubeSpace, 2016e).

Power subsystem

The on-board power subsystem must be able to provide the payload and the rest of satellite subsystems with enough power for a flawless operation in the different modes. The most power consuming elements are the remote sensing payload and the communications subsystem. The satellite will have three different operation modes:

a) **Observation mode:** After receiving a command from the dedicated computer, the camera will capture an image and send it back to the computer. This will take place when the satellite is in the sunlight zone.

b) **Processing mode:** Once the computer receives the image sent by the camera, it processes it (processes the raw data, performs geometric and radiometric correction and geolocates every pixel in the image), carries out a classification task for feature recognition and creates a GIS map layer showing the relevant features for the specific application.

c) **Communications mode:** In this mode the satellite communicates with the ground station, receiving telecommands (uplink) and sending telemetry (downlink).

To maximize resources, opportunities such as when the region on the Earth under the satellite is covered by clouds or in night-time, both of which preclude the system from taking useful images, the satellite should be used for image processing and communications with the ground station.

The tasks and level of power required by the most demanding components are represented in the following table.

Table 3.7: Tasks and power requirements of the most power demanding subsystems in the different operation modes.

Subsystem		Observing mode		Processing mode		Communications mode	
		Tasks	Power	Tasks	Power	Tasks	Power
Payload	HS Camera	Receive command, capture and send image	Maximum	None	Idle	None	Idle
	Dedicated computer	Send command and receive image	Medium	Process and classify the image	Maximum	None	Idle
Comm. Subsystem		None	Idle	None	Idle	Receive TM and send TC	Maximum

Power will be provided by solar panels and stored in a battery. It must then be distributed to the other satellite subsystems: ADCS, OBDH, communications and. The following table represents the power budget for PyrSat.

Table 3.8: PyrSat power budget (not including the EPS subsystem).

Subsystem		**Power demand**		
ADCS	**CubeControl**	250 Mw		
	CubeSense	150 Mw nominal; 360 mW peak		
	CubeTorquer	NA		
	CubeCoil	NA		
	CubeWheel	120 Mw nominal; 720 mW peak		
	GPS receiver and antenna	191 mW		
OBDH: CubeComputer		200 mW		
Total power demand when the satellite is not tasked (idle state)		0.91 - 1.72 W		
Operation mode		*Observation*	*Processing*	*Communications*
Comm. subsystem	**Passive S-band antenna**	NA	NA	NA
	UHF/S-band Transceiver	Idle	Idle	UHF receiver: 109 – 231 mW (nominal 125 mW) S-band transmitter: Up to 5.38 W
Payload	**HS LS100 camera**	1.6 W	Idle	Idle
	Jetson TX1 dedicated computer	8 – 10 W	8 – 10 W typical CUDA load 15 W peak	Idle
Total power demand		10.51 – 13.32 W	8.91 – 16.72 W	Up to 1.95 W uplink Up to 7.1 W downlink

Table 3.8 shows the absolute minimum and maximum power demand of the system. The maximum value will be requested in processing mode and corresponds to the TX1 computer's peak power demand. However, although the power subsystem must be able to meet this power demand to ensure fully operational capabilities, it is important to consider that in most scenarios this will not be the case. This is the image processing tasks requested from the dedicated computer will not be as computationally demanding as other applications, such as gameplay or the most demanding vision routines, that may produce this power peak. Indeed, with the purpose of benchmarking the TX1,

developers at Nvidia tested Caffe AlexNet Neural Networks image classifier on the computer and it was able to classify 258 images per second with a power demand of 5.7 W (Franklin, 2015).

Electrical power system:

The selected EPS is produced by NanoAvionics for a basic price of €3 000. The low power configuration, in principle sufficient for this mission, provides 23 Wh. It contains a battery of two cells.

The input from the solar panels is converted into battery power, with a design that achieves maximum efficiency even in adverse situations such as low light or highly dynamic charging environment (e.g. when the satellite is spinning).

The power system incorporates a fail-safe design for the case of a microcontroller malfunction that allows activating an emergency mode in which selected emergency channels will maintain the satellite operational. Additionally, the system has a watchdog timer to reset the microcontroller in the case of a fault.

The input and output converter efficiency are over 90 %. Its power consumption is not specified but through comparison with similar systems is assumed to be below 1 W. It features three regulated voltage trails, namely 3.3 V, 5 V and a third configurable one in the range of 3 V – 18V. All these rails can produce a maximum output power of 20 W. Unregulated voltage can induce a maximum power of 28 W. The EPS can handle an input voltage in the range of 2.5 to 18 V, with a maximum input power per converter of 25 W and a maximum charging power of 10 W.

Its dimensions are 92.9 mm x 89.3 mm x 25 mm and its mass is 300 g (NanoAvionics, n.d.a).

In conclusion, a maximum power of 20 W (when the battery is fully charged) will be provided, for a maximum demand below 17.72 W (including the EPS) in the processing mode. Thus, the electrical power system should be able to cope with all the required tasks.

Solar panels:

In view of these power requirements, a configuration of three body-mounted side 3U solar panels provided by ISIS was considered appropriate. Each side solar panel can provide a maximum of 6.9 W in direct solar incidence, which means a total of 13.8 W with two of the CubeSat are illuminated by the sun. The nominal voltage supply of the cells is 3 V, although configurations of 5 and 8 V can be supplied on demand. The cells are made of GaAs and have an efficiency of 30 %. They have a thickness of 2.5 mm and weight (for each 3U side panel) 150 g. ISIS solar panels have flight heritage since 2013 (ISIS, 2016a).

Figure 3.18: Custom solar panels by ISIS (ISIS, 2016a).

Out of the 13.8 W power supply provided by two side solar panels, the maximum charging power of the battery is 10 W. If the power dissipated in the satellite when it is in charging mode and all the subsystems are in an idle or sleeping mode is 2 W, the charging power will be 8 W. This means the battery will take 2 hours and a half to be charge up to its full capacity (23 Whr). Since the orbital period is 95.21 min and only half of the orbit (47.61 min) will be in sunlight, the battery will be fully charged after 3.15 orbits, or 5 hours (3.15 times the orbital period). This time must be taken into account when planning the mission operations.

Direct correspondence with ISIS revealed that the price of each 3U panel is €4 950 including the harnessing, a protective cover, test reports of the solar arrays cells' performance and the customization of the mechanical and electrical layout. Thus, the total cost will be €14 850.

The degradation of the solar arrays over time must been considered in the design. ISIS (2016a) states that their solar cells are radiation tolerant for a minimum of two years, which corresponds to the required mission operational life (PSR 10).

Structure

In order to comply with the primary objectives of the mission, the satellite must adopt the CubeSat standard, which will dictate the spacecraft structure. The number of CubeSat units for the satellite will be the minimum necessary to accommodate the payload and all the subsystems, and so reduce the development and launch cost. Considering the size of the rest of subsystems, a 3U form factor will be selected for this mission. The structure provider will be ISIS.

The mass of the ISIS 3U CubeSat structure is 304.3 g. The dimensions of the outside envelope are 100 mm x 100 mm x 340.5 mm and those of the inside envelope are approximately 98.4 x 98.4 x 98.4 mm (ISIS and CubeSatShop.com, n.d.). Depending on the configuration the price can vary from €3 650 to €3 900. This structure has flight heritage since 2013 (ISIS, n.d.).

3.1.4. Overview of the whole system

Figures 3.19 and 3.20 show a schema of the designed satellite (front view and a bottom-up view). Three of the lateral faces (30 x 10 cm) will be covered by solar panels. The S-band and the CubeSense nadir sensor will be mounted on the fourth lateral face that will accommodate also the aperture of the hyperspectral camera. The CubeSense sun sensor will have its aperture on the opposite lateral face to that one of the nadir sensor and so will be necessary to accommodate it among the 3U lateral solar panels. The UHF antenna will be mounted on one of the two CubeSat bases (10 x 10 cm).

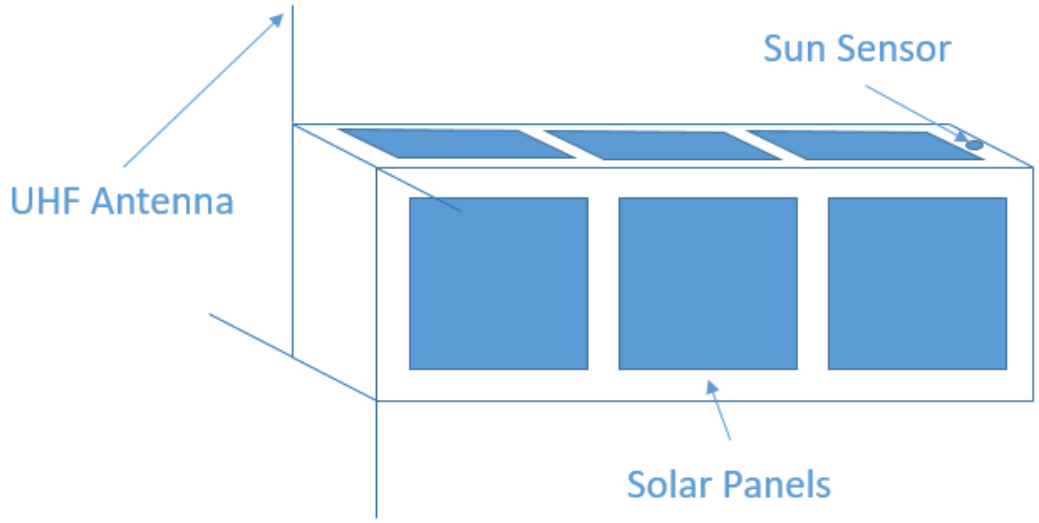

Figure 3.19: Front view of the PyrSat satellite.

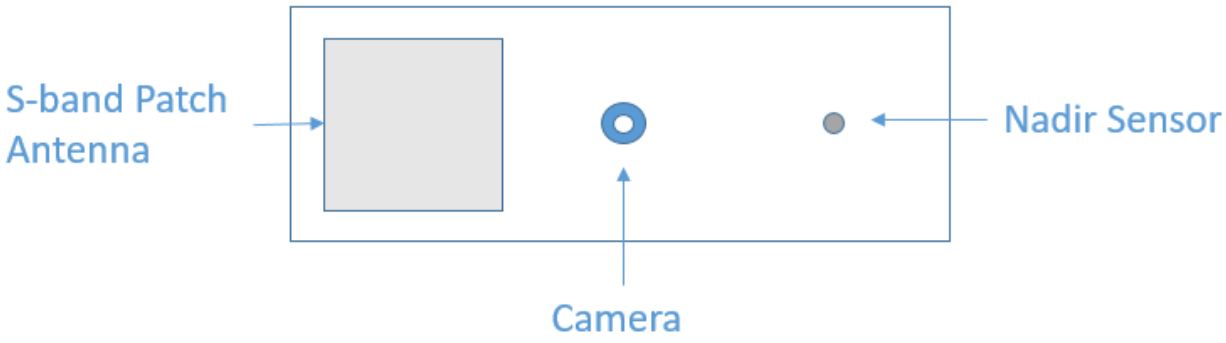

Figure 3.20: Bottom-up view of the PyrSat satellite.

Table 3.9: Overall system properties.

Subsystem			Dimensions	Mass	Price (June 2017)
ADCS	**CubeControl (CubeSpace)**		90 x 96 mm	56 g	€4 800
	CubeSense (CubeSpace)		40 x 31 x 19 mm	80 g	€4 800
	CubeTorquer (CubeSpace)		18 x 14 x 62 mm (with brackets and PCB)	28 g	€1 600
	CubeCoil (CubeSpace)		90 x 96 x 6 mm (no PCB or fasteners)	46 g	
	CubeWheel small (CubeSpace)		28 x 28 x 26.1 mm	60 g	€4 300
	GPS system (SkyFox Labs)	**Receiver**	71.1 × 45.7 × 11 mm	24 g	€6 900
		Antenna	98 × 98 × 14.5 mm	50 g	€1 900
OBDH: CubeComputer (CubeSpace)			90 x 96 x 10 mm	70 g	€4 500
Comm. subsystem	**Passive S-band antenna (Endurosat)**		98 x 98 x 12 mm	64 g	€3 000
	UHF Antenna (EnduroSat)		98 x 98 x 1.6 mm	85 g	€3 000
	UHF/S-band Transceiver (Endurosat)		90.2 x 95.9 x 25.2 mm	125 g	€7 000
Payload	**HS LS100 camera (XIMEA)**		26 x 26 x 31 mm	32 g	€17 700
	Jetson TX1 dedicated computer (Nvidia)		50 x 87 mm	144 g	€279
	+ Orbitty Carrier (Connect Tech's)		50 x 87 mm	41 g	€141
Power subsystem	**3U side solar panels (x4) (ISIS)**		2.5 mm thick	150 g x 3 = 450 g	€4 950 x 3 = €14 850
	EPS (NanoAvionics)		92.9 x 89.3 x 25 mm	300 g	€3 000
Structure: 3U CubeSat structure (ISIS)			Outside envelope: 100 x 100 x 340.5 mm Inside envelope: ~ 98.4 x 98.4 x 98.4 mm	304.3 g	€3 650 - €3 900
Overall system			Outside envelope: ~ 105 x 105 x 343.7 mm	1.96 kg	€81 420 - €81 670

Table 3.9 summarizes the system design, excluding the power requirements already covered in Table 3.8.

The prices in this Table are expressed in Euros. The prices were converted to South African Rands from Euros and US Dollars according to the conversion rate of the 13th of February 2018. On this date, 1 USD = 0.81 EUR.

In relation to the satellite overall mass, it is important to consider that Table 3.9 does not include the mass of all the bolts, cables and other structural and electrical connection elements. The actual final satellite mass will be then somewhat over the mass shown in the Table.

3.1.5. Orbital lifetime and end-of-life disposal

In order to comply with requirements PSR 30 and PSR 31, the satellite must remain in orbit (i.e. without re-entering the atmosphere) for a minimum of two years but the end-of-life disposal must be done within a maximum of 25 years after the mission end-of-life.

The impact of the atmosphere on an Earth orbit is significant in orbits below 500 km. This altitude corresponds to the approximate position of the thermopause that divides the two upper layers of the atmosphere: the Thermosphere and the Exosphere. Indeed, the average altitude of the thermopause is 700 km, although it varies with solar activity from 500 km to 1000 km (Braeunig, 2014).

The few air molecules that the atmosphere contains at that altitude cause atmospheric drag on the satellites, which makes them naturally decay. In the LEO region, the atmospheric density is determined by the space weather, in particular by the solar flux and the particles coming from the magnetosphere. These effects are expressed by means of the Solar Radio Flux (F10.7) and the Geomagnetic Index (Ap). Both indices are date-dependent, since they depend on the precise solar and geomagnetic activity on an initial date (i.e. the launch date, when the satellite is injected in the application orbit).

The atmosphere model valid from where the atmospheric density can be derived for an altitude comprised between 100 and 500 km is defined by the following system of equations:

$$T = 900 + 2.5\,(F10.7 - 70) + 1.5\,Ap \qquad [\mathrm{K}]$$

$$m = 27 - 0.012\,(h - 200) \qquad 180 < h\,[km] < 500$$

$$H = \frac{T}{m} \qquad [\mathrm{km}]$$

$$\rho = 6x10^{-10}\,exp\,(-\frac{h - 175}{H}) \qquad [\mathrm{kg\,m^{-3}}]$$

The atmospheric drag experienced by a satellite in orbit in, the opposite direction to its motion, can be expressed as:

$$D = \frac{1}{2}\rho v^2\,A\,C_d$$

where ρ is the atmospheric density, v is the orbital velocity, A is the cross-sectional area of the satellite, perpendicular to its direction of motion, and C_d is the drag coefficient, that acquires an approximate value of 2 at the altitudes where satellites generally fly. The cross-sectional area and the drag coefficient are normally englobed into what is called the "efficient cross-sectional area", with $A_e = A\,Cd$. Introducing the expression for the atmospheric drag in Newton's second law and using energy considerations for a circular orbit, the variation of the orbital radius and period with time can be deducted as (IPS Radio & Space Services, 1999):

$$\frac{dP}{dt} = -3\pi a\rho\frac{Ae}{m}$$

Finally, the decay time can be calculated iterating this equation and that of the orbital period shown earlier in this Chapter (Section 3.1.1. of this dissertation) and the atmospheric model. The F10.7 value generally used is the mean value calculated over the 90 days previous to the initial date (IPS Radio & Space Services, 1999).

Isana Kashiwai (n.d.) developed an online orbital decay calculator based on the previous analysis. The input parameters are the satellite mass and cross-sectional area, the initial orbital altitude, Solar Radio Flux (F10.7) and the Geomagnetic Index (Ap). These two last variables can be obtained online from a website where the Belgium organization Parsec vzw updates the space weather parameters, daily (SpaceWeatherLive, 2018). SpaceWeatherLive.com obtains these parameters from the NOAA / NWS Space Weather Prediction Center. For a hypothetic launch on the 31st of December 2017, start date for the SDK orbital propagation in Section 3.1.1., the F10.7 90 days mean was 73 and the observed Ap, 2. With these values, a satellite mass of 2 kg (derived from Table 3.9 and adding some margin for bolts and cables), a cross-sectional area of 0.01 m^2 (10 cm x 10 cm) and a 550 km initial altitude the resulting evolution of the orbit with time is expressed in Table 3.10. Re-entry is assumed to occur at an altitude of 180 km. With exception of the heaviest satellites, any satellite at that altitude will have a lifetime or only a few hours (IPS Radio & Space Services, 1999).

Although in principle this analysis is only true for an orbit under 500 km, it constitutes a fair approximation to the specific case of this mission, with an orbit of 550 km.

As can be seen in Table 3.10 the orbital lifetime of a satellite of these characteristics launched into space on a day with a space weather activity similar to that of the 31st of December of 2017 is approximately 43425.29 days. This figure corresponds to 120.62 years. Because this time is much longer than the 25-year end-of-life disposal requirement, some external means of Active Debris Removal (ADR) will be necessary. Because research on ADR mechanisms is needed to ensure a sustainable access to space and it is a currently popular research line, the PyrSat team could engage with a research facility or university and put the CubeSat at their disposition for research purposes upon the end-of-life of the mission. This option would promote research at the same time than ensuring the safe satellite disposal and non-contamination of the LEO region.

Table 3.10: Orbital decay due to atmospheric drag.

TIME(days)	HEIGHT(km)	PERIOD(mins)	MEAN MOTION(rev/day)	DECAY(rev/day^2)
0	550	95.61	15.05	0
7575.5	539.99	95.43	15.08	0
14585.4	529.99	95.22	15.12	0
20283.39	519.99	95.02	15.15	0
24902.79	509.99	94.81	15.18	0
28637.79	499.99	94.6	15.22	0
31649.69	489.99	94.4	15.25	0
34072.09	479.99	94.19	15.28	0
36015.09	469.99	93.98	15.32	0
37569.59	459.99	93.78	15.35	0
38809.89	449.99	93.57	15.38	0
39796.79	439.99	93.37	15.42	0
40580.09	429.99	93.16	15.45	0
41200.19	419.99	92.96	15.49	0
41689.69	409.99	92.75	15.52	0
42075.09	399.99	92.55	15.55	0.0001
42377.69	389.99	92.34	15.59	0.0001
42614.69	379.99	92.14	15.62	0.0001
42799.89	369.99	91.93	15.66	0.0002
42944.09	359.99	91.73	15.69	0.0002
43056.19	349.99	91.52	15.73	0.0003
43142.99	339.99	91.32	15.76	0.0004
43210.19	329.98	91.12	15.8	0.0006
43261.89	319.98	90.91	15.83	0.0007
43301.69	309.97	90.71	15.87	0.001
43332.19	299.97	90.51	15.9	0.0013
43355.49	289.97	90.3	15.94	0.0017
43373.29	279.96	90.1	15.98	0.0023
43386.79	269.98	89.9	16.01	0.003
43397.09	259.95	89.69	16.05	0.004
43404.89	249.9	89.49	16.09	0.0054
43410.79	239.81	89.29	16.12	0.0072
43415.19	229.81	89.08	16.16	0.0096
43418.49	219.84	88.88	16.2	0.0129
43420.99	209.74	88.68	16.23	0.0174
43422.89	199.43	88.47	16.27	0.0237
43424.29	189.17	88.26	16.31	0.0322
43425.29	179.31	88.26	16.31	0.0322

3.2. Ground segment

There will be a master ground station (integrated with the mission operations centre) and a network of auxiliary downlink-only ground stations that will download the data from the satellite and transmit them to the master ground station via the Internet. The master ground station will then transmit the data product to the end users. All the on-ground data transfers will be done via Internet.

Users will submit applications for requested observations directly to the master ground station via the Internet, which will be scheduled according to a priority ranking. Once downloaded, the mission product will be transmitted to the users via the Internet. The ground operators can also select an option to download additional information necessary to simulate or recreate the whole HS image to evaluate the system performance and correct possible errors.

Figure 3.21: Antenna for the VHF/UHF/S-band ground kit (NanoAvionics, n.d.b).

Low-cost ground stations for CubeSats are also commercially available. NanoAvionics offers a complete VHF/UHF/S-band ground station kit for the price of €25 125. It includes:

- Yaesu FT-817, a HF/VHF/UHF self-contained multi-mode Portable Transceiver or SDR USRP B210, a Dual Channel Transceiver (70 MHz - 6GHz) with housing (Optional).
- SCS Tracker DSP TNC that supports 300Bd AFSK (audio-frequency shift keying), 1200Bd AFSK and 9600/19200 FSK (G3RUH).
- SPID RAS azimuth and elevation rotator including controller with rotator dish mounting.
- Parabolic Mesh dish kit of 1.5 meter diameter and 6mm mesh.
- High Gain (up to 15 dBD gain) UHF Yagi antenna array available in three polarizations: vertical, horizontal and circular.
- Hispico S-band receiver assembled in a 19” rack.
- S-band FEED, including: RX-Antenna, LNA, filter, bias-tee for powering, connectors and housing and 50m RF-cable to the receiver.
- Main power switch for full remote control.

It also comes with all the necessary software pre-installed in a Linux server. The ground station software comprises three modules:

- Mission Control Software (MCS)

- Hamlib: Standard data protocol to communicate using radio equipment.
- GPredict: It allows satellite tracking and Doppler effect estimation.

Remote operation of the ground station is also possible (NanoAvionics, n.d.b).

3.3. User segment

The users of the data will be GIS analysts able to interpret the vegetation fire risk and burn scar products and combine it with other thematic information. The final users, who will translate the data to action, will mainly be firefighting units and decision makers. The data will be produced on demand according to the users' needs.

Users will request observations via the Internet to the ground segment. Later they will receive a notification stating the scheduled time of their observation. Finally, once the data have been captured and the product has been developed on-board the spacecraft, it will be downloaded to the closest available ground station, sent to the master ground station and retransmitted to the user via the Internet.

3.4. Launch segment

3.4.1. Launch vehicle

The launch cost is the most expensive element in a CubeSat project.

Many the current CubeSat launches are done on converted Russian rockets by companies such as Eurokot or Kosmotras. Currently, the launch cost on Kosmotras is about US$50 000 per single cube (1U).

CubeSats can also be launched as a secondary payload on larger rockets, with a cost in the range of (US$2.7K - US$12K)/kg.

There are also other punctual opportunities, mainly research-based, that offer free launches. For example, the NASA's CubeSat Launch Initiative offers universities and schools in America a free launch opportunity on board rockets that are going to be launched (Madry, 2016).

Additionally, there are some services developed specifically for CubeSats:

- The Japanese ISS module has an airlock that can be used to launch CubeSats. However, the cost of this service is unknown.
- The project Nanoracks also launches from the ISS, with a price of US$85 000 per cube.
- Sherpa Containerized, by Spaceflight Industries, offer launch to LEO for 3U - 12U CubeSats at a cost of US$295 – US$995 (Madry, 2016).

The specific choice of a launch provider for this project will depend on the availability of different systems. Because the satellite does not have autonomous propulsion capability, the launcher will inject it directly in the operational orbit (h = 550 km; i = 97 °, LTAN = 10:10 AM).

Alternatively, ISIS Launch Services could be used. ISIS offers small satellite developers piggyback launch possibilities where the company organizes every aspect of the launch campaign: launch acquisition and coordination; technical interface control; launch deployer and interface hardware; full campaign management; logistics coordination and support and launch vehicle integration (ISIS, 2018).

3.4.2. Launch interface

The selected CubeSat deployer is ISIPOD by ISIS, to use in combination with the ISIS Launch Services or to be purchased independently.

The 3U configuration has a mass of 2 kg and the dimensions of the envelope are 182 mm (H) x 127 mm (W) x 414 mm (L). The typical payload mass is 3 kg and the maximum, 6 kg.

ISIPOD does not have a battery nor employs pyrotechnics and protects the satellite from the outer environment. Furthermore, it is compatible with numerous launch vehicles, which will increase the number of launch opportunities (ISIS, 2016b).

Chapter IV. Autonomous on-board image analysis and classification

The objective of this Chapter is to discuss the on-board image processing software architecture for PyrSat. Due to the limited time and resources available for this work, this software has not been developed and will remain as future work. This Chapter is intended to serve as a reference document for the future development of the software platform by the project software engineers of PyrSat.

Firstly, the problem to be addressed by this software platform will be presented. Secondly, there will be an introduction to the basic theoretical aspects of image processing, such as spectral and geometrical correction methods. Finally, the specific characteristics of the image processing software tools for the PyrSat mission will be described. That is, the development environment (i.e. the software and programming languages used), the software development process and the final software product that will be installed on-board the payload data microprocessor.

This preliminary work is intended to inform for the development of the software at a later stage.

4.1. Problem statement

Hyperspectral remote sensing can be extremely useful for a variety of applications, due to its ability to capture information about the sensed objects in hundreds of narrow bands over a wide region of the electromagnetic spectrum. However, the large size of hyperspectral images poses highly demanding requirements on the downlink and requires:

1. Complex ground station infrastructure, including high-performance antennae.

2. Skilled image processing specialists to convert the complex hyperspectral data into meaningful products useful for the end-users.

3. Huge on-board storage capability.

4. Limited data download time, which triggers a longer on-board storage need, and precludes capturing of new images until the memory is read out.

5. In order to cope with the demanding downlink requirements, the satellite's communications subsystem must be able to achieve a high performance.

These requirements ultimately result in a highly costly and complex system, only affordable for a limited number of users.

Thus, the main goal of this project is to change this paradigm and create on-board the final data product to be directly retransmitted to the end users by the ground station. The format of this product will be a shape file (GIS layer) representing burned areas and a categorization of the vegetation fire risk level. The burned area product will only represent two categories (burned / non-burned) and the fire risk maps will represent four risk levels (low / moderate / high / extreme). The ground operators may alternatively

select to download the raw data for analysis on the ground and for system performance evaluation. Lastly, the downloaded product shall be accompanied by ancillary data such as the date and time of the capture as well as the level of confidence of the derived product. All these aspects are explicit in the mission requirements PSR 16 to PSR 21.

4.2. Image processing fundamentals

In order to convert the hyperspectral raw data into a meaningful shape file representing only the information of interest, the data must undergo the following transformations:

4.2.1. Radiance to reflectance

When analysing hyperspectral data, there are two main physical attributes of the sensed surface and reflected light that must be taken into consideration: spectral reflectance and spectral radiance.

- The *spectral reflectance* is the ratio of reflected energy to incident energy as a function of wavelength; it is characteristic of each material and so can be used to differentiate them. The *spectral curve* or *spectral signature* is the plot of the reflectance of a certain object over different wavelengths in the electromagnetic spectrum. Acute depressions of this curve are called *absorption bands* and their positions are useful for discriminating materials. Reflectance values are expressed on a scale ranging from 0 to 1 or as a percentage and are unitless.

  Due to the often limited spatial resolution of remote sensing sensors, the radiation coming from different individual materials or *end members* can be mixed in the same pixel, resulting in *composite or mixed spectra*.

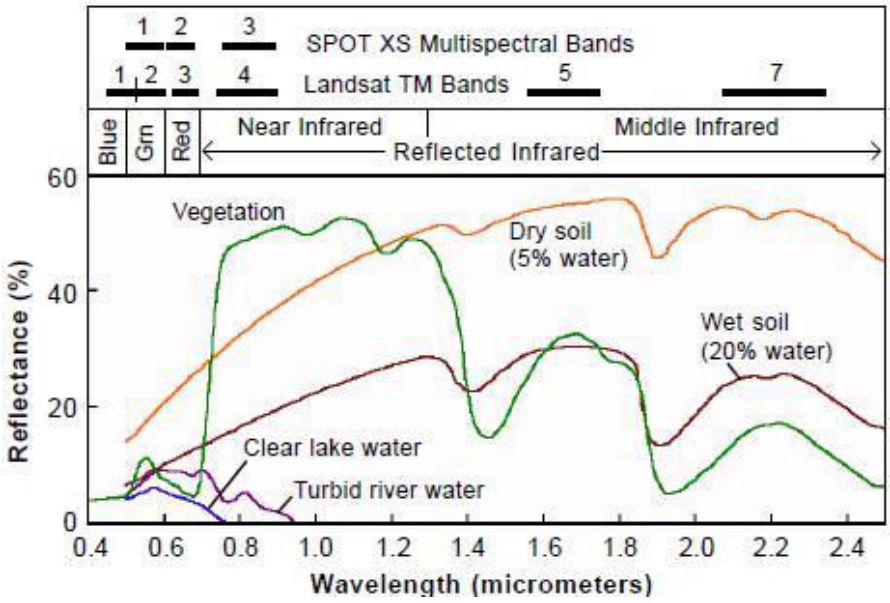

Figure 4.1: Spectral response of different features and the spectral bands of the SPOT XS and Landsat TM instruments (MicroImages, 2012).

- *Spectral radiance* is the signal strength measured by the sensor and represents the amount of reflected light that arrives at the detector as a function of wavelength. It is not only affected by the spectral reflectance of the sensed objects, but also by the solar spectrum, the interaction of this radiation with the atmosphere in its downward and upward passes, the lighting conditions and characteristics of the specific sensor. These factors affect the ability to retrieve the reflectance values of sensed features and introduce within-scene variability (MicroImages, 2012).

  Figure 4.2 shows the average of the brightness measured by the AVIRIS sensor in 25 images of a bright dry lake bed surface in the Cuprite, Nevada. Since the natural spectral signature of this area is relatively flat and featureless, the shape of the curve corresponds to the solar spectrum with atmospheric absorption bands (MicroImages, 2012).

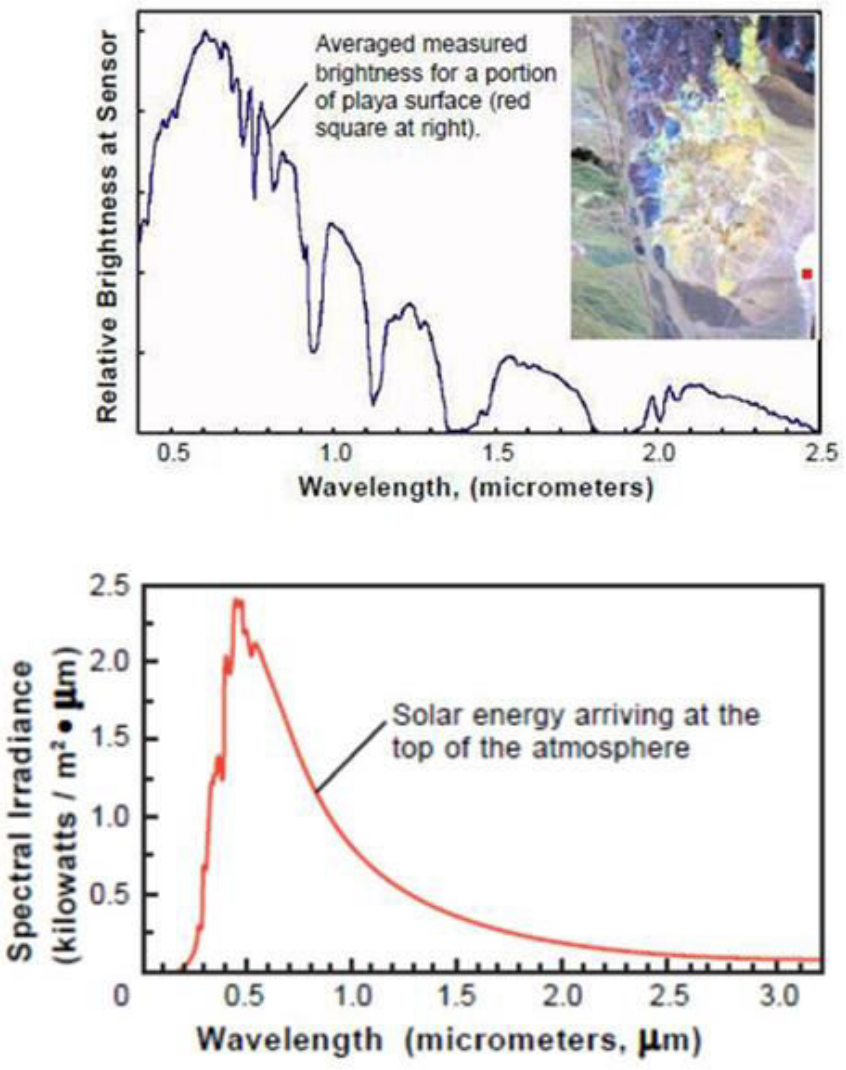

Figure 4.2: Influence of the solar spectrum (bottom) and atmospheric effects in the spectral radiance of a bright dry lake bed surface in Cuprite, Nevada, as measured by the sensor AVIRIS at an altitude of 20 km (top) (MicroImages, 2012).

Sources of radiometric distortion

In order to convert radiance values into surface reflectance it is necessary to account for the following factors (MicroImages, 2012):

a. **Illumination factors:** Three different aspects affecting the illumination of a scene must be taken into consideration. Firstly, because the radiance will be affected by the incident solar energy, i.e. *source illumination* [Figure 4.2], its spectrum at the time an image was captured must be known, assumed or derived from another measurement. The spectral dependence of source illumination affects band-to-band relativity. Secondly, the energy reflected from a target on the ground depends on the amount of solar energy illuminating it, which in turns depends on the *angle of incidence* or *illumination geometry*. The illumination geometry varies with the changing position and elevation of the sun during the day and through the year. The illumination geometry is also determined by the shape of the surface (slope angle and direction), and can produce variations even within a single scene. Lastly, *shadowing* can also occur due to clouds, topographic obstacles and other features, such as tree canopy, and diminishes the amount of energy reflected to the sensor.

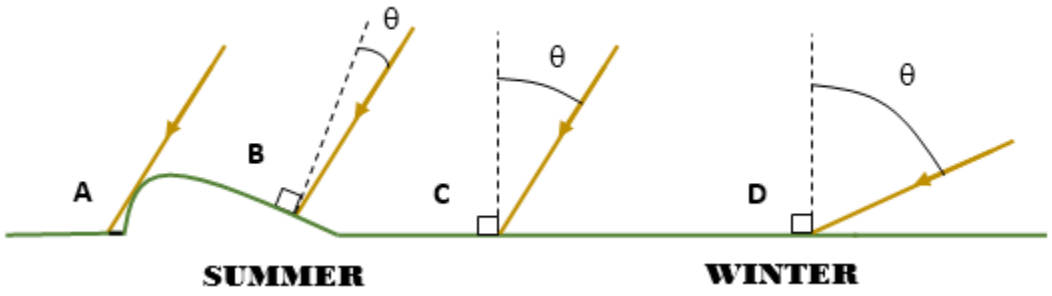

Figure 4.3: Different illumination conditions derived from shadowing (A) and different incidence angles (B, C and D).

b. **Atmospheric effects:** The energy emitted by the sun propagates isotropically through space, its intensity diminishing with increasing distance in accordance with the inverse-square law. The power density at a certain distance from the sun is the *irradiance* and can be measured in watts per square metre (Wm^{-2}). The power density that the Earth scatters in a certain direction is called *radiance* and is expressed as density per solid angle in watts per square metre per steradian ($Wm^{-2}sr^{-1}$). Both of these quantities are wavelength dependent and thus can be also expressed as spectral magnitudes, called *spectral irradiance* and *spectral radiance*, and with units $Wm^{-2}\mu m^{-1}$and $Wm^{-2}\mu m^{-1}sr^{-1}$, respectively (Richards, 2013).

The presence of the atmosphere has two effects on travelling light energy: scattering and absorption by atmospheric particles. The latter is a selective process that converts light into heat. The strongest radiation attenuations are caused at specific wavelengths by molecules of

oxygen, carbon dioxide, ozone and water. There are two scattering mechanisms, caused either by the air molecules themselves, *Rayleigh scattering*, or by larger particles present in the atmosphere, such as aerosols, called *aerosol scattering* or *Mie scattering*. Although both are wavelength dependent, some especially large particles such as those found in fogs, clouds and dust can make the Mie scattering wavelength independent. Because of absorption and scattering, not all the radiation emitted by the sun reaches the Earth's surface, and not all the radiation reflected by the Earth's surface reaches the sensor. The amount of energy that does cross the atmosphere, relative to that that would be transmitted in the absence of atmosphere, is called *transmittance* and it can be referred to in both downward and upward directions (Richards, 2013).

Figure 4.4 shows the effects that the atmosphere has on the solar radiation that crosses it. *Sky irradiance* is the radiation that arrives at a certain pixel on the ground from directions in the sky besides the one on a direct path from the sun. It can be radiation coming from the sun that is scattered to the said pixel through an undefined and diffuse path or radiation emitted by the surrounding pixels that is bounced back to the ground. *Pathirradiance* represents the amount of radiation that is registered by the sensor from sources other than the onein the direct path from a given pixel. It can be radiation directly from the sun that is scattered up by the atmosphere before it reaches the ground or radiation coming from adjacent pixels on the ground (Richards, 2013).

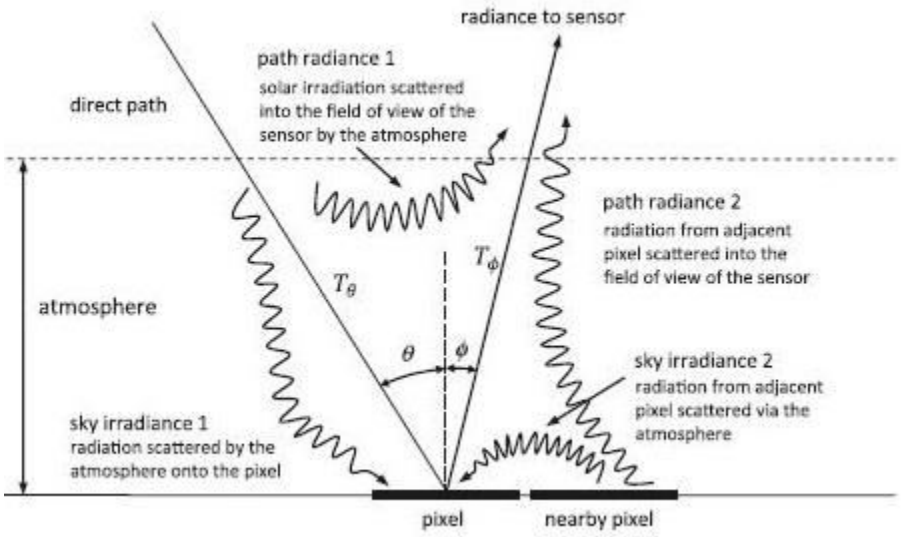

Figure 4.4: Effect of the atmosphere on solar radiation illuminating a pixel on the ground and reaching a sensor (Richards, 2013).

A combined effect of the atmosphere and the solar curve previously discussed derives from the interference of both. Part of the solar light is selectively absorbed by the atmosphere and thus modifying the radiance recorded by the sensor in certain wavelengths. The main absorption features are caused by oxygen, carbon dioxide and water vapour. Some other solar light is scattered by the atmosphere and complicates the signal, as part of this radiation never reaches

the sensor and some other part is directly scattered from the atmosphere to the sensor, without passing by the surface (Richards, 2013).

c. **Sensor effects:** When the energy reflected from an object reaches a sensor, the radiance is converted into an electric signal that is later scaled and quantized into discrete integer values representing radiance values (MicroImages, 2012). Radiometric errors can be due to calibration differences among sensors, to *detector offsets*, in which some signal, often called *dark current*, is produced even without incoming radiation, or to differences in the transfer characteristics of different detectors within an array. Also, mismatches among the detectors in pushbroom sensors can give rise to longitudinal striping in the image. Lastly, a momentary sensor or communication link failure can cause the loss of one of more lines of data or of individual pixels in a certain band. This results in black lines or black pixels in the image (Richard, 2013).

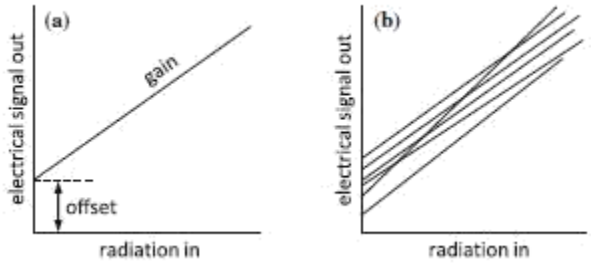

Figure 4.5: (a) Linear radiation detector transfer characteristic, and (b) hypothetical mismatches in detector characteristics for different pixels or regions in a detector (Richards, 2013).

Radiometric correction

A comprehensive method to convert radiance into real reflectance values must take into consideration all the factors described above, namely, the solar spectrum, atmospheric effects and sensor gain. In mathematical terms, the ground reflectance spectrum is multiplied by these effects, in a wavelength-by-wavelength fashion, to produce the recorded spectrum. The effects of the sensor internal noise (sensor offset) and the atmospheric path radiance originating from scattering are incorporated in an additive way (MicroImages, 2012).

a. **Normalization for the solar spectrum:** In order to compensate for the wavelength dependence of incident solar radiation, the solar emissivity must be used (such as the curve shown in Figure 4.2) to normalize the recorded data. A very simplistic approach that may be valid in the case of broadband sensors is to assume that the sun emits like a black body. However, in the case of narrowband sensors, such as hyperspectral sensors, this approximation is not acceptable and the real solar emissivity must be accounted for (Richards, 2013).

b. **Atmospheric correction:** The typical procedure to apply atmospheric correction to a hyperspectral image is structured as follows (Richards, 2013):

1. Conversion of raw recorded pixel digital numbers (DN) to radiance.

2. Compensation for the solar spectral curve as described earlier. The input radiances are converted to apparent reflectances of the surface by dividing them by the solar irradiance above the atmosphere.

3. Compensation for atmospheric absorption and scattering. This transforms the apparent reflectances into scaled surface reflectances. To accomplish this step, information on the scattering and absorptive characteristics of the gases present in the atmosphere is necessary. There are libraries of data for most atmospheric components, HITRAN being the most widely used. However, the majority of these gases do not have a significant effect on the image and so excluding them from the corrections does not generally lead to significant errors. The most important gases are ozone (O_3), carbon dioxide (CO_2), nitrous oxide (N_2O), carbon monoxide (CO), methane (CH_4) and oxygen (O_2). Ozone is the only one that varies with latitude and season, although it can be modelled as constant for a given image. The rest can be assumed to have constant effects across images. The water vapour effects are generally more difficult to account for, as the water vapour amount in the atmosphere varies with the humidity and can vary even within the same image (Richards, 2013). Different software packages are available for atmospheric correction. For example, ATCOR 2 and 3 are used for the atmospheric correction of spaceborne remote sensing images; ATCOR 4 is used for the correction of airborne images. ENVI also has a module for atmospheric correction called FLAASH.

4. Finally, real surface reflectances are obtained from scaled surface reflectances incorporating topographic effects. If no topographic information is available, the surface is supposed Lambertian and real reflectances are thus equal to scaled reflectances (Richards, 2013). A Lambertian surface is *a surface that appears uniformly bright from all directions of view and reflects the entire incident light* (AZoOptics, 2014). These final reflectance values may still incorporate the effect of topographic shading (MicroImages, 2012).

c. **Correction of sensor effects:** On the assumption that the signals recorded by all the pixels in a sensor are statistically similar, with the same or almost the same mean brightness and standard deviation, mismatches among pixels in a certain band can be corrected. In most cases this assumption is reasonable. In order to correct the mismatches, a pixel must be taken as reference and the mean and standard deviation of its corresponding image lines must be calculated. Later, the brightness of the rest of pixels must be adjusted so their statistical values match those of the reference pixel. This is called *destriping* and can be done applying the following analytical expression:

$$y = \frac{\sigma_d}{\sigma_i} x + m_d - \frac{\sigma_d}{\sigma_i} m_i$$

where x is the original brightness for a given pixel, y is the adjusted or destriped value, σ_d and m_d are the reference mean and standard deviation values and m_i and σ_i are the mean and standard deviation of the pixel under consideration.

Considering only first and second order derivatives for destriping produces imperfect results. However, more complex models are generally not recommended for sensors with numerous pixels (Richards, 2013).

Black pixels and lines can be corrected using a method commonly called *infilling* or *inpainting* that consists of assigning to a black pixel the average value of its surroundings (Richards, 2013).

d. **Image based methods:** Other methods try to correct errors of different nature directly from the recorded information in the sensor. They are:

d.1. The Flat Field Method: This method requires that the image includes a spectrally uniform area. Because the reflectance curve of this area should be relatively flat, i.e. featureless, it can be assumed that the measured difference in spectra is due to solar irradiance and atmospheric scattering and absorption. Thus, the radiance values of each pixel can be converted to relative reflectance by dividing each pixel spectrum by the flat field spectrum. In order to avoid mistaking sensor noise for atmospheric effects, the flat field must be bright, with high reflectance values. One disadvantage of this method is that any spectral absorption feature in the flat field spectrum will produce spurious features in the calculated relative reflectance curve. Residual effects of shadowing and atmospheric path radiances could also be triggered by great elevation differences within the scene (Richards, 2013, and MicroImages, 2012).

d.2. Average Relative Reflectance Conversion: The first step in this conversion method is to scale the radiance values so that their sum is constant over the entire image. By doing so, topographic and other varying brightness effects are removed. Then, the mean spectrum of the whole image is calculated and used to normalize image spectra. This method is based on the assumption that the scene is heterogeneous enough to cancel out any spectral variations. In cases where this is not true, spurious spectral features will be added to the calculated spectrum (MicroImages, 2012).

d.3. Haze Removal by Dark Subtraction: The goal of this method is to account for the additive effect of path radiance not considered in the two previous methods and that is important for the visible and near infrared bands (MicroImages, 2012). It makes the assumption that every band of data for a certain scene should have some pixels with zero brightness but that atmospheric path radiance has introduced a constant level to each pixel in each band. Thus, the way of correcting it is to determine the minimum brightness value in each band and subtract it from every pixel in that band (Richards, 2013).

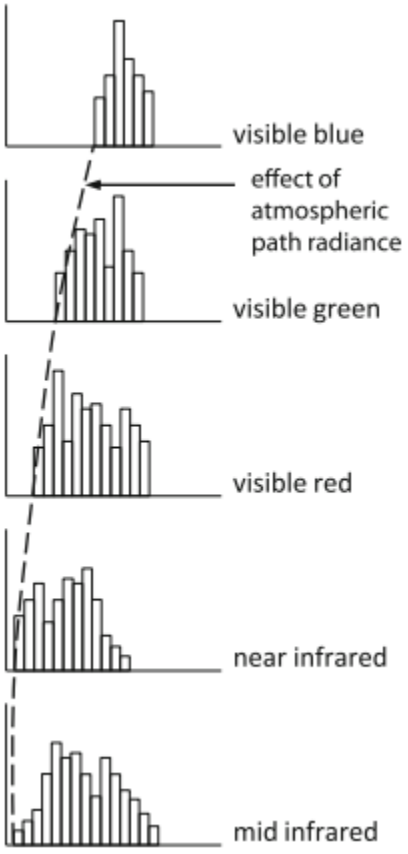

Figure 4.6: Effect of the path radiance resulting from atmospheric scattering in different spectral regions (Richards, 2013).

Geometric distortion

In addition to radiometric errors, there are also geometric errors and their effects in the images can be very severe. These geometrical errors can be due to the following factors:

- The rotation of the Earth during image acquisition.
- Variations in platform altitude, attitude and velocity.
- The wide field of view of some sensors.
- The curvature of the Earth.
- The finite scan rate of some sensors.
- Other optical or mechanical distortions in the sensor.

These distortions can be systematic, i.e. they are predictable and can be precisely modelled, or non-systematic or random (Levin, 1999 and Toutin, 2004). The different geometric distortions are shown in Figure 4.7 and are (Levin, 1999 and Richards, 2013):

<u>Non-systematic distortions:</u>

- *Altitude variance:* Changes in the sensor platform altitude or in the terrain elevation cause scale distortions, at constant angular IFOV and field of view.

- *Platform attitude changes:* A satellite's attitude is defined by the angles yaw, pitch and roll. Changes in these angles can, respectively, lead to image rotation, along-track and across track displacement.

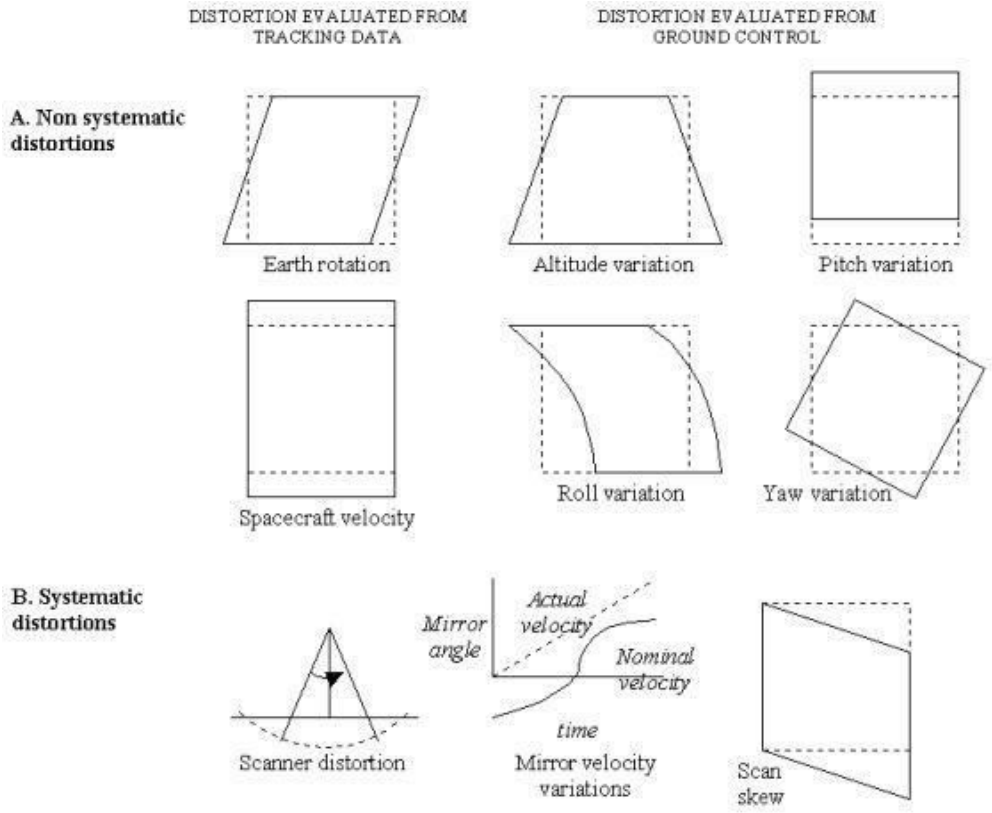

Figure 4.7: Geometric distortions of Landsat images (Levin, 1999).

Systematic distortions:

- *Scan skew:* For imaging systems in which the ground swath is skewed with respect to the ground track, the forward motion of the platform during the time a mirror completes a scan results in geometric distortions as shown in Figure 4.7.

- *Mirror-scan velocity variance:* Sensor scan nonlinearities occur in line scanners with oscillating mirrors. In these, the mirror scan rate is constant during the image scan until it reaches the line extreme and needs to slow down in order to reverse direction. This rate change causes a displacement distortion of the recorded pixels in the along-track direction.

- *Panoramic distortion:* Remote sensing imaging systems have a constant IFOV that results in the effective size of the pixels at the extremities of the images being larger. Thus and because they have to "fit in the same image pixel size", they look compressed in the image. The Earth curvature can have the same effect in images taken by sensors with wide swath width.

- *Platform velocity:* Changes in the satellite's velocity can arise due to orbit eccentricity and the non-sphericity of the Earth. These velocity changes result in scale changes in the along-track direction. This distortion is greater for linescan sensors.

- *Earth rotation:* Because the time of image capture is finite, once again more in linescan sensors that record an image line at a time, the Earth rotation during this time will cause geometric distortions. As the Earth rotates from west to east, the last image line captured will be placed more to the west than the first one captured when the image recording started. Thus, the later scanned lines will be incorrectly shifted to the east.

Geometric correction

In order to be able to use the satellite's products in combination with other GIS data, the images must be geometrically corrected and represented in the same format, i.e. ortho-images, or units of terrain-geocoded data.

The geometric distortions can be corrected either through 2D/3D empirical models or through 2D/3D physical and deterministic models. The first methodology includes 2D/3D polynomial and 3D rational functions, that establish a relationship between the image coordinates and the terrain coordinates through the definition of ground control points (GCP). 2D/3D physical models represent the physical reality of the viewing scenario, including the platform, the sensor, the Earth and in some cases a map projection (Toutin, 2004).

The sensor provider often specifies the geometric distortions caused by instrumentation characteristics. For example, XIMEA (2016) describes the common distortions and the corrections that should be applied to the images taken by their sensors. Figure 4.8 represents the processing chain recommended by XIMEA to convert the raw image into the corrected hyperspectral cube, for both snapshot and line scan sensors. It is relevant to recall here that the LS100 sensor proposed for this project is a line scan sensor.

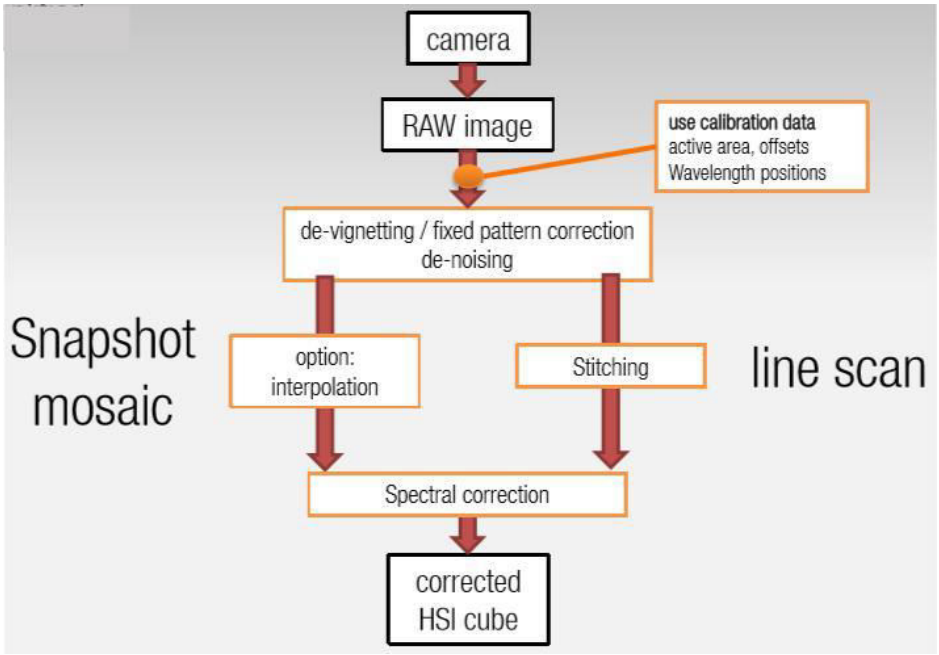

Figure 4.8: Data correction chain for XIMEA sensor images (XIMEA, 2016b).

Finally, if the Earth and atmosphere models, the sensor model and the satellite's ephemeris data (i.e. position, attitude and velocity) as well as the image capture time are known, the image can be geometrically corrected through geolocation. This consists of assigning to each image point expressed in image coordinates (pixel line and row) terrain coordinates on the Earth's surface (latitude, longitude and altitude).

4.2.2. Classification

Remote sensing image classification consists of automatically clustering pixels with similar properties under a set of classes that represent different objects on the Earth's surface. It is an important research topic within the image processing community, with numerous defined techniques. These can be categorized based on pixel information or based on training samples (Ablin and Sulochana, 2013).

Based on pixel information, different classification methods can be performed depending on the information they use. In this way, *per pixel or pixel-wise classification* processes the entire scene in a pixel-by-pixel fashion. The main drawback of this approach is that each pixel is classified as belonging only to one class and so mixed pixel effects are ignored, which makes it not suitable for many applications. Furthermore, because they do not consider spatial information, these methods can suffer from 'salt and pepper effects' (i.e. a final classification map that looks noisy) which would reduce the classification accuracy (Miao and Shi, 2015). On the contrary, *sub-pixel classifiers*, with spectral mixture analysis being the most popular method, take mixed pixels into consideration. This is thus generally more appropriate for a larger number of scenes, as heterogeneous landscapes or the limited spatial resolution of some sensors often result in mixed pixels. However, it still remains difficult to assess the accuracy of these approaches. *Per-field* or *object-based classifiers* incorporate the information of the surrounding area in the classification of a given pixel. In object-based classification, the image is first segmented into groups and then not only the individual pixels but also these groups are classified. Although the accuracy achieved is generally higher, if the segmentation of the image into different objects is not accurate it can lead to an erroneous classification. Besides spectral and spatial information, *knowledge-based classifiers* make also use of available ancillary data, e.g. digital elevation models or thematic maps. Similarly to per-field classifiers, *contextual classifiers* also utilise the information of neighbouring pixels to classify a given pixel, with the difference that it classifies pixel by pixel and not clusters of them. By doing so, the model includes spatial information, increasing the classification accuracy. Finally, combining the results of *multiple classifiers* through, for example, a product rule, a sum rule or thresholds generally increases the classification accuracy (Ablin and Sulochana, 2013).

As for **image classification based on training samples**, it can be supervised or unsupervised. In *supervised classification*, the training samples are already classified in known classes that the algorithm must learn during the training in order to be able to classify other images. Linear and logistic regression, gradient descent, Neural Networks (NN) and Support Vector Machines (SVM) are some supervised classifiers. *Unsupervised classifiers* automatically group pixels with similar characteristics in different clusters that the image analyst must recognize and label later. Examples of unsupervised classifiers are the K-means algorithm and some dimensionality reduction methods such as Principal Component Analysis (PCA) and anomaly detection (Ablin and Sulochana, 2013 and Ng, 2017a).

Ablin and Sulochana (2013) concluded in their study that Machine Learning approaches perform better than others such as Maximum Likelihood. Furthermore, they state that a combination of different classifiers achieve the best results.

Luo and Chanussot (2009), Marée at al. (2009), Santos et al. (2013) and Miao and Shi (2015) all agree that kernel-based methods (and in particular SVM) outperform other traditional techniques in hyperspectral image classification. Furthermore, SVM is able to deal with high dimensional data and reduced training sets. The authors also conclude in their work that incorporating spatial information in the classification instead of relying only on spectral data improves the classification accuracy and makes the predictions smoother, avoiding the salt and pepper effects previously mentioned. However, in cases where the objects to be classified are small in size this may not be true as their spatial structure is likely to be disrupted in the image segmentation step (Miao and Shi, 2015). Another important remark of these authors' research is that fusing different information sources and the results of different classifiers generally improves the classification accuracy.

The basic scheme of a supervised learning problem is represented in Figure 4.9. Its goal is to *learn*, based on a previously labelled or classified training set, a predictor function to assign to the input data X the output Y. The input parameters X are generally the features of the objects to be assessed. The output variable Y can be continuous in the case of a regression problem (such as the prediction of house prices) or discrete if the problem being addressed is a classification problem. The predictor function is traditionally called the *hypothesis function*.

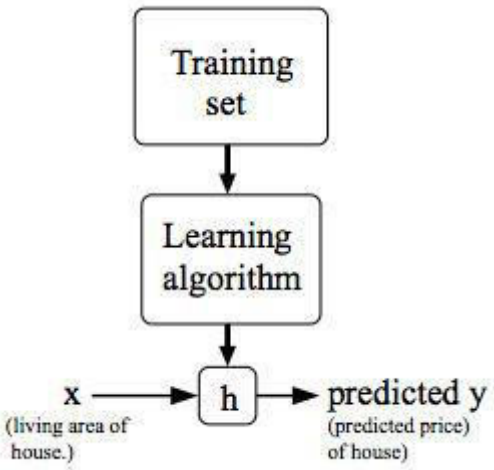

Figure 4.9: General scheme of a supervised learning problem, for the case of a regression problem such as the prediction of house prices (Ng, 2017a).

Neural Networks (NN)

Neural Networks (NN) were devised with the aim to mimic the brain. As such, their basic unit is the neuron and replicates a neuron in the brain. Figure 4.10 shows the scheme of a biological neuron and the model of the neuron as a logistic unit in the NN. The image on the left represents a biological neuron and its connections. In this image, the dendrites constitute the chains through which the inputs get to the cell body where, after interacting with each other, they produce an output through the axon. The image on the right shows the neuron scheme for NN, where the inputs interact through an activation function $h_{\theta}(x)$ to produce an output (Ng, 2017c).

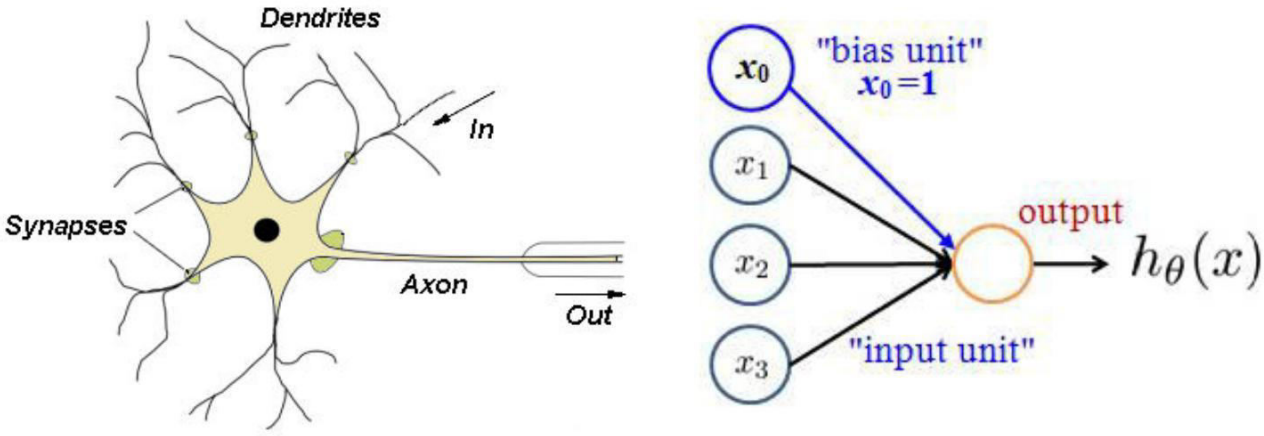

Figure 4.10: (Left) Biological neuron and its connections (Golda, 2005) and (Right) neuron model (Ng, 2017d).

In this model, the so-called *input layer,* consisting in the features vector, is transformed in the intermediate or *hidden layers* to finally produce the *output layer*, containing the hypothesis function. The nodes in the hidden layers, also known as activation units, operate on the input coming from the previous layer through the *sigmoid (logistic) activation functions*, expressed as:

$$g(\theta x) = \frac{1}{1 + e^{-\theta^T x}}$$

where Θ, sometimes called *weights*, are the parameters that will define the Neural Network structure and that must be learnt.

In the case of one hidden layer, the model can be represented as the following scheme:

$$\begin{bmatrix} x_0 \\ x_1 \\ x_2 \\ x_3 \end{bmatrix} \rightarrow \begin{bmatrix} a_1^{(2)} \\ a_2^{(2)} \\ a_3^{(2)} \end{bmatrix} \rightarrow h_\theta(x)$$

$$a_1^{(2)} = g(\theta_{10}^{(1)} x_0 + \theta_{11}^{(1)} x_1 + \theta_{12}^{(1)} x_2 + \theta_{13}^{(1)} x_3)$$

$$a_2^{(2)} = g(\theta_{20}^{(1)} x_0 + \theta_{21}^{(1)} x_1 + \theta_{22}^{(1)} x_2 + \theta_{23}^{(1)} x_3)$$

$$a_3^{(2)} = g(\theta_{20}^{(1)} x_0 + \theta_{31}^{(1)} x_1 + \theta_{32}^{(1)} x_2 + \theta_{33}^{(1)} x_3)$$

$$h_\theta(x) = a_1^{(3)} = g\left(\theta_{10}^{(2)} a_0^{(2)} + \theta_{11}^{(2)} a_1^{(2)} + \theta_{12}^{(2)} a_2^{(2)} + \theta_{13}^{(2)} a_3^{(2)}\right)$$

where $a_i^{(j)}$ represents the activation of unit *i* in layer *j* and $\Theta^{(j)}$ the matrix of weights controlling the function mapping from layer *j* to layer *j+1*. If layer *j* has s_j units and layer *j+1* has s_{j+1}, the dimension of $\Theta^{(j)}$ will be $s_{j+1} \times (s_j+1)$. It must be taken into consideration that when passing the nodes of each layer as inputs of the following layer, a bias unit will be added which value is 1. In particular, here they are x_0 a d $\Theta_0^{(j)}$. This process of obtaining the hypothesis function from the input layer is called *feedforward propagation.*

In order to learn the weights matrices, a somewhat similar process must be performed but in the inverse order (i.e. from the previously calculated hypothesis function or output layer to the input layer). This is called *forward-backward propagation* and is done using a training

set with already classified samples. Further details on the computations involved in Neural Networks fall out of the scope of this study but can be found in (Ng, 2017c and 2017d).

Support Vector Machines (SVM)

Support Vector Machine (SVM) classifiers consist of defining a separating hyperplane or *decision boundary* to divide the ensemble of different samples into separated classes. They are often referred to as *large margin classifiers*, as the searched decision boundary will be the one resulting in the largest minimum distance to the samples. It constitutes an optimization problem, in which the goal is to find the parameters θ that minimize the following expression (Ng, 2017e and OpenCV, 2014):

$$\min_{\theta} C\sum_{i=1}^{m}\left[y^{(i)}cost_1\left(\theta^T x^{(i)}\right)+\left(1-y^{(i)}\right)cost_0(\theta^T x^{(i)})\right]+\frac{1}{2}\sum_{j=1}^{n}\theta_j^2$$

for a hypothesis function:

$$h_\theta(x)\begin{cases}1\ if\ \ (\theta^T x)\gg 0\\ 0\ \ otherwise\end{cases}$$

where x is the input variable or the features, y is the output $\theta^T x$ the target variable, θ represents the parameters to be learnt from the training examples and cost (corresponds to the cost function, i.e. a measure of the accuracy of the hypothesis function and how much it diverges from the target variable y. C is a parameter that must be selected beforehand. The parameter C controls the influence of each support vector. It allows to "ignore" some examples that are extremely unusual or mislabelled, avoiding poorly fit models. This implementation of SVM is called a "soft margin classifier", as opposed to traditional SVM classifiers, that try to separate all positive and negative examples (Ng, 2017e).

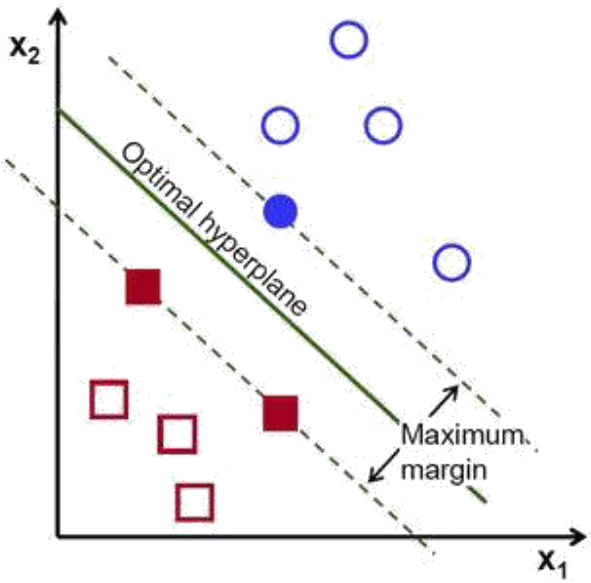

Figure 4.11: Simplification of the SVM problem for a linearly separable case (OpenCV, 2014).

Figure 4.11 shows a simplification of the SVM classifier for a linearly separable case. In cases where the classes are not separable by a linear decision boundary, the practice in SVM is to substitute the input variables or features *x* by *kernels.* These are similarity functions defined in base of the proximity of the samples to a set of defined *landmarks* $l^{(i)}$, normally selected among the training data set. A variety of similarity functions can be used, among which a widely used one is the Gaussian kernel:

$$f = similarity(x, l^{(i)}) = \exp(-\frac{\|x - l^{(I)}\|^2}{2\,\sigma^2})$$

where σ^2 is called the bandwidth parameter and dictates how fast the metric decreases as the examples are further apart. In this case, the SVM parameters to trade-off are C and σ^2 (Ng, 2017e).

Principal Component Analysis (PCA)

Principal Component Analysis (PCA) is an unsupervised learning algorithm for data dimensionality reduction. There are two possible motivations for dimensionality reduction, namely, data compression and data visualization. The former is interesting for this project in order to reduce the necessary on-board memory and computing time.

For a given n-dimensional dataset, PCA intends to find a lower k-dimensional surface (i.e. a 2D plane for a 3D dataset or a 1D line for 2D data) defined by k vectors $k^{(1)}$, $k^{(2)}$, ..., $k^{(k)}$ onto which to project the data so as to minimize the projection error. In order to do this, the data must be first pre-processed by means of a feature scaling, with the goal of obtaining a new dataset in which all the features are in a comparable scale. Then, the covariance matrix must be computed from these features. Finally, an eigen vector decomposition must be performed. The resulting vectors will define the targeted lower-dimensional surface (Ng, 2017f).

4.3. Image processing for PyrSat

4.3.1. Developing environment

Implemented libraries – OrfeoToolBox and Earth Observation CFI

OrfeoToolBox (OTB) is an open-source software library for remote sensing image processing developed by the French Centre National d'Études Spatiales (CNES) written in C++ and that is ideally suited for this project (CNES, 2017). It will be used for both atmospheric correction and classification.

For geolocation, the Earth Observation CFI software will be used. It is developed by the European Space Agency and consists of a library of precompiled functions in C for timing, coordinate conversions, orbit propagation, satellite pointing calculations and target visibility calculations. The software is openly available from ESA's Earth Observation System Support for any user involved in Earth Observations missions, either in preparation or exploitation, (ESA, 2017).

Image processing tools

The OTB libraries are callable from QGIS or Monteverdi, the latter being a-priori included in the downloadable OTB package. Both are image processing environments that allow users to visually follow the transformations performed on the images. Development on QGIS is preferred, due to the fact that it is an open source platform and more widely distributed. However, since Monteverdi was

developed as a tool to demonstrate OTB capabilities, some functions work better on this platform. In order to develop a high-level software tool, OTB can be called from Python. Finally, C++ will be used to create a full Application Programming Interface (API).

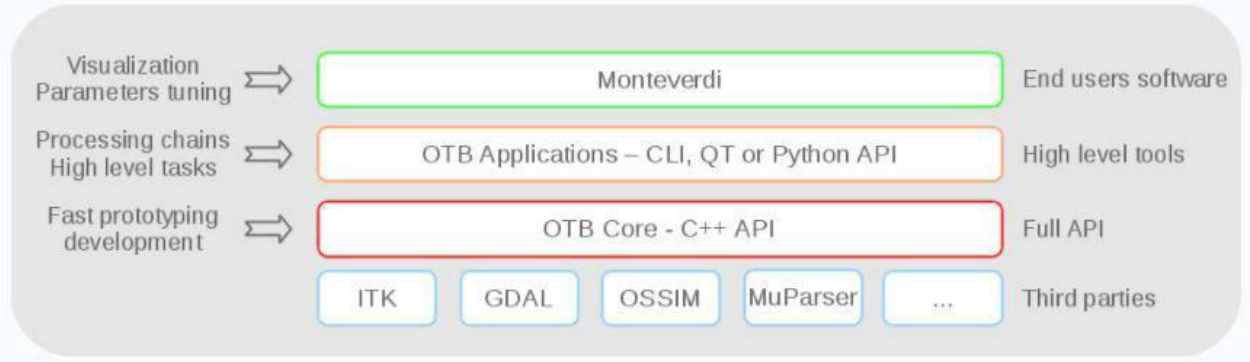

Figure 4.12: Scheme of use of the OTB libraries (CNES, n.d.).

a) *QGIS:*

QGIS is an open source Geographic Information System (GIS) developed by the Open Source Geospatial Foundation (OSGeo) and distributed under the GNU General Public License. It can run on multiple operating systems (Linux, Unix, Mac OSX, Windows and Android) and support numerous geospatial data formats and functionalities (QGIS, n.d.).

Orfeo ToolBox can be used from QGIS, either through applying the processing toolbox tools directly on the images or through the in-built Python console.

b) *Monteverdi:*

Monteverdi was born as a simple software tool with the capability of showing users what Orfeo ToolBox was able to do. Later, because of its popularity in the user community, it was further developed as a robust stand-alone image processing toolkit.

It has some features that are especially suitable for processing of satellite Earth observation images. Firstly, its *high performance*, achieved through a hardware accelerated rendering engine, allows for very rapidly image processing even for full size images. Secondly, its *sensor geometry support* capability permits viewing raw images directly in the sensor geometry. Lastly, it is highly *powerful* and can access all the applications in OTB (OTB Team, 2017).

Final software product

Due to its higher reliability and robustness, and because it is the language in which the core of OTB is written, the on-board final software product will be written in C++. This is in line with the current tendency in the space sector regarding programming languages used for the on-board software.

For example, the programming languages used by the European Space Agency (ESA) are Ada, C/C++ and Java. C is used for payloads, Digital Signal Processing software, small instruments and some platforms. It is also often used by automatic code generators, for less critical software and whenit is the language in which the development team has the most expertise. C++ is however less suitable for on-board software because of its poorer semantic control and ESA recommends to carefully

consider its choice. Two documents are available for assessing the suitability of using C++. One is the *Embedded C++ (EC++) standard* within the *ESA C/C++ coding standard* and the other one are the *guidelines for using object-oriented programs on-board aircraft* by the Aerospace Vehicle Systems Institute (ESA, n.d.c).

As for NASA, the Laboratory for Reliable Software (LaRS) at the Jet Propulsion Laboratory (JPL) can be taken as a reference. The mission of the LaRS is *to achieve long-term improvements in the reliability ofJPL's mission-critical software system* (JPL, 2016). The preferred programming language for writing critical code is C, as stated by the JPL scientist Gerard J. Holzmann in its work *The Power of Ten–Rules for Developing Safety-Critical Code* (2014). Software engineers at JPL also use the *guideline JPL Institutional Coding Standard for the C Programming Language* (2009). However, for non-critical software the organisation also uses other languages. Indeed, they have also defined guidelines for the use of C++ and Java. For C++ programming, NASA developed in 2005 the guideline *C++ Coding Standards and* Style Guide (Jun, Shoan and Stevens, 2005).

4.3.2. Development architecture

Atmospheric correction

OTB offers only model-based atmospheric correction in four steps (CNES, 2017):

1. Digital number to luminance correction.
2. Luminance to reflectance image correction.
3. Atmospheric correction for TOA (top of atmosphere) to TOC (top of canopy) reflectance estimation.
4. Correction of the adjacency effects taking into account the neighbourhood contribution.

The inputs needed for this application are (CNES, 2017):

- Atmospheric correction parameters: Physical atmospheric parameters at the time of the image capture (i.e. atmospheric pressure, water vapour content, aerosol information...)
- Acquisition correction parameters: Sensor related and viewing geometry information at the time of the capture (i.e. solar angles, spectral resolution...)

During the development of the software it will be necessary to study also image-based radiometric correction. These methods are not included in OTB and thus it will be necessary to implement them manually.

The accuracy of both approaches should be assessed, including images with a wide range of different atmospheric conditions. Then, the methods should be automated in order to implement them in the on-board processor. The preferred approach in a real case will be model-based but, because atmospheric data at the acquisition time and location will not always be available, the best performing image-based algorithm should be ready for use as a back-up. It is possible that different image-based algorithms are more suitable in different atmospheric and imaging conditions. Therefore, the possibility of incorporating more than one algorithm from which it is possible to automatically choose the best one to implement in a specific scenario should be considered. However, it must also be taken into consideration that this approach would require more of the

available on-board processing resources. Its practical value and possibilities of implementation should thus be carefully studied.

Classification

OrfeoToolBox offers several possible supervised and non-supervised classification methods.

Since the data product of the satellite must be a final classification map, supervised classification is preferred for this work. Also, the target classes are well defined: burned/non-burned for the burned area product and four levels of vegetation fire risk for the fire risk product. The supervised classifiers present in OTB are:

- Support Vector Machine (SVM):
  - LibSVM (based on libSVM)
  - SVM (based on OpenCV, itself based on libSVM)
- Normal Bayes classifier.
- Boost classifier.
- Decision Tree (DT).
- Random Forest (RF).
- Gradient Boosted Tree (GBT).
- K – Nearest Neighbours (KNN).
- Artificial Neural Networks (ANN).

OTB has the possibility of learning from samples or from images (CNES, 2017). It also permits the fusion of classification maps obtained with different methods in order to obtain a more robust and precise final classification map. This can be done with two methods:

- Majority Voting: Chooses the more frequent class label for each pixel.
- Dempster Shafer: This method is more adaptive than the Majority Voting and is based on the Dempster Shafer theory. It takes into consideration the confidence levels in the classification maps achieved with different classifiers (CNES, 2017).

After the production of a classification map, it can also be regularized to obtain more homogeneous areas in the image. This is done with majority voting, taking the neighbourhood into consideration (CNES, 2017). However, in order to avoid losing image information, this approach is not going to be considered in the present study.

Classification pipeline:

Figure 4.12 shows the proposed classification pipeline for the development of the best suitable software, explained in greater detail in this section. This architecture is based on the typical image classification pipeline: image acquisition, image pre-processing, feature extraction and classification. Here the term *feature* refers to the attributes considered for the classification.

The first step in the classification pipeline of this project is image acquisition from some source. Working on the images, different features including red and NIR wavebands and spectral indices will be considered for the classification. Through principal component analysis (PCA), a subset will be extracted from the feature space and used for classification. Then the SVM and ANN classifiers available in OTB, as well as a fusion of both, will be trained and tested. Different feature subsets will be used in conjunction with different classifiers and the accuracy for each combination will be assessed. In this way, the combination producing the best results will be identified for its final implementation in the on-board computer.

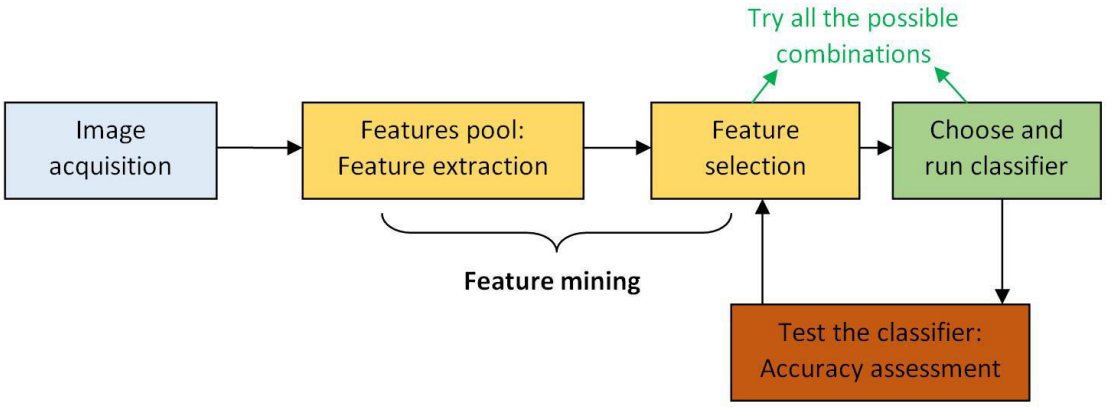

Figure 4.13: Classification pipeline.

a. Image acquisition

The images selected for classification training and validation should contain scenes taken before and after a fire. That is, for the burned area product the scene must contain burned areas taken after a fire. For the vegetation fire risk product, the scene must contain an area where a fire is known to have occurred, before it did.

The images should also be as similar as possible to the images taken by the XIMEA MQ022HG-IM-LS100-NIR camera proposed for this project, in terms of spectral coverage and spectral and spatial resolution.

The ground truthing will be done visually from the MODIS burned area product, which is updated monthly. Alternatively, the case of simulating images from spectral libraries can also be considered for a consistent validation.

b. Feature extraction

The features considered will be the reflectance in the different wavebands observed by the sensor and spectral indices to correlate them. To simulate how the proposed XIMEA MQ022HG-IM-LS100-NIR camera works and assess its utility for this application, only the wavebands it can sense will be considered. That is, 100+ bands in the range between 600 and 975 nm (red, red-edge and NIR), in steps of 4nm. Each band has dimensions of 2048 x 8 pixels, in a detector of 2048 x 1088 pixels (XIMEA, 2016b).

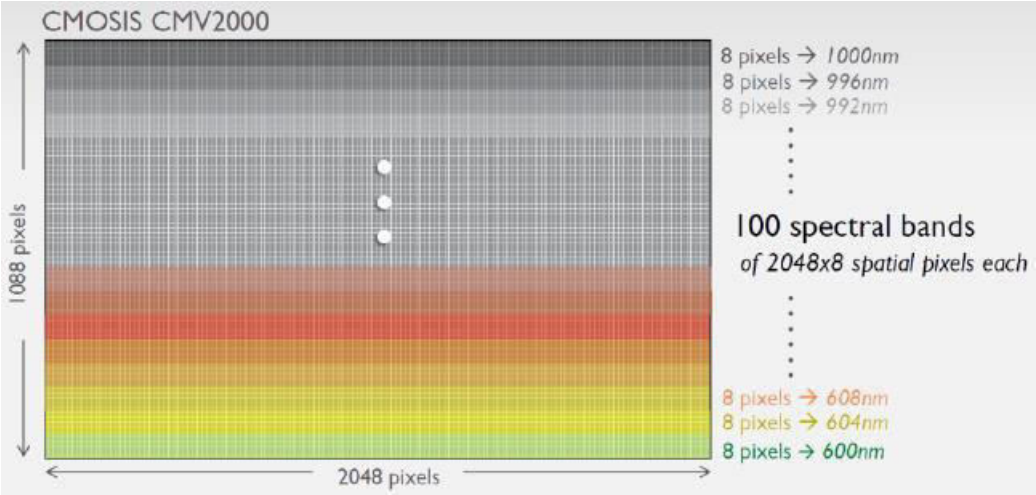

Figure 4.14: XIMEA MQ022HG-IM-LS100-NIR filter layout (XIMEA, 2016b).

By introducing dependability among bands through spectral indices, it is possible to cope with the spectral variability introduced by different factors such as lightning conditions and atmospheric and sensor effects. It will also give a physical meaning to the spectra.

Multiple indices correlate the red and NIR bands sensed by the camera in question to derive vegetation characteristics and soil characteristics. An exhaustive compilation of spectral indices for agriculture is provided in the online R documentation for the Remote Sensing Tool Box (Leutner, 2010). The ones that only use the red and NIR bands and will thus be used as additional features are:

- Corrected Transformed Vegetation Index (CTVI):

$$CTVI = \frac{NDVI + 0.5}{\sqrt{|NDVI + 0.5|}}$$

- Global Environmental Monitoring Index (GEMI):

$$GEMI = n\,(1 - 0.25\,n) - \frac{red - 0.125}{1 - red}$$

$$\text{with } n = \frac{2 * (NIR^2 - red^2) + 1.5 * NIR + 0.5 * red}{NIR + red + 0.5}$$

- Modified Soil Adjusted Vegetation Index (MSAVI):

$$MSAVI = NIR + 0.5 * (0.5 * \sqrt{(2 * NIR + 1)^2 - 8\,(NIR - 2 * red)}\,)$$

- Modified Soil Adjusted Vegetation Index 2 (MSAVI2):

$$MSAVI2 = \frac{2 * (NIR + 1) - \sqrt{(2 * NIR + 1)^2 - 8\,(NIR - 2 * red)}}{2}$$

- Normalised Difference Vegetation Index (NDVI):

$$NDVI = \frac{NIR - red}{NIR + red}$$

- Normalised Ratio Vegetation Index (NRVI):

$$NRVI = \frac{\frac{red}{NIR} - 1}{\frac{red}{NIR} + 1}$$

- Ratio Vegetation Index (RVI):

$$RVI = \frac{red}{NIR}$$

- Simple Ratio Vegetation Index (SR):

$$SR = \frac{NIR}{red}$$

- Transformed Vegetation Index (TVI):

$$TVI = \sqrt{\frac{NIR - red}{NIR + red} + 0.5}$$

- Transformed Vegetation Index (TTVI):

$$TTVI = \sqrt{\left|\frac{NIR - red}{NIR + red} + 0.5\right|}$$

Of these indices, OTB only includes GEMI, MSAVI, MSAVI2, NDVI and RVI. The rest must be manually coded. Spectral indices incorporated in OTB that make use of red and NIR wavelengths and that have not been mentioned include (CNES, 2017):

- Infrared Percentage Vegetation Index (IPVI) (Payero, Neale and Wright, 2004):

$$IPVI = \frac{NIR}{NIR + red}$$

- Perpendicular Vegetation Index (PVI):

$$PVI = \frac{NIR - a_0 * red - a_1}{\sqrt{1 + a_1^2}}$$

with a_0 and a_1 the intercept and slope of the soil line, respectively (Payero, Neale and Wright, 2004).

- Soil-Adjusted Vegetation Index (SAVI):

$$SAVI = \frac{NIR - red}{NIR + red + L} * (1 + L)$$

where *L* is a correction factor whose value depends on the vegetation cover (zero for total cover, one for low vegetation cover) (SEOS Project, 2017).

- Transformed Normalized Difference Vegetation Index (TNDVI) (Deering et al., 1975):

$$TNDVI = \sqrt{NDVI + 0.5}$$

- Transformed Soil Adjusted Vegetation Index (TSAVI) (Payero, Neale and Wright, 2004):

$$TSAVI = \frac{a_1 * (NIR - a_1 * red - a_0)}{red + a_1 * NIR - a_1 * a_0}$$

- Weighted Difference Vegetation Index (WDVI) (Payero, Neale and Wright, 2004):

$$WDVI = NIR - a_1 * red$$

As can be observed, a number of indices exist for vegetation using optical and NIR bands. The possibility to incorporate bands in the SWIR wavelengths to compare the accuracy in the results, in order to assess the real suitability of the selected sensor for this application and possibly consider other options, could also be contemplated. SWIR wavelengths would incorporate the region between 1500 and 1750 nm, where water has high absorption. Information about the water content and the possibility of adding water-specific spectral indices would be of great interest for fire-related applications.

Furthermore, the incorporation of additional bands in the visible would allow the use of other indices also included in OTB that could improve the classification accuracy. These are the Atmospherically Resistant Vegetation Index ARVI (blue, red and NIR), the Angular Vegetation Index AVI (green, red and NIR) (CNES, 2017), Enhanced Vegetation Index EVI (blue, red, NIR) (The IDB Project, n.d.) and the Transformed Soil Atmospherically Resistant Index TSARVI (red-blue and NIR) (Bannari et al., 1995).

c. Feature selection

In order to retain only the relevant features to distinguish the different classes, OTB utilises various data dimensionality reduction methods. This will also lighten the computational cost of the classification. These methods are (CNES, 2017):

- Principal Component Analysis (PCA)
- Noise-Adjusted Principal Components Analysis
- Maximum Noise Fraction transform
- Fast Independent Component Analysis
- Maximum Autocorrelation Factor transform

Because of its higher usage in hyperspectral image classification, PCA will be used in this study. The only inputs for this operation are the number of PCs required as output and the image (CNES, 2017).

To avoid losing information unnecessarily, the algorithm must be first implemented without applying PCA. Only if the computational load exceeds the processing capability should PCA be performed.

d. Classifiers

From the literature available on hyperspectral image classification using Machine Learning, it can be deduced that kernel-based algorithms outperform traditional image classification algorithms. This is especially true for the case of SVM for hyperspectral images. Also, combining different classifiers generally produces better results.

Bicalho Santos, de Albuquerque Araújo and Menotti (2013) combined six different methods to obtain a more accurate classification map. Namely, they studied three feature representations based on spectral and spatial information and two learning algorithms, SVM and Neural Networks. The combining approach was based on Weighted Linear Combinations (WLG) using Genetic Algorithms (GA), which achieves better results than Majority Vote and Average rules. SVM proved to be effective in dealing with high dimensional data and small training sets.

Miao and Shi (2016) also stated that SVM has better accuracy in pixel-wise classification. The spectral-spatial classification outperformed the state-of-the-art methods in use at that time.

Because of the high dimensionality of hyperspectral images, their classification methods must be able to operate with a lot of different features. In this frame, Neural Networks perform better than other methods such as logistic regression (Ng, 2017c). On its side, SVM is a large margin classifier and thus normally assures more efficient separation of the data and lower classification error (Ng, 2017e).

Thus, SVM, ANN and the combination of both will be implemented in this work. Finally, a combination of both classifiers through decision fusion will be also analysed.

e. Accuracy assessment

The classification accuracy will be assessed by means of:

- Overall accuracy (OA): number of well classified samples divided by the number of test samples.
- Average accuracy (AA): Average of class classification accuracy.

- Kappa coefficient of agreement κ: Percentage of agreement corrected by the amount of agreement that could be expected due to chance alone.
- Class accuracy: Percentage of correctly classified samples for a given class.

Geolocation

The moment when geolocation is carried out will have different effects on the overall system performance. On the one hand, geolocating the image after classification will trigger a lower computational effort, as only the relevant pixels must be classified in order to produce the geolocated shape file and will not affect the classification accuracy if the only features considered are spectral reflectance over different wavelengths and radiometric indices (per-pixel classification). On the other hand, a classification of a geolocated image would enable the incorporation of spatial information as a classification feature (object-based classification), increasing the classification accuracy, but also increasing the computational load. One consideration that must be constantly taken into account for the PyrSat mission, is that due to the autonomy of the image processing tasks, every possible step to increase accuracy should be taken. Thus, the first approach (i.e. classification after geolocation) seems to be a more appropriate method for the mission and will be chosen at this stage. However, the ratio of improvement in accuracy to computational load must be assessed during the development of the entire payload software.

The geolocation tool will be based on a project previously developed by the author in the Remote Sensing Laboratory of the Spanish National Institute for Aerospace Technology (INTA): OPTOS_EOCFI, a software tool for the geolocation of CubeSat images. This SW tool is based on the Earth

Observation CFI libraries by ESA. Although it was developed for the Spanish satellite OPTOS, it could be easily adaptable to any other satellite. OPTOS had an on-board panchromatic camera called APIS that featured a CMOS detector. Both will be involved in the definition of the software (Estébanez, 2015 and 2016).

Figure 4.15 shows a diagram flow of the software architecture of OPTOS_EOCFI. Four functions are used in the process:

- *az_el*, which defines the sensor model by means of the azimuth and elevation angles of each pixel's line of sight based on the characteristics of the CMOS detector and the APIS camera: the dimensions of the detector, the pixel size and the focal length.
- Telemetry processing: There are two kinds of APIS science telemetry:
    - On the one hand there is the image information telemetry that contains orbital and attitude information relative to two different times: just before and just after the capture of the image, as well as these two times and the time of the capture. The *processor_INFO* function produces the information correspondent to the capture time through interpolation of the two other measurements.
    - On the other hand, there is the image data telemetry that contains the detector configuration parameters and the actual image. These configuration parameters allow the user to choose a region of interest (ROI) in the detector in order to take smaller images that need less memory and less time to be transmitted to ground,

and are the initial pixel row and line and the dimensions of the ROI. The *processor_DATA* function extracts and saves these metadata.

- The *OPTOS_eo* geolocation function uses as inputs the results of the previous functions. That is, the time and information relative to the time of the capture, the CMOS configuration parameters and the azimuth and elevation angles of each pixel in the image. It also makes use of a Digital Elevation Model (DEM), specifically the ACE 2 model with a resolution of 9 arcsec, and the Earth's precession and rotation parameters provided by the IERS (International Earth Rotation and Reference Systems Service) in periodical bulletins. With all this information it calculates and prints the geographic coordinates of each pixel through the implementation of the EOCFI libraries (Estébanez, 2015 and 2016).

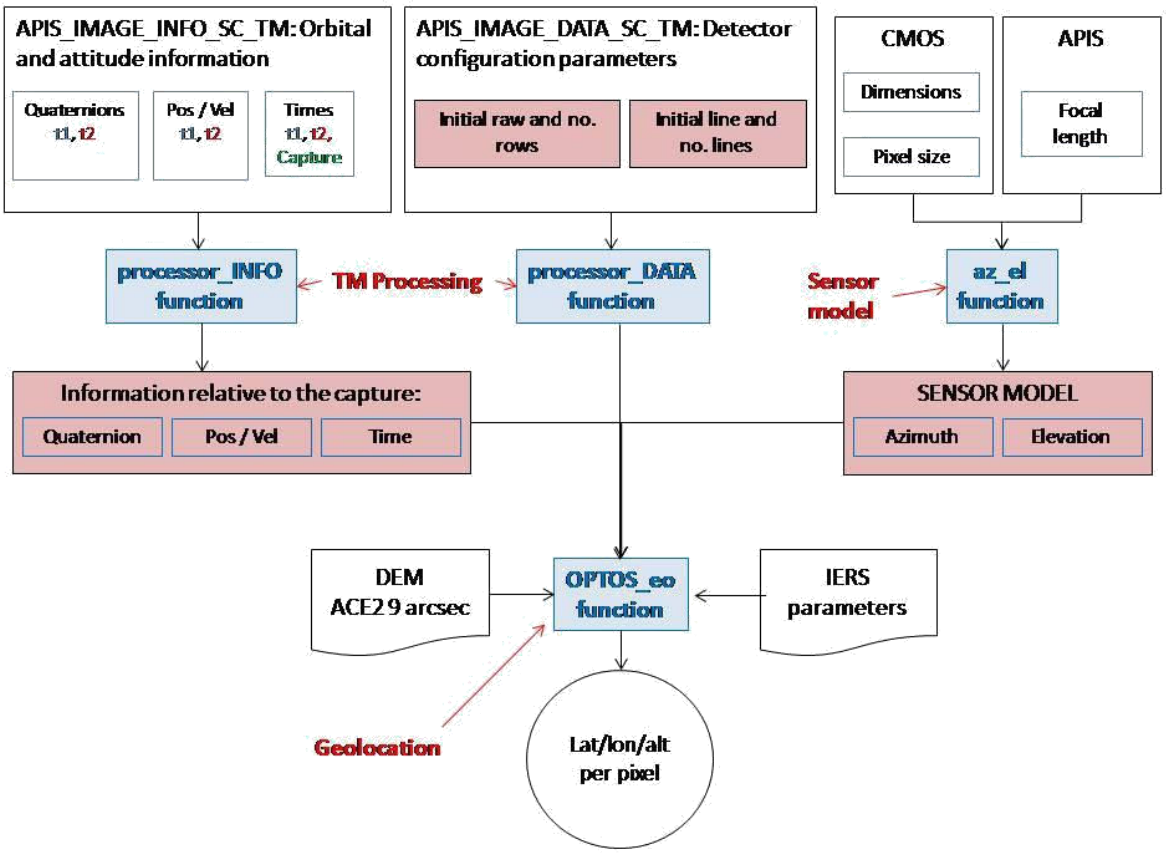

Figure 4.15: OPTOS_EOCFI software architecture (Estébanez, 2016).

In order to adapt this process to the PyrSat mission, it will be necessary to take into consideration the different telemetry formats and sensor model (i.e. dimensions of the detector, pixel size and focal length). In the case of the sensor model it must also be considered that while APIS was a snapshot sensor, the LS100 camera by XIMEA is a linescan sensor. Apart from these issues, the rest of the image analysis and classification process should be the same. It is important to note that this geolocation method avoids the use of ground control points (GCPs), making the process more easily automated.

4.3.3. Final software product

Once the software has been developed and the best methods have been identified, they will be implemented in C++ in the NVIDIA Jetson TX1 computer. Only this final software product will be thus launched to space and used by the satellite to process the mission data. During this implementation and before declaring it operative, the software must be tested to confirm that the results obtained in operation in orbit are the same that those obtained during the development phase.

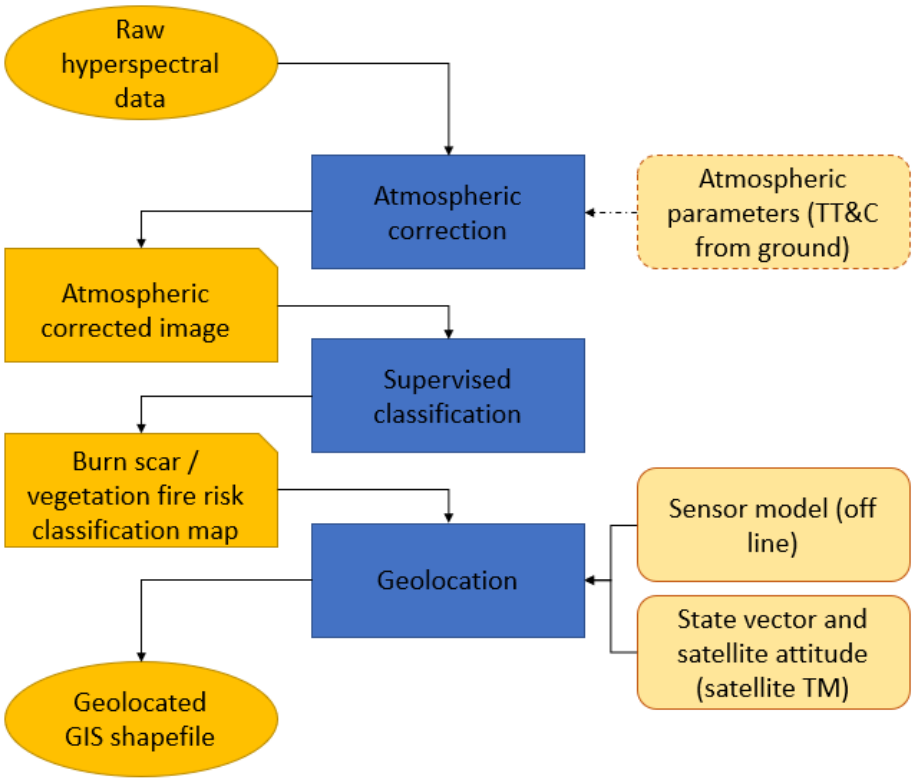

Figure 4.16: Software architecture and data flow for PyrSat.

The on-board software architecture and data flow are represented in Figure 4.16. Three consecutive tasks are carried out in order to obtain the final data product from the raw hyperspectral data:

1. **Atmospheric correction**: In different circumstances, image-based methods or modelling methods will be applied. For the latter, ground operators must upload atmospheric parameters to the satellite via the TT&C link. A decision factor will be for example the availability of atmospheric data and the particular atmospheric conditions in a given date and location.

2. **Supervised classification**: Only the already trained and validated classifier will be installed on the on-board processor, so that an input image will be directly classified in order to obtain a classification map of either burned areas or vegetation fire risk.

3. **Geolocation**: Direct geolocation will be performed using the sensor model and the satellite orbital data (i.e., state vector and attitude). These parameters will be derived directly by the satellite and expressed in its telemetry. As opposed to the traditional image geolocation, where all the image pixels are geolocated, only the perimeter of the GIS layer polygons will

be geolocated in this project. This will reduce the computing demand and also minimise the size of the final data product.

Finally, the derived mission data product will be a shape file containing the geolocated perimeter of the GIS polygons forming the different thematic areas for each application (i.e. burned areas and vegetation fire risk maps).

Chapter V. Schedule, cost and funding

This Chapter will describe the schedule and cost of the PyrSat's whole life-cycle as well as sources of funding. To start with, the typical phases of a space mission will be introduced and identified in the PyrSat mission. Later, a time scale will be given to the different phases of the mission, so as to achieve the objectives while complying with the requirements of the project. Further on, a cost estimate for the mission life-cycle will be calculated. Finally, possible sources of funding for the project will be discussed.

5.1. Schedule

In line with the requirement PSR 24, the mission shall be developed within two years. The fact that all the satellite components are COTS, most of them being already qualified for space conditions, and the on-board scientific software is open source make this requirement more easily achievable.

NASA defines seven project phases in a space mission, and identifies a series of key decision points and major reviews as a result of these different phases. This structure is represented in Figure 5.1.

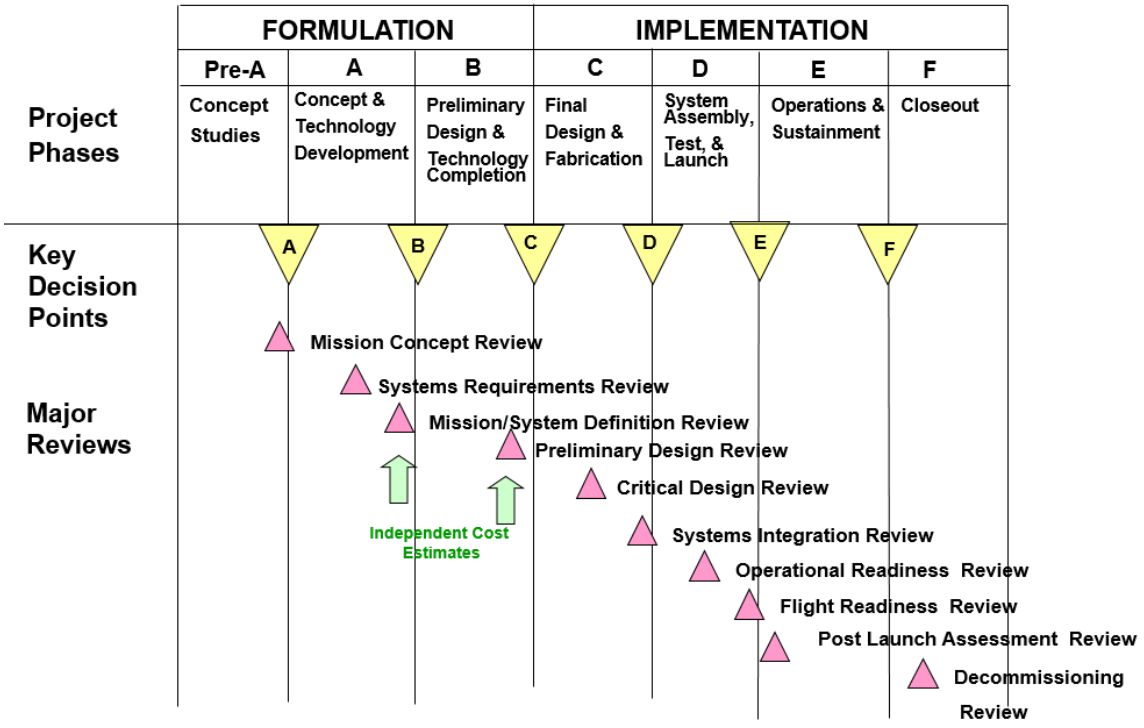

Figure 5.1: Space mission life-cycle as defined by NASA (NASA, n.d.d).

This work covers the three first phases of the project: concept studies, concept and technology development and preliminary design and technology completion. The preceding Chapters of this dissertation have addressed the conceptual design of PyrSat and the consideration of using only COTS components for all the mission (satellite and ground station) hardware. Thus, the next phase to carry out should be the Final Design and Fabrication.

5.1.1. Final design and Fabrication

The Final Design and Fabrication phase includes activities such as developing and refining the overall design and elaborating engineering data including satellite plans, the necessary tests, specifications and procedures. The result of this phase shall be translatable into manufacturing plans that describe detailed procedures for assembly and identify inspections and test requirements, facilities where these operations should be carried out and the required personnel.

Upon the completion of this phase, the **Critical Design Review (CDR)** will be produced before moving on to phase D: System Assembly, Test and Launch. The CDR documents the maturity of the design and verifies that it is appropriate to support proceeding with full-scale fabrication, assembly, integration, and test. It ensures that the flight and ground system development and mission operations are feasible, meeting the mission requirements within the defined cost and schedule constraints (NASA, 2009).

5.1.2. System Assembly, Test and Launch

First of all, the satellite COTS components must be ordered. Although all of them will be ordered at the same time, higher priority will be given to the hyperspectral camera and the dedicated computer (both the NVIDIA Jetson TX1 board and the Orbitty carrier) that form the heart of the payload.

While waiting for the delivery of the components, the development of the on-board payload software will be finished, with a view to incorporating it into the dedicated computer as soon as it is available. Once the hyperspectral camera is received, compatibility of the camera and its related sensor will be tested. These tests will be used to characterise the optical performance of the camera/sensor system. The results of these tests will be incorporated in the image processing and analysis software. Later on, the compatibility of this camera/sensor system with the Jetson computer, installed on the Orbitty carrier, must be also tested. Laboratory tests will be complimented with tests performed using an aerial platform. Indeed, conducting a flight campaign to as a payload proof-of-concept test is generally a necessary step in space missions.

Upon receipt of all the components, the **Systems Integration Review (SIR)** will be scheduled. This review ensures that all the necessary components are available and ready to be integrated into the satellite. Furthermore, all the integration facilities, the necessary support personnel and the integration plans and procedures are ready for integration (NASA, 2009).

All the flight hardware must be subjected to the pertinent space qualification tests in order to demonstrate that the hardware and software design is suitable and that the satellite will survive the stresses and conditions experienced during the launch and in-orbit. This includes (Wertz and Larson, 1999):

- *Vibration test:* This test qualifies the survivability of components to the vibrations produced when the launch vehicle acoustics couple with the engine rumble through its structural mount. The test normally consists of inducing a random signal spectrum in the frequency range of 20 – 2000 Hz.

- *Shock test:* The shock test simulates the stresses experienced by the satellite in its separation from the launch vehicle and the stresses that can be induced by explosive release

devices such as aerodynamic fairing separation mechanisms or satellite separation bolts. The test consists of a shock pulse in the form of a complex wave that triggers a mechanical response over a wide range of frequencies.

- *Thermal vacuum test:* This test demonstrates the spacecraft's ability to survive the extremes of temperature and thermal fluctuations experienced in orbit. The spacecraft is mounted on a temperature controlled base plate inside a vacuum chamber. The vacuum chamber's walls contain thermal shrouds for cooling or heating. The satellite is then subjected to thermal cycles that simulate the temperature variations it will experience in space. These temperature cycles are obtained by conductive transfer to the base plate and radiative transfer to the chamber's walls. In order to qualify for space, the component must be able to tolerate these temperature variations, including the temperature extremes without any failure (Wertz and Larson, 1999).

Generally, these qualification tests are conducted in a sequence such as to match the expected stresses during the launch phase and in orbit. An example of such a sequence, extracted from Wertz and Larson (1999), is represented in Figure 5.2.

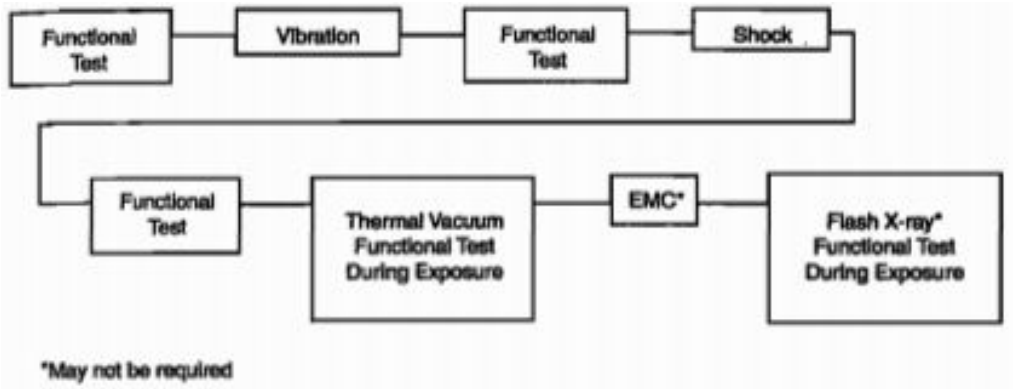

Figure 5.2: Flow of qualification testing for components. A component is qualified by a series of functional tests and exposure to environmental conditions. In the figure, EMC stands for electromagnetic compatibility (Wertz and Larson, 1999).

The functional test represents tests in which the performance of the components is checked. The flash X-ray test is carried out for components that must survive nuclear weapons effects and simulates the prompt radiation dose. This test will not be conducted on PyrSat components. Finally, EMC stands for electromagnetic compatibility (Wertz and Larson, 1999).

There are three different possible qualification methods (Wertz and Larson, 1999):

- *Dedicated qualification test*, in which a separate set of qualification components is tested at qualification levels and later this same set or a second qualification set is integrated in the spacecraft and tested at qualification levels.
- *Qualify the first set of flight hardware* or *protoflight approach*, in which the first set of flight components are tested at qualification levels, then integrated into the spacecraft and tested again at qualification levels and finally this same unit is launched.
- *Qualify by similarity*, in which qualification is just based on demonstrating that the component and the environment are identical to previously qualified hardware.

Since most of PyrSat's components are COTS, and in order to minimize the cost of the project, the protoflight approach will be followed. Thus, there will be no qualification articles and the hardware will be directly designed to all qualification requirements. On the one hand, this approach has the advantage that the mission is partially demonstrated, saving time and cost. On the other hand, it also poses some risks derived from the testing of the flight article (Welch, 2010).

Here it must be taken into consideration that most of the COTS components have already been successfully qualified for space. Table 5.1 summarizes the satellite hardware elements and corresponding tests. Most of the COTS components have flight heritage and are qualified for space. In these cases, the subsystems will be tested only once integrated in the whole spacecraft. This reduces the number of component-level tests necessary to the momentum wheel CubeWheel Small and the payload, that comprises elements not designed for space. Even after contacting NanoAvionics, there is no available information on the tests of the EPS. Thus, unless further information is received before the EPS is received, it will be necessary to perform qualification tests on this system in order to ensure its survivability in space.

In order to optimize resources, CubeWheel Small and the EPS will be qualified at a component-level upon their receipt. The fact that CubeWheel Small has been designed to work in combination with the rest of CubeSpace ADCS should ensure that it will have an appropriate performance at a subsystem-level. In the case of the payload, its integration and proof-of-concept will be carried out before the qualification tests.

At this point all the subsystems are assumed space qualified and we shall then assemble the whole spacecraft and perform the *integrated system test* (IST).

The ground station will be ordered from NanoAvionics at the same time as the satellite components. Upon receipt of the ground station equipment, it will be installed and tested. These tests will include issues such as verifying the correct performance of the steerable antenna.

If the system test produces any undesired results, the appropriate modifications will be made. Once the ground station passes all its qualification tests, the mission development can proceed to the next phase: test the compatibility of the satellite with the ground station and the correct reception and sending of telemetry and telecommands.

The full development process must be documented, including all test results, even if unsatisfactory, so as to be able to trace the development, testing and qualification of the system, and to use these documentation as a fault-finding tool and as in in-house development resource for future missions.

Table 5.1: Satellite hardware and relative test information (CubeSpace, 2016a, 2016b, 2016c, 2016d and 2016e; EnduroSat, 2016a and 2016b; XIMEA, 2016 and n.d.; Connect Tech Inc., 2017;ISIS, 2016 and n.d.a., Surrey n.d. and 2014).

Component		Vibration test	Shock test	Thermal vacuum test	Additional commentaries	Space flight heritage
ADCS	**CubeControl**	Successful	Evidence of test is lacking – Assumed successful	Successful	Also radiation test (TID)	Used on QB50 precursor satellites
	CubeSense	Successful	Evidence of test is lacking – Assumed successful	Successful	Also radiation test (TID)	Used on QB50 precursor satellites
	CubeTorquer	Successful	Evidence of test is lacking – Assumed successful	Successful	---	Used on QB50 precursor satellites
	CubeCoil	Successful	Evidence of test is lacking – Assumed successful	Successful	---	Used on QB50 precursor satellites
	CubeWheel small	**Necessary**	**Necessary**	Successful	---	Wheel design based on momentum wheels used on QB50 precursor satellites
	GPS: Antenna and receiver	Successful – On-board the Pegasus satellite (PEGASUS Team, 2017a)	Successful – On-board the Pegasus satellite (PEGASUS Team, 2017a)	Successful – On-board the Pegasus satellite (PEGASUS Team, 2017a)	N.A.	Flown on the Austrian satellite Pegasus within the European project QB50 – Information obtained through direct correspondence with SkyFox Labs. Successful in-orbit commissioning of the GPS (PEGASUS Team, 2017b)
OBDH: CubeComputer		Successful	Evidence of test is lacking – Assumed successful	Successful	Also radiation tests (TID @ 20 krad, SEE @ 60 MeV)	ADCS OBC on QB50 precursor satellites
Comm.	Passive S-band	Successful:	Successful	Successful:	Tests follow the ESA	None

subsystem	antenna	Random Vibration Sine Vibration		Thermal Cycling Thermal Vacuum	standard ECSS-E-ST-10-03C and GEVS: GSFCSTD-7000A	
	UHF Antenna	Successful: Random Vibration Sine Vibration	Successful	Successful: Thermal Cycling Thermal Vacuum	Tests follow the ESA standard ECSS-E-ST-10-03C and GEVS: GSFCSTD-7000A	None
	UHF/S-band Transceiver	Successful: Random Vibration Sine Vibration	Successful	Successful: Thermal Cycling Thermal Vacuum	Tests follow the ESA standard ECSS-E-ST-10-03C and GEVS: GSFCSTD-7000A	None
Payload	HS LS100 camera	**Necessary**	**Necessary**	**Necessary**	XIMEA states space exploration as a possible application due to the camera's robustness	None
	Jetson TX1 dedicated computer	**Necessary**	**Necessary**	**Necessary**	The board will be protected by the Orbitty Carrier Maximum TX1 TTP (thermal transfer plate): 80 °C	None
	Orbitty Carrier	**Necessary**	**Necessary**	**Necessary**	Operating temperature range of -40 °C to 85 °C	None
Power subsystem	3U side solar panels	Successful	Successful	Successful: Thermal Cycling Thermal Vacuum	Additional tests: Total Ionizing Dose Continuity Isolation Flasher Test Solar Cells crack test	Flight heritage in different missions since 2013
	EPS	TBD - No information available Manufacturer has been contacted but there has been no response yet	TBD - No information available Manufacturer has been contacted but there has been no response yet	TBD - No information available Manufacturer has been contacted but there has been no response yet		TBD - No information available. Manufacturer has been contacted but there has been no response yet
3U CubeSat structure		Successful	Successful	Successful: Thermal Cycling Thermal Vacuum	---	Flight heritage in different missions since 2013; the ISIS 1U CubeSat structure has flight heritage since 2012

The deliverable resulting from the system validation will be the **Operational Readiness Review (ORR)**. The ORR examines the system characteristics and procedures used in operation and certifies that the mission is ready to be operational. This includes all mission elements: from flight and ground hardware and software, to personnel, procedures and user documentation (NASA, 2009).

Besides the ORR, the review that serves as the final "go-no go" review to proceed with the satellite launch is the **Flight Readiness Review (FRR)**. The FRR ensures that the system can be safely and successfully launched and further operated. It also certifies, expanding on the ORR, that the system is operationally ready (NASA, 2009).

At this point, the launch will be procured and the satellite will be transported to the launch site and integrated in the launch vehicle to be finally launched. In order to alleviate the workload and to potentially accelerate the time to launch, one possibility is hiring ISIS launch services. ISIS offers numerous launch opportunities on different launch vehicles, most of them having capacity for 3U CubeSats, an achievable orbital altitude including 550 km and to Sun-synchronous injection orbits (ISIS, 2018). ISIS also has an office in Cape Town, which would greatly facilitate interaction with the launch service provider.

In February 2018, ISIS successfully carried out or supported thirteen launch campaigns, launching 259 CubeSats and one microsatellite on-board different launch vehicles. Figure 5.3 shows the launch sites from which the diverse missions have been launched.

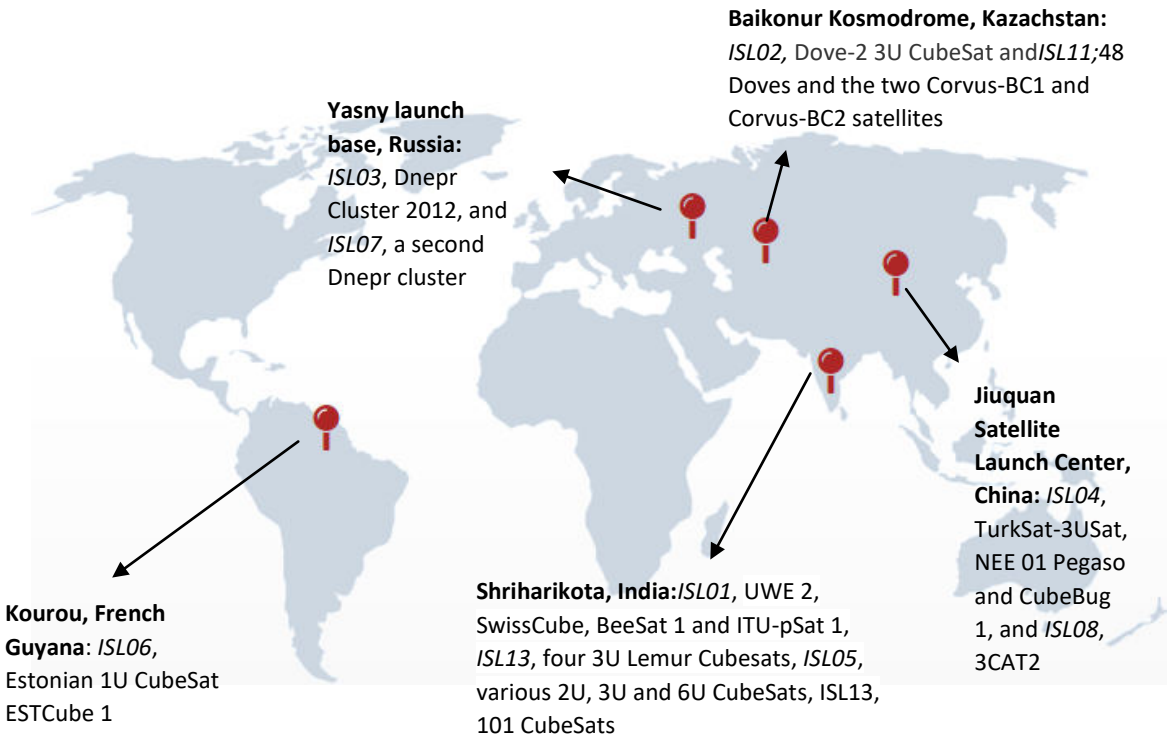

Figure 5.3: ISIS Launch Services' past launch campaigns, since the first launch in 2009 until the most recent one in February 2018 (ISIS, 2018).

5.1.3. Operations and Sustainment

Once the satellite has been launched, the first phase will be commissioning, in which its in-orbit performance after separation will be checked. The duration of this phase is estimated to be on the order of two months.

After successfully being commissioned, the **Post-Launch Assessment Review (PLAR)** will take place. The PLAR determines the readiness of the spacecraft to proceed with full operations after it has been deployed. Besides the status of the spacecraft, it also evaluates the status of the overall project plans and the ability to successfully conduct the rest of the mission (NASA, 2009).

Only after successfully being commissioned will the satellite be declared operational. During its operational life, users will request certain observations to the mission operators, who in turn will task the satellite to perform those observations. When the satellite captures an image, it processes it and sends the final data product to the ground station, to be then transmitted to the users. There will be a master ground station (integrated with the mission operations centre) and a network of auxiliary downlink-only ground stations that will download the data from the satellite and transmit them to the master ground station via the internet. The master ground station will then transmit the product to the end users. All the on-ground data transfers will be done via internet. The ground operators will be responsible for scheduling the observations according to the users' needs and priorities.

The ground segment will be also in charge of the flight software maintenance and the identification and rectification of software errors.

In accordance with the duration requirement PSR10, the operational phase of the mission will be of a minimum of two years. If after this time the satellite is still in a good operational condition, continuation of the operational life will be maintained until the satellite fails or re-enters the atmosphere.

5.1.4. Closeout.

The operational life of the satellite will be maintained until it fails or naturally re-enters the atmosphere. If the former occurs before the latter, the satellite will be passivated (i.e. all remaining sources of energy will be discharged). The final review to be delivered is the **Decommissioning Review (DR)**. The review establishes the decision to decommission the project and evaluates the readiness of the satellite for a safe end-of-life disposal (NASA, 2009).

5.1.5. Overall mission schedule

Table 5.2: Mission schedule.

Phase	Activities	Duration
1. Final design	a. Design revision b. Elaboration of manufacturing plans and other engineering data	One month
2.Satellite subsystems and ground station acquisition	a. Payload acquisition b. Subsystems acquisition c. Ground station acquisition	a. One month b. Six months c. Four months
3.Payload preparation	a. Integration and compatibility test b. Software development	Six months
4.Payload proof-of-concept	Flight campaign for system (camera-computer-software) validation	One month
5. Subsystems qualification test	a. Reaction wheel and EPS qualification test b. Payload qualification test	a. Two weeks b. Two weeks
6.Satellite assembly	Subsystems integration	Two weeks
7.Satellite qualification test	Qualification test of the overall system	Two weeks
8.Ground station preparation	a. Installation of the ground station b. Final checks as for example steerable antenna performance c. Operations training	One month
9.Satellite and ground station compatibility test	Telemetry and telecommands links check	One week
10. Launch preparation	a. Satellite transportation to the launch site b. Satellite integration on-board the launch vehicle	One month
11.Launch	Launch	N.A.
12.Commissioning	Commissioning phase	Two months
13.Operations and maintenance	a. Operations phase b. On-board software maintenance	Up to two years by requirement, potentially longer
14.End of operational life	Electronic degradation and end of operational capability	N.A.

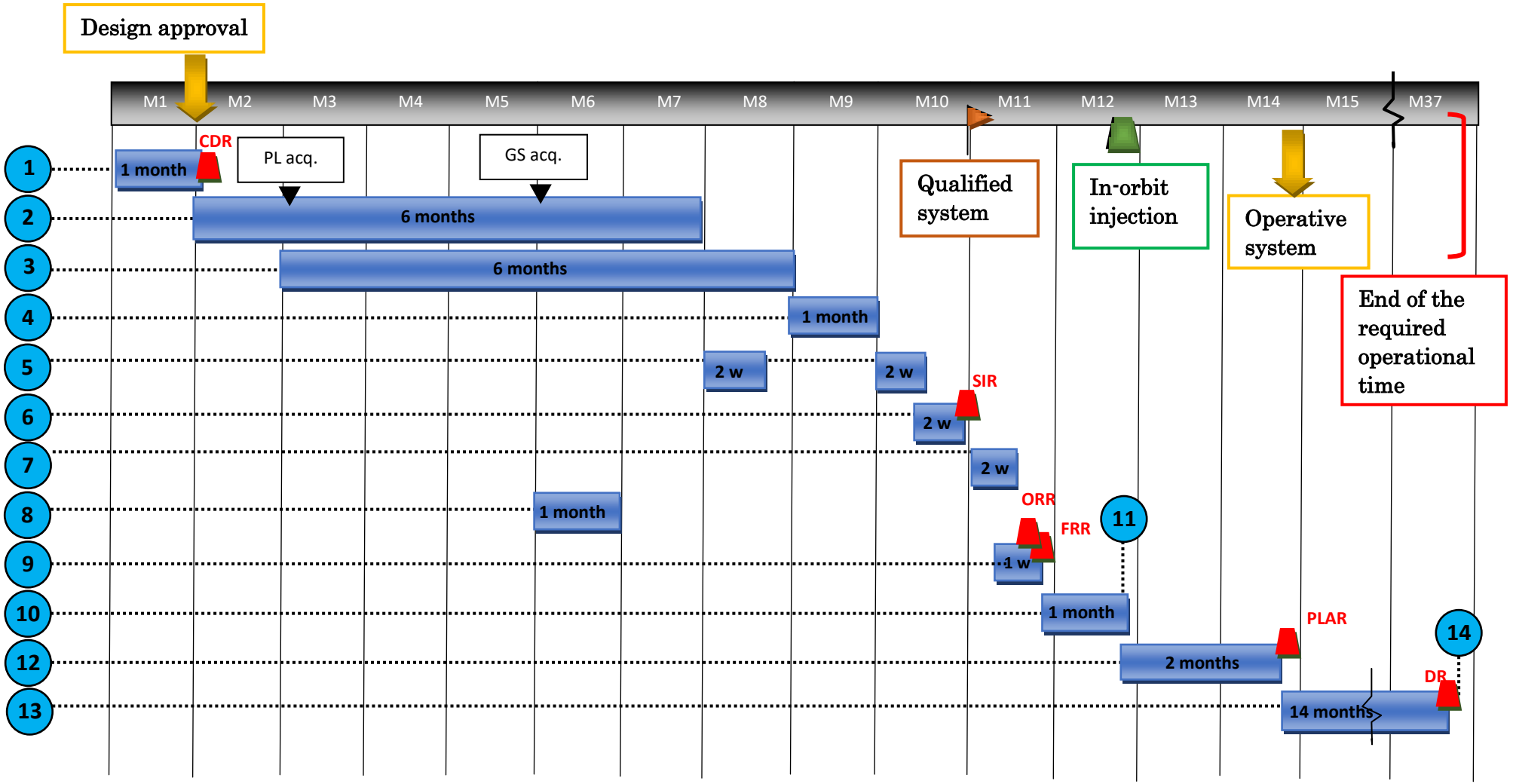

Figure 5.4: PyrSat mission timeline. Refer to Table 5.2 for a description of the mission phases.

As can be seen in Figure 5.4, if everything goes according to plan the mission will be ready to launch in one year and three weeks. This is eleven months below the two-year requirement PSR 24. This time will allow some margin to accommodate adverse circumstances such as delays in access to test facilities, delays in the setting up of tests and possible redesigns required after testing, while still complying with requirement PSR 24.

5.2. Mission cost estimate

As stated in Chapter 2, the primary objective of this mission is *to build a low-cost satellite able to produce on-board vegetation fire risk and burned area maps based on hyperspectral data*. Other hyperspectral satellites have been launched before and on-board processing is being introduced in a number of space missions. However, the most powerful characteristic of PyrSat is to develop those technologies for a low-cost CubeSat. Indeed, the main motivation for this project was to offer the benefits of hyperspectral imagery to communities for whom space has traditionally been out of reach as a tool to solve real-world problems.

Thus, cost has been the main design driver in the mission design. The goal has been to achieve the required functionalities and performance at a minimum cost. This design approach is often referred to as *design-to-cost*.

5.2.1. Space Mission Work Breakdown Structure

Probably the most comprehensive way of estimating the life-cycle cost of a mission is through a Work Breakdown Structure (WBS), as represented in Figure 5.5.

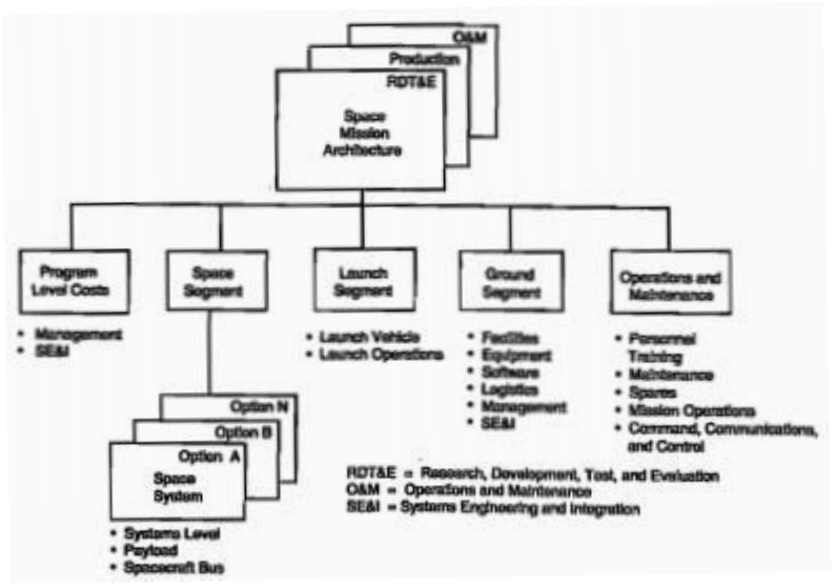

Figure 5.5: Representative Work Breakdown Structure (Wertz and Larson, 1999).

Three phases are differentiated in the mission life cycle (Wertz and Larson, 1999):

1. *Research, Development, Test and Evaluation (RDT&E).* This phase comprises design, analysis and test of breadboards, brassboards, prototypes and qualification units. Traditionally, it also covers protoflight units and one-time ground station costs.

2. *Production.* This phase covers the production and launch of flight units, including technology development for system components. The Theoretical First Unit (TFU) is often used as a tool for modelling costs and represents the estimated cost of the first satellite launched. In space missions comprising only one satellite, the TFU is the flight article itself. In constellations with various satellites, the successive replacement satellites are part of the Operations and Maintenance phase. The cost of these replacement satellites is estimated through a learning curve from the TFU cost.
3. *Operations and Maintenance (O&M).* This phase's costs consist of on-going operations and maintenance costs. This includes spacecraft replacements in a constellation, software maintenance and ground station operations.

5.2.2. Cost evaluation for PyrSat

In order to apply the WBS cost evaluation mentioned above to this particular mission, its characteristics must be defined:

- All the satellite components are COTS. This will reduce the research, design, test and evaluation times and costs.

- Due to the cost and schedule limitations and also the flight heritage of most of the proposed satellite subsystems, the production will follow a protoflight approach.

  Thus, the traditional two first phases of the WBS, Research, Development, Test and Evaluation (RDT&E), and production, will be modified. The first phase will be reduced to the design of the mission and the system design selection among the commercially available components. The scientific flight software will also be developed in this phase. The first integration and test of the whole system will be part of the production phase.

- The PyrsSat space mission will in principle consist of only one satellite, although in the future the setting up of a constellation could be considered after a successful in-orbit demonstration of the first unit. Thus, the operations and maintenance phase will only consist of the flight software maintenance and ground operations for one spacecraft.

- All the staff involved in the mission after its launch will be based at the master ground station. Ground station operators will be responsible for communicating with the satellite and also for carrying out all mission tasks, including marketing, public communication and communication with the users.

- For a first estimation of the overall life-cycle cost the engineer salaries are based on the average salary of a software engineer in South Africa as of February 2018. This figure has been taken from the PayScale website (www.payscale.com). This salary is deemed a good estimate for all the engineers involved in the PyrSat space mission.

- The management cost has been based on the assumption that a project manager will be employed in the space mission during the four-year period of the mission

development and operations. The figure used is the average salary for a technical project manager in South Africa as of February 2018. This figure has been taken from the PayScale website (www.payscale.com).

- However, if the project was developed as a university project, students could participate in it. This would give them a hands-on-training on space missions and reduce the overall project cost. In this case, the project manager will be a university professor supervising the team and thus the management cost will be his/her salary during the four-year project life. Furthermore, in South Africa the State handles the licensing process of projects developed in academic institutions and there are no costs for the academic institutions.

- In order to have an estimate for the payload proof-of-concept flight campaign, the Remote Sensing Laboratory at the Spanish National Institute for Aerospace Technology (INTA) was contacted. The Laboratory carries out flight campaigns for different national and international customers to test their equipment on-board a CASA 212 airplane. The flight campaigns can be arranged through the European Facility for Airborne Research (EUFAR) (EUFAR, 2018).

  The cost per hour of a flight campaign at INTA is 5380 Euros, including the flight and the distribution of the data to the user. A simple flight needs three to four hours and generally a project needs more than one flight. The typical requirement for EUFAR is eight to ten hours per project. Additionally, costs of third party instrument integration are generally associated with one or two flight days but in the case of PyrSat, because the payload is small and relatively simple, the baseline tariff of only 8 to 10 hours would apply. Thus, the flight campaign would have a cost of up to 53 800 Euros.

- The test and integration of the satellite could potentially be free of charge, counting with the support of the South African space industry. As a university user, we will have free access to the integration and test facilities at Houteq in Grabouw. Both tasks could be carried out by students with technical and engineering support from some local industry partner, or from the South African National Space Agency (SANSA), as a form of in-kind contribution to the project. An example of such collaboration is the CubeSat ZACUBE-1, developed by the Cape Peninsula University of Technology (CPUT) in collaboration with SANSA. The CubeSat was designed and built by postgraduates students within the CubeSat programme at the French South African Institute of Technology (F'SATI) (Cape Peninsula university of Technology, 2013). ZACUBE-1 was successfully launched in 2013.

- Because during the development of this dissertation it has not been possible to obtain a figurative price for ISIS satellite launching services, the launch cost has been estimated based on the price that companies such as Eurokot or Kosmotras, which offer launching opportunities on-board converted Russian rockets, charge. In the case of Kosmotras, this cost is about US$50 000 per single cube (Madry, 2016). Thus, being PyrSat a 3U CubeSat, the launching cost will be US$150 000.

In view of these considerations, the estimated costs are defined in Table 5.3.

Table 5.3: Life-cycle cost for the PyrSat mission.

WBS	Element				Cost	
Program Level Cost	Management				1 project manager x 4 years x €26 800 = €107 200	
	Final design: - Revision of the design - Elaboration of manufacturing plans - Contracts definition for tests and launch				1 engineer x 1 month x €1 800 = €1 800	
	Regulatory and licensing costs				N.A.	
Space Segment	PL SW (Because the payload software is open source, its only cost will be labour)				1 software engineer x 6 months x €1 800 = €10 800	
					HW cost	*Test*
	TFU	ADCS	CubeControl		€4 800	N.A.
			CubeSense		€4 800	N.A.
			CubeTorquer		€1 600	N.A.
			CubeCoil			N.A.
			CubeWheel small		€4 300	TBD (Potentially none)
			GPS	Antenna	€1 900	N.A.
				Receiver	€6 900	N.A.
		OBDH: CubeComputer			€4 500	N.A.
		Comm. subsystem		Passive S-band antenna	€3 000	N.A.
				UHF antenna	€3 000	N.A.
				UHF/S-band Transceiver	€7 000	N.A.
		Payload		HS LS100 camera	€17 700	TBD (Potentially none)
				Jetson TX1 dedicated computer	€279	TBD (Potentially none)
				Orbitty Carrier	€141	TBD (Potentially none)
		Power subsystem		3U side solar panels	€4 950 x 3 = €14 850	N.A.
				EPS	€3 000	TBD (Potentially none)
		3U CubeSat structure			€3 900	N.A.
	Payload proof-of-concept - Flight campaign				€53 800	
	Satellite integration				TBD (Potentially none)	
	Integrated system test				TBD (Potentially none)	
Launch Segment	Launch service				€150 000	
Ground Segment	Ground station equipment HW and SW				€25 150 x 2 GS = €50 300	
Operations and Maintenance	Ground segment operations and support.				(2 years x 2 ground stations (Cape Town and Barcelona) x 3 people at a time at each ground station during summer months and 2 people during winter months x 3 shifts of 8 hours in order to have permanent presence at each ground station. 2 GS x 2 yrs x (9pp x 6 months x €1 800 + 6pp x 6 months x €1 800) = €648 000		
Life-cycle cost					**€1 103 570**	

As shown in the Table, the overall mission life-cycle cost will be €1 103 570, with €251 970 for development (management during the mission development, final design, spacecraft software and hardware and ground segment software and hardware), €150 000 for the launch and €701 600 for operations and maintenance (management and ground segment operation during the required two-year operational mission). Out of the life-cycle cost, €767 800 is human-power cost (management, final design, payload software development and ground segment operation), €131 970 is hardware cost (satellite components and ground stations), €203 800 is services (flight campaign and launch) and finally, the mission software cost is "hidden" in the previous figures: the on-board software is open source and the ground segment software is included in the ground station cost. This cost breakdown is represented in Tables 5.4 and 5.5.

Table 5.4: Life-cycle cost breakdown by mission phases (development, launch and operations & maintenance).

Mission phase	**Cost**
Development	€251 970
Launch	€150 000
Operation and maintenance	€701 600
Overall cost	**€1 103 570**

Table 5.5: Life-cycle cost breakdown into resource type (human-power, hardware, software and services).

Resource type	**Cost**
Human-power	€767 800
Hardware	€131 970
Software	N.A.
Services	€203 800
Overall cost	**€1 103 570**

This cost ensures that requirement PSR 22, targeting a development and launch cost of under €500 000, is met. It is worth noting the low-cost of the whole 4-years mission, including development, launch and operation, that becomes more apparent when compared to similar missions. For example, Mandl et al. (2016) estimate a cost of one million US Dollars for the development of each 6U CubeSat in the *Hyperspectral Cubesat Constellation for Rapid Natural Hazard Response* proposed by NASA. This cost is comparable to the overall life-cycle cost of the PyrSat mission.

5.3. Funding

The project costs will be covered through a mixture of university funding, research grant funding and crowdsourcing and subscriptions. By following a design-to-cost philosophy, we will contain costs to the levels affordable by universities. By drawing in a number of university partners, the development times and costs may be further contained.

Crowdsourcing will be motivated among the general public. The two main factors to engage possible contributors will be the global and constant problem of wild fires and the proof of concept of this innovative technology. Incentives could be some sort of involvement in the

project, such project follow-up, outreach activities in academic institutions, workshops and visits to the ground segment to learn about the daily operations of space missions.

Although the current data produced by the satellite will be open, value added services will be available for subscribed users. This will comprise derived products such as historical data, historical analysis or data already combined with other sources of geographic information, according to the user needs.

An essential key to obtaining crowd sourcing will be marketing of the project, by sharing its evolution and achieved milestones and activities on social media platforms and at public events such as space symposia.

The project will have a dedicated website and Instagram and Facebook accounts. In the first phase, public awareness about the problem that wild fires represent in Africa and the world will be raised and small hints of the project will be shared, in order to create public interest. The website will contain information about the project, the space mission characteristics, a collection of data products represented as an interactive map, ways to collaborate and a section only for subscribed users. The project development, interesting facts and achieved milestones will be shared both on Instagram and Facebook. These two accounts will also direct the public to the website.

Chapter VI. Regulatory and space policy issues

Space missions involve a number of legal aspects that must be considered during their design and development. Because of the special nature of space, different to any environment on the Earth, space activities are governed by a special international legal regime. There are a series of international treaties, principles and soft law instruments that regulate space activities. The goal of this chapter is to define the legal frame within which the PyrSat project should be developed and all the legal and policy issues that must be taken into consideration.

The first part of the chapter presents an overview of international space law, including its origins, its fundamental principles, treaties and other soft law instruments, as well as national regulatory mechanisms. The second part of the chapter treats the regulatory issues applicable to the PyrSat space mission, both at an international and national level, for all the states involved in the project.

6.1. Introduction to space law

6.1.1. The foundations of space law

At the beginning of the space era, the different nature of space gave rise to a need for an equally different legal regime to that of any environment on Earth (terrestrial, maritime or aerial). International space law originated as a response to this new need, as the necessary international legal framework for all space activities.

Because space law was written as *public international law*, it is applicable to entities with international legal personality. That is, States and international intergovernmental organisations such as the UN or ESA. The main legislative body that develops laws and principles regulating space activities is the UN Committee on the Peaceful Uses of Outer Space (UN COPUOS). COPUOS was founded in 1959 *to govern the exploration and use of space for the benefit of all humanity: for peace, security and development* (COPUOS, 2018a). Since its establishment, the number of Member States in COPUOS has increased from twenty-four to eighty-four. At the moment, it is one of the biggest committees in the UN. Additionally, there are a number of States and intergovernmental and non-governmental entities with an observer status (COPUOS, 2018b).

There are two subsidiary bodies in charge of carrying out the technical work in COPUOS: The Legal Subcommittee and the Scientific and Technical Subcommittee, both established in 1961. COPUOS reports to the Special Political and Decolonization Committee (Fourth Committee) of the General Assembly, which adopts an annual resolution on International cooperation in the peaceful uses of outer space (COPUOS, 2018a, and United Nations, 2018). Absolute consensus of all Member States is necessary in order to reach any decision in COPUOS and its subcommittees (Martinez, 2017).

6.1.2. Space law Treaties and Principles

Expanding on the Declaration of Legal Principles Governing the Activities of States in the Exploration and Use of Outer Space, adopted by the UN General Assembly in 1963, the *Treaty on Principles Governing the Activities of States in the Exploration and Use of Outer Space, including the Moon and Other Celestial Bodies*, generally referred to as the **Outer Space Treaty (OST) (1967)**, was adopted by the General Assembly in its resolution 2222 (XXI) of 19 December 1966. It provided the basic framework for international space law, reason why it is often seen as the *Magna Carta* of space law (UNOOSA, 2008a).

The OST contains seventeen articles, including a series of principles that define the nature of outer space as a specific legal regime and that serve as the basis for subsequent space law treaties. UNOOSA (n.d.) states these principles as follows:

- *The exploration and use of outer space shall be carried out for the benefit and in the interests of all countries and shall be the province of all mankind.*
- *Outer space shall be free for exploration and use by all States.*
- *Outer space is not subject to national appropriation by claim of sovereignty, by means of use or occupation, or by any other means.*
- *States shall not place nuclear weapons or other weapons of mass destruction in orbit or on celestial bodies or station them in outer space in any other manner.*
- *The Moon and other celestial bodies shall be used exclusively for peaceful purposes.*
- *Astronauts shall be regarded as the envoys of mankind.*
- *States shall be responsible for national space activities whether carried out by governmental or non-governmental entities.*
- *States shall be liable for damage caused by their space objects.*
- *States shall avoid harmful contamination of space and celestial bodies*

These principles were the basis to the further development of international space law, embodied in four other treaties and additional so-called “soft-law”.

Only one year after the OST, the *Agreement on the Rescue of Astronauts, the Return of Astronauts and the Return of Objects Launched into Outer Space*, or the **Rescue Agreement (1968)**, entered into force. It establishes that States shall *take all possible steps to rescue and assist astronauts in distress and promptly return them to the launching State* and upon request*, provide assistance to launching States in recovering space objects that return to Earth outside the territory of the Launching State* (UNOOSA, 2017a).

Expanding on Article VII of the OST, the *Convention on International Liability for Damage Caused by Space Objects*, commonly known as the **Liability Convention (1972)**, obtained the consensus of the General Assembly in 1972. It identifies the Launching State as liable for any damage that its space objects cause in space, on the surface of the Earth or on an aircraft in the air. Liability is absolute for damage caused on the surface of the Earth or to aircraft in flight, but fault-based for damage caused to other space objects in space. The Convention also defines the procedures to claim compensation for such damages (UNOOSA, 2017b).

The *Convention on Registration of Objects Launched into Outer Space*, so-called the **Registration Convention (1976)**, was developed as a means to assist in the identification of

the Launching State of a certain space object in order to ease the implementation of the Outer Space Treaty, the Rescue Agreement and the Liability Convention. As an expansion of the 1961 United Nations Register of Objects Launched into Outer Space, established in the 1961 Resolution 1721B (XVI), it dictates that States parties to the Convention shall maintain a register of all their objects launched into Outer Space. The Secretary General of the UN shall be given all this information and he or she must then make it openly available to all other States (UNOOSA, 2017c). To date, over 92 percent of all satellites, probes, landers, manned spacecraft and space station flight elements launched into outer space have been registered with the Secretary General of the United Nations, either under the Registration Convention or GA Resolution 1721B (XVI) (UNOOSA, 2018a).

The last UN Treaty adopted by COPUOS was *the Agreement Governing the Activities of States on the Moon and Other Celestial Bodies*, often referred to as the **Moon Agreement (1979)**. The Agreement was developed from 1972 to 1979, when it was adopted. However, it was not until 1984 when Austria, the needed fifth country for the Agreement to enter into force, signed it. The Agreement elaborated on the issues related to the Moon and other celestial bodies contained in the OST. That is, their non-militarisation, non-appropriation and non-contamination and the peaceful uses of outer space. In order to achieve these goals, the United Nations must be informed of the location and purpose of any station established on any celestial body. The Agreement also reiterates the "res-communis" nature of the resources obtainable from celestial bodies and dictates that an international regime must be reached to govern their exploitation when it is about to become feasible (UNOOSA, 2017d). To date, such a regime has not been developed.

Table 6.1: Status of the UN Treaties as at February 2018 according to COPUOS (2017), and updated according to (UNOOSA, 2018b), represented by means of the number of States that have ratified, signed or recognized the different treaties.

	Outer Space Treaty	Rescue Agreement	Liability Convention	Registration Convention	Moon Agreement
Ratification, acceptance, approval accession or succession	105 + 3 (Accession by New Zealand, Armenia and Finland in January 2018)	95	94	63	17 + 1 (Accession by Armenia in January 2018)
Signature	25	24	20	4	4
Declaration of acceptance of rights and obligations	0	2	3	3	0

Besides the above treaties, COPUOS has over the years also defined a series of principles that should guide the use and exploration of outer space. They were enacted as instruments of soft law, i.e. they are not legally binding upon States but represent the "best practice". However, they could become binding upon private actors by their inclusion in national law. The first of principles were adopted in the UN General Assembly resolution 1962 (XVIII) of 13 December 1963, *Declaration of Legal Principles Governing the Activities of States in the Exploration and Uses of Outer Space*, known as the *Declaration of Principles* (UNOOSA, 1963a).

As the space sector evolved and space technology and applications advanced, later General Assembly resolutions added other principles to guide the practices of States in the conduct of their space activities in several areas. These are:

- The *Principles Governing the Use by States of Artificial Earth Satellites for International Direct Television Broadcasting*, or *the Broadcasting Principles* (UNOOSA, 1982).
- The *Principles Relating to Remote Sensing of the Earth from Outer Space*, or the *Remote Sensing Principles* (UNOOSA, 1986).
- The *Principles Relevant to the Use of Nuclear Power Sources in Outer Space*, or the Nuclear *Power Sources Principles* (UNOOSA, 1992).
- The *Declaration on International Cooperation in the Exploration and Use of Outer Space for the Benefit and in the Interest of All States, Taking into Particular Account the Needs of Developing Countries*, or the *Benefits Declaration* (UNOOSA, 1996).

Besides these treaties and principles, other soft law instruments developed by the UN comprise guidelines and resolutions. These include, among others, the COPUOS Space Debris Mitigation Guidelines.

6.1.3. Radiofrequency regulation

The International Telecommunication Union (ITU), is the United Nations agency specialized in information and communication technologies (ICTs). It is in charge of regulating the radiofrequencies and orbital slots internationally as well as defining networks and technical standards to ensure a worldwide harmonization of radiofrequency allocation and utilization. The agency's goal is also to provide ICTs to remote communities worldwide (ITU, 2017a).

At an international level, there are three intergovernmental binding treaties that dictate the applicable law regarding radiofrequency allocation and usage. These are the ITU Constitution, the ITU Convention and the ITU Radio Regulations (Johnson, 2014).

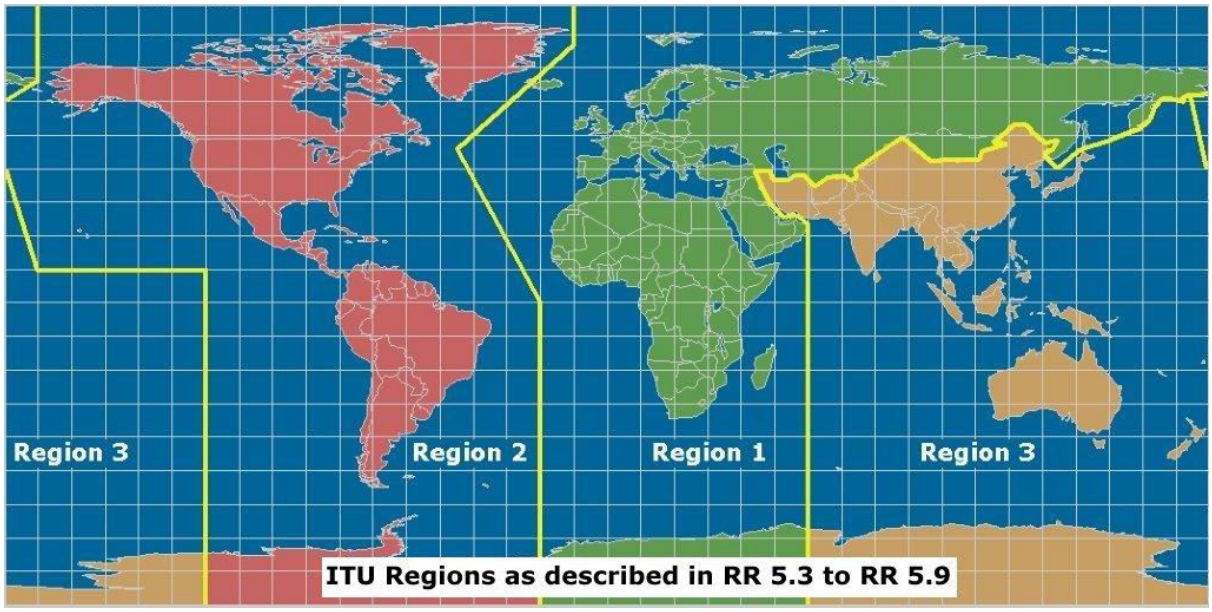

Figure 6.1: ITU regions (ITU, 2017b).

The ITU manages the radiofrequency spectrum by dividing the world in three regions and assigning different frequencies to each one of them (ITU, 2017b). Figure 6.1 shows this division. Additionally, nine different satellite services are identified within the ITU regulations and are: Fixed Satellite Services, Mobile Satellite Services, Earth Exploration Services, Space Research Services, Space Operations Services, Radiodetermination Satellite Services, Inter-Satellite Services and Amateur-Satellite Services. The spectrum is then divided into bands, with either exclusive or shared allocations over these services (Johnson, 2014).

Every space mission must undergo a coordination process in order to avoid interference with other users of the radio spectrum. The ITU recommends starting the process of frequency coordination early in the project so as to save time and resources. In terms of frequency allocation, including coordination, planning, notification and registration, the ITU relies on specific mandatory and voluntary regulatory procedures. The organization maintains the Central International Frequency Register (MIFR) that must be consulted prior selecting a frequency for a new space mission (Johnson, 2014).

At a national level, the national regulatory bodies coordinate the allocated frequencies between the different national space missions. Considering other users within the same region, these national administrators are responsible for determining the type of license that best suits a satellite service while posing the least interference to others and to register said satellite in the MIFR (Johnson, 2014).

Additionally, the International Amateur Radio Union (IARU) is in charge of managing the radio spectrum nationally and internationally among radio amateurs around the world and advising prospective satellite builders in their frequency domain (IARU, 2017a). It was organized in 1925 in Paris, France, and is divided into three Regional Organizations that correspond to the three radio ITU regions (IARU, 2017b).

6.1.4. National space law

Countries ensure that their nationals comply with international space law through domestic regulatory mechanisms. In some countries, the national space agencies are the bodies in charge of defining national legislation. While the most advanced space fairing countries have a complete and detailed space law, others may not have enacted any regulations specific to space activities. In these cases, possible sources of applicable law are telecommunications regulations, laws concerning hazardous activities or aviation legislation. In general terms, States are responsible for regulating, authorizing, licensing and supervising all space activities carried out by their nationals, both governmental and private entities (Johnson, 2014).

6.2. Space law applicable to the PyrSat project

International space law recognizes the Launching State of a particular mission as liable for any damage that it may cause. According to the Article VII of the OST (UNOOSA, 1966), a Launching State may be the State that:

a) *Launches an object into outer space, including the moon and other celestial bodies.*
b) *Procures the launching of an object into outer space, including the moon and other celestial bodies.*
c) *From whose territory an object is launched.*

d) *From whose facility an object is launched.*

The case of the PyrSat project is particularly complex. According to the first definition in the previous list, South Africa would be the Launching State. However, the preferred launching option at this phase of the project is to hire the services of the company ISIS to coordinate the whole launch. ISIS is a company from Netherlands that offers launches on-board launch vehicles of different nationalities. For instance, the launches planned for 2018 will be on-board USA, Asian, European and Russian vehicles. The States from whose territory the launches will take place will also vary in the different launching opportunities (ISIS, 2018).

Also, there will be a ground station in Barcelona that will send telecommands and receive telemetry from and to the satellite. This must be taken into consideration for the frequency regulations.

Furthermore, this being a remote sensing mission, the 1986 COPUOS' Principles Relating to the Remote Sensing of the Earth from Outer Space may apply and impact the data use and policy.

Lastly, the satellite's components may be subject to export regulations depending on their country of origin. In the case of this project, these countries are: Bulgaria (EnduroSat), Canada (Connect Tech), Czech Republic (SkyFox Labs), Germany (Ximea), Lithuania (NanoAvionics), Netherlands (ISIS), South Africa (CubeSpace and NewSpace) and United States of America (Nvidia).

Even the nationality of the people working in the project may trigger some legal considerations for the countries of which they are nationals.

6.2.1. Registration and liability

In the scope of this work and taking into account the uncertainty in the exact launch option, only the status of space law in South Africa and Netherlands will be considered for registration and liability issues. Table 6.2 shows the ratification status of the UN Treaties for these countries.

Table 6.2.1: Status of the UN Treaties in South Africa and Netherlands (COPUOS. 2017). R = Ratified

	Outer Space Treaty	Rescue Agreement	**Liability Convention**	**Registration Convention**	Moon Agreement
South Africa	**R**	R	**R**	**R**	-
Netherlands	**R**	R	**R**	**R**	R

National space law in South Africa is dictated by the *South African Space Affairs Act*, passed in 1993 and amended in 1995 (Government of South Africa, 1993 and 1995). In the case of Netherlands, it is the *Dutch Rules Concerning Space Activities and the Establishment of a Registry of Space Objects, or the Space Activities Act* (2006), that plays this role (Government of Netherlands, 2006).

Because the satellite will be produced, owned and operated in South Africa, this will be the State of Registry. Thus, the satellite will be registered with the South African Council for Space Affairs (Government of South Africa, 1993).

As stated in the Registration Convention, the South African government will be then responsible for submitting this information to the Secretary General of the United Nations (UNOOSA, 2017c). Generally, registration with the UN is done after launch. The UN provides a registration information submission form (the UN Register of Space Objects application form) written in six languages that must be filled in for this purpose. This registration form is available both electronically and in hard copy form through the State of Registry's Permanent Mission to the UN. Later in the mission life, re-registration may be necessary if the spacecraft is sold or control over it is transferred, as well as if it de-orbits. In terms of UN Resolution 62/101 on recommendations on enhancing registration practice, States are also encouraged to provide on a voluntary basis additional information such as the decay rate or the moment when the satellite becomes non-functional (UNOOSA, 2008b).

The states involved in the project and that do the function of launching states as described in section 6.2 should reach an agreement on how to share the liability in case of accidental damage to third parties. However, the particular case of Netherlands as launch provider is dubious. According to Palkovitz and Masson-Zwaan (as cited in Johnson, 2014) not only do they not consider non-propelled satellites in their space regulations, for understanding "space activities" only as requiring active space control, but they also do not deem a private procurement of a launch sufficiently relevant to implicate state liability. Thus, they are not willing to assume any liability derived from these activities.

6.2.2. Technology Transfer aspects

Due to the possible dual-use nature of advanced technology used in space projects and also to avoid unfair trade and use of technology, such as for the benefit of foreign manufacturers who did not invest in research and development, many nations restrict the exporting of their space technologies, hardware and intellectual property. These restrictions can materialize in the form of multilateral instruments, such as regulations or Codes of Conduct, or unilateral legislation (Johnson, 2014).

In order to avoid future conflicts of interest, during the development of the PyrSat project it is essential to take into consideration these restrictions. It is important to bear into mind that the satellite will be manufactured in South Africa and then exported to the country from where it will be launched. The launch site location is still uncertain and will only be known when a launch contract with ISIS is established.

Table 6.3 shows all satellite components with their country of origin with their applicable regional export regulations. Table 6.4 shows the international arrangements of which the countries involved in the project are members.

Table 6.3: PyrSat satellite's components and applicable export regulations.

Subsystem		Provider	Nationality	Applicable regional export regulations
ADCS	**CubeControl, CubeSense, CubeTorquer, CubeCoil and CubeWheel small**	CubeSpace	**South Africa**	International Trade Administration Act, 2002, (Act 71 of 2002) Customs and Excise Act, 1964, (Act 91 of 1964). Promotion to Administrative Justice Act, 2000, (Act 3 of 2000). Promotion to Access to Information Act, 2000, (Act 2 of 2000).
	GPS system (receiver and antenna)	SkyFox Labs	**Czech Republic**	Council Regulation (EC) No. 428/2009
OBDH: CubeComputer		CubeSpace	**South Africa**	Act 71 of 2002, Act 91 of 1964, Act 3 of 2000 and Act 2 of 2000
Comm. subsystem	**Passive S-band antenna**	Endurosat	**Bulgaria**	Council Regulation (EC) No. 428/2009
	UHF/S-band Transceiver	Endurosat		
Payload	**HS LS100 camera**	XIMEA	**Germany**	Council Regulation (EC) No. 428/2009
	Jetson TX1 dedicated computer	Nvidia	**USA**	Arms Export Control Act (AECA), Export Administration Act (EAA)
	+ Orbitty Carrier	Connect Tech's	**Canada**	Revised Statutes of Canada, R.S.C., 1985, c. E-19
Power subsystem	**3U side solar panels (x4)**	ISIS	**Netherlands**	Council Regulation (EC) No. 428/2009
	EPS	NanoAvionics	**Lithuania**	Council Regulation (EC) No. 428/2009
Structure: 3U CubeSat structure		ISIS	**Netherlands**	Council Regulation (EC) No. 428/2009

Table 6.4: International arrangements of which the provider countries of the PyrSat project are members.

	South Africa	Czech Republic	Bulgaria	Germany	USA	Canada	Lithuania	Netherlands
Wassenaar Arrangement	X	X	X	X	X	X	X	X
Australia Group	-	X	X	X	X	X	X	X
Nuclear Suppliers Group	X	X	X	X	X	X	X	X
Missile Technology Control Regime	X	X	X	X	X	X	-	X
Zangger Committee	X	X	X	X	X	X	-	X
Hague Code of Conduct	X	X	X	X	X	X	X	X

The **Wassenaar Arrangement on Export Controls for Conventional Arms and Dual-Use Goods and Technologies (WA)** was established in the year 1996 as a tool to promote regional and international security and stability, through transparency and responsibility in the trade of arms and dual-use items. Member States comply with the WA through their national policies and apply export controls to items established in the WA Control Lists. That is, the *Munitions List* and the *List of Dual-Use Goods and Technologies* (Wassenaar Arrangement, 2017a).

The **Australia Group (AG)** met for the first time in 1985, with 15 participating States, as a reaction to the use of chemical weapons by Iraq in the war Iran-Iraq. Since then, annual meetings have occurred and the number of AG Participants States has increased to 41 plus the European Union (AustraliaGroup.net, 2007a). The AG is an informal arrangements of countries, all parties to the Chemical Weapons Convention (CWC) and the Biological Weapons Convention (BWC), that seek to minimize the risk for chemical and biological weapon (CBW) proliferation through their national export controls (AustraliaGroup.net, 2007b).

Also as a reaction to the misuse of technology transferred for peaceful uses, the **Nuclear Suppliers Group (NSG)** originated in 1974 following the explosion of a nuclear device by a non-nuclear-weapon State. The goal of the NSG is to minimize the risk of nuclear weapons (NW) proliferation as a result of nuclear trade. For this purpose, the NSG Guidelines were published in 1978 by the International Atomic Energy Agency (IAEA) as the instructions and obligations to apply by States to nuclear trade so as to ensure nuclear items are not misused for NW proliferation (Nuclear Suppliers Group, n.d.).

The **Missile Technology Control Regime (MTCR)** was officially announced in 1987 (James Martin Center for Nonproliferation Studies, 2017) in *to restrict proliferation of missiles, complete rocket systems, unmanned air vehicles, and related technology for those systems capable of carrying a 500 kilogram payload at least 300 kilometres, as well as systems intended for the delivery of weapons of mass destruction (WMD).* In order to do so, the MTCR lists all items that must be subject to export controls in the *MTCR Equipment, Software and Technology Annex*. Member States are then responsible to comply with this export control list and to issue pertinent export licenses within their territory (Missile Technology Control Regime, n.d.).

In 1999, MTCR partners started discussions to reduce global missile proliferation, first internally and later with other "non-MTCR States". These discussions took then the form of negotiations open universally to all States to participate. In a negotiations session in the Hague, the **Code of Conduct against Ballistic Missile Proliferation (the Hague Code of**

Conduct) was established. The Code is open for voluntary subscription and provides a forum for ballistic missile non-proliferation (Missile Technology Control Regime, n.d.). Since its establishment, the number of subscribed States increased from 93 to 139 as of June 2017 (Hague Code of Conduct, 2017). Subscribing States commit themselves to provide pre-launch notifications on ballistic missiles (BM) and space-launch vehicles (SLV), as well as to submit an annual declaration of their national policies on BM and SLV (Federal Ministry for Europe, Integration and Foreign Affairs, 2018).

To end with, the Zangger Committee originated in the meetings carried out between 1971 and 1974 by a group of 15 countries suppliers or potential suppliers of nuclear material and equipment. The aim of the Group was to meet the obligations of article III, paragraph 2 of the Nuclear Non-Proliferation Treaty (NPT), *to harmonize the interpretation of nuclear export control policies for NPT Parties*. The Committee maintains a Trigger List containing nuclear-related strategic goods with the aim to assist NPT Parties in identifying items subject to export controls. To date, the Committee is composed of 39 members including all the nuclear weapon states (NWS) as defined in the NPT (Zangeer Committee, n.d.a and n.d.b). The NWS are the States officially recognized as having nuclear weapons by the NPT. That is, China, France, Russia (formerly Soviet Union), United Kingdom, and the United States (Arms Control Association, 2018).

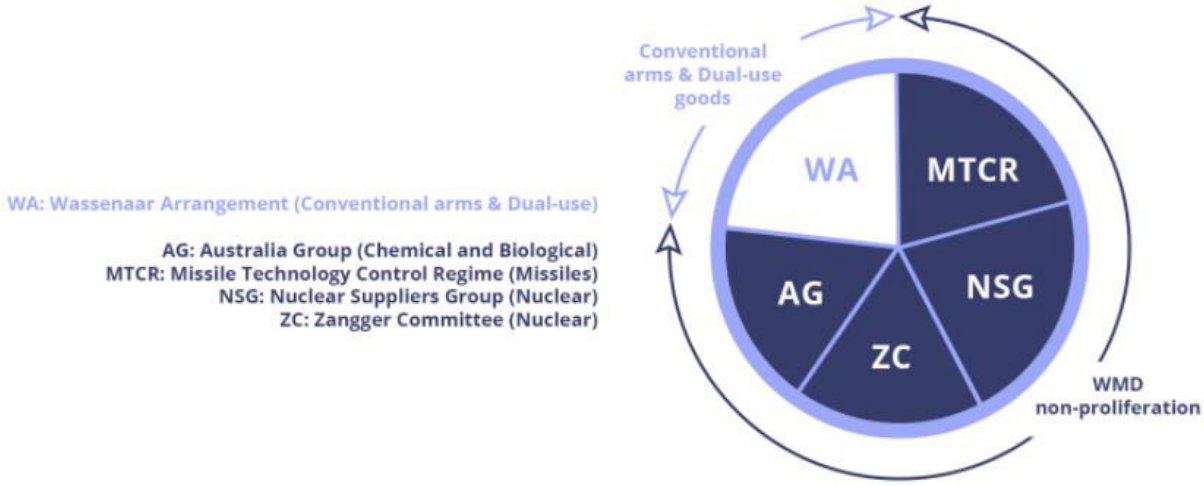

Figure 6.2: Application areas of the international trade arrangements (Wassenaar Arrangement, 2017b).

In order to comply with the international arrangements of which States are member, States implement national or regional trade regulation mechanisms. In the case of the **European Union and therefore Bulgaria, Czech Republic, Germany, Lithuania and Netherlands** in this project, the exports of dual-use items in are regulated by the Council Regulation (EC) No. 428/2009 of 5 May 2009, whose goal is to *set up a Community regime for the control of exports, transfer, brokering and transit of dual-use items* (The Council of the European Union, 2009). For this purpose, the "Regulation" establishes a set of common control rules, exports control list and guidelines for a harmonized implementation (European Commission, 2014).

In this way, certain dual-use items contained in the EU Control List or that may involve public security or human rights can only leave the European Union with an export authorization. These are:

- Items contained in the EU Control List.

- Items that, although not listed in the EU Control List, are believed to be *intended for use in connection with a biological, chemical, nuclear weapons or ballistic missile weapons programme, or for use in violation of an arms embargo*. These restrictions are made under a "catch-all clause".
- Under certain conditions, EU Member States can also impose additional restrictions to items that may involve public security or human rights (European Commission, 2014).

The Control List (Annex I of the Council Regulation (EC) No. 428/2009) is derived from decisions adopted in international control regimes, i.e. – the Australia Group (AG), the Nuclear Suppliers Group (NSG), the Wassenaar Arrangement and the Missile Technology Control Regime (MTCR) (European Commission, 2014). It divides the dual-use items into ten categories numbered from 0 to 10 - namely - Nuclear materials, facilities and equipment; Special materials and related equipment; Materials processing; Electronics; Computers; Telecommunications and ”information security”; Sensors and lasers; Navigation and avionics; Marine and Aerospace and Propulsion (The Council of the European Union, 2009).

In **Canada**, exports control are regulated by the R.S.C., 1985, c. E-19 *Export and Import Permits Act*, first redacted in 1985 and latest updated in 2017. Sections 3 of this Act states that the Governor in Council may establish a control list to regulate the export of certain items (Parliament of Canada, 1985).

Following section 3 of the Export and Import Permits Act, the SOR/89-202 *Export Control List* was established in 1989 and last amended in 2017. The Export Control List contains the items on the Wassenaar Arrangement Dual-Use List. In this list, goods and technology are divided into the following seven groups: Dual use; Munitions; Nuclear non-proliferation; Nuclear-related dual use; Miscellaneous goods and technology; Missile technology control regime and Chemical and Biological Weapons Non-proliferation. These groups are subject to export controls subject to the country of destination and varying between the different groups (Parliament of Canada, 1989).

As for the **Unites States**, there are two acts that govern the exports. On the one hand, the Arms Export Control Act (AECA) of 1976allows the US Department of State to regulate the International Traffic in Arms Regulations (ITAR) based on the United States Munitions List (USML) through the Directorate of Defense. Larger space missions normally operate under the ITAR (Johnson, 2014). The 22 U.S.C. 2778 of the Arms Export Control Act constitutes the Chapter 39 (sections 2751 to 2801) of the Title 22 - Foreign Relations and Intercourse of the United States Code of Federal Regulations (CFR) (US Department of State, 2016). Title 22 of the CFR can be accessed online at (US Department of State, n.d.)

The United States Munitions List (USML) can be found in Part 120 of the Title 22 of the CFR. It divides the regulated items into twenty-one categories related to defence.

On the other hand, the US Export Administration Act (EAA) of 1979 (US Congress, 1979) authorizes the US Directorate of Commerce to manage the Export Administration Regulations (EAR), covering the items listed in the Commerce Control List (CCL).

There is a trend in small satellite missions to utilize components included in the Commerce Control List (US Bureau of Industry and Security, 2017), which generally lessens the constraints on exports (Johnson, 2014). As the export control lists of other countries previously

mentioned, the US CCL (Supplement No. 1 to Part 774 of the EAR) includes, among others, the items contained in the Wassenaar Arrangement Dual-Use List.

The CCL assigns to the controlled items different Export Control Classification Numbers (ECCN). The ECCN are alphanumeric codes that describe an item and identify its export licensing requirements. The Control List is divided into the following ten categories, numbered from 0 to 10: Nuclear and Miscellaneous; Materials, Chemicals, Microorganisms and Toxins; Materials Processing; Electronics; Computers and Telecommunications; Information Security; Sensors and Lasers; Navigation and Avionics; Marine and Aerospace and Propulsion. Then each category is divided into five different groups - Systems, Equipment and Components; Test, Inspection and Production Equipment; Material; Software and Technology (US Bureau of Industry and Security, 2016).

Finally, once the satellite is integrated in **South Africa** it will be transported to the launch site. Thus, the satellite will have to meet the South African export regulations. The export regulatory body is the International Trade Administration Commission of South Africa (ITAC), established through the International Trade Administration Act (Act 71 of 2002). The Act 71 of 2002 establishes that the import and export of certain goods designated by regulation must be subject to control through a permit system, as well as the functions that ITAC shall undertake. ITAC is responsible for trade (import and export) control and management and technical advice to the Department of Trade and Industry of the Republic of South Africa (dti). Its main goal is *to create an enabling environment for fair trade, through the efficient and effective administration of trade instruments* (The dti, n.d.).

The Government of South Africa establishes the goods submitted to export control in the Export Control list, Government Notice No. R. 92 published in Government Gazette No. 35007 in 2012 (ITAC, 2012), and amended in the Government Notice No. 1292 published in the Government Gazette No. 39567 in 2015 (ITAC, 2015). Exporters of goods included in this list, as well as importers of other controlled items, must comply with the South African legislation as described in the following instruments: ITA Act of 2002, Customs and Excise Act of 1964, Promotion to Administrative Justice Act of 2000 and Promotion to Access to Information Act of 2000 (ITAC, 2011).

Because of the general level of detail of the export control lists and the current state of design of the PyrSat satellite, a thorough study of these documents for each satellite component is deemed out of the scope of this thesis. However, it must be carried out in a later phase of the mission design.

6.2.3. Radiofrequency aspects

Article 1.56 of the ITU Radio Regulations defines amateur services as:

> *A radiocommunication service for the purpose of self-training, intercommunication and technical investigations carried out by amateurs, that is, by duly authorized persons interested in radio technique solely with a personal aim and without pecuniary interest* (ITU, 2016).

The next article of the RR, 1.57, refines the definition of amateur-satellite services as:

A radiocommunication service using space stations on Earth satellites for the same purposes as those of the amateur service (ITU, 2016).

Since the PyrSat project's main goal is technology demonstration and scientific research, and not having a financial interest other than the necessary funding to support the mission, it can be categorized as an amateur service. The frequencies used by the designed satellite's communications subsystem are in accordance with this. In particular, a passive S-band antenna and an UHF/S-band transceiver provided by Endurosat will be used. The uplink frequency will be 430 - 440 MHz, in the UHF band, and the downlink frequency will be 2400 - 2480 MHz, in the S band (EnduroSat, 2016b). Furthermore, both South Africa and Spain are located in ITU Region 1. Within this region, South Africa is part of what the ITU defines as the "African Broadcasting Area", being part of the African territories situated between the parallels 40° South and 30° North (Radio Regulations, 5.10.a and 5.11). On its side, Spain is contained in the "European Broadcasting Area", bordered on the South by the parallel 30° North and on the East and West by the lines delimiting the ITU Region 1 (Radio Regulations, 5.14).

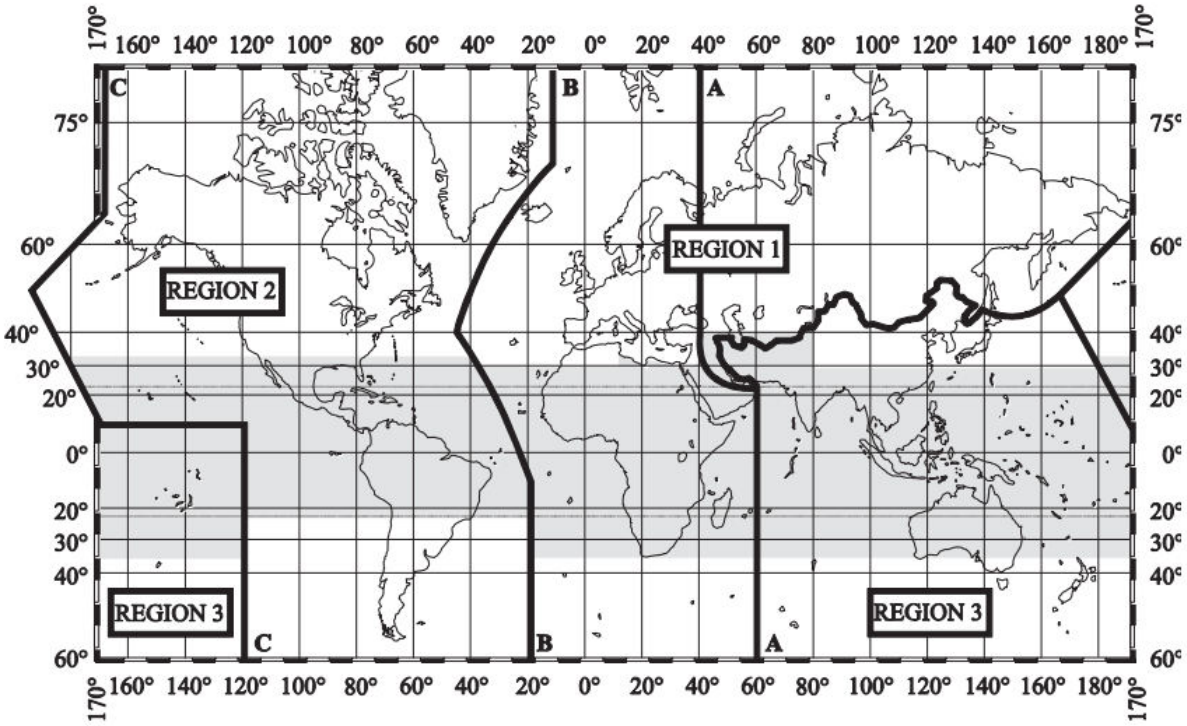

Figure 6.3: World division in ITU Regions. The shaded part represents the Tropical zones (ITU, 2016).

According to the ITU table of frequency allocation, the range of the spectrum between 430 and 440 MHz (the proposed uplink frequency range for PyrSat) in the ITU Region 1 is reserved to amateur services and radiolocation. The range between 432 and 438 MHz is additionally reserved for active Earth observation (Radio Regulations, Article 5). In ITU Region 1, the band 433.05 to 434.79 MHz, among others, is designated for industrial, scientific and medical (ISM) applications (Radio Regulations, 5.138). Thus, the use of this sub-band by the satellite telecommunications should be avoided, in order to avoid interferences with other services.

The radiofrequency bands between 2400 and 2480 MHz (the proposed frequency range of PyrSat downlink) have a different allocation in ITU Region 1. The range between 2300 and 2450 MHz in this Region is reserved to fixed satellite, amateur and radiolocation services. On its side, the range between 2450 and 2483.5 MHz is dedicated to fixed mobile and

radiolocation services (Radio Regulations, Article 5). The band 2400 – 2500 MHz is also designated for industrial, scientific and medical (ISM) applications and thus services operating within these bands must accept harmful interferences (Radio Regulations, 5.150).

Article 25 of the ITU Radio Regulations dictates the legislation applicable to amateur services. Regarding the communication between the ground stations in Spain and Barcelona, the ITU establishes that international communication between amateur stations must be allowed except from when one of the countries involved is opposed to such communication (Radio Regulations, 25.1), be limited to communication incidental to the purposes of the amateur services and to remarks of a personal character (Radio Regulations, 25.2). Additionally, international communication between amateur radio stations should not be encrypted except for command signals exchanged between Earth command stations and space stations in the amateur satellite service (Radio Regulations, 25.2A).

The ITU also establishes that Administrations must determine the conditions to issue a radio amateur license as well as verify the operational and technical competences of any person wishing to operate a radio amateur station (Radio Regulations, 25.5 and 25.6).

Because there will be ground stations in South Africa and Spain, both countries shall be listed in the service area of the space mission when sending a filing to the ITU. However, the satellite project license will be issued only for one country and solely their national regulatory administrator will communicate with the ITU Radiocommunications Bureau (Johnson, 2014). Given the fact that the satellite will be registered in South Africa, it seems reasonable that also this country's radio administration should manage the frequency coordination process with the ITU. This role will correspond to the Independent Communications Authority of South Africa (ICASA). ICASA is the South African National Administrative unit for the ITU, and co-ordinates frequency allocation, registration and licensing within the country. It was established by the Independent Communications Authority of South Africa Act of 2000, as Amended (ICASA, 2017).

In the case of Spain, the regulatory body responsible for radiofrequency spectrum management is the Secretariat of State for the Information Society and the Digital Agenda, of the Ministry of Energy, Tourism and the Digital Agenda (Spanish Ministry of Energy, Tourism and the Digital Agenda, n.d.). The source of applicable law to do this task is the Royal Decree 123/2017 of 24th of February 2017, which approves the regulations on the use of the radioelectric public domain. This Royal Decree was published in the Official State Gazette (BOE by its acronyms in Spanish) of 8th of March 2017 (Spanish Ministry of Energy, Tourism and the Digital Agenda, 2017).

Additionally, contact with regional or national amateur radio societies as well as the IARU should be made. Both South Africa and Spain are represented in the IARU Region 1, according to the ITU Regions. The two countries have IARU Member Societies that should be contacted for the development of the project. In the case of South Africa, this Society is the South African Radio League (SARL) and in the case of Spain it is the Spanish Amateur Radio Association (Union de Radioaficionados Españoles, URE) (IARU, n.d.).

The IARU also has a Satellite Frequency Coordination division that can help in telecommands and telemetry planning as well as radiofrequencies operations. They will also issue a frequency coordination letter for PyrSat's operators to submit to the national frequency regulatory administrator (Johnson, 2014).

6.2.4. Data policy

The PyrSat mission is conceived to primarily produce observations of the territories of both South Africa and Spain, although during the mission life and if resources (i.e. processing power, on-board memory and satellite power) sensing other States should also be considered. As encouraged in the UN Principles Relating to Remote Sensing of the Earth from Outer Space, this would promote international cooperation (Principles II and V), safeguard the Earth's environment (Principle X) and protect a wider extent of population from wild fires (Principle XI).

Principles X and XI state that when remote sensing activities produce information that can be used to *avert any phenomenon harmful to the Earth's natural environment* or that *may be useful to States affected by natural disasters,* the sensing State shall share this information with other States concerned as promptly as possible. Furthermore, Principle XIII provides that sensed States must have access to the primary and processed remote sensing data *on a non-discriminatory basis and on reasonable cost terms* as soon as these data are produced (UNOOSA, 1986).

Finally, due to the amateur nature of the satellite service, and in accordance with the Article 25, point 25.2A1A (RR25-1), of the ITU Radio Regulations, the transmission to and from the amateur satellite must be open and clear for other licensed amateur radio operators. The only exceptions are the control signals exchanged between the ground stations and the satellite (ITU, 2016).

6.2.5. End-of-life disposal and space debris mitigation

Space debris is a rapidly growing and severe problem affecting to all space users. Although the creation of debris is not prohibited by international law, it must be avoided in order to achieve a cooperative and sustainable access to and use of space.

Figure 6.4: Space debris environment in Earth orbit (UNOOSA, 2010).

In 2002 the Inter-Agency Space Debris Coordination Committee (IADC), formed by fourteen space agencies and governmental bodies from around the world, developed a set of technical guidelines for space debris mitigation (Johnson, 2014). Based on these guidelines, and taking

into consideration the UN treaties and principles on outer space, the Working Group on Space Debris of UN established a set of guidelines, the *Space Debris Mitigation Guidelines of the Committee on the Peaceful Uses of Outer Space* (2007), to serve as a common framework to avoid or minimize the growing problem of space debris. It was endorsed in the resolution 62/217 of the General Assembly.

These guidelines contain various recommendations to consider during the development, operation and termination of the PyrSat mission.

Firstly, the satellite must be designed so as to minimize the potential of debris release (Guideline 1) and break-ups (Guideline 2) during normal operations.

Secondly, the mission profile must be designed so as to *limit the probability of accidental collision in orbit* (Guideline 3). This will affect the orbit parameters and is of special relevance for this mission because of its specific characteristics: Sun-synchronous design orbit and no autonomous propulsion. The LEO region is highly populated and therefore is, together with the GEO region, the most vulnerable area for space debris problems. Additionally, Sun-synchronous orbits are widely used for remote sensing missions, which increases the risk of accidental collision. Finally, because PyrSat does not have autonomous propulsion capability, collision avoidance manoeuvres will not be possible.

Thirdly, at the mission end-of-life, appropriate measures must be taken to minimize the potential for post-mission break-ups resulting from stored energy (Guideline 5). This includes discharging the electrical storage devices. To conclude, Guideline 6 encourages States *to limit the long-term presence of spacecraft and launch vehicle orbital stages in the low-Earth orbit (LEO) region after the end of their mission*, because of the high concurrence of space debris in this region, but does not provide any specific time requirement for de-orbiting of satellites. However, the revised *IADC Space Debris Mitigation Guidelines* (IADC, 2007), fixed this limit at 25 years. Taking into consideration the initial orbital altitude of this mission, the satellite will remain in orbit for a considerably longer time than 25 years (Section 3.1.5 of this dissertation, on *Orbital lifetime and end-of-life disposal*). Thus, active debris removal (ADR) will be necessary in order to meet this IADC guideline.

Chapter VII. Conclusions and future work

This dissertation has presented the preliminary design of an intelligent hyperspectral 3U CubeSat Earth Observation mission for forest fire observation and mitigation. The main goals of the mission are scientific investigation and technology demonstration. A preliminary selection of the spacecraft, its subsystems and the payload, as well as the application orbit, the user segment, ground segment and launch segment has been evaluated. The work also covers major policy and regulatory issues related to the mission.

The use of COTS components and on-board processing using open-source software signify a cost-effective solution to offer the benefits of hyperspectral imagery to communities for whom space data has traditionally been out of reach as a tool to solve real-world problems. In particular, PyrSat has an overall approximate mass of 2 kg and could be built for under €82 000. The spatial resolution at an altitude of 550 km is 67.57 m (across-track) x 95.39 m (along-track), with a swath width of 138.29 km x 103.71 km.

It is important to note that this work intends to serve as an example of application of the Space Mission Analysis and Design (SMAD) process for future space missions of these characteristics and presents only a preliminary space mission design. Additionally, because the available time for the development of this project was limited, it was not possible to implement a hardware version of PyrSat, nor the software functionalities described in Chapter IV. Thus, some further issues should be taken into consideration if the space mission were to be developed.

Firstly, the possible alternatives or complements to a one-satellite mission or a constellation should be thoroughly evaluated in terms of cost, efficiency and coverage. For example, high-altitude platforms (HAPs) have been used in other fire management services, such as the European project OSIRIS (Lewyckyj, Biesemans and Everaerts, 2007).

Secondly, a further analysis of the mission should incorporate elements such as a consideration of possible ground segment architectures, computing capabilities of the satellite once the software functionalities are developed, precise uplink-downlink requirements from and to the ground station and a simulation of all the satellite subsystems working together. Such a simulation could be done using a commercial tool such as Simulink. Furthermore, although the primary goal of the PyrSat mission is technology demonstration and thus a constellation would not be formed until the first satellite has been successfully demonstrated in orbit, the design parameters of a potential constellation should also be evaluated. This includes parameters such as coverage, frequency of coverage, response time and trade-off between coverage and number of satellites to optimize the cost of the constellation.

Finally, once the design was thoroughly studied and a design decision was made, this theoretical work should be implemented and tested in hardware. Possible development risks could include non-space-qualification of some satellite subsystems, in particular the hyperspectral sensor and dedicated computer defining the payload. In that case, the use of alternative components should be considered.

Nonetheless, it is important to emphasize that the main goal of this dissertation was to present an example of the SMAD process for a low-cost intelligent hyperspectral CubeSat for fire management. As such, it would serve the need for a classical Phase A mission concept analysis for the PyrSat mission concept. Should the mission advance to the next phase, the design decisions presented herein should be re-evaluated and further examined.

References

Ablin R and Sulochana C H. (2013). *A Survey of Hyperspectral Image Classification in Remote Sensing*. International Journal of Advanced Research in Computer and Communication Engineering Vol. 2, Issue 8, August 2013. ISSN (Print): 2319-5940. ISSN (Online): 2278-1021

AFIS. (n.d.). *AFIS* [ONLINE] Available at: http://www.afis.co.za [Accessed: June 2017]

AFIS. (2017). *AFIS Viewer* [ONLINE] Available at: https://southernafrica.afis.co.za/ [Accessed: June 2017]

Ager AA, Preisler H K, Arca B, Spano D and Salis M. (2013). *Wildfire risk estimation in the Mediterranean area.* Envirometrics. Special Issue Paper. Wiley Online Library. DOI: 10.1002/env.2269 [PDF ONLINE] Available at: https://www.fs.fed.us/psw/publications/preisler/psw_2014_preisler002_ager.pdf [Accessed: June 2017]

Anderson I, Imandaand Muhnandar I. (1999). *Vegetation Fires in Sumatra, Indonesia: A first look at vegetation indices in relation to fire occurrence*. Forest Fire Prevention and Control Project. European Union and Ministry of Forestry and Estate Crops.

Antunes S. (2012). *LEO Temperatures* in 'DIY Satellite Platforms: Building a Space-Ready General Base Picosatellite for Any Mission'. Published by O'Reilly Media, Inc [ONLINE] Available at: https://www.safaribooksonline.com/library/view/diy-satellite-platforms/9781449312756/ch01s05.html [Accessed: January 2016]

Antunes Daldegan G., Abílio de Carvalho Júnior O., Fontes Guimarães R., Trancoso Gomes R. A., de Figueiredo Ribeiro F. and McManus C. (2014). *Spatial Patterns of Fire Recurrence Using Remote Sensing and GIS in the Brazilian Savanna: Serra do Tombador Nature Reserve, Brazil*. Remote Sensing 2014, 6, 9873-9894, DOI: 10.3390/rs61098734

Arms Control Association. (2018). *Nuclear Weapons: Who Has What at a Glance.* [ONLINE] Available at: https://www.armscontrol.org/factsheets/Nuclearweaponswhohaswhat [Accessed: February 2018]

Arrow Electronics. (2018). *NVIDIA Jetson TX2 Module* [ONLINE] Available at: https://www.arrow.com/en/products/900-83310-0001-000/nvidia [Accessed: February 2018]

AustraliaGroup.net. (2007a). *The Origins of the Australia Group*. The Australia Group [ONLINE] Available at: http://www.australiagroup.net/en/origins.html [Accessed: February 2018]

AustraliaGroup.net. (2007b). *The Origins of the Australia Group*. The Australia Group [ONLINE] Available at: http://www.australiagroup.net/en/introduction.html [Accessed: February 2018]

Australian Geoscience. (2015). *Category: Analysis Ready Data.* Data Cube [ONLINE] Available at: http://www.datacube.org.au/wiki/Category:Analysis_Ready_Data [Accessed: June 2017]

AZoOptics. (2014). *What is a Lambertian Surface?* Editorial Feature [ONLINE] Available at: https://www.azooptics.com/Article.aspx?ArticleID=790 [Accessed: March 2017]

Bannari A, Morin D, Bonn F and Huete A R. (1995). *A review of vegetation indices*. Remote Sensing Reviews, 13: 1. pp. 95 — 120. DOI: 10.1080/02757259509532298 [PDF ONLINE] Available at: http://dx.doi.org/10.1080/02757259509532298 [Accessed: September 2017]

Bannon D. (2009). *Hyperspectral imaging: Cubes and slice* [ONLINE] Available at: http://www.nature.com/nphoton/journal/v3/n11/full/nphoton.2009.205.html[Accessed: May 2016]

Bastarrika A., Chuvieco E., Martín M.P. (2011). *Mapping burned areas from Landsat TM/ETM+ data with a two-phase algorithm: Balancing omission and commission errors.* Remote Sensing of Environment Volume 115, Issue 4, 15 April 2011, Pages 1003–1012. Science Direct [PDF ONLINE] Available at: http://www.sciencedirect.com/science/article/pii/S0034425710003433 [Accessed: May 2017]

Bense T. (2007). *Procesamiento de las imágenes satelitales (continuación)*. In Tutorial – Introduccion a la Percepcion Remota [ONLINE] Available at: http://www.teledet.com.uy/tutorial-imagenes-satelitales/procesamiento-imagenes-satelitales-1.htm [Accessed: January 2017]

Bicalho Santos A, de Albuquerque Araújo A and Menotti D. (2013). *Combining Multiple ClassificationMethods for Hyperspectral Data Interpretation*. IEEE JOURNAL OF SELECTED TOPICS IN APPLIEDEARTH OBSERVATIONS AND REMOTE SENSING, VOL. 6, NO. 3, JUNE 2013 [PDF ONLINE] Available at: http://ieeexplore.ieee.org/stamp/stamp.jsp?arnumber=6490435 [Accessed: March 2017]

Boain R. (2004). *A-B-Cs of Sun-synchronous Orbit Mission Design*. 14 AAS/AIAA Space Flight Mechanics Conference. Maui, Hawaii, 2004 [PDF ONLINE] Available at: https://trs.jpl.nasa.gov/bitstream/handle/2014/37900/04-0263.pdf?sequence=1 [Accessed: June 2017]

Braeunig R. (2014). *Atmospheric Models*. Rocket & Space Technology [ONLINE] Available at: http://www.braeunig.us/space/atmmodel.htm [Accessed: February 2018]

Capderou M. (2005). Orbit Relative to the Sun. Crossing Times. In: *Satellites. Orbits and missions*. France: Springer-Verlag, pp 265 - 291 [PDF ONLINE] Available at: http://www.atmo.arizona.edu/students/courselinks/spring09/atmo656b/SunSynchCrossTimeDrift.pdf [Accessed: June 2017]

Carrielo F. and Anderson L. O. (2007). *Multitemporal analysis of the spectral response of scars of burned areas using Landsat/ETM sensor.*Geoscience and Remote Sensing Symposium, 2007. IGARSS 2007. IEEE International. 23-28 July 2007. Barcelona, Spain. DOI: 10.1109/IGARSS.2007.4423681

California Polytechnic Institute of Technology. (n.d.). CubeSat. California Polytechnic Institute of Technology [ONLINE] Available at: http://www.cubesat.org [Accessed: June 2017]

CNES, Centre National d'ÉtudesSpatiales. (2017). *TheORFEO Tool Box Software Guide. Updated for OTB-5.10.0*. OTB Development Team [PDF ONLINE] Available at:https://www.orfeo-toolbox.org/packages/OTBSoftwareGuide.pdf [Accessed: July 2017]

CNES, Centre National d'ÉtudesSpatiales. (n.d.). *Start using Orfeo ToolBox. Orfeo ToolBox* - Orfeo is not a black box [ONLINE] Available at: https://www.orfeo-toolbox.org/start/ [Accessed: September 2017]

Cochrane M A. (2003). Fire science for rainforests. Nature. Vol 421. 27 February 2003. Pp. 913-919 [PDF ONLINE] Available at: https://pdfs.semanticscholar.org/dbb4/a92166ef11e25f929377d167f4f021040efd.pdf [Accessed: January 2018]

ConnectTech. (2017). *Orbitty Carrier for NVIDIA® Jetson™ TX2 and Jetson™ TX1* [PDF ONLINE] Available at: http://www.connecttech.com/pdf/ASG003.pdf [Accessed: June 2017]

COPUOS. Committee on the Peaceful Uses of Outer Space. (2017). *Status of International Agreements relating to activities in outer space as at 1 January 2017.* Legal Subcommittee Fifty-sixth session Vienna, 27 March-7 April 2017 Item 5 of the provisional agenda* Status and application of the five United Nations treaties on outer space. A/AC.105/C.2/2017/CRP.7. 23 March 2017. Vienna.

COPUOS. (2018a). *Committee on the Peaceful Uses of Outer Space.* United Nations Office for Outer Space Affairs [ONLINE] Available at: http://www.unoosa.org/oosa/en/ourwork/copuos/index.html [Accessed: February 2018]

COPUOS. (2018b). *Members of the Committee on the Peaceful Uses of Outer Space.* United Nations Office for Outer Space Affairs [ONLINE] Available at: http://www.unoosa.org/oosa/en/ourwork/copuos/index.html [Accessed: February 2018]

Cosine. (2016). *HyperScot. Real time hyperspectral land and vegetation inspection* [ONLINE] Available at: http://hyperscout.nl/ [Accessed: February 2018]

CubeSpace. (n.d). *CubeControl. Sensor/Actuator Board* [ONLINE] Available at: https://www.cubespace.co.za/componentscontrol [Accessed: June 2017]

CubeSpace. (2016a). *CubeControl. Actuator and Sensor Interface Board* [PDF ONLINE] Available at: https://www.isispace.nl/brochures/CubeControl_Brochure%20CubeSpace.pdf [Accessed: June 2017]

CubeSpace. (2016b). *CubeTorquer&CubeCoilMagnetorquers for CubeSats* [PDF ONLINE] Available at: https://www.cubesatshop.com/wp-content/uploads/2016/06/CubeTorquer-CubeCoil-Brochure-August-2016.pdf [Accessed: June 2017]

CubeSpace. (2016c). *CubeSense*. *Fine Sun and Nadir Sensor*. http://41.185.8.177/~cubespac/ClientDownloads/Brochures/CubeSense%20-%20Brochure%20%5Bv1.0%5D.pdf [PDF ONLINE] Available at: [Accessed: June 2017]

CubeSpace. (2016d). *CubeWheel. Reaction/Momentum Wheel* [PDF ONLINE] Available at: https://www.cubesatshop.com/wp-content/uploads/2016/06/CubeWheel-Brochure-August-2016.pdf [Accessed: June 2017]

CubeSpace. (2016e). *CubeComputer. General Purpose On-board Compute* [PDF ONLINE] Available at: https://www.cubesatshop.com/wp-content/uploads/2016/06/CubeComputer-Brochure-August-2016.pdf [Accessed: June 2017]

Deering D W, Rouse J W, Haas R H and Schell J A. (1975). 'Measuring forage production of grazing units from Landsat MSS data'. In: Cook J.J. (Ed.), *Proceedings of the Tenth International Symposium onRemote Sensing of Environment* (Ann Arbor, 1975), Vol. 2, pp.1169-1178.Ann Arbor, Michigan,USA.

Department of Commerce of the United States of America. (n.d.). *Advanced Very High Resolution Radiometer (AVHRR).*NOAA. Comprehensive Large Array-Data Stewardship System (CLASS) National Oceanic and Atmospheric Administration (NOAA). [ONLINE] Available at: http://www.sciencedirect.com/science/article/pii/S0034425710003433 [Accessed: May 2017]

Dimitriou A, Mantakas G, Kouvelis S. (2001). *An analysis of key issues that underlie forest fires and shape subsequent fire management strategies in 12 countries in the Mediterranean basin.* Final report prepared by Alcyon for WWF Mediterranean Programme Office and IUCN. May 2001 [PDF ONLINE] Available at: http://ec.europa.eu/environment/forests/pdf/meeting140504_wwfsecondocument.pdf [Accessed: June 2017]

EnduroSat. (2016a). *USER MANUAL.Communication Module* [PDF ONLINE] Available at: https://www.endurosat.com/modules-datasheets/COMM_User_Manual_Rev1.6.pdf?x65766 [Accessed: June 2016]

EnduroSat. (2016b). *USER MANUAL S-Band Patch Antenna Type I* [PDF ONLINE] Available at: https://www.endurosat.com/modules-datasheets/S_Band_Patch_User_Manual.pdf [Accessed: June 2016]

EnduroSat. (2017). *USER MANUAL UHF Antenna* [PDF ONLINE] Available at: https://www.endurosat.com/modules-datasheets/S_Band_Patch_User_Manual.pdf [Accessed: February 2018]

EnMAP. (n.d.). *Mission - EnMAP Hyperspectral Imager.*Earth Observation Center EOC of DLR [ONLINE] Available at: http://www.enmap.org/?q=mission [Accessed: May 2017]

eoPortal Directory. (2018). *GomX-4 [ONLINE]* Available at: https://directory.eoportal.org/web/eoportal/satellite-missions/g/gomx-4 [Accessed: February 2018]

eoPortal Directory. (n.d*.) EO-1 (Earth Observing-1)*[ONLINE] Available at: https://directory.eoportal.org/web/eoportal/satellite-missions/e/eo-1#Zqch411c5Kram [Accessed: January 2017]

ESA. (2017). Earth Observation CFI Software. Earth Observation Mission Support [ONLINE] Available at: https://eop-cfi.esa.int/index.php/mission-cfi-software/eocfi-software [Accessed: February 2018]

ESA. (2018). *Hand-sized hyperspectral camera to fly on ESA's next CubeSat*[ONLINE] Available at: http://www.esa.int/Our_Activities/Space_Engineering_Technology/Hand-sized_hyperspectral_camera_to_fly_on_ESA_s_next_CubeSat[Accessed:February 2018]

ESA. (n.d.a). *Overview.* Copernicus. Observing the Earth [ONLINE] Available at: http://www.esa.int/Our_Activities/Observing_the_Earth/Copernicus/Overview4 [Accessed: January 2018]

ESA. (n.d.b). *Sentinel-3 SLSTR Technical Guide.* Sentinel Online [ONLINE] Available at: https://sentinels.copernicus.eu/web/sentinel/technical-guides/sentinel-3-slstr [Accessed: January 2018]

ESA. (n.d.c). *Coding Languages*. ESA software engineering and standardisation [ONLINE] Available at: http://www.esa.int/TEC/Software_engineering_and_standardisation/TECRFBUXBQE_0.html [Accessed: July 2017]

Estébanez M. (2015). *Georreferenciación de las imágenes de la cámara APIS a bordo del satélite OPTOSmediante la implementación de librerías Earth Observation CFI de ESA.* Bachelor's thesis. Bachelor'sDegree in Aerospace Engineering.School of Aeronautics and Space Engineering. Technical University of Madrid.

Estébanez M. (2016). *OPTOS_EOCFI–A software tool for the geolocation of Cubesat images.*3rd International African CubeSat Workshop, CPUT. Cape Town. 25 Feb 2016.

EUFAR. (2018). *Aircraft: CASA 212 RS - INTA*. European Facility for Airborne Research [ONLINE] Available at: http://www.eufar.net/aircrafts/23 [Accessed: February 2018]

Euroconsult. (2017). *Government Spending in Space Programs Reaches $62 Billion in 2016* [ONLINE] Available at: http://euroconsult-ec.com/30_May_2017 [Accessed: February 2018]

European Commission. (n.d.a). *Welcome to EFFIS.* COPERNICUS. Emergency Management Service [ONLINE] Availble at: http://effis.jrc.ec.europa.eu [Accessed: May 2017]

European Commission. (2014). *The EU Dual Use Export Control Regime [PDF ONLINE*] Available at: http://trade.ec.europa.eu/doclib/docs/2014/february/tradoc_152181.pdf [Accessed: December 2017]

European Commission. (n.d.b). *Global Wildfire Information System (GWIS).* COPERNICUS. Emergency Management Service [ONLINE] Availble at:http://gwis.jrc.ec.europa.eu/ [Accessed: May 2017]

European Commission. (n.d.c). *Fire Damage Assesment.* COPERNICUS. Emergency Management Service [ONLINE] Availble at: http://effis.jrc.ec.europa.eu/about-effis/technical-background/fire-damage-assesment/ [Accessed: June 2017]

Federal Ministry for Europe, Integration and Foreign Affairs. (2018). *HCOC – ICC/Executive Secretariat.* Federal Ministry for Europe, Integration and Foreign Affairs. Republic of Austria [ONLINE] Available at: https://www.bmeia.gv.at/en/european-foreign-policy/disarmament/weapons-of-mass-destruction/hcoc-iccexecutive-secretariat/ [Accessed: February 2018]

Flasse S. P., Trigg S. N., Ceccato P. N., Perryman A. H., Hudak A.T., Thompson M. W., Brockett B. H., Drame M., Ntabeni T., Frost P. E., Landmann T., le Roux J. L.. (2004). *Remote sensing of vegetation fires and its contribution to a fire management information system.* In:Goldammer, J.; de Ronde, C., eds. Fire Management Handbook for Subsaharan Africa. The Hague: SPB Publishing. p. 58-211.

Franklin D. (2015). *NVIDIA® Jetson™ TX1 Supercomputer-on-Module Drives Next Wave of Autonomous Machines [ONLINE]* Availble at: https://devblogs.nvidia.com/nvidia-jetson-tx1-supercomputer-on-module-drives-next-wave-of-autonomous-machines/ [Accessed: February 2018]

Fuchs E., Stein E., Strunz G., Strobl C. and Frey C. (2015). *Fire monitoring – The use of medium resolution satellites (AVHRR, MODIS, TET) for long time series processing and the*

implementation in user driven applications and services. The International Archives of the Photogrammetry, Remote Sensing and Spatial Information Sciences. Volume XL-7/W3, 2015. 36TH International Symposium on Remote Sensing of Environment. 11-15 May 2015, Berlin, Germany

Golda A. (2005). Introduction to neural networks. [ONLINE] Available at: http://home.agh.edu.pl/~vlsi/AI/intro/ [Accessed: September 2017]

Government of South Africa. (1993). *Space Affairs Act*. Statutes of the Republic of South Africa - Trade and Industry No. 84 of 1993 [ONLINE] Available at: http://www.unoosa.org/oosa/en/ourwork/spacelaw/nationalspacelaw/south_africa/space_affairs_act_1993E.html [Accessed: December 2017]

Government of South Africa. (1995). *Space Affairs Amendment Act*. No. 1530. 6 October 1995. No. 64 of 1995: Space Affairs Amendment Act, 1995. Office of the President [ONLINE] Available at: http://www.unoosa.org/oosa/en/ourwork/spacelaw/nationalspacelaw/south_africa/space_affairs_amendment_act_1995E.html [Accessed: December 2017]

Government of Netherlands. (2006). *Rules Concerning Space Activities and the Establishment of a Registry of Space Objects (Space Activities Act)* [ONLINE] Available at: http://www.unoosa.org/oosa/en/ourwork/spacelaw/nationalspacelaw/netherlands/space_activities_actE.html [Accessed: December 2017]

Hagen N, Kester R, Gao L and Tkaczyk T. (2012). *Snapshot advantage: a review of the light collection improvement for parallel high-dimensional measurement systems.* National Center for Biotechnology Information, U.S. National Library of Medicine [ONLINE] Available at: https://www.ncbi.nlm.nih.gov/pmc/articles/PMC3393130/ [Accessed: January 2016]

Hagolle O. (2014). *The product level names, how they work ?* Séries Temporelles [ONLINE] Available at: http://www.cesbio.ups-tlse.fr/multitemp/?p=3202 [Accessed: June 2017]

Hague Code of Conduct. (2017). *The Hague Code of Conduct against Ballistic Missile Proliferation (HCoC)*. HCoC. The Hague Code of Conduct [ONLINE] Available at: http://www.hcoc.at/?tab=what_is_hcoc&page=description_of_hcoc [Accessed: February 2018]

Halle W and Terzibaschian T. (n.d.). *Satelliten* . FireBIRD. DLR [ONLINE] Available at: http://www.dlr.de/firebird/desktopdefault.aspx/tabid-9106/17971_read-42454/ [Accessed: June 2017]

Hellen F. (2017). *Didi Abuli (დიდიაბული) vu par Sentinel2-A*. Séries Temporelles [ONLINE] Available at: http://www.cesbio.ups-tlse.fr/multitemp/?tag=sentinel-2 [Accessed: June 2017]

Hochberg E, Robert D, Dennison P and Hulley G. (2015). *Special issue on the Hyperspectral Infrared Imager (HyspIRI): Emerging science in terrestrial and aquatic ecology, radiation balance and hazards.* Remote Sensing of Environment. Volume 167, 15 September 2015, Pages 1-5. Elsevier [PDF ONLINE] Available at: http://www.sciencedirect.com/science/article/pii/S0034425715300420 [Accessed: May 2017]

Holzmann G. (2014). *The Power of Ten–Rules for Developing Safety Critical Code* [PDF ONLINE] Available at: http://pixelscommander.com/wp-content/uploads/2014/12/P10.pdf [Accessed: September 2017]

Hudak A.T. corresponding author and Brockett B. H. (2004). *Mapping fire scars in a southern African savannah using Landsat imagery.* International Journal of Remote Sensing, 25:16, 3231-3243, DOI: 10.1080/01431160310001632666

IADC. (2017). *IADC Space Debris Mitigation Guidelines.* Issued by Steering Group and Working Group 4. IADC Action Item number 22.4. IADC-02-01 Revision 1 September 2007 [PDF ONLINE] Available at: http://www.unoosa.org/documents/pdf/spacelaw/sd/IADC-2002-01-IADC-Space_Debris-Guidelines-Revision1.pdf [Accessed: December 2017]

IARU. (2017a). *Worldwide Voice of Radio Amateurs*. IARU – International Amateur Radio Union [ONLINE] Available at: http://www.iaru.org/ [Accessed: December 2017]

IARU. (2017b). *About*. IARU – International Amateur Radio Union [ONLINE] Available at: http://www.iaru.org/about.html [Accessed: December 2017]

IARU. (n.d.). *IARU Member Societies*. IARU – International Amateur Radio Union [ONLINE] Available at: http://www.iaru.org/member-societies.html [Accessed: January 2017]

ICASA. (2017). *Welcome to ICASA.* ICASA - The Independent Communications Authority of South Africa [ONLINE] Available at: https://www.icasa.org.za/ [Accessed: December 2017]

IPS Radio & Space Services. (1999). *Satellite Orbital Decay Calculations.* Australian Government. Bureau of Meteorology [PDF ONLINE] Available at: http://www.sws.bom.gov.au/Category/Educational/Space%20Weather/Space%20Weather%20Effects/SatelliteOrbitalDecayCalculations.pdf [Accessed: February 2018]

Irons J, Taylor M and Rocchio L. (2017). History. Landsat Science. NASA [ONLINE] Available at: https://landsat.gsfc.nasa.gov/about/history/ [Accessed: June 2017]

Kashiwai I. (n.d.). *Satellite Orbital Decay Prediction* [ONLINE] Available at: http://www.lizard-tail.com/isana/lab/orbital_decay/ [Accessed: February]

ISIS. (2016a). *Solar Panels [PDF ONLINE*] Available at: https://www.cubesatshop.com/wp-content/uploads/2016/06/ISIS-Solar-Panels-Brochure-v1.pdf [Accessed: January 2017]

ISIS. (2016b). *CubeSat Deployers* [PDF ONLINE] Available at: https://www.isispace.nl/wp-content/uploads/2016/02/ISIS-CubeSat-Deployers-Brochure-v1.pdf [Accessed: February 2018]

ISIS. (2018). *Launch services*. ISIS [ONLINE] Available at: https://www.isispace.nl/launch-services/ [Accessed:February 2018]

ISIS. (n.d.). *3-Unit CubeSat structure* [ONLINE] Available at: https://www.isispace.nl/product/3-unit-cubesat-structure/ [Accessed: January 2017]

ISIS and CubeSatShop.com. (n.d.). *CubeSat Structures [PDF ONLINE*] Available at: https://www.cubesatshop.com/wp-content/uploads/2016/06/ISIS_CubeSat-Structures_Brochure_v.7.11.pdf [Accessed: January 2017]

ITAC. (2011). *Export Control. Legislation*. International Trade Administration Commission of South Africa. [ONLINE] Available at: http://www.itac.org.za/pages/services/import--export-control/export-control [Accessed: February 2018]

ITAC. (2012). *Export Control*. International Trade Administration Commission of South Africa. Government Notice No. R. 92. Government Gazette No. 35007, pp. 47-59. 10 February 2012 [PDF ONLINE] Available at: http://www.itac.org.za/upload/gg35007_nn92-Export-control-10-Feb-2012.pdf [Accessed: February 2018]

ITAC. (2015). *Export Control*. International Trade Administration Commission of South Africa. Government Notice No. R. 1291. Government Gazette No. 39567, pp. 6-7. 31 December 2015 [PDF ONLINE] Available at: http://www.itac.org.za/upload/gg35007_nn92-Export-control-10-Feb-2012.pdf [Accessed: February 2018]

ITU. (2016). *Radio Regulations. Articles.* Edition of 2016 [PDF ONLINE] Available at: http://search.itu.int/history/HistoryDigitalCollectionDocLibrary/1.43.48.en.101.pdf [Accessed: December 2017]

ITU. (2017a). *Overview.* ITU - Committed to connecting the world [ONLINE] Available at: https://www.itu.int/en/about/Pages/overview.aspx [Accessed: December 2017]

ITU. (2017b).*ITU Regions [ONLINE]* Available at: https://www.itu.int/en/ITU-R/terrestrial/broadcast/PublishingImages/bcd%20images/ITU%20regions.jpg [Accessed: December 2017]

James Martin Center for Nonproliferation Studies. (2017). *Missile Technology Control Regime (MTCR)*. NTI. Building a safer world [ONLINE] Available at: http://www.nti.org/learn/treaties-and-regimes/missile-technology-control-regime-mtcr/ [Accessed: February 2018]

Johnson C. (2014). *Chapter 5: Legal and Regulatory Considerations of Small Satellite Projects* in 'Small Satellite Program Guide', 1st Edition.Eds: Alonso-Perez M V, Qedar R [PDF ONLINE] Available at: https://swfound.org/media/188605/small_satellite_program_guide_-_chapter_5_-_legal_and_regulatory_considerations_by_chris_johnson.pdf [Accessed: December 2017]

JPL. (2009). *JPL Institutional Coding Standard for the C Programming Language.* JPL DOCID D-60411 [PDF ONLINE] Available at: http://lars-lab.jpl.nasa.gov/JPL_Coding_Standard_C.pdf [Accessed: September 2017]

JPL. (2016).*Laboratory for Reliable Software (LaRS) at the Jet Propulsion Laboratory*. Jet PropulsionLaboratory. California Institute of Technology. NASA [ONLINE] Available at: http://lars-lab.jpl.nasa.gov/ [Accessed: September 2017]

Jun L, Shoan W and Stevens H. (2005). C++ Coding Standards and Style Guide. NASA Technical Reports Server [PDF ONLINE] Available at: https://ntrs.nasa.gov/archive/nasa/casi.ntrs.nasa.gov/20080039927.pdf [Accessed: September 2017]

Killough B. (2015). *CEOS Data Cube Concept and Prototype Project Plans*. WGISS-39. May 11-13, 2015 [ONLINE] Available at: http://slideplayer.com/slide/5255009/ [Accessed: May 2017]

Klein D., Fischer C., Heldens W., Stein E., Holzer-Popp T., Baier F., Hedelt P., Lorenz E., Frey C., Strobl C., Valks P., Minet C., Eyring V., Jöckel P., Bugliaro L., Künzer C., Terzibaschian T., Conrad C., Knoefel P., Rücker G. (2013). *FireBIRD Science Plan and Concept of Data Use.* German Remote Sensing Data Center, Earth Observation Center. DLR.[PDF ONLINE] Available at: http://www.dlr.de/firebird/en/Portaldata/79/Resources/dokumente/FireBIRD_concept_of_data_use_v1.pdf [Accessed: May 2017]

Leutner B. (2010). Spectral Indices. R Documentation. [ONLINE] Available at: http://bleutner.github.io/RStoolbox/rstbx-docu/spectralIndices.html [Accessed: March 2017]

Levin N. (1999). *Fundamentals of Remote Sensing*. 1st Hydrographic Data Management course, IMO - International Maritime Academy, Trieste, Italy [PDF ONLINE] Available at: http://www.geoservis.ftn.uns.ac.rs/downloads/ISP/1999-fundamentals-of-remote-sensing.pdf [Accessed: September 2017]

Lewyckyj N, Biesemans J and Everaerts J. (2007). *OSIRIS: a European project using a High Altitude Platform for forest fire monitoring.* In book: Safety and Security Engineering II, Edition: 2007. WIT press, Ed: M. Guarascio M, Brebbia C A and Garcia F, pp.205-213.

Lorenz E, Mitchell S, Säuberlich T, Paproth C, Halle W and Frauenberger O. (2015). *Remote Sensing of High Temperature Events by the FireBird Mission.* ISPRS15, Berlin, Germany [ONLINE] Available at: http://elib.dlr.de/104106/ [Accessed: May 2017]

Luo and Chanussot. (2009). *Hyperspectral Image Classification Based on Spectral and GeometricalFeatures*. GIPSA-Lab [PDF ONLINE] Available at: http://www.gipsa-lab.grenoble-inp.fr/~jocelyn.chanussot/publis/ieee_mlsp_09_luo_Based.pdf [Accessed: January 2017]

Madry S. (2016). *Space Transportation Systems Spaceports, and Cubesats.* MPhil in Space Studies, course 2016. SpaceLab. University of Cape Town, South Africa

Mandl D, Crum G, Handy M, Huemmrich K, Ong L, Holt B and Maharaja R. (2016). *Hyperspectral Cubesat Constellation for Natural Hazard Response (Follow-on).*30thAnnual AIAA/USU Conference on Small Satellites.SSC16-XII-02.[PDF ONLINE] Available at: https://ntrs.nasa.gov/archive/nasa/casi.ntrs.nasa.gov/20160009139.pdf[Accessed: January 2016]

Marée R, Stévens B, Geurts P, Guern Y and Mack P. (2009). *A Machine Learning Approach for MaterialDetection in Hyperspectral Images*. Open Repository and Bibliography ORBI. University of Liege.[PDF ONLINE] Available at: http://orbi.ulg.ac.be//bitstream/2268/14710/1/maree-subcubes-otcbvs-cvpr09.pdf [Accessed: January 2017]

Martinez P. (2017). *Status update on the LTS discussions in UN COPUOS. Relevance to small satellite activities.* Peter Martinez Chair, UN COPUOS WG on LTS. IAC2017, Adelaide, September 2017.[PDF ONLINE] Available at: http://www.unoosa.org/documents/pdf/psa/activities/2017/SouthAfrica/slides/Presentation55.pdf [Accessed: February 2018]

Matsunaga T, Tsuchida S, Iwasaki A, Tanii J, Kahimura O and Rokugawa S. (2011). *Current Status of Hyperspectal Imager Suite (HISUI)*. 2011 HyspIRI Science Workshop Aug 23-25,

2011 Washington DC [PDF ONLINE] Available at: https://hyspiri.jpl.nasa.gov/downloads/2011_Workshop/day2/23.1108_HISUI_HyspIRIWS_06.pdf [Accessed: May 2017]

Miao Z and Shi W. (2016). A New Methodology for Spectral-Spatial Classification of Hyperspectral Images. Journal of Sensors, vol. 2016, Article ID 1538973,2016. doi:10.1155/2016/1538973 [ONLINE] Available at: https://www.hindawi.com/journals/js/2016/1538973/ [Accessed: March 2017]

MicroImages. (2012). Introduction to Hyperspectral Imaging with TNTmips® [PDF ONLINE] Available at: http://www.microimages.com/documentation/Tutorials/hyprspec.pdf [Accessed: July 2017]

Missile Technology Control Regime. (n.d.). *Objectives of the MTCR*. Missile Technology Control Regime [ONLINE] Available at: http://mtcr.info/deutsch-ziele/ [Accessed: February 2018]

NanoAvionics. (n.d.a). *Electrical Power System "EPS". CubeSat Electrical Power System "EPS".* CubeSat Solar Panels & Power Systems *[ONLINE]* Available at: http://n-avionics.com/cubesat-components/solar-panels-and-power-systems/cubesat-electrical-power-system-eps/ [Accessed: June 2017]

NanoAvionics. (n.d.b). *CubeSat UHF/VHF/S-Band Ground Station Kit CubeSat Ground Station Kits [ONLINE]* Available at: http://n-avionics.com/cubesat-components/ground-station-kits/cubesat-uhf-vhf-s-band-ground-station-kit/ [Accessed: June 2017]

NASA. (2005). *Autonomous SciencecraftExperiment.*Jet Propulsion Laboratory.California Institute of Technology [ONLINE] Available at: http://ase.jpl.nasa.gov/[Accessed: January 2016]

NASA. (2009). *NASA Systems Engineering Processes and Requirements w/Change 1 (11/04/09).* Appendix G. Technical Review Entrance and Success Criteria [PDF ONLINE] Available at: https://nodis3.gsfc.nasa.gov/npg_img/N_PR_7123_001A_/N_PR_7123_001A_.pdf [Accessed: February 2017]

NASA. (2016). *Landsat 7 Science Data Users Handbook* [PDF ONLINE] Available at: https://landsat.gsfc.nasa.gov/wp-content/uploads/2016/08/Landsat7_Handbook.pdf [Accessed: June 2017]

NASA. (2017). Welcome to HyspIRI Mission Study Website - HyspIRI Mission Study. Jet Propulsion Laboratory. California Institute of Technology [ONLINE] Available at: https://hyspiri.jpl.nasa.gov/ [Accessed: May 2017]

NASA. (n.d.a). *AVHRR Pathfinder.* Physical Oceanography Distributed Active Archive Center (PODAC). Jet Propulsion Laboratory. California Institute of Technology. NASA [ONLINE] Available at: https://podaac.jpl.nasa.gov/AVHRR-Pathfinder [Accessed: June 2017]

NASA. (n.d.b). *Earth Smallsats Main Image.* Global Climate Change. Vital signals of the planet [ONLINE] Available at: https://climate.nasa.gov/system/news_items/main_images/2512_Earth-smallsats-MAIN-IMAGE-768px-80.jpg [Accessed: June 2017]

NASA. (n.d.c). *Sun-synchronous Orbits for the Earth Solar Power Satellite System.* Mission Planning Resources Library. Sun Synchronous Orbits [ONLINE] Available at: http://design.ae.utexas.edu/mission_planning/mission_resources/orbital_mechanics/Sun_Synchronous_Orbits.pdf [Accessed: February 2018]

NASA. (n.d.d). *The Project Life Cycle Module. Exploration Systems Engineering, version 1.0* [PDF ONLINE] Available at: http://origins.sese.asu.edu/ses405/Class%20Notes/Project_LC_Module_V.10_PAS.pdf [Accessed: February 2017]

National Treasury Republic of South Africa. (2016). *Estimates of National Expenditure 2016.* Abridged Version. ISBN: 978-0-621-44244-1. RP: 15/2016 [PDF ONLINE] Available at: http://www.treasury.gov.za/documents/national%20budget/2016/ene/FullENE.pdf [Accessed: June 2017]

NewSpace. (2016). *GPS RECEIVER* [PDF ONLINE] Available at: https://www.cubesatshop.com/wp-content/uploads/2016/07/NewSpace-GPS-Receiver.pdf [Accessed: June 2017]

Ng A. (2017a). Online Machine Learning course in Coursera. Stanford University [ONLINE] Available at: https://es.coursera.org/learn/machine-learning [Accessed: January 2017]

Ng, A. (2017b). Model Representation. Introduction [ONLINE] Available at: https://www.coursera.org/learn/machine-learning/supplement/cRa2m/model-representation [Accessed: September 2017]

Ng A. (2017c). *Neural Networks: Representation*. Online Machine Learning course in Coursera. Stanford University [ONLINE] Available at: https://es.coursera.org/learn/machine-learning [Accessed: January 2017]

Ng A. (2017d). *Neural Networks: Learning*. Online Machine Learning course in Coursera. Stanford University [ONLINE] Available at: https://es.coursera.org/learn/machine-learning [Accessed: January 2017]

Ng A. (2017e). *Support Vector Machines*. Online Machine Learning course in Coursera. StanfordUniversity [ONLINE] Available at: https://www.orfeo-toolbox.org/CookBook/Monteverdi.html [Accessed: September 2017]

Ng A. (2017f). *Unsupervised Learning*. Online Machine Learning course in Coursera. Stanford University [ONLINE] Available at: https://es.coursera.org/learn/machine-learning [Accessed: January 2017]

Nuclear Suppliers Group. (n.d.). *NSG Timeline.* Nuclear Suppliers Group [ONLINE] Available at: http://www.nuclearsuppliersgroup.org/en/history1 [Accessed: February 2018]

OpenCV. (2014). *Introduction to Support Vector Machines*. OpenCV 2.4.13.3 documentation. OpenCV Tutorials. Machine Learning [ONLINE] Available at: http://docs.opencv.org/2.4/doc/tutorials/ml/introduction_to_svm/introduction_to_svm.html [Accessed: October 2017]

OTB Team. (2017). Monteverdi. OTB CookBook. [ONLINE] Available at: https://es.coursera.org/learn/machine-learning [Accessed: January 2017]

Parliament of Canada. (1988). *Export and Import Permits Act.An Act respecting the export and transfer of goods and technology and the import of goods.* R.S.C., 1985, c. E-19. Last amended on September 21, 2017 [PDF ONLINE] Available at: http://laws-lois.justice.gc.ca/PDF/E-19.pdf [Accessed: January 2018]

Parliament of Canada. (1989). *Export Control List.* SOR/89-202. Last amended on September 21, 2017 [PDF ONLINE] Available at: http://laws-lois.justice.gc.ca/PDF/E-19.pdf [Accessed: January 2018]

Payero J O, Neale C M U and Wright J L. (2004). *Comparison of Eleven Vegetation Indices for Estimating Plant Height of Alfalfa and Grass*. Applied Engineering in Agriculture. Vol. 20(3), pp.385-393. American Society of Agricultural Engineers [PDF ONLINE] Availa le at: https://naldc.nal.usda.gov/download/10026/PDF [Accessed: September 2017]

PEGASUS Team. (2017a). *Testing*. PEGASUS. [ONLINE] Available at: http://www.pegasus-fhwn.at/testing/ [Accessed: February 2017]

PEGASUS Team. (2017b). *Updates*. PEGASUS. [ONLINE] Available at: http://www.pegasus-fhwn.at/updates/ [Accessed: February 2017]

Pereira J. (2007). *Remote Sensing of Fire.* Lecture D4L1: Fires and burned area detection. ESA. In the Advanced Training Course on Land Remote Sensing at the Instituto Superior de Estatística e Gestao de Informaçao, Universidade Nova de Lisboa (ISEGI-UNL)

Perry M, Alea P, Cully M, McCullough M, Sanneman P and Teti N. (2001). *Earth Observing-1 Spacecraft Bus.*15th Annual/USU Conference on Small Satellites.SSC01-V-6 [ONLINE] Available at: http://digitalcommons.usu.edu/cgi/viewcontent.cgi?article=1986&context=smallsat [Accessed: January 2016]

QGIS. (n.d.). *QGIS - The Leading Open Source Desktop GIS*. [ONLINE] Available at: http://www.qgis.org/en/site/about/index.html [Accessed: September 2017]

Richards J A. (2013). *Correcting and Registering Images*. In Remote Sensing Digital Image Analysis pp 27-77. Springer-Verlag Berlin Heidelberg. DOI: 10.1007/978-3-642-30062-2_2

Roy D. (2016). *Prototyping a Landsat-8 Sentinel-2 Global Burned Area Product.* International Journal of Remote Sensing, 25:16, 3231-3243, DOI: 10.1080/01431160310001632666

SEOS Project. (2017). *Vegetation Indices.* Remote Sensing and GIS in Agriculture [ONLINE] Available at: http://www.seos-project.eu/modules/agriculture/agriculture-c01-s04.html [Accessed: September 2017]

Soukup M, Gailis J, Fantin D, Jochemsen A, Aas C, Baeck P, Benhadj I, Livens S, Delauré B, Menenti M, Gorte B, Hosseini Aria SE, Esposito M and van Dijk C. (2016). *HyperScout: Onboard Processing of Hyperspectral Imaging Data on a Nanosatellite*. Small Satellites, System & Services Symposium (4S), At Valletta, Malta. May 2016.

Spanish Ministry of Energy, Tourism and the Digital Agenda. (2017). *Real Decreto 123/2017, de 24 de febrero, por el que se aprueba el Reglamento sobre el uso del dominio público radioeléctrico.* Boletin Oficial del Estado. No. 57. Sec. I. Pg. 17029. Wednesday 8th of March 2017 [PDF ONLINE] Available at: https://www.boe.es/boe/dias/2017/03/08/pdfs/BOE-A-2017-2460.pdf [Accessed: January 2018]

Spanish Ministry of Energy, Tourism and the Digital Agenda. (n.d.). *Espectro radioeléctrico.* Spanish Ministry of Energy, Tourism and the Digital Agenda. Secretariat of State for the Information Society and the Digital Agenda [ONLINE] Available at: http://www.minetad.gob.es/TELECOMUNICACIONES/ESPECTRO/INFORMACION/Paginas/informacion-general.aspx [Accessed: January 2018]

Sterling Arnold S, Nuzzaci R and Gordon-Ross A. (2012).*Energy Budgeting for Cubesats with an Integrated FPGA.*Department of Electrical and Computer Engineering, University of Florida, Gainesville, FL 32611

Stöckli R. (n.d). Images. Earth Observatory. When everyday is Earth Day. NASA [ONLINE] Available at: https://Earthobservatory.nasa.gov/IOTD/view.php?id=2421 [Accessed: June 2017]

Saglam B., Bilgili E., Durmaz B. D., Kadiogullari A. I. and Kücük Ö. (2008*). Spatio - Temporal Analysis of Forest Fire Risk and Danger Using LANDSAT Imagery.* Sensors 2008, 8, 3970-3987, DOI: 10.3390/s8063970

SkyFox Labs. (2017). *Space-Friendly Active GPS-L1 Patch Antenna. piPATCH-L1*. Product Datasheet. Rev. C/2017 [PDF ONLINE] Available at: http://www.skyfoxlabs.com/pdf/piPATCH-L1_Datasheet_rev_C.pdf [Accessed: February 2018]

SkyFox Labs. (2018). S*pace-Friendly CubeSat GPS Receiver/Next Generation. piNAV-NG*. Product Datasheet. Rev. F/2018 [PDF ONLINE] Available at: http://www.skyfoxlabs.com/pdf/piNAV-NG_Datasheet_rev_F.pdf [Accessed: February 2018]

SpaceWeather.com. (2018). *Solar activity report. Joint USAF/NOAA Report of Solar and Geophysical Activity.* Viewing archive of Sunday, 31 December 2017 [ONLINE] Available at: https://www.spaceweatherlive.com/en/archive/2017/12/31/rsga [Accessed: February]

Surrey. 2014. *SGR-05U Subsystem* [PDF ONLINE] Available at: https://www.sst-us.com/getfile/d3991938-d829-4d05-82aa-3e421dc3d10a [Accessed: July 2016]

Surrey. n.d. *SGR-05U - Space GPS Receiver* [ONLINE] Available at: https://www.sst-us.com/shop/satellite-subsystems/global-positioning-systems-gps-receivers/sgr-05u-space-gps-receiver [Accessed: July 2016]

The Council of the European Union. (2009). *Regulations*. *Council Regulation (EC) No 428/2009 of 5 May 2009. Setting up a Community regime for the control of exports, transfer, brokering and transit of dual-use items*. Official Journal of the European Union. L 134/1 [ONLINE] Available at: http://trade.ec.europa.eu/doclib/docs/2013/august/tradoc_151691.pdf#page=12 [Accessed: December 2017]

The dti. (n.d.). *Import and Export Control.* Department: Trade and Industry. Republic of South Africa [ONLINE] Available at: http://www.dti.gov.za/trade_investment/import_export_control.jsp [Accessed: February 2018]

The IDB Project. (n.d.). *Index: Enhanced Vegetation Index***.** [ONLINE] Available at: http://www.indexdatabase.de/db/i-single.php?id=16[Accessed: September 2017]

Thenkabail P. S., Enclona E. A., Ashton M. S., Legg C., De Dieu M. J. (2004). *Hyperion, IKONOS, ALI and ETM+ sensors in the study of African rainforests.* Remote Sensing of Environment Volume 90, Issue 1, 15 March 2004, Pages 23–43. Science Direct [PDF ONLINE] Available at: http://www.sciencedirect.com/science/article/pii/S0034425703003560 [Accessed: May 2017]

Thompson D, Bornstein B, Bue B, Tran D, Chien S, Castaño R. (2012). *Hyperspectral Feature Detection On-board the Earth Observing One Spacecraft Using Superpixel Segmentation and Endmember Extraction [PDF ONLINE*] Available at: http://ml.jpl.nasa.gov/papers/thompson/Thompson_2012_iSAIRAS_c.pdf [Accessed: January 2016]

Toutin T. (2004). *Review article: Geometric processing of remote sensing images: models, algorithms andmethods.*International Journal of Remote Sensing, 20 May, 2004, vol. 25, NO. 10. pp. 1893 - 1984.

Tsela P., Wessels K., Botai J., Archibald S., Swanepoel D., Steenkamp K., Frost P. (2014). *Validation of the Two Standard MODIS Satellite Burned-Area Products and an Empirically-Derived Merged Products in South Africa.* Remote Sensing. 2014, 6(2), 1275-1293; DOI:10.3390/rs6021275[PDF ONLINE] Available at: http://www.mdpi.com/2072-4292/6/2/1275 [Accessed: May 2017]

United Nations. (2018). *Special Political and Decolonization (Fourth Committee).* General Assembly of the United Nations [ONLINE] Available at: http://www.un.org/en/ga/fourth/ [Accessed: February 2018]

UNOOSA. (1963). *Declaration of Legal Principles Governing the Activities of States in the Exploration and Use of Outer Space*. Resolution 1962 (XVIII) of the General Assembly [PDF ONLINE] Available at: http://www.unoosa.org/pdf/publications/st_space_11rev2E.pdf [Accessed: December 2017]

UNOOSA. (1982). *Principles Governing the Use by States of Artificial Earth Satellites for International Direct Television Broadcasting*. Resolution 37/92 of the General Assembly [ONLINE] Available at: http://www.unoosa.org/oosa/en/ourwork/spacelaw/principles/dbs-principles.html [Accessed: December 2017]

UNOOSA. (1986). *Principles relating to remote sensing of the Earth from space*. Resolution 41/65 of the General Assembly [ONLINE] Available at: http://www.un.org/documents/ga/res/41/a41r065.htm [Accessed: December 2017]

UNOOSA. (1992). *Principles Relevant to the Use of Nuclear Power Sources in Outer Space*. Resolution 47/68 of the General Assembly [ONLINE] Available at: http://www.unoosa.org/oosa/en/ourwork/spacelaw/principles/nps-principles.html [Accessed: December 2017]

UNOOSA. (1996). *Declaration on International Cooperation in the Exploration and Use of Outer Space for the Benefit and in the Interest of All States, Taking into Particular Account the Needs of Developing Countries*. Resolution 51/122 of the General Assembly [ONLINE] Available at: http://www.unoosa.org/oosa/en/ourwork/spacelaw/principles/space-benefits-declaration.html [Accessed: December 2017]

UNOOSA. (2008a). *Treaty on Principles Governing the Activities of States in the Exploration and Use of Outer Space, including the Moon and Other Celestial Bodies*. Resolution 2222 (XXI) of the General Assembly. In "United Nations Treaties and Principles on Outer Space and related General Assembly resolutions" [PDF ONLINE] Available at: http://www.unoosa.org/pdf/publications/st_space_11rev2E.pdf [Accessed: December 2017]

UNOOSA. (2008b). *Recommendations on enhancing the practice of States and international intergovernmental organizations in registering space objects.* Resolution 62/101 of the General Assembly. Sixty-second session. Agenda item 31. 10 January 2008. A/RES/62/101 [PDF ONLINE] Available at: http://www.unoosa.org/pdf/gares/ARES_62_101E.pdf [Accessed: February 2018]

UNOOSA. (2010). *Space Debris Mitigation Guidelines of the Committee on the Peaceful Uses of Outer Space* [ONLINE] Available at: http://www.unoosa.org/pdf/publications/st_space_49E.pdf [Accessed: December 2017]

UNOOSA. (2017a). *Agreement on the Rescue of Astronauts, the Return of Astronauts and the Return of Objects Launched into Outer Space.* Resolution 2345 (XXII) of the General Assembly [ONLINE] Available at: http://www.unoosa.org/oosa/en/ourwork/spacelaw/treaties/introrescueagreement.html [Accessed: December 2017]

UNOOSA. (2017b). *Convention on International Liability for Damage Caused by Space Objects*. Resolution 2777 (XXVI) of the General Assembly [ONLINE] Available at: http://www.unoosa.org/oosa/en/ourwork/spacelaw/treaties/introliability-convention.html [Accessed: December 2017]

UNOOSA. (2017c). *Convention on Registration of Objects Launched into Outer Space*. Resolution 3235 (XXIX) of the General Assembly [ONLINE] Available at: http://www.unoosa.org/oosa/en/ourwork/spacelaw/treaties/introregistration-convention.html [Accessed: December 2017]

UNOOSA. (2017d). *Agreement Governing the Activities of States on the Moon and Other Celestial Bodies*. Resolution 34/68 of the General Assembly [ONLINE] Available at: http://www.unoosa.org/oosa/en/ourwork/spacelaw/treaties/intromoon-agreement.html [Accessed: December 2017]

UNOOSA. (2018a). *United Nations Register of Objects Launched into Outer Space* [ONLINE] Available at: http://www.unoosa.org/oosa/en/spaceobjectregister/index.html[Accessed: February 2018]

UNOOSA. (2018b). *Status of International Agreements relating to Activities in Outer Space*. *Latest Depository Notifications*. United Nations Office for Outer Space Affairs [ONLINE] Available at: http://www.unoosa.org/oosa/en/ourwork/spacelaw/treaties/status/index.html [Accessed: February 2018]

US Bureau of Industry and Security. (2017). *The Commerce Control List*. Supplement No. 1 to Part 774 of the EAR [ONLINE] Available at: https://www.bis.doc.gov/index.php/documents/regulation-docs/435-part-774-the-commerce-control-list/file [Accessed: January 2018]

US Bureau of Industry and Security. (2017). *Commerce Control List*. Bureau of Industry and Security. U.S. Department of Commerce. Where Industry and Security Intersect [ONLINE] Available at: https://www.bis.doc.gov/index.php/regulations/commerce-control-list-ccl [Accessed: January 2018]

US Congress. (1979). *The Export Administration Act of 1979*. Amended and enacted December 17, 2004 [PDF ONLINE] Available at: https://legcounsel.house.gov/Comps/The%20Export%20Administration%20Act%20Of%201979.pdf [Accessed: January 2018]

US Department of State. (2016). *The Arms Export Control Act*. US Department of State. Directorate of Defense Trade Controls [ONLINE] Available at: https://www.pmddtc.state.gov/regulations_laws/aeca.html [Accessed: January 2018]

US Department of State. (n.d.). *Title 22. Foreign Relations and Intercourse*. In 'US Code of Federal Regulations' [ONLINE] Available at: http://uscode.house.gov/view.xhtml?req=granuleid%3AUSC-prelim-title22&saved=%7CKHRpdGxlOjIyIHNlY3Rpb246MSBlZGl0aW9uOnByZWxpbSkgT1IgKGdyYW51bGVpZDpVU0MtcHJlbGltLXRpdGxlMjItc2VjdGlvbjEp%7CdHJlZXNvcnQ%3D%7C%7C0%7Cfalse%7Cprelim&edition=prelim [Accessed: January 2018]

USDA-ARS Jornada Experimental Range, BLM-AIM Program, and Idaho Chapter of The Nature Conservancy. (2013). Normalized Difference Vegetation Index. The Landscape Toolbox. Tools & Methods for Effective Land Health Monitoring [ONLINE] Available at: http://wiki.landscapetoolbox.org/doku.php/remote_sensing_methods:normalized_difference_vegetation_index [Accessed: January 2018]

Vassili Group. (n.d.). *Latest and Fastest Ka-Band Internet Space Satellite Technology*. Global Internet Provider - We Connect Continents [ONLINE] Available at: http://www.vassili-group.com/space-satellites---internet.html [Accessed: June 2017]

Varshney P and Arora M. (2004). *Advanced Image Processing Techniques for Remotely Sensed Hyperspectral Data.* Springer Berlin Heidelberg. ISBN: 9783662056059 (online) • 9783540216681. DOI: 10.1007/978-3-662-05605-9

Verhegghen A., Eva H., Ceccherini G., Achard F., Gond V., Gourlet-Fleury S. and Omar Cerutti P. (2016). *The Potential of Sentinel Satellites for Burned Area Mapping and Monitoring in the Congo Basin Forests.* Remote Sensing 2016, 8(12), 986,DOI:10.3390/rs8120986

VITO NV. (2010). *SPOT 4*. VEGETATION [ONLINE] Available at: http://www.vgt.vito.be/pages/VegetationProgramme/spot4.htm [Accessed: June 2017]

Wassenaar Arrangement. (2017a). *Funding Documents*. Public documents, Volume I. Wassenaar Arrangement on Export Controls for Conventional Arms and Dual-Use Goods and Technologies. WA-DOC (17) PUB 001 [PDF ONLINE] Available at: http://www.wassenaar.org/wp-content/uploads/2015/06/WA-DOC-17-PUB-001-Public-Docs-Vol-I-Founding-Documents.pdf [Accessed: February 2018]

Wassenaar Arrangement. (2017b). *About us. Overview*. The Wassenaar Arrangement on Export Controls for Conventional Arms and Dual-Use Goods and Technologies [ONLINE] Available at: http://www.wassenaar.org/about-us/ [Accessed: February 2018]

Welch J. (2010). *Flight Unit Qualification Guidelines*. Aerospace report no. TOR-2010(8591)-20. U.S. Space Programs Mission Assurance Improvement Workshop.

Wertz J and Larson W. (1999). *Space Mission Analysis and Design*. Space Technology Library volume 8. Springer Netherlands, 1999. ISBN: 1-881883-10-8 (pb) 0-7923-5901-1 (hb)

XIMEA. (2016a). *xiSpecHyperspectral Cameras Brochure* [PDF ONLINE] Available at: https://www.ximea.com/files/brochures/xiSpec-Hyperspectral-cameras-2015-brochure.pdf [Accessed: January 2016]

XIMEA.(2016b). *Hyperspectral imaging data correction and standardization, mobileapplications*.SpectroNet Collaboration Forum 2016. Fraunhofer IIS, Dresden [PDF ONLINE]Available at: https://www.ximea.com/support/attachments/5981/SpectroNet-2016-03-Ximea-V02.pdf [Accessed: April 2017]

XIMEA. (n.d.). *MQ022HG-IM-LS100-NIR [ONLINE]* Available at: https://www.ximea.com/en/products/hyperspectral-cameras-based-on-usb3-xispec/mq022hg-im-ls100-nir [Accessed: July 2016]

Zangger Committee. (n.d.a). *History*. Zangger Committee [ONLINE] Available at: http://zanggercommittee.org/history.html [Accessed: February 2018]

Zangger Committee. (n.d.b). *Zangger Committee*. Zangger Committee [ONLINE] Available at: http://zanggercommittee.org/ [Accessed: February 2018]

Zhang L, Liu Y, Zhang X, Wang J, Zeng L, Xue Y and Tong Q. (2014). *Progress in Chinese Satellite Hyperspectral Missions*. Institute of Remote Sensing and Digital Earth. Chinese Academy of Sciences [PDF ONLINE] Available at: https://www.grss-ieee.org/wp-content/uploads/2014/12/2014_07_ISIS_Session1_Mission/1030_zhanlf-IGARSS-20140716.pdf [Accessed: May 2017]

ANNEX A.
Accesses of the on-board sensor in an orbit with LTAN at 10:10 to Cape Town

Access	Start Time (UTCG)	Stop Time (UTCG)	Duration (sec)
1	3 Dec 2017 09:18:35.994	3 Dec 2017 09:18:50.937	14.943
2	4 Dec 2017 09:15:12.979	4 Dec 2017 09:15:27.927	14.948
3	20 Dec 2017 20:37:00.226	20 Dec 2017 20:37:15.172	14.946
4	21 Dec 2017 20:33:37.222	21 Dec 2017 20:33:52.167	14.945
5	31 Dec 2017 09:18:47.703	31 Dec 2017 09:19:02.648	14.945
6	1 Jan 2018 09:15:24.694	1 Jan 2018 09:15:39.644	14.951
7	17 Jan 2018 20:37:11.936	17 Jan 2018 20:37:26.885	14.949
8	18 Jan 2018 20:33:48.925	18 Jan 2018 20:34:03.868	14.943
9	28 Jan 2018 09:18:59.407	28 Jan 2018 09:19:14.349	14.942
10	29 Jan 2018 09:15:36.402	29 Jan 2018 09:15:51.352	14.950
11	14 Feb 2018 20:37:23.640	14 Feb 2018 20:37:38.590	14.950
12	15 Feb 2018 20:34:00.625	15 Feb 2018 20:34:15.568	14.943
13	25 Feb 2018 09:19:11.104	25 Feb 2018 09:19:26.049	14.945
14	26 Feb 2018 09:15:48.104	26 Feb 2018 09:16:03.053	14.949
15	14 Mar 2018 20:37:35.340	14 Mar 2018 20:37:50.291	14.950
16	15 Mar 2018 20:34:12.321	15 Mar 2018 20:34:27.264	14.943
17	25 Mar 2018 09:19:22.796	25 Mar 2018 09:19:37.743	14.947
18	26 Mar 2018 09:15:59.803	26 Mar 2018 09:16:14.751	14.948
19	11 Apr 2018 20:37:47.041	11 Apr 2018 20:38:01.992	14.951
20	12 Apr 2018 20:34:24.017	12 Apr 2018 20:34:38.959	14.942
21	22 Apr 2018 09:19:34.492	22 Apr 2018 09:19:49.439	14.947
22	23 Apr 2018 09:16:11.504	23 Apr 2018 09:16:26.451	14.948
23	9 May 2018 20:37:58.749	9 May 2018 20:38:13.703	14.954
24	10 May 2018 20:34:35.718	10 May 2018 20:34:50.664	14.946
25	20 May 2018 09:19:46.191	20 May 2018 09:19:50.752	4.561
26	21 May 2018 09:16:23.211	21 May 2018 09:16:38.158	14.947
27	6 Jun 2018 20:38:10.464	6 Jun 2018 20:38:25.416	14.952
28	7 Jun 2018 20:34:47.429	7 Jun 2018 20:35:02.375	14.946
29	18 Jun 2018 09:16:34.929	18 Jun 2018 09:16:49.875	14.947
30	4 Jul 2018 20:38:22.191	4 Jul 2018 20:38:37.147	14.956
31	5 Jul 2018 20:34:59.152	5 Jul 2018 20:35:14.098	14.946
32	16 Jul 2018 09:16:46.657	16 Jul 2018 09:17:01.603	14.946
33	1 Aug 2018 20:38:33.925	1 Aug 2018 20:38:48.884	14.959
34	2 Aug 2018 20:35:10.884	2 Aug 2018 20:35:25.830	14.946
35	13 Aug 2018 09:16:58.392	13 Aug 2018 09:17:13.338	14.946
36	14 Aug 2018 09:13:41.762	14 Aug 2018 09:13:50.288	8.526
37	29 Aug 2018 20:38:45.668	29 Aug 2018 20:38:57.721	12.053
38	30 Aug 2018 20:35:22.620	30 Aug 2018 20:35:37.566	14.946
39	10 Sep 2018 09:17:10.129	10 Sep 2018 09:17:25.075	14.946
40	11 Sep 2018 09:13:47.072	11 Sep 2018 09:14:02.029	14.957
41	26 Sep 2018 20:38:57.404	26 Sep 2018 20:38:57.496	0.091
42	27 Sep 2018 20:35:34.355	27 Sep 2018 20:35:49.301	14.946
43	8 Oct 2018 09:17:21.860	8 Oct 2018 09:17:36.806	14.946
44	9 Oct 2018 09:13:58.809	9 Oct 2018 09:14:13.765	14.956
45	25 Oct 2018 20:35:46.079	25 Oct 2018 20:36:01.025	14.947
46	5 Nov 2018 09:17:33.577	5 Nov 2018 09:17:48.523	14.946
47	6 Nov 2018 09:14:10.532	6 Nov 2018 09:14:25.486	14.954
48	22 Nov 2018 20:35:57.786	22 Nov 2018 20:36:12.733	14.947
49	23 Nov 2018 20:32:48.191	23 Nov 2018 20:32:49.753	1.562

Global Statistics

Min Duration	41	26 Sep 2018 20:38:57.404	26 Sep 2018 20:38:57.496	0.091
Max Duration	33	1 Aug 2018 20:38:33.925	1 Aug 2018 20:38:48.884	14.959
Mean Duration				13.969
Total Duration				684.495

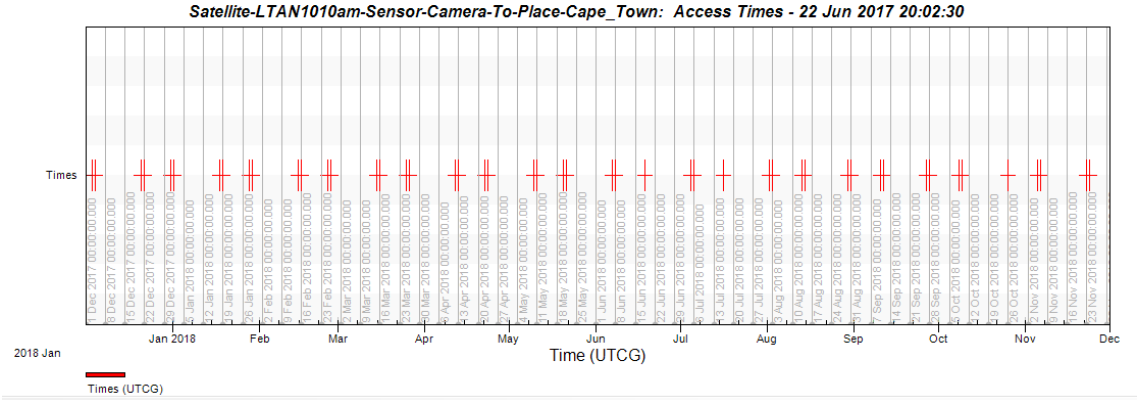

ANNEX B - Accesses of the on-board sensor in an orbit with LTAN at 10:10 to Barcelona

Access	Start Time (UTCG)	Stop Time (UTCG)	Duration (sec)
1	4 Dec 2017 09:35:20.253	4 Dec 2017 09:35:35.282	15.028
2	5 Dec 2017 09:31:57.257	5 Dec 2017 09:32:12.279	15.022
3	9 Dec 2017 22:30:10.255	9 Dec 2017 22:30:25.275	15.021
4	10 Dec 2017 22:26:47.248	10 Dec 2017 22:27:02.277	15.029
5	1 Jan 2018 09:35:31.966	1 Jan 2018 09:35:46.996	15.029
6	2 Jan 2018 09:32:08.963	2 Jan 2018 09:32:23.984	15.021
7	6 Jan 2018 22:30:21.961	6 Jan 2018 22:30:36.985	15.024
8	7 Jan 2018 22:26:58.961	7 Jan 2018 22:27:13.989	15.028
9	29 Jan 2018 09:35:43.674	29 Jan 2018 09:35:58.700	15.026
10	30 Jan 2018 09:32:20.665	30 Jan 2018 09:32:35.687	15.021
11	3 Feb 2018 22:30:33.664	3 Feb 2018 22:30:48.683	15.020
12	4 Feb 2018 22:27:10.667	4 Feb 2018 22:27:25.694	15.027
13	26 Feb 2018 09:35:55.377	26 Feb 2018 09:36:10.405	15.028
14	27 Feb 2018 09:32:32.363	27 Feb 2018 09:32:47.384	15.021
15	3 Mar 2018 22:30:45.358	3 Mar 2018 22:31:00.381	15.023
16	4 Mar 2018 22:27:22.368	4 Mar 2018 22:27:37.394	15.027
17	26 Mar 2018 09:36:07.076	26 Mar 2018 09:36:22.105	15.029
18	27 Mar 2018 09:32:44.057	27 Mar 2018 09:32:59.078	15.020
19	31 Mar 2018 22:30:57.050	31 Mar 2018 22:31:12.074	15.023
20	1 Apr 2018 22:27:34.066	1 Apr 2018 22:27:49.092	15.026
21	23 Apr 2018 09:36:18.779	23 Apr 2018 09:36:33.808	15.029
22	24 Apr 2018 09:32:55.754	24 Apr 2018 09:33:10.778	15.024
23	28 Apr 2018 22:31:08.744	28 Apr 2018 22:31:23.767	15.023
24	29 Apr 2018 22:27:45.768	29 Apr 2018 22:28:00.793	15.025
25	21 May 2018 09:36:30.488	21 May 2018 09:36:45.518	15.030
26	22 May 2018 09:33:07.459	22 May 2018 09:33:22.483	15.024
27	26 May 2018 22:31:20.449	26 May 2018 22:31:30.001	9.552
28	27 May 2018 22:27:57.477	27 May 2018 22:28:12.502	15.025
29	28 May 2018 22:24:39.592	28 May 2018 22:24:49.440	9.848
30	18 Jun 2018 09:36:42.209	18 Jun 2018 09:36:57.242	15.033
31	19 Jun 2018 09:33:19.175	19 Jun 2018 09:33:34.199	15.024
32	24 Jun 2018 22:28:09.197	24 Jun 2018 22:28:24.221	15.025
33	25 Jun 2018 22:24:46.128	25 Jun 2018 22:25:01.165	15.037
34	16 Jul 2018 09:36:53.942	16 Jul 2018 09:37:08.972	15.030
35	17 Jul 2018 09:33:30.901	17 Jul 2018 09:33:45.926	15.024
36	22 Jul 2018 22:28:20.926	22 Jul 2018 22:28:35.951	15.024
37	23 Jul 2018 22:24:57.862	23 Jul 2018 22:25:12.900	15.038
38	13 Aug 2018 09:37:05.681	13 Aug 2018 09:37:20.715	15.034
39	14 Aug 2018 09:33:42.636	14 Aug 2018 09:33:57.660	15.024
40	19 Aug 2018 22:28:32.662	19 Aug 2018 22:28:47.686	15.024
41	20 Aug 2018 22:25:09.606	20 Aug 2018 22:25:24.640	15.034
42	10 Sep 2018 09:37:17.423	10 Sep 2018 09:37:32.459	15.036
43	11 Sep 2018 09:33:54.372	11 Sep 2018 09:34:09.397	15.024
44	16 Sep 2018 22:28:44.398	16 Sep 2018 22:28:59.422	15.024
45	17 Sep 2018 22:25:21.348	17 Sep 2018 22:25:36.379	15.031
46	8 Oct 2018 09:37:29.157	8 Oct 2018 09:37:44.193	15.037

47	9 Oct 2018 09:34:06.103	9 Oct 2018 09:34:21.128	15.025
48	14 Oct 2018 22:28:56.126	14 Oct 2018 22:29:11.150	15.024
49	15 Oct 2018 22:25:33.082	15 Oct 2018 22:25:48.115	15.033
50	5 Nov 2018 09:37:40.882	5 Nov 2018 09:37:51.501	10.620
51	6 Nov 2018 09:34:17.821	6 Nov 2018 09:34:32.846	15.025
52	7 Nov 2018 09:31:01.067	7 Nov 2018 09:31:09.874	8.807
53	11 Nov 2018 22:29:07.838	11 Nov 2018 22:29:22.862	15.024
54	12 Nov 2018 22:25:44.799	12 Nov 2018 22:25:59.829	15.030

Global Statistics

Min Duration	52	7 Nov 2018 09:31:01.067	7 Nov 2018 09:31:09.874	8.807
Max Duration	37	23 Jul 2018 22:24:57.862	23 Jul 2018 22:25:12.900	15.038
Mean Duration				14.633
Total Duration				790.167